PHILOSOPHY DOCTOR THESIS

Polymer optical fiber gratings for microwave photonics and communications applications

Author

Rui Min

Supervisors

Dr. Beatriz Ortega Tamarit

Dr. Carlos Alberto Ferreira Marques (external)

Departamento de Comunicaciones

Universitat Politècnica de València

Valencia, June 2019

Acknowledgements

I would like to show my sincere acknowledgements to my supervisor Prof. Beatriz Ortega, Dr. Carlos Marques and short-term co-supervisor Dr. David Saez for their tremendous support since without their help, I would not have been able to complete the work presented in this thesis.
I would also like to thank Prof. Ole Bang, Prof. Christophe Caucheteur and Prof. Victor Torres for a short visit in their group and longtime collaboration during my PhD study, to be honest, this has been very important to finish this thesis.
I wish to express my gratitude to all my present and past colleagues, for the helpful conversations on the scientific challenges and problems which have appeared on the way and have allowed me to get new perspectives.
Beyond the professional environment, I would like to thank all my friends since we shared a lot of time after work and I will always miss those evenings in good company.
I would like to thank my parents since they always support me in any decision.
To my dear wife Mo, she is an essential support to me and living with her is the best thing has ever occurred to me. She is a source of understanding, love, affection and accepts me with all my faults. She has made possible the finishing of this Ph.D. thesis.

Rui Min

Valencia 19/06/2019

Abstract

With the continuing development of material and fabrication technologies over the last three decades, the transmission attenuation of polymer optical fibers (POF) has been greatly decreased. POFs are advantageous for home networks as well as storage interconnections and have significant advantages for many sensing applications, including high elastic strain limits, high fracture toughness, high flexibility in bending, high sensitivity to strain and potential negative thermo-optic coefficients.

This thesis improved the laser irradiation technology for POF and investigated special grating devices in POF for optical communication, microware photonics and sensing. In particular, we developed fast POF grating fabrication technology with a detailed study and optimization of the polymer optical fiber Bragg grating (POFBG) fabrication parameters. Highlights of the results include an 8 dB uniform POFBG with one single Nd:YAG (266nm) laser pulse (8 ns) based on BDK doped fiber, which is the shortest time ever reported for POFBG fabrication. The irradiation of polymer optical fibers using different materials under 248 nm KrF laser system allowed to demonstrate a better performance compared with 325 nm Kimmon laser system. Furthermore, uniform FBGs in step-index TS doped POF were achieved with less than 1 second by means of controlling pulse repetition and low pulse energy. Finally, the study of low UV pulse power irradiation for fabricating stable gratings allowed to save energy in the POF grating fabrication process, as one of the main goals for mass production.

Based on the improved fabrication technology, we focused on the fabrication of different grating structures: a phase-shifted FBG was fabricated by using two 15 ns 248 nm KrF pulses overlapped by Moiré method; the first tunable chirped FBG was achieved by using a single laser short pulse, which opened the applications based on chirped POF -BGs; also a novel thermal annealing method was proposed to obtain chirped POFBGs based on uniform FBGs, and proved as the ever published most convenient way to achieve chirped POFBG; and finally, long period gratings have been also achieved by using a short time fabrication process, specially when compared with previous research.

Finally, based on the grating devices obtained throughout this work, several potential applications have been proposed in this thesis. Similarly, to silica chirped FBG, chirped FBG in POF have many potential applications in optical communications and sensing area. This document described the potential strain sensing application based on tunable chirped POFBG; also, the thermal detection application in bio-medical systems; and the potential of tunable dispersion devices in optical communications, i.e., dispersion compensation or microwave photonics.

Resumen

Con el continuo desarrollo de materiales y tecnologías de fabricación durante las últimas tres décadas, la atenuación de la transmisión de las fibras ópticas de polímero (POF) se ha reducido considerablemente. Las POF son ventajosas para las redes domésticas, así como para las interconexiones de almacenamiento, y tienen ventajas significativas para muchas aplicaciones de detección, que incluye el límite alto de tensión elástica, alta resistencia a la fractura, alta flexibilidad en la flexión, alta sensibilidad a la tensión y coeficientes termoópticos negativos.

Esta tesis consigue mejorar la tecnología de irradiación con láser para POF e investiga dispositivos especiales basados en redes de difracción en POF para comunicaciones ópticas, microondas, fotónica y detección. En particular, desarrollamos la tecnología de fabricación rápida de FBGs en POF con un estudio detallado y la optimización de los parámetros de fabricación de redes de difracción de Bragg en fibra (FBG). Los resultados más destacados incluyen un FBG uniforme de 8 dB con un solo pulso láser Nd: YAG (26 nsm) (8 ns) basado en fibra dopada con BDK, que es el tiempo más corto presentado hasta ahora para la fabricación de FBGs en POF. La irradiación de fibras ópticas de polímero utilizando diferentes materiales basado en el láser KrF a 248 nm permitió demostrar un mejor rendimiento en comparación con el sistema que emplea el láser He-Cd a 325 nm. Además, se fabricaron FBGs uniformes en POFs de índice escalón dopadas con TS en menos de 1 segundo mediante la repetición de pulsos con baja energía. Finalmente, el estudio de la irradiación UV con pulsos de baja energía para la fabricación de redes de difracción estables permitió ahorrar energía en el proceso de fabricación de FBGs en POF, como uno de los principales requisitos para la producción en masa.

Basándonos en la tecnología de fabricación mejorada, nos centramos en la fabricación de redes de difracción con diferentes estructuras: se fabricó un FBG con desplazamiento de fase utilizando dos pulsos de 15 ns a 248 nm KrF superpuestos por el método de Moiré; el primer FBG con chirp sintonizable se logró utilizando un solo pulso corto del láser, que abrió nuevas perspectivas a las aplicaciones basadas en redes de difracción con chirp en POF; también se propuso un nuevo método basado en gradientes térmicos para obtener FBG con chirp en POF basadas en FBG uniformes, y se demostró como la forma más conveniente publicada hasta la fecha para lograr este tipo de FBGs no uniformes en POF; y, finalmente, también se han fabricado redes de difracción de largo período utilizando un proceso de fabricación de corto tiempo, especialmente en comparación con investigaciones anteriores.

En la última parte de la tesis, y en base a los dispositivos basados en redes de difracción obtenidos a lo largo de este trabajo, se han propuesto varias aplicaciones . De manera similar a los FBG en fibra de sílice, los FBGs con chirp en POF tienen muchas aplicaciones futuras en las áreas de comunicaciones ópticas y de los sensores. Este documento describe la aplicación de detección de tensión basada en una FBG con chirp sintonizable en POF, su aplicación para detección térmica en sistemas biomédicos; e ilustra el potencial de los dispositivos de dispersión sintonizables en el campo de las comunicaciones ópticas, bien como compensación de dispersión o en fotónica de microondas.

Resum

Amb el continu desenvolupament de materials i tecnologies de fabricació durant les últimes tres dècades, l'atenuació de la transmissió de les fibres òptiques de polímer (POF) s'ha reduït considerablement. Els POF són avantatjosos per a les xarxes domèstiques, així com per a les interconnexions d'emmagatzematge, i tenen avantatges significatius per a moltes aplicacions de detecció, inclosos els límits de tensió elàstica alta, alta resistència a la fractura, alta flexibilitat en la flexió, alta sensibilitat a la tensió i potencials coeficients termoópticos negatius.

Aquesta tesi va millorar la tecnologia d'irradiació amb làser per a POF i va investigar dispositius basats en xarxes difracció de Bragg (FBG) especials en POF per a comunicació òptica, microones, fotònica i detecció. En particular, desenvolupem la tecnologia de fabricació ràpida de FBG en POF amb un estudi detallat i l'optimització dels paràmetres per a la seua fabricació. Els punts destacats dels resultats inclouen un FBG uniforme de 8 dB amb un sol pols del làser Nd: YAG (266 nm) (8 ns) basat en fibra dopada amb BDK, que és el temps més curt reportat per a la fabricació de POF FBG. La irradiació de fibres òptiques de polímer utilitzant diferents materials sota el sistema de làser KrF a 248 nm va permetre demostrar un millor rendiment en comparació amb el sistema de làser Kimmon de 325 nm. A més, els FBG uniformes en el POF dopat amb TS d'índex escalonat es van aconseguir amb menys d'1 segon mitjançant la repetició de polsos de control i l'energia baixa de pols. Finalment, l'estudi de la irradiació d'energia de pols per a la fabricació de FBGs estables va permetre estalviar energia en el procés de fabricació de FBGs en POF, com un dels principals objectius de la producció en massa.

Basant-nos en la tecnologia de fabricació millorada, ens centrem en la fabricació de diferents estructures de xarxes de difracció: es va fabricar un FBG amb desplaçament de fase utilitzant dos polsos de 15 ns a 248 nm KrF superposats pel mètode de Moiré; el primer FBG amb chirp sintonitzable es va aconseguir utilitzant un sol pols curt de làser, que va obrir les aplicacions basades en FBG amb chirp en POF; també es va proposar un nou mètode amb gradients tèrmics per a obtindre FBG en POF basat en FBG uniformes, i es va demostrar com la forma més convenient publicada fins hui per a aconseguir FBG POF estimulada; i, finalment, també s'han aconseguit xarxes de llarg període utilitzant un procés de fabricació de curt temps, especialment en comparació amb investigacions anteriors.

Finalment, sobre la base dels dispositius de xarxes de difracció obtinguts al llarg d'aquest treball, s'han proposat diverses aplicacions potencials en aquesta tesi. De manera similar que per als FBG amb silici, el FBG amb chirp en POF té moltes aplicacions potencials en comunicacions òptiques i a l´àrea de sensors. Aquest document descriu l'aplicació de detecció de tensió basada en FBG amb chirp sintonitzable en POF; a més, l'aplicació de detecció tèrmica en sistemes biomèdics; i el potencial dels dispositius de dispersió sintonitzables en les comunicacions òptiques, com per eixample a la compensació de dispersió o a la fotònica de microones.

Contents

List of Figures

List of Tables

Chapter 1

Introduction

1.1 State of the art and motivation

1.1.1 Polymer optical fibers

Polymer optical fibers (POFs) are optical fibers made of polymer materials with attractive characteristics compared with silica fibers, such as low Young's modulus, high failure strain, high flexibility and biocompatibility. The first commercially available optical fiber with deuterated polymer was produced by *DuPont* in 1963 [1]. From the middle of the last century, optical fibers are under research with the aim of transmitting high speed data. Although some of the first optical fibers were made of polymer with beeswax as the cladding material [2], silica fibers were also under intense research since their first proposal as transmission medium by *Kao* and *Hockman* [2]. At that time the transmission loss of silica fibers was high, but theoretical predictions allowed to propose pure glass as fiber material able to transmit light over 100 km. In a few years, the purity of silica material was significantly improved, and losses were reduced up to 2 dB/km at 850 nm, 0.5 dB/km at 1300 nm and 0.2 dB/km at 1550 nm. Therefore, most of the research was conducted in the silica optical fiber technology and current silica optical fiber networks form the backbone of the modern telecommunications systems where the loss is about 0.15 dB/Km at the telecom wavelength region [3].

The absorption loss of polymer materials is higher compared with silica although Rayleigh scattering is a dominant mechanism in both cases. In polymers, the main absorption contribution is due to the harmonics of the C-H vibration [4]. In 1975, The Mitsubishi Rayon commercialized the very first step-index POF "EsKa". Then, other two Japan companies, Asahi Chemical and Toray, also did that during 1970s. Intense research demonstrated the transmission loss close to the theoretical limit of PMMA POF with 150 dB/km at 650 nm wavelength during 1980s [5]. In terms of graded-index (GI) POF, the very first Poly(methyl methacrylate) (PMMA) core GI POF was reported by *Ohtsuka et al.* in 1976 [6], where the attenuation of GI POF composed of Methyl methacrylate (MMA) and vinyl benzoate was about 1000 dB/km, much higher than step-index POF [7]. Years later, the group of *Prof. Koike* found fluorinated materials to improve the transparency of polymer fibers with lower losses (50 dB/km over 650 nm~1300 nm) and extend the transmission window up to infrared region, which made components design for silica fiber also valid for polymer optical fibers [8]. "Lucina" perfluorinated polymer fibers by Asahi Glass Co., then called CYTOP in 2000 [9] were the first commercial product for real applications. However, this technology received a substantial boost when *Chromis*, a company in USA, licensed the manufacture process of prefluorinated polymer optical fiber [10], as the lower loss commercial fiber. In spite of continuous research by *Chromis*, the fabrication expenditures of fluorinated polymer are still much higher compared with silica fiber. Therefore, this is the reason why the most common material for polymer fiber is PMMA which is cheaper, although it shows higher transmission loss at visible range. Figure 1.1 shows the spectral attenuation behavior of PMMA POF, CYTOP POF and silica optical fibers.

Both the step-index POF (SI-POF) and GI-POF mentioned above are multimode fibers, but *Kuzyk et al.* obtained single mode step-index PMMA POF for the first time for more than 20 years [11] and *Tam´s* group also reported low loss, single mode fluorinated fiber in 2010 [12]. However, the main limitation for commercial POFs is to achieve single mode performance in the low transmission loss band with low fabrication costs due to the technology limitations.

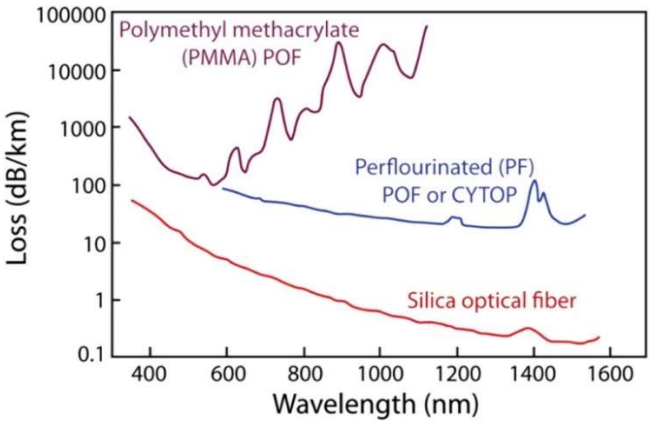

Figure 1.1 Spectral attenuation of polymer and silica optical fibers. [13]

The mature of photonic crystal fiber technology attracted the attention of polymer optical fiber research community, which was firstly invented by *Birks et al.* in 1997 in silica structures [14]. Then, *Large et al.* obtained the very first photonic crystal fiber with polymer materials in 2001 [15] allowing to obtain endless single-mode performance in POF [15]. According to this promising result, different materials such as Topas [16], Zeonex [17] and polycarbonate [18] were used to obtain microstructured polymer optical fiber (mPOF). Topas polymer belongs to the collection of cyclic olefin copolymers (COCs), a kind of optical thermoplastics that are chemically inert, with a very low moisture uptake, good optical transmission and high water barrier [19]. Zeonex belongs to cyclo olefin polymers, an amorphous homopolymer of norbornene [20]. Polycarbonate is an engineered plastic which exhibits excellent clarity and impact strength, and also shows larger available temperature range compare with PMMA material [21]. However, the main limitation of mPOF is the coupling to step-index silica fiber since, so far, there is no commercial method for coupling between mPOF and step-index silica fiber. Current research leads to several kinds of step-index POF with single mode performance [22][23], which indicates this technology is becoming mature.

Polymer optical fiber technology achieved the loss theoretical limit in 80s, which imposed a slow down in their development [15]. Furthermore, large core POF was demonstrated with enormous potential to be used in automotive engineering with benefits such as high bandwidth, low weight, immunity to electromagnetic, easy handing and install. After this media system based on POF was firstly introduced by BMW in the 7th series [24], a lot of automotive factories were interested on such kind of systems and more than 22 car models use POF in multimedia services system.

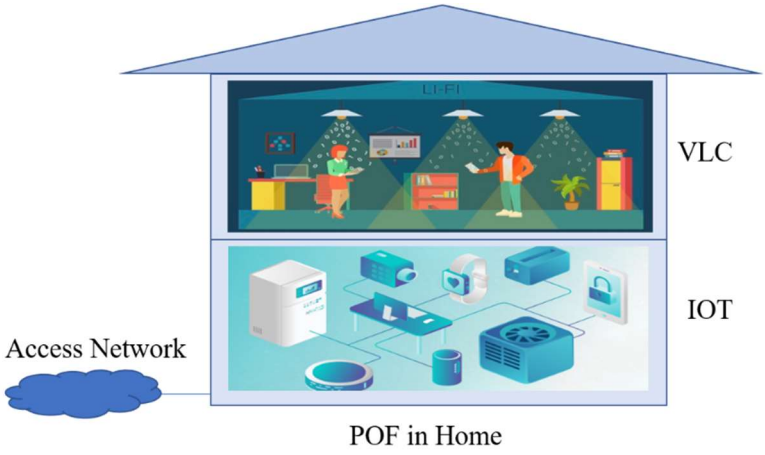

Figure 1.2 Potential application for POF in Home network.

Afterwards, the first application of POF in a large central office telecom platform is successful in 2001 [25]. Since then, the application scenarios were extended to longer

transmission distance (Fiber in home network). The demand of high capacity increase from long-haul system to short range communication links, and POFs with large core, low weight and higher transmission capacity are good candidates for short range communications in fiber to the home (FTTH) applications. Figure 1.2 shows the potential use of POFs in home networks, where the fiber allows to visible light communication (VLC) and smart home Internet of Things (IoT). The group of professor *Koike* drives continue research towards data transmission at high speed based on POF. Since they reported high bandwidth 2.5 Gb/s 100 m data transmission using GI POF at 650 nm wavelength in 1995 [26], they worked on high bandwidth GI-POF with low penalties in 2003 [27] and developed 120 Gb/s GI POF and the ballpoint pen interconnect technology for uncompressed 4K/8K video transmission in 2016 [28]. Another examples in the European framework allowed to achieve 2.5 Gb/s signal transmission over 300 m (@645 nm), 550 m (@840 nm and @1310 nm) in 2001 [29]. Focusing on the short range in home networks, other achievements in the literature include 4.7 Gbit/s discrete multi-tone (DMT) signal transmission over 50m multi-Core SI-POF [30]. Recently, a 2 GB/s bidirectional real time link using 5 WDM visible channels over 50 m step index POF was reported by *Pinzon et al.* [31]. Gigabit per second transmission over short-range step-index plastic optical fiber based on a laser diode (LD) as the optical source has been implemented using multi-level pulse amplitude modulation (PAM-M) scheme with simultaneous transmission of 16-QAM 40 MHz bandwidth WLAN, 64-QAM LTE-A bands [32]. Also, 1.7 Gb/s 4-PAM baseband signal over 50 m of 1-mm core diameter GI POF [33] has been demonstrated for in home network, showing the enormous potential for POF in home networks, which is still an emerging area under research.

Figure 1.3 Potential applications of sensing based on POF.

The use of POFs for sensing applications is growing fast during the recent years [34]. PMMA based POFs are mainly used due to its lower Young's modulus compare with silica fiber, higher thermo-optic coefficient [35] and low cost. Additionally, PMMA has biological compatibility which is important for biomedical applications.

Sensing technology based on intensity variation represents one of the first optical fiber sensing technologies, and in general, all sensors include a light source, optical fiber, optical spectrum analyzer or photo detector. Figure 1.3 shows potential applications of sensing based on POF such as structural health monitoring [36], medical instrument [37], environment monitoring [38], mechanical measurement [39] and chemical detectors [40]. Although the literature shows an extense number of implementations and examples, several of them are mentioned in the following for the sake of illustrating the variety of applications of POF sensors. *Durana et al.* presented a POF sensor for monitoring the deflection of aircraft flap under different load conditions and showed good signal repeatability and stability with low cost [36]. *Bilro et al.* [37] reported a wireless and wearable system for monitor human gait with a portable and low cost package. *Junior et al.* presented a fully portable, wearable

and low cost sensor for joint angle assessment based on POF curvature sensor with high repeatability and low error [41]. *Shan et al.* introduced a differential method in reflective intensity modulation angular POF sensor with a high sensitivity [42]. *Sequeira et al.* investigated D-shape POF sensor to be used for chemical and biochemical sensing [40]. The major disadvantage of intensity-based sensors is related with the stability of the light source, which usually introduces errors in the measurement and limits the resolution. However, self-referencing or dynamic compensation [39] can be used to improve the sensitivity of these sensors.

Brillouin scattering technology is also an attractive sensing solution based on optical fibers which has been extensively explored using silica fibers [43] in spite of the fragility and limited strain of these fibers. Oppositely, POF shows a high flexibility to be exploited under large strains. *Mizuno et al.* reported the first stimulated Brillouin scattering in POF with 1 m CYTOP fiber [44] which could be used for high accuracy temperature detection. *Minardo et al.* [45] reported low resolution distributed temperature sensing based on Brillouin optical frequency domain analysis, then *Hayashi et al.* [46] presented the first demonstration of distributed temperature and strain sensing with a centimeter order spatial resolution using Brillouin optical correlation domain reflectometry. Brillouin scattering technology in POF is suitable for long distance structural health monitoring.

1.1.2 Polymer fiber gratings

Grating devices in fibers belong to two main types depending on the mode coupling mechanism: counter-directional coupling is the responsible mechanism in fiber Bragg gratings (FBGs) whereas co-directional coupling happens in long period gratings (LPGs).

Fiber Bragg grating (FBG) is a periodic modulation of the refractive index along the length of an optical fiber, produced through the exposure of the fiber core to an intense optical interference pattern. The periodic structure in a FBGs acts like a selective mirror for the wavelength that satisfies the Bragg condition expressed as:

$$\lambda_{\text{Bragg}} = 2n_{eff}\Lambda \tag{1.1}$$

where Λ is the grating period and n_{eff} is the average effective refractive index along the periodic structure. Therefore, such component reflects one wavelength and transmits all others as Figure 1. 4 shows with a wavelength-specific dielectric mirror response.

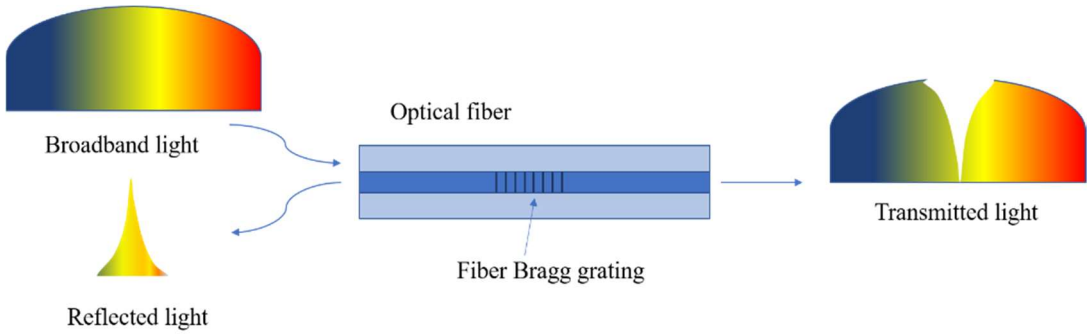

Figure 1.4 FBG transmission and reflection.

The ability of the FBGs to act as mirrors could find application such as band stop filters in dispersion compensators [47], Raman amplifiers [48] and wavelength division multiplexers [49]. Also, they can be used for sensing purposes, such as strain, temperature and humidity measurements since these parameters have an impact on the period and the refractive index, and accordingly, the resonant wavelength shifts.

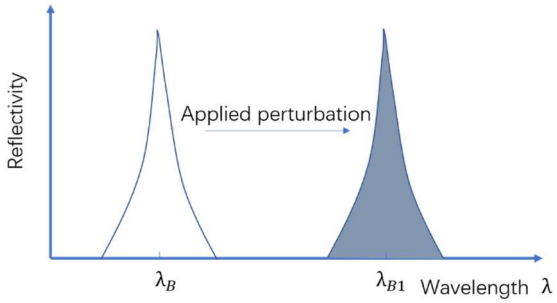

Figure 1.5 Reflectivity response shift.

A variation in the environmental parameters, for instance, temperature and strain, influence both the pitch and the refractive index of the grating layers perturbing the spectral properties of the FBG, as shown in Figure 1.5, and such perturbation in the spectrum is commonly utilized for sensing applications. We can calculate the shift of the Bragg wavelength due to a uniformly applied strain and temperature changes with the following expression:

$$\Delta\lambda_B = 2\left[\Lambda\frac{\partial n_{eff}}{\partial l} + n_{eff}\frac{\partial\Lambda}{\partial l}\right]\Delta l + 2\left[\Lambda\frac{\partial n_{eff}}{\partial T} + n_{eff}\frac{\partial\Lambda}{\partial T}\right]\Delta T \tag{1.2}$$

The first term in the above equation contains information about the applied deformation. The shift of the Bragg wavelength due to the strain term *l* is:

$$\Delta\lambda_B = 2\left[\Lambda\frac{\partial n_{eff}}{\partial l} + n_{eff}\frac{\partial\Lambda}{\partial l}\right]\Delta l \tag{1.3}$$

Where $\frac{\partial n_{eff}}{\partial l}$ is the variation of the effective refractive index induced by the strain and $\frac{\partial\Lambda}{\partial l}$ is the change of pitch with *l*, $\frac{\partial n_{eff}}{\partial T}$ is the variation of the effective refractive index induced by the temperature *T*.

LPG is also based on a periodic modulation of the refractive index of the fiber core along of the direction of propagation of the light as shown in Figure 1.6, but in this case, the core mode couples to co-propagating cladding modes and different attenuation bands are produced at the wavelengths where the resonance condition is satisfied:

$$\lambda_{\text{res}} = \Lambda * \Delta n \tag{1.4}$$

Where Δ n =n_{co}-n_c is the difference between the effective refractive indices of the core fundamental mode and the *i* th cladding mode. As can be clearly seen from this relation the resonance wavelength is determined by the effective refractive indices of the core and cladding modes, so that any geometrical, photo-induced, thermal-induced, or mechanically induced change (periodic) will modify the position of the resonance wavelength. This property makes fiber LPGs so useful for applications in fields as diverse as optical sensing, biological and chemical sensing, as wavelength dependent loss elements in telecommunication systems and laser and many more.

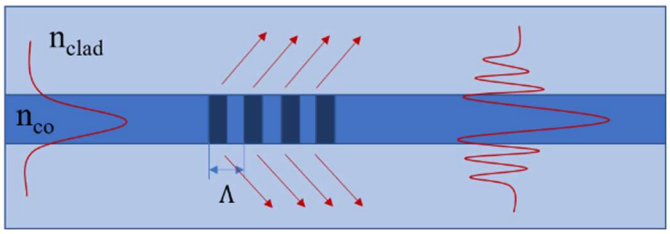

Figure 1.6 LPG transmission graph.

In 1978, *Hill et al.* [50] discovered the photosensitivity of germano-silicate optical fibers and since then, silica FBG has been found widespread and important applications, mostly for the stabilization of the pump laser diodes that are used in Erbium-doped Fiber Amplifiers

[51], for distributed arrays of strain, acoustic and temperature sensors [52], and to a lesser extent for wavelength multiplexing [53], for gain flattening in optical communication systems [54], for dispersion compensation [55] and increasingly as cavity for fiber lasers [56].

Similarly, the *Bell* laboratories discovered the PMMA photosensitivity around 1970s by means of 325 nm wavelength UV radiation [57], which is the preferred wavelength for changing the refractive index change of this material. The refractive index modification in PMMA material is due to several mechanisms, basically photo polymerization, photo degradation and cross-linking change between the polymer material chains, which also depend on the power and the wavelength of the irradiated light. *Kopietz et al.* [58] reported that PMMA material irradiated with a low pressure mercury lamp and observed a decrease of PMMA refractive index in a first stage of illumination, followed by an index increase until saturation. The process was explained as an increase of the presence of new monomers under UV radiation, followed by a second stage where a photo-polymerization of those monomers prevails until the saturation of the refractive index during 1980s. *Yu et al.* [59] reported refractive index modification by means of photo-isomerization, where polymers with different dopants, i.e. trans-4-stilbenemethanol and MMA–EMA–BzMA present different refractive index change under 325 nm wavelength UV radiation.

The 248 nm wavelength is a preferred irradiation wavelength for silica fiber [60], and can also be employed for PMMA fibers. *Wochnowski et al.* [61] reported on the formation of photoproducts in the exposed areas under low flounce and low repetition rates of UV laser system. They observed a refractive index increase during the beginning of the irradiation because of the volume contraction by *Van der Waal's* interactions due to the complete separation of the polymer side chain. At the end, the refractive index decreases due to the degradation of the polymer structure.

The first FBG in POF was reported in 1999 [35] with a step-index POF while *Dobb et al.* [62] reported the first FBG in mPOF in 2005. Although phase mask technology is the preferred choice for fabricating FBGs in POF, other inscription methods have also been reported, such as interferometry [63][64] or direct writing with a femtosecond laser [65][66]. Published papers on POF gratings applications such as strain [67], temperature [68] and humidity [69] sensing show the interest and potential of these devices. Recent achievements include Bragg gratings fabricated on microstructured polymer optical fiber (mPOF) with high temperature Topas, Zeonex and polycarbonate [19][20][21] and Bragg gratings inscribed in the low loss perfluorinated fiber (CYTOP) using an fs laser [66].

However, the photosensitivity of pure PMMA fiber is quite low [70], and several research groups focus on doped POF to enhance the photosensitivity. The first fabricated grating in doped polymer fiber [71] was reported by *Peng's* group with a step-index PMMA fiber which core was doped with an organic dye. Some years later, the same group reported another fiber with the core doped with ethyl and benzyl methacrylate with a low concentration of initiator and chain transfer to improve the photosensitivity [72], obtaining the inscription of FBGs during 85 min with -28 dB transmission at the central wavelength. *Tam´s* group doped the core of the fiber with a photoisomer which changes from the trans-structure to the cis-structure under UV radiation, providing a negative index change [59] and obtained -10 dB Bragg grating with 10 min irradiation. In the literature we also find other techniques to improve the FBG fabrication process in polymer fibers, such as *Saez et al.* [70], who employed uniform benzyl dimethyl ketal (BDK) doped mPOF, as a simpler alternative than using step index POF with extra dopants such as ethyl methacrylate in the core to compensate the reduction of the refractive index of the BDK dopant. *Hu et al.* [73] used the selected center hole doping technique to obtain uniform BDK distribution in its core without any drastic loss increase. The first POFBG inscribed successfully using 248 nm UV beam during 30 seconds was demonstrated due to low flounce and low repetition rate, this work opened up a new area for Bragg grating irradiation in POF [74]. *Pospori et al.* [75] fabricated FBGs with BDK doped POF under 248 nm wavelength and obtained one strong Bragg gratings by using a single short laser pulse, which is even suitable for tower drawing FBG irradiation. More recently, *Tam´s* group investigated a new dopant material, diphenyl disulphide, which leads to a positive refractive change with a low ultraviolet dose, obtaining FBGs after 7 ms of 325 nm UV irradiation of an step-index POF [76].

However, grating fabrication using 248 nm UV beam still needs further investigations

towards the technology maturity before commercial application, similar as grating devices in silica fiber. Furthermore, flexible grating structures in POF are attractive to exploit the advantages of POF compared with silica fiber, as one of the main aims of this PhD work.

1.2 Objectives of the thesis

The general objective of this thesis is the proposal and development of polymer fiber grating devices for applications in optical communications, microwave photonics and bio-sensing fields.

The general objective is achieved by fulfilling the following specific objectives:

- Fabrication of uniform fiber Bragg gratings using different polymer materials, either in step index or microstructured fibers.
- Optimization of the FBG and LPG fabrication process by reducing the optical power, pulse duration and inscription time among other critical parameters.
- Fabrication of polymer fiber gratings with different structures.
- Fabrication of chirped fiber Bragg gratings in polymer fibers.
- Characterization of stability, thermal, strain and humidity response of the fabricated gratings.
- Demonstration of potential applications such as strain measurements, thermal detection and variable dispersion devices.

1.3 Structures of the thesis

This thesis has been written as a compendium of publications, which follows the Universitat Politecnica de Valencia regulation (approved by the Consejo de Gobierno on 15/12/2011 and modified on 25/04/2013) about doctoral studies in its article 11 "Doctoral thesis", point 4.e. According to it, the structure of the thesis is the following:

Chapter 1, “Introduction”, provides a full description of the state of the art of polymer optical fibers and fiber gratings in this type of fibers which clearly motivates the realization of the presented work. According to it, the chapter presents the definition of the general and specific objectives of the Thesis and how it is structured to fulfill all of them.

Chapter 2, “Optimization of fabrication process”, describes the work and results obtained in five papers where a single Nd:YAG laser pulse is demonstrated to fabricate gratings on BDK doped fiber, fast fabrication of gratings in different materials is achieved using a 248 nm KrF laser, Bragg gratings have been written using low pulse energy and FBGs centered at 600 nm have been obtained in perfluorinated fibers.

Chapter 3, “Fabrication of different types of gratings“, presents the results on gratings fabrication included in four papers where phase shifted FBGs in POF, tunable chirped FBGs in POF using a uniform phase mask with only one short pulse and also using thermal annealing method and finally, long period gratings have been fabricated.

Chapter 4, “Novel applications of polymer fiber gratings”, includes three papers proposing novel applications such as strain sensing based on tunable chirped POF FBG, thermal profile detection as biosensors or variable dispersion devices for communications or microwave photonic systems.

Chapter 5, “General discussion of the results”, analyzes the presented results and discusses about the quality of the novel contributions and achievements, as well as the main limitations found all throughout the work.

Chapter 6, “Conclusions and future research line”, summarizes the main results obtained in this thesis and also the prospects of future research in this field

1.4 References

1. H. M. Schleinitz and P. G. Stephan, "Process for low attenuation methacrylate optical fiber," U.S. patent 842166 (1979).
2. K. C. Kao and G. A. Hockham, "Dielectric-fibre surface waveguides for optical frequencies," Proc. Inst. Electr. Eng. **113**(7), 1151–1158 (1966).
3. M.C.J.Large, L. Poladian, G.W.Barton, and M. A. van Eijkelenborg, Microstructured Polymer Optical Fibres (Springer, 2008).
4. W. Groh, "Overtone absorption in macromolecules for polymer optical fibers," Macromol. Chem. Phys. **189**(12), 2861–2874 (1988).
5. S.Minami, "The development and applications of pof review and forecast," in *Third International Conference on Plastic Optical Fibres* (The European Institute for Communications and Networks, 1994), pp. 27–31.
6. Y. Ohtsuka and Y. Hatanaka, "Preparation of light-focusing plastic fiber by heat-drawing process," Appl. Phys. Lett. **29**(11), 735–737 (1976).
7. Y. Koike, Y. Kimoto, and Y. Ohtsuka, "Studies on the Light-Focusing Plastic Rod. 12: The GRIN Fiber Lens of Methyl Methacrylate-Vinyl Phenylacetate Copolymer," Appl. Opt **21**(6), 1057–1062 (1982).
8. Y. Koike and M. Naritomi, "Graded-refractive-index optical plastic material and method for its production," U.S. patent 5783.636 (1998).
9. Y. Koike and T. Ishigure, "High-bandwidth plastic optical fiber for fiber to the display," J. Light. Technol. **24**(12), 4541–4553 (2006).
10. "Chromis Giga POF," https://chromisfiber.com/product-category/gigapof-fibers/.
11. M. G. Kuzyk, "Guest-host polymer fibers for nonlinear optics," Appl. Phys. Lett. **8**, (1991).
12. G. Zhou, C. F. J. Pun, H. Y. Tam, A. C. L. Wong, C. Lu, and P. K. A. Wai, "Single-mode perfluorinated polymer optical fibers with refractive index of 1.34 for biomedical applications," IEEE Photonics Technol. Lett. **22**(2), 106–108 (2010).
13. N. Ioannides, E. B. Chunga, A. Bachmatiuk, I. G. Gonzalez-Martinez, B. Trzebicka, D. B. Adebimpe, D. Kalymnios, and M. H. Rümmeli, "Approaches to mitigate polymer-core loss in plastic optical fibers: A review," Mater. Res. Express **1**(3), (2014).
14. T. A. Birks, J. C. Knight, and P. S. J. Russell, "Endlessly single-mode photonic crystal fiber," Opitcs Lett. **22**(13), 961–963 (1997).
15. M. C. J. Large, M. A. van Eijkelenborg, A. Argyros, J. Zagari, S. Manos, N. A. Issa, I. Bassett, and S. Fleming, "Microstructured polymer optical fibre," Opt. Express **9**(7), 319–327 (2001).
16. G. Emiliyanov, J. B. Jensen, O. Bang, P. E. Hoiby, L. H. Pedersen, E. M. Kjær, and L. Lindvold, "Localized biosensing with Topas microstructured polymer optical fiber," Opt. Lett. **32**(5), 1059–1059 (2007).
17. A. Argyros, J. Anthony, R. Leonhardt, and M. C. J. Large, "Terahertz transmission in Zeonex polymer waveguides," in *Proc. 8th Int. Photon. Electromagn. Crystal Structures Meeting* (2009), pp. 5–9.
18. M. A. van Eijkelenborg, A. Argyros, S. G. Leon-saval, M. A. Van Eijkelenborg, A. Argyros, and S. G. Leon-saval, "Polycarbonate hollow-core microstructured optical fiber," Opt Lett **33**(21), 2446–2448 (2008).
19. C. Markos, A. Stefani, K. Nielsen, H. K. Rasmussen, W. Yuan, and O. Bang, "High-Tg TOPAS microstructured polymer optical fiber for fiber Bragg grating strain sensing at 110 degrees.," Opt. Express **21**(4), 4758–4765 (2013).
20. G. Woyessa, A. Fasano, C. Markos, A. Stefani, H. K. Rasmussen, and O. Bang, "Zeonex microstructured polymer optical fiber: fabrication friendly fibers for high temperature and humidity insensitive Bragg grating sensing," Opt. Mater. Express **7**(1), 286–295 (2017).
21. A. Fasano, G. Woyessa, P. Stajanca, C. Markos, A. Stefani, K. Nielsen, H. K. Rasmussen, K. Krebber, and O. Bang, "Fabrication and characterization of polycarbonate microstructured polymer optical fibers for high-temperature-resistant fiber Bragg grating strain sensors," Opt. Mater. Express **6**(2), 649–659 (2016).
22. G. Woyessa, A. Fasano, A. Stefani, C. Markos, K. Nielsen, H. K. Rasmussen, and O. Bang, "Single mode step-index polymer optical fiber for humidity insensitive high temperature fiber Bragg grating sensors," Opt. Express **24**(2), 1253–1260 (2016).

23. X. Cheng, J. Bonefacino, B. O. Guan, and H. Y. Tam, "All-polymer fiber-optic pH sensor," Opt. Express **26**(11), 14610–14616 (2018).
24. U. H. P. Fischer, M. Haupt, and M. Joncic, "Optical Transmission Systems Using Polymeric Fibers," (2002).
25. G. J. Grimes, "POF applications in broadband networks," in *Proceedings 27th European Conference on Optical Communication* (2002), (1), pp. 16–17.
26. T. Ishigure, E. Nihei, S. Yamazaki, K. Kobayashi, and Y. Koike, "2.5Gbit/s 100m data transmission using graded-index polymer optical fibre and high- speed laser diode at 650nm wavelength," Electron. Lett. **31**(6), 467–469 (1995).
27. T. Ishigure, K. Makino, S. Tanaka, and Y. Koike, "High-bandwidth graded-index polymer optical fiber enabling power penalty-free gigabit data transmission," J. Light. Technol. **21**(11), 2923–2930 (2003).
28. Y. Koike and A. Inoue, "High-Speed Graded-Index Plastic Optical Fibers and Their Simple Interconnects for 4K/8K Video Transmission," J. Light. Technol. **34**(6), 1551–1555 (2016).
29. H. P. A. Van Den Boom, W. Li, P. K. Van Bennekom, I. Tafur Monroy, and G. D. Khoe, "High-capacity transmission over polymer optical fiber," IEEE J. Sel. Top. Quantum Electron. **7**(3), 461–470 (2001).
30. H. Yang, E. Tangdiongga, S. C. J. Lee, C. Okonkwo, H. P. A. Van Den Boom, and S. Randel, "4 . 7 Gbit / s Transmission over 50m Long 1mm Diameter Multi-core Plastic Optical Fiber," in *OFC* (2010), pp. 7–9.
31. P. J. Pinzón, I. Pérez, and C. Vázquez, "Visible WDM System for Real-Time Multi-Gb/s Bidirectional Transmission over 50-m SI-POF," IEEE Photonics Technol. Lett. **28**(15), 1696–1699 (2016).
32. I. N. Osahon, S. Rajbhandari, and W. O. Popoola, "Performance comparison of equalization techniques for SI-POF multi-gigabit communication with PAM- M and device non-linearities," J. Light. Technol. **36**(11), 2301–2308 (2018).
33. F. Forni, Y. Shi, N. C. Tran, H. P. A. Van Den Boom, E. Tangdiongga, and A. M. J. Koonen, "Multiformat wired and wireless signals over large-core plastic fibers for in-home network," J. Light. Technol. **36**(16), 3444–3452 (2018).
34. K. Peters, "Polymer optical fiber sensors - A review," Smart Mater. Struct. **20**(1), (2011).
35. Z. Xiong, G. D. Peng, B. Wu, and P. L. Chu, "Highly Tunable Bragg Gratings in Single-Mode Polymer Optical Fibers," IEEE Photonics Technol. Lett. **11**(3), 352–354 (1999).
36. G. Durana, H. Poisel, J. Zubia, I. Saez, and J. Gomez, "Monitoring the vertical deflection of a flap rudder using a novel fibre optical strain sensor," 18th Int. Conf. Plast. Opt. Fibers **9**(10), 3–7 (2009).
37. L. Bilro, J. G. Oliveira, J. L. Pinto, and R. N. Nogueira, "A reliable low-cost wireless and wearable gait monitoring system based on a plastic optical fibre sensor," Meas. Sci. Technol. **22**(4), (2011).
38. Y. M. Wong, P. J. Scully, R. J. Bartlett, K. S. C. Kuang, and W. J. Cantwell, "Plastic optical fibre sensors for environmental monitoring: Biofouling and strain applications," Strain **39**(3), 115–119 (2003).
39. A. G. Leal-Junior, A. Frizera, and M. J. Pontes, "Dynamic Compensation Technique for POF Curvature Sensors," J. Light. Technol. **36**(4), 1112–1117 (2018).
40. F. Sequeira, L. Bilro, A. Rudnitskaya, M. Pesavento, L. Zeni, and N. Cennamo, "Optimization of an Evanescent Field Sensor based on D-Shaped Plastic Optical Fiber for Chemical and Biochemical Sensing," Procedia Eng. **168**, 810–813 (2016).
41. A. G. Leal-Junior, A. Frizera, L. M. Avellar, and M. J. Pontes, "Design considerations, analysis, and application of a low-cost, fully portable, wearable polymer optical fiber curvature sensor," Appl. Opt. **57**(24), 6927 (2018).
42. M. Shan, R. Min, Z. Zhong, Y. Wang, and Y. Zhang, "Differential reflective fiber-optic angular displacement sensor," Opt. Laser Technol. **68**, 124–128 (2015).
43. M. Niklès, L. Thévenaz, and P. A. Robert, "Simple distributed fiber sensor based on Brillouin gain spectrum analysis," Opt. Lett. **21**(10), 758–760 (1996).
44. Y. Mizuno, M. Kishi, K. Hotate, T. Ishigure, and K. Nakamura, "Observation of stimulated Brillouin scattering in polymer optical fiber with pump–probe technique," Opt. Lett. **36**(12), 2378–2380 (2011).
45. A. Minardo, R. Bernini, and L. Zeni, "Distributed temperature sensing in polymer optical fiber by BOFDA," IEEE Photonics Technol. Lett. **26**(4), 387–390 (2014).
46. N. Hayashi, Y. Mizuno, and K. Nakamura, "Distributed brillouin sensing with centimeter-order spatial resolution in polymer optical fibers," J. Light. Technol. **32**(21), 3397–3401

(2014).
47. K. M. Feng, J. X. Cai, V. Grubsky, D. S. Starodubov, M. I. Hayee, S. Lee, X. Jiang, A. E. Willner, and J. Feinberg, "Dynamic Dispersion Compensation in a 10-Gb/s Optical System Using a Novel Voltage Tuned Nonlinearly Chirped Fiber Bragg Grating," IEEE Photonics Technol. Lett. **11**(3), 373–375 (1999).
48. J. H. Lee, Y. M. Chang, Y. Han, H. Chung, S. H. Kim, and S. B. Lee, "Raman amplifier-based long-distance remote, strain and temperature sensing system using an erbium-doped fiber and a fiber Bragg grating," Opt. Express **12**(15), 3515–3520 (2004).
49. A. Iocco, H. G. Limberger, R. P. Salathé, L. A. Everall, K. E. Chisholm, J. A. R. Williams, and I. Bennion, "Bragg grating fast tunable filter for wavelength division multiplexing," J. Light. Technol. **17**(7), 1217–1221 (1999).
50. K. O. Hill, Y. Fujii, D. C. Johnson, and B. S. Kawasaki, "Photosensitivity in optical fiber waveguides: Application to reflection filter fabrication," Appl. Phys. Lett. **32**, 647 (1978).
51. B. F. Ventrudo, G. A. Rogers, G. S. Lick, D. Hargreaves, and T. N. Demayo, "Wavelength and intensity stabilisation of 980nm diode lasers coupled to fibre bragg gratings," Electron. Lett. **30**(25), 2147–2149 (1994).
52. A. D. Kersey, M. A. Davis, H. J. Patrick, M. LeBlanc, M. K. P. Koo, C. G. Askins, M. A. Putnam, and E. J. Friebele, "Fiber Grating Sensors," J. Light. Technol. **15**(8), 1442–1463 (1997).
53. F. Bilodeau, D. C. Johnson, S. Thériault, B. Malo, J. Albert, and K. O. Hill, "An All-Fiber Dense-Wavelength-Division Multiplexer/Demultiplexer Using Photoimprinted Bragg Gratings," IEEE Photonics Technol. Lett. **7**(4), 388–390 (1995).
54. J.-C. Dung, S. Chi, and S. Wen, "Gain flattening of erbium-doped fibre amplifier using fibre Bragg gratings," Electron. Lett. **34**(6), 555–556 (2002).
55. N. M. Litchinitser, B. J. Eggleton, and D. B. Patterson, "Fiber Bragg gratings for dispersion compensation in transmission: Theoretical model and design criteria for nearly ideal pulse recompression," J. Light. Technol. **15**(8), 1303–1313 (1997).
56. L. Y. Shao, X. Dong, A. P. Zhang, H. Y. Tam, and S. He, "High-resolution strain and temperature sensor based on distributed Bragg reflector fiber laser," IEEE Photonics Technol. Lett. **19**(20), 1598–1600 (2007).
57. W. J. Tomlinson, I. P. Kaminow, E. A. Chandross, R. L. Fork, and W. T. Silfvast, "Photoinduced Refractive Index Increase in Poly(methylmethacrylate) and its Applications," Appl. Phys. Lett. **16**(12), 486–489 (1970).
58. E. K. M.Kopietz, M.D.Lechner, D.G.Steinmeier, J.Marotz, H.Franke, "Light-induced refractive index changes in polymethylmethacrylate (PMMA) blocks," Polym. Photochem. **5**(1), 109–119 (1984).
59. J. Yu, X. Tao, and H. Tam, "Trans-4-stilbenemethanol-doped photosensitive polymer fibers and gratings," Opt. Lett. **29**(2), 156–158 (2004).
60. K. P. Chen, P. R. Herman, and R. Tam, "Strong fiber Bragg grating fabrication by hybrid 157- and 248-nm laser exposure," IEEE Photonics Technol. Lett. **14**(2), 170–172 (2002).
61. C. Wochnowski, S. Metev, and G. Sepold, "UV-laser-assisted modification of the optical properties of polymethylmethacrylate," Appl. Surf. Sci. **154**, 706–711 (2000).
62. H. Dobb, D. J. Webb, K. Kalli, A. Argyros, M. C. J. Large, and M. A. van Eijkelenborg, "Continuous wave ultraviolet light-induced fiber Bragg gratings in few- and single-mode microstructured polymer optical fibers," Opt. Lett. **30**(24), 3296–3298 (2005).
63. H. Y. Liu, H. B. Liu, G. D. Peng, and P. L. Chu, "Observation of type I and type II gratings behavior in polymer optical fiber," Opt. Commun. **220**(4–6), 337–343 (2003).
64. H. B. Liu, H. Y. Liu, G. D. Peng, and P. L. Chu, "Novel Growth Behaviors of Fiber Bragg Gratings in Polymer Optical Fiber under UV Irradiation with Low Power," IEEE Photonics Technol. Lett. **16**(1), 159–161 (2004).
65. A. Stefani, M. Stecher, G. E. Town, and O. Bang, "Direct writing of fiber Bragg grating in microstructured polymer optical fiber," IEEE Photonics Technol. Lett. **24**(13), 1148–1150 (2012).
66. A. Lacraz, M. Polis, A. Theodosiou, C. Koutsides, and K. Kalli, "Femtosecond Laser Inscribed Bragg Gratings in Low Loss CYTOP Polymer Optical Fiber," IEEE Photonics Technol. Lett. **27**(7), 693–696 (2015).
67. X. Chen, C. Zhang, D. J. Webb, G. D. Peng, and K. Kalli, "Bragg grating in a polymer optical fibre for strain, bend and temperature sensing," Meas. Sci. Technol. **21**(9), (2010).
68. C. Zhang, W. Zhang, D. J. Webb, and G.-D. Peng, "Optical fibre temperature and humidity sensor," Electron. Lett. **46**(9), 643 (2010).

69. W. Zhang, D. J. Webb, and G. D. Peng, "Investigation into time response of polymer fiber bragg grating based humidity sensors," J. Light. Technol. **30**(8), 1090–1096 (2012).
70. D. Sáez-Rodríguez, K. Nielsen, H. K. Rasmussen, O. Bang, and D. J. Webb, "Highly photosensitive polymethyl methacrylate microstructured polymer optical fiber with doped core," Opt. Lett. **38**(19), 3769–3772 (2013).
71. G. D. Peng, Z. Xiong, and P. L. Chu, "Photosensitivity and gratings in dye-doped polymer optical fibers," Opt. Fiber Technol. **5**(2), 242–251 (1999).
72. Y. Luo, Q. Zhang, H. Liu, and G.-D. Peng, "Gratings fabrication in benzildimethylketal doped photosensitive polymer optical fibers using 355 nm nanosecond pulsed laser," Opt. Lett. **35**(5), 751–753 (2010).
73. X. Hu, G. Woyessa, D. Kinet, J. Janting, K. Nielsen, O. Bang, and C. Caucheteur, "BDK-doped core microstructured PMMA optical fiber for effective Bragg grating photo-inscription," Opt. Lett. **42**(11), 2209–2212 (2017).
74. R. Oliveira, L. Bilro, and R. Nogueira, "Bragg gratings in a few mode microstructured polymer optical fiber in less than 30 seconds," Opt. Express **23**(8), 10181–10187 (2015).
75. A. Pospori, C. A. F. Marques, O. Bang, D. J. Webb, and P. André, "Polymer optical fiber Bragg grating inscription with a single UV laser pulse," Opt. Express **25**(8), 9028–9038 (2017).
76. J. Bonefacino, H.-Y. Tam, T. S. Glen, X. Cheng, C.-F. J. Pun, J. Wang, P.-H. Lee, M.-L. V. Tse, and S. T. Boles, "Ultra-fast polymer optical fibre Bragg grating inscription for medical devices," Light Sci. Appl. **7**(3), 17161 (2018).

Chapter 2

Optimization of POF gratings fabrication process

2.1 Bragg gratings inscription in POF with a single pulse

[JP.1] L. Pereira, R. Min, X. Hu, B. Ortega, C. Marques, C. Caucheteur, P. Antunes J. Pinto, "Polymer optical fiber Bragg grating inscription with a single Nd:YAG laser pulse " Optics Express, 26(10), 18096-18104, 2018.

2.1.1 Introduction

The study and development of Fiber Bragg Gratings (FBGs) began in the 1970s with *Hill's* work on the non-linear properties of silica optical fibers (SOFs) doped with germanium [1]. In this study, an interference pattern was introduced into the core of an optical fiber, resulting in a periodic modulation of the refractive index of the core. These results led to a huge effort by the scientific community to improve the FBGs manufacturing. In 1989 [2], *Meltz et al.* demonstrated a strong variation in the core's refractive index when SOFs doped with germanium were irradiated by a periodic pattern originated by the intersection of two coherent ultraviolet (UV) beams. The fabrication of FBGs improved drastically in 1993 [3], with the introduction of the phase mask for side inscription, providing a method for mass fabrication due to the simplicity of the technique, easy alignment, stability, reproducibility and flexibility of the process for producing apodized and chirped gratings [4]. Recently, polymer optical fibers (POFs) have been used as an alternative to SOFs in data transmission over short distances and in sensing applications [5]. Although POFs have higher transmission losses, they also have several advantages over SOFs, including lower Young's modulus and higher elastic strain limits [6], enabling them to be used as strain [7], stress [8], bending [9], refractive index [10] and pressure sensors [11]. Additionally, POFs have a negative thermo-optic coefficient and high sensitivity to temperature [12]; and the standard polymer poly(methyl methacrylate) (PMMA) has affinity to water [13], allowing to monitor humidity based parameters. Furthermore, polymers display excellent compatibility with organic materials, giving them great potential for biomedical applications [14][15]. The first FBGs were inscribed in POF in 1999 by *Peng et al.* [16], using two illumination wavelengths, 248 and 325 nm, to create different gratings. Since then, the most common UV light used to manufacture Polymer Optical Fiber Bragg Grating (POFBG) remains the continuous wave (CW) low power He-Cd laser operating at 325 nm, which is an affordable and accessible laser for grating inscription. It is typically the preferred option to avoid any ablation issues due to high energy [17], and to obtain deeper penetration of the radiation in the material [18]. Lately, other lasers with different wavelengths in the UV region have also been used to fabricate POFBGs, in particular the KrF laser operating at 248 nm [19][20][21] which allows to decrease the POFBG inscription time due to the higher absorption of the PMMA for shorter wavelengths.

However, in ref [22] the authors reported a periodic ablation on the fiber surface when the 248 nm wavelength was used, due to the higher absorption of PMMA in shorter UV wavelengths [21]. Furthermore, using low energy density as well as low repetition rate from a 248 nm laser, a refractive index modification in PMMA bulk material was confirmed without introducing the ablation effect [19]. In this way, the key factors to avoid the ablation effect are

the use of low energy density, low repetition rate and also low number of pulses as recently reported in different reports using different polymers [19][20][21][23], in contrast with the reported in [16][17]. After the first laser pulse with an energy lower than the ablation threshold, the polymer structure changes and there is a refractive index modification. Thus the refractive index change is due to an incubation phenomenon well below the material ablation threshold. This index change could be caused by the complete side chain removal of the material molecule leading to a densification [24]. As most polymers are intrinsically photosensitive, FBG inscription in different polymers is possible without doping [23]. Despite the photosensitivity mechanisms not being fully understood, the chemical structure of the polymer can be altered either by photo-polymerization, or by photo-crosslinking, or by photodegradation [24][25]. All these mechanisms can possibly co-exist under UV irradiation, and which one prevails over the other depends on the irradiation conditions: laser wavelength, intensity and total exposure time [24].

The fabrication of Bragg gratings in undoped POFs can be a time consuming process, and as the exposure time increases, the higher are the risks of damaging the POF and compromising the stability of the grating [23][25]. Usually, to obtain a strongly reflective signal using the 30 mW CW HeCd laser, the minimum exposure time is about 20 minutes for step-index (SI) PMMA-POF [26], and that time can easily increase for microstructured POFs (mPOFs) [25]. Increasing the UV beam intensity, the exposure time can drop to a few minutes [27], showing a dependency between grating inscription time and laser power. For the 248 nm excimer KrF laser, the inscription time for undoped PMMA-POF is less than 30 seconds [19][23], due to the higher absorption of the material at this wavelength. The inscription time can be reduced to less than 1 second by doping the core of the POF. The fastest time for POFBG fabrication is 15 ns [21][28][29], the duration of only one UV laser pulse, using a single mode (SM) PMMA-mPOF doped with benzildimethylketal (BDK) to enhance the photosensitivity of the core. When the fiber is irradiated by the appropriate wavelengths (about 250 nm and 344 nm) [30], the photo-polymerization process starts, with the BDK acting as a photo-initiator. Exploring the photosensitivity in those UV bands, in particularly around 250 nm where the spectral absorption is higher [30], is possible to use alternative UV sources for fast fabrication of POFBGs. Using this principle, the implementation of smaller dimension and cheaper lasers in the fabrication of POFBGs is increasingly important to develop simple and viable inscription systems and potentially reduce POFBGs fabrication costs. We report the inscription of POFBGs using only one pulse of the fourth harmonic of a Nd:YAG laser system (operating at 266 nm). This wavelength has been implemented before to fabricate Bragg gratings in SOF, through pulsed [31][32] and CW lasers [33]. Regarding the inscription of POFBGs, there are no data available until now, and we believe this is the first demonstration using this wavelength. The Bragg grating was inscribed with one pulse in a BDK-doped mPOF, with a pulse duration about 8 ns, which is to our knowledge the fastest photo-inscription time for POFBGs to date as well as the lowest pulse energy employed for this purpose.

2.1.2 Experimental setup

The optical fiber used to inscribe the POFBGs was a 3-ring hexagonal step index PMMA mPOF with a BDK-doped core [34], manufactured at *DTU Fotonik*. The doping process was performed at 51.5 °C, improving the diffusion speed of the BDK and decreasing the time of the process [34]. Because of the smooth nature of the core, we believe the BDK is uniformly distributed in the core, without generating large scatterings. The average hole diameter and pitch in the fiber are 1.5 μm and 3.79 μm, respectively. Thus, the ratio of the hole diameter to the pitch was calculated to be 0.4, confirming that the mPOF is endlessly SM [35]. The diameters of the core and the cladding are 6 μm and 150 μm, respectively. The mPOF pieces of length about 20 cm were cleaved with a hot blade [36]and glued into FC/PC connectors in order to simplify the POFBG interrogation. Before the inscription, the mPOFs were preannealed during 24 hours at 70 °C to reduce the internal stress in the fiber originating from the fabrication process. This heat treatment reduces the POFBG sensor hysteresis and the inscription time and increases the grating stability [37][38], which can be further improved by also annealing the preform before drawing [39]. Figure 2.1.1 presents the inscription setup,

based on the phase mask technique. A pulsed Q switched Nd:YAG laser system (LOTIS TII LS-2137U Laser) lasing at the fourth harmonic (266nm) was employed to produce the POFBGs, using pump lamp repetition rate of 1 Hz and the Q-Switch mode as single shot. The laser beam profile is circular, the diameter is about 8 mm and the divergence is $\leqslant$1.0 mrad. The laser beam is focused onto the fiber core using a plano-convex cylindrical lens with effective focal length of 320 mm. The effective spot size of the beam on the fiber surface is 8 mm in width and about 30 μm in height. Experimental setup was aligned and tested before the inscription in order to focus the UV beam onto the core of the fiber and obtain an effective POFBG inscription. A single 8 ns pulse with a pump energy of 23.6 J and measured pulse energy of 72 μJ was used to inscribe the grating in a pre-annealed PMMA-mPOF.

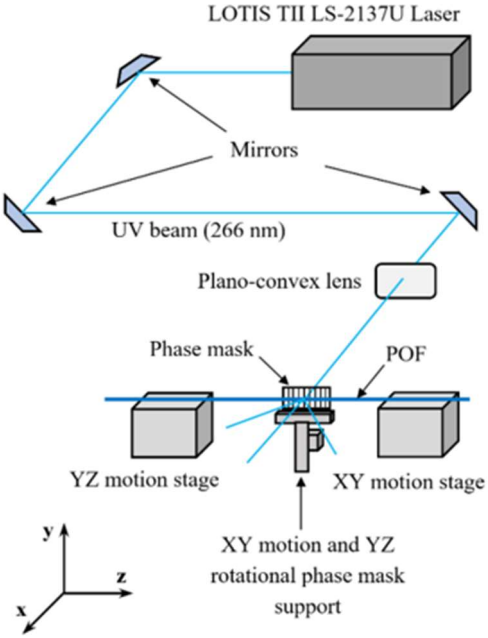

Figure 2.1.1 Sketch of the experimental setup based on phase mask technique.

It shall be noted that this pulse energy is the lowest value reported for the Bragg gratings inscription and it is several orders lower than the pulse energy used in the recent published reports using 248 nm laser system [21][28][29]. The phase mask employed is 10 mm in length with a period of Λ_{PM}= 567.8 nm, designed to operate at 248 nm. It can produce gratings in PMMA-POFs with the Bragg wavelengths around 844 nm. To monitor the grating spectrum in transmission and in reflection, a super luminescent diode (Superlum SLD-371-HPI) and an optical spectrum analyzer (Yokogawa AQ637B) were used. An 850 nm 50:50 ratio SM-silica optical coupler was used for monitoring the reflection spectrum.

2.1.3 Results and discussion

The transmission and reflection spectra of the inscribed POFBG (with 8 mm in length) with a single 266 nm pulse is shown in Figure 2.1.2. The Bragg wavelength is located at 840.460 nm, and shifted from 844 nm because the fiber was placed with some tension on the inscription setup [40]. Just after the illumination with a single laser pulse, the grating growth was almost instantaneous, reaching the saturation level in few seconds after the exposure. We believe the fast grating growth is due to the high concentration and uniform distribution of the dopant BDK in the core, since the saturation level of other POFBGs inscriptions using a single laser pulse [21] took several minutes. The reflective signal (green) has about 30 dB of reflective power and a Full Width at Half Maximum (FWHM) of 237 pm. The transmission rejection (red) is about 8 dB and the FWHM is 84 pm. Therefore, the grating reflectivity is approximately 84% and the maximum refractive index change in the core material is $\Delta n = 0.5*10^{-4}$. By comparing these results to POFBGs in PMMA-mPOF doped

with BDK inscribed with a single pulse from the KrF 248 nm laser [21][28], the reflectivity of the grating was lower, however, the pulse energy employed (72μJ) was also inferior (approximately by a factor of 87). When comparing to the results available regarding the production of POFBGs in the same mPOF [34], using a 400 nm femtosecond pulsed laser system, we achieved higher reflectivity in a much reduced inscription time

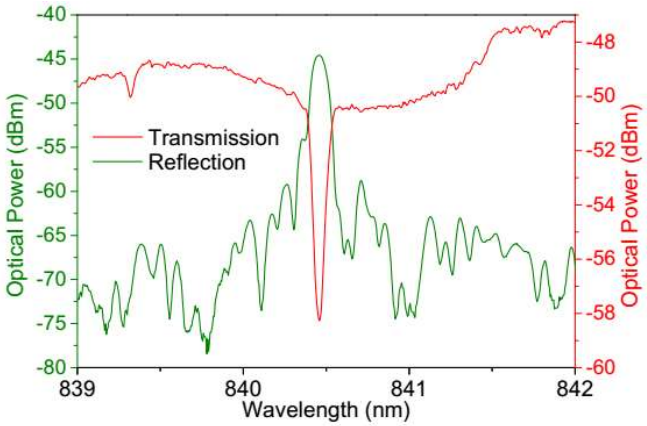

Figure 2.1.2 Reflection/transmission spectra of the inscribed POFBG using a single pulse of 266 nm laser.

It is known that the necessity of keeping the laser and inscription setup stable for several minutes is critical to achieve stable gratings. Also, the reduction of the gratings inscription time can also improve the FBG stability [26]. In addition, the pre-annealing treatment made on the fibers can influence the grating stability. For this reason, the POFBGs transmission spectra were monitored for 40 days at room temperature (controlled environments conditions) to verify any instability on the grating strength, bandwidth and central wavelength. Figure 2.1.3 presents the results obtained for each POFBG in terms of grating strength, bandwidth and central wavelength, which were monitored over 40 days by measuring them every 2 days. Figures 2.1.3(a) and 2.1.3(b) show the gratings transmission spectra and bandwidth, respectively, whereas Figure 2.1.3(c) presents the central wavelength of the POFBG. The results show a variation lower than 0.6 dB in the strength of the grating after 40 days. In addition, the bandwidth of the POFBG remains almost constant showing no significant change. For most sensing applications using FBGs, the change in the parameter to be monitored is related to the central wavelength variation, such stable wavelength (see Figure 2.1.3(c)) enables the use of the presented setup for fast inscription of POFBGs in the monitoring of different parameters, in many different applications. It shall be noted that we inscribed more similar gratings and a very similar behavior was achieved.

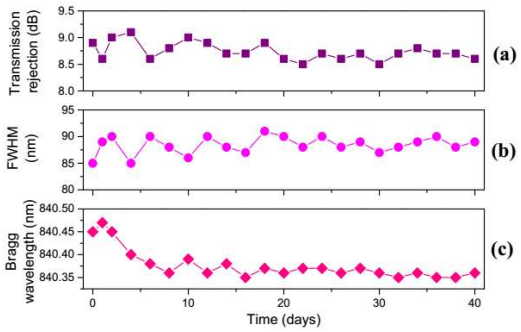

Figure 2.1.3 Stability of BDK-doped POFBG after 40 days. (a) Gratings strength, (b) bandwidth and (c) central wavelength.

The temperature and strain response of the POFBG was studied to analyze the grating stability and sensing properties. Figure 2.1.4(a) shows the transmission spectra of the POFBG under different temperatures. The temperature was increased from 22 °C up to 52 °C, by steps of 5 °C. In each step, the temperature was kept constant over 20 minutes to ensure

thermal stabilization and then the measurement was collected. Figure 2.1.4(b) shows the thermal tuning of the Bragg wavelength, and the obtained temperature sensitivity, after the linear fit, was −54.50 ± 1.45 pm/°C. From 22 °C up to 47 °C, the transmission rejection increased almost linearly with temperature, with a total variation of 2.13 dB.

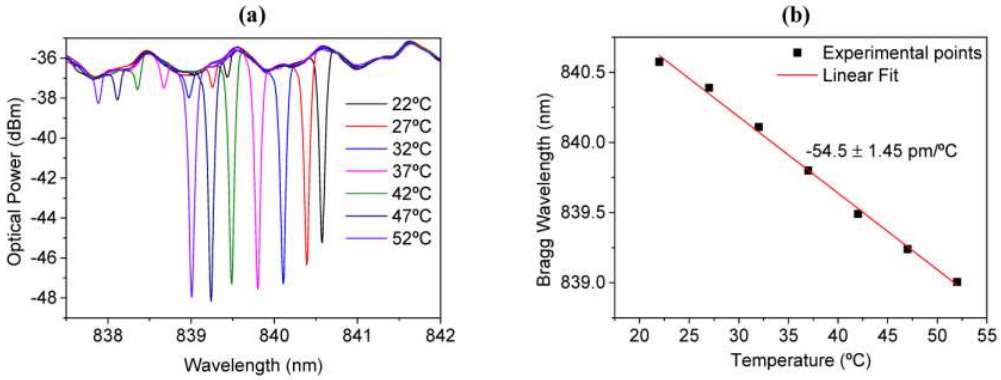

Figure 2.1.4 (a) Transmission spectra of the POFBG at different temperatures; (b) Bragg wavelength tuning with increasing temperature.

The strain characterization was performed by fixing the fiber between a fixed and a manual translating stage, with 10 µm resolution. The transmission spectra of the POFBG, when different percentages of strain are applied, are shown in Figure 2.1.5(a). The fiber was stretched up to 1.26 %, with 0.14 % steps (5 min. to ensure stabilization), resulting in a total Bragg wavelength tuning of 8.9 nm. The displacement of the Bragg wavelength with increasing strain is presented in Figure 2.1.5(b), and the obtained strain sensitivity was 0.710 ± 0.004 pm/με. Figure 2.1.5(c) shows the scattering of the measurement points around the fit line, from which the calculated standard deviation was found to be 48 pm. Improving precision in setting the fiber elongations can further decrease that result and the sensitivity error, which increases the measurement resolution. The transmission rejection during strain measurements had a nonlinear behavior and variated between −43.2 dB and −44.7 dB.

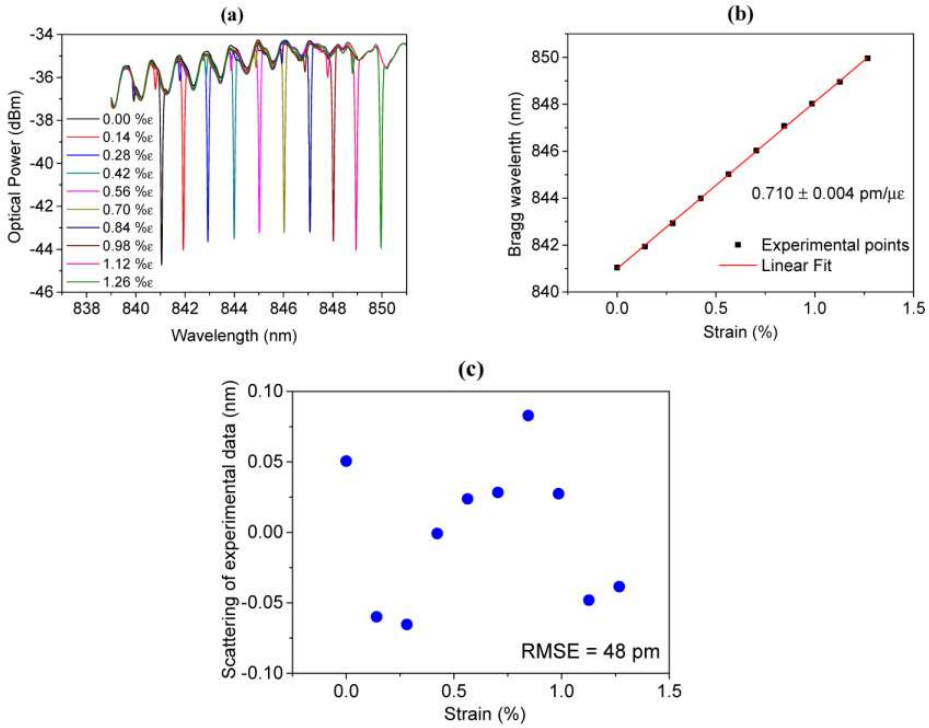

Figure 2.1.5 (a) Transmission spectra of the POFBG at different strains;(b) Bragg wavelength tuning with increasing strain; (c) scattering of experimental points around the fit line with a Root Mean Square Error (RMSE) of 48 pm.

Cyclic testing was also performed to investigate any thermal and strain hysteresis during increasing and decreasing steps. Three full cycles were performed to compare the sensitivity range for increasing and decreasing response under different levels of strain and temperature. Table 2.1.1 summarizes the sensitivities obtained for each cycle and the associated hysteresis. All cycles show good approximations for increasing-decreasing sensitivities and a low level of hysteresis, i.e., the maximum difference in sensitivity between increasing and decreasing experiments.

Table 2.1.1 Sensitivity analysis for each cycle and hysteresis

	Strain Sensitivity		Strain Sensitivity	
	Increasing	Decreasing	Increasing	Decreasing
Cycle 1	0.710	0.722	-54.5	-54.8
Cycle 2	0.725	0.719	-54.3	-53.9
Cycle 3	0.718	0.724	-54.7	-54.3
Maximum hysteresis	0.012		0.6	

2.1.4 Conclusion

In conclusion, we demonstrate for the first time a POFBG inscription in a BDK-doped PMMA-mPOF using a single low energy pulse from a Q-switched Nd:YAG laser system, operating at 266 nm. The grating exhibits more than 84 % reflectivity, and a refractive index change of 0.5×10^{-4} in the core of the fiber. The POFBG stability after the inscription was analyzed by monitoring the grating strength, FWHM and central wavelength over 40 days, showing no significant changes in any of those parameters. Also, the strain and temperature sensitivities was studied and found to be 0.710 ± 0.004 pm/με and −54.50 ± 1.45 pm/°C, respectively. The comparison of the POFBGs inscribed with the laser system presented in this work and with the KrF 248 nm laser system show a significant reduction in the pulse energy to obtain stable gratings using a single pulse. We believe the high concentration and the uniform distribution of the dopant contributed to the fast grating growth after the exposure. Nevertheless, the fiber reported in [41] and used in different works with the KrF 248 nm laser system [21][28][29], was tested with this laser (@266 nm) and we achieved Bragg gratings with identical spectral quality employing just one pulse (72 μJ the lowest pulse energy to inscribe Bragg gratings in PMMA fiber). These results show the potential to reduce POFBG production costs, by employing cheaper laser systems (the laser system employed in this work is about 5 times cheaper when compared to the KrF 248 nm excimer laser system and the femtosecond laser system) and reducing the inscription time to a pulse width (in this case to 8 ns). In addition, the maintenance of the current laser system is much easier and cheaper. For example, it does not need a periodic supply of high-purity excimer gases as the KrF 248 nm laser system does. Furthermore, this report can bring new developments in different research groups around the world using alternative UV sources for fast fabrication of FBGs in different polymer materials.

2.2 Bragg gratings inscription in POFs made of different materials

[JP.2] C. Marques, R. Min, A. Leal Junior, P. Antunes, A. Fasano, G. Woyessa, K. Nielsen, H. K. Rasmussen, B. Ortega, O. Bang, "Fast and stable gratings inscription in POFs made of different materials with pulsed 248 nm KrF laser" Optics Express, 26(2), 2013-2022, 2018.

2.2.1 Introduction

Optical fiber sensors are compact, lightweight, allow multiplexing systems, present electromagnetic immunity and electrical isolation [13]. Although optical fiber sensors are commonly made of silica fibers, advances in polymer processing [10], characterization [42] and fiber Bragg grating (FBG) inscription [21] enable the application of polymer optical fibers (POFs) in sensing applications. POFs present additional advantages when compared with their silica counterparts, which include flexibility in bending, higher fracture toughness, and lower Young's Modulus that provides higher sensitivity in strain sensing applications [43]. In addition, the biocompatibility and non-brittle nature of POFs means that they are clinically acceptable and can be employed in in-vivo applications [44]. Such advantages of POF sensors enable their application to measure parameters like temperature [45], strain [46] humidity [38], curvature [47], acceleration [48], and liquid level [11]. Furthermore, POF sensors are employed in biomedical applications such as antibody [14][49] and glucose sensors [15].

Of all POF materials, polymethyl methacrylate (PMMA) is yet the most employed material in POF production [43]. However, PMMA has a low glass transition temperature (*Tg*) compared to some of the other polymer materials for fiber fabrication, such as polycarbonate (PC), which can limit its application at higher temperatures [46]. Furthermore, the higher moisture absorption capability of PMMA can harm its application in temperature or strain sensing where a humidity cross-sensitivity is undesirable [50]. In order to mitigate the issue of humidity cross-sensitivity, POFs made of cyclic olefin copolymer such as Topas grade 8007 [50][51] and 5013 [52][53] and cyclic olefin homopolymer such as Zeonex 480R [54] can be employed. Gratings inscribed in fiber made of these materials demonstrated a humidity sensitivity at least 30 times lower than that of PMMA POFBGs. However, the glass transition temperature can vary significantly among different grades of Topas. For instance, Topas 8007 presents *Tg* of only 78 °C, which is even lower than the PMMA glass transition temperature [51] and which implies that fiber cleaving parameters are quite different for POFs made of PMMA and Topas [36]. The low glass transition temperature of Topas 8007 fibers severely limits the range of temperature sensing. In order to combat this, POFs made of another grade of Topas with a Tg of 134 °C was demonstrated [52][53]. Another polymer material employed for high temperature and strain sensing is Zeonex 480R, which has a *Tg* of 138 °C. Zeonex 480R material presents further advantages compared to Topas 5013 such as superior drawability that allow a more robust fabrication of microstructures in the fiber [54]. Both Topas and Zeonex have low loss at THz frequencies and have been applied extensively in this field also [55][56][57]. In addition to the aforementioned POF materials, polycarbonate (PC) polymer can also be used for fiber fabrication [58]. PC has a Tg of 145 °C, which is higher that of Topas 5013 and Zeonex 480R [46]. Furthermore, PC POFs can withstand higher stresses when compared with PMMA and Topas POFs [46]. The inscription of polymer optical fiber Bragg gratings (POFBGs) has been made with different setups throughout the years. An appropriate wavelength regime is around 650 nm, where PMMA has low material loss, but the more common wavelength for POFBGs is around 850 nm, which we will also focus on here [59][60], since the polymer presents high losses at the 1550 nm region [60]. Conventionally, the inscription of POFBGs is made with the phase mask technique using continuous wave (CW) 325 nm HeCd UV lasers [58]. With this laser, the writing time in POFs was ranging from few to hundreds of minutes depending on the polymer material the fibers were made from, the inscription power, the structure of the fibers, and so on [36][46][53][55].

These inscription times can be significantly reduced by doping the fiber, which can be made with trans-4-stilbenemethanol (TS) that can also increase the grating reflectivity [61][62]. Benzyl dimethyl ketal (BDK) PMMA POFs also demonstrated inscription times as short as 4 minutes with a He-Cd CW laser [41] and to 40 seconds with a femtosecond laser [34] or even to 1 pulse using a KrF pulsed laser [21].

However, such doped POFs [63] are more expensive and difficult to fabricate. In addition, they are unsuitable for in-vivo applications and the dopants employed generally lead to higher transmission losses in the final sensor [39]. Since most polymers are intrinsically photosensitive, the doping is not necessary for gratings inscription [27] and the only issue of undoped POFs is the longer inscription time. Such long inscription times lead to some challenges related to the necessity of higher stability of the setup during inscription [50]. Furthermore, shorter inscription times are important for the grating stability after inscription [27]. Nevertheless, the time taken for a POFBG inscription can be reduced by several orders of magnitude with the application of a 248 nm laser with low fluence and repetition rate through the phase mask technique [19]. It was also demonstrated that the inscription time can be lowered by performing a thermal treatment on the fiber preforms [39]. To establish general POFBG technology it is extremely important to have a general FBG writing set-up that is suitable for all different polymer materials with different sensing properties. Direct femtosecond writing is one such technology [15][64], but it is very expensive. In order to use UV writing to obtain low inscription times for undoped POFs made of different materials, this paper presents FBG inscription in several different POFs using both a pulsed KrF @ 248 nm laser and a CW HeCd @ 325 nm laser with all fiber pieces properly pre-annealed. The comparison between the POFBGs obtained with both setups is made with respect to the inscription time, bandwidth and strength. In addition, the reflection and transmission spectra of the gratings obtained with the pulsed laser system are presented. Also, the POFBG stability is assessed by analyzing the grating variation over several days. This work investigated the inscription of gratings in POFs made of different materials using pulsed UV KrF @248 nm laser. The results obtained are compared with those gratings inscribed in the same fibers but with a continuous UV HeCd @325 nm laser system. The comparison between the POFBGs obtained with both setups is made with respect to the inscription time, bandwidth and strength. In addition, the reflection and transmission spectra of the gratings obtained with the pulsed laser system are presented. Also, the POFBG stability is assessed by analyzing the grating variation over several days.

2.2.2 Experimental results

The POFs used for the grating fabrications were PMMA, Topas 8007, Topas 5013, Zeonex 480R and Polycarbonate microstructured polymer optical fibers (mPOFs), and Topas-Zeonex step index POF [53]. All the POFs employed were fabricated at *Technical University of Denmark (DTU)* as presented in [27][46][52][53][54]. Table 2.2.1 presents the dimensions of each fiber, such as the cladding structure, hole diameter and pitch for mPOFs and the core and cladding diameters for step-index POFs. Furthermore, the *Tg* of each fiber is also presented.

Table 2.2.1 Dimension and Tg of each POFs employed for the grating fabrication

POFs	Type	Cladding Structure	Hole diameter/pitch ()	Core/Cladding Diameter ()	*Tg*(C)
PMMA [27]	Microstructure	3 rings hexaganal	1/3.75	8/125	110
Topas 8007 [50]	Microstructure	2 rings hexaganal	2/6	~9/240	78
Topas 5013 [52]	Microstructure	3 rings hexaganal	2.2/6	~10/130	134
Topas 5013 core-Zeonex 480R cladding	Step-index	-	V=2.38 at 850 nm	4.8/150	134

step index POF [65]					
Zeonex 480R [54]	Microstructure	3 rings hexaganal	2.2/5.5	8.8/150	138
Polycarbonate [46]	Microstructure	3 rings hexaganal	1.75/4.375	7/150	145

Annealing is a heat treatment during which the fiber on a temperature close to the glass transition temperature for some hours [37]. Such treatment provides a reduction of the internal stress in the fiber created during fabrication process. For this reason, it reduces the POFBGs sensors hysteresis, and can also decrease the inscription time and increase the grating stability [39]. The annealing can be made before the grating inscription (pre-annealing) or after the inscription (post-annealing). If it is made after the grating inscription, the annealing can lead to a blue-shift of the Bragg wavelength [38] . All fibers except of PC were pre-annealed, PC has a high refractive index of about 1.58 and the Bragg wavelength was therefore outside the analyzer wavelength range (830-870 nm). Post-annealing was therefore made on this fiber in order to blue-shift the Bragg wavelength and to be seen on the analyzer [38]. Although the post-annealing at high humidity conditions and an optimization of the annealing time can provide larger blue-shifts, the goal here is a blue-shift sufficient only to obtain a Bragg wavelength within the analyzer range, which was achieved with the annealing time employed. Table 2.2.2 presents the annealing parameters employed for each POF used for the gratings inscription. Since it cannot be higher than the material *Tg*, the annealing temperature needs to be different for each POF material. For this reason, the annealing temperature of the Topas fiber with low *Tg* is only 60 °C and the one employed for the PMMA mPOFs is 80 °C, whereas, the annealing temperatures of the materials with higher Tg are higher than 100 °C.

Table 2.2.2 The annealing parameters applied for the POFs used for grating inscription

POFs	Annealing Type	Temperature ()	Annealing time (h)
PMMA mPOFs	Pre-annealing	80	24
Topas 8007 mPOFs	Pre-annealing	60	24
Topas 5013 mPOFs	Pre-annealing	115	24
Topas 5013 core-Zeonex480R cladding step index POF	Pre-annealing	115	24
Zeonex 480R mPOF	Pre-annealing	120	24
Polycarbonate mPOFs	Pre-annealing	130	30

Figure 2.2.1 presents the inscription setup, which is based on a pulsed 248 nm KrF Bragg Star Industrial-LN excimer laser, emitting 15 ns pulses at a repetition rate of 1 Hz. The setup presents mirrors, focal lens and a slit with 4.5 mm width to position the UV beam on the phase mask employed. The laser beam profile is a rectangular Tophat function with dimensions 6.0 × 1.5 mm^2 and divergence 2 × 1 $mrad^2$. The laser beam is focused onto the fiber core using a plano-convex cylindrical lens (Newport CSX200AR.10) with effective focal length of 200 mm. The effective spot size of the beam on the fiber surface is 20.0 μm in width and 32.4 μm in height. The setup presented in Figure 2.2.1 employs the phase mask technique, where a phase mask for 248 nm operation with a 10 mm length is used and its period is 567.8 nm. The FBG is inscribed in the fiber that is placed close to the phase mask with two 3D translational stages to guarantee the correct positioning of the fiber and avoid undesired bending of the POF.

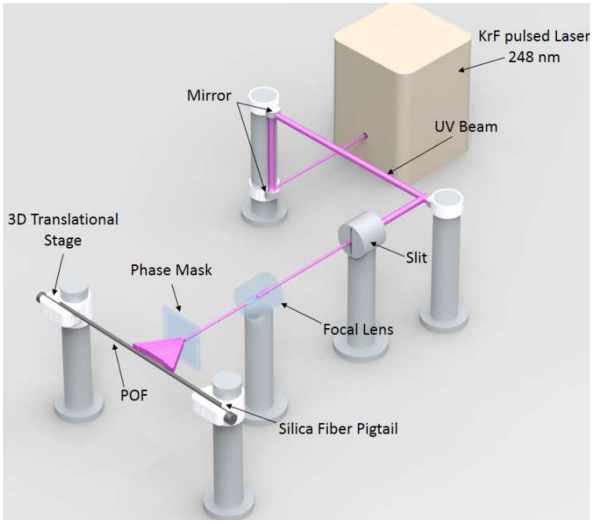

Figure 2.2.1 Setup employed for the POF FBGs inscription.

The POFs were cleaved with a hot blade on a plate using the suitable temperature reported for each fiber [27][36][37][46][52][53], which were butt-coupled with a silica pigtail. In order to carry out the inscription experiments, the POFs sections were UV-glued (LOCTITE AA 3936) to two 8° angled silica fiber pigtails on both sides of the POFs. The index matching UV-glue used between fibers could avoid Fabry–Pérot cavity effects and the angled silica fiber could reduce the Fresnel reflections generated in the interface between silica fiber and UV-glue because of large refractive index difference between cured UV-glue (refractive index ~1.49) and silica fiber. Provided by the manufacturer, the tensile strength of the UV glue is 2780 psi after curing. Since the splice is the weakest part in POFBG applications, we have further increased the strength of the splicing part. An epoxy resin was dip-coated on the UV-glue splice, in order to increase its resistance. The FBGs were inscribed at the same distance from the two glue points to compare the reflected FBGs strength. All gratings were inscribed with a total length of 4.5 mm. To interrogate the reflection and transmission spectra of the gratings we used a super luminescent diode and an optical spectrum analyzer OSA). A 50/50 optical coupler was used for the reflection spectrum.

2.2.3 Results and discussion

The gratings inscribed in the aforementioned fibers with the setup presented in Figure 2.2.1 are compared with those gratings inscribed with the CW 325 nm HeCd laser for the same fibers. The grating inscription results obtained in the literature with the 325 nm laser are presented in Table 2.2.3 with respect to the inscription time, full width at half maximum (FWHM) and grating reflectivity.

Table 2.2.3 POFBGs inscription with the CW UV HeCd laser at 325 nm

POFs	Inscription time (min)	FWHM (nm)	Reflectivity	Grating Length (mm)
PMMA mPOF [27]	7	0.40	26	3
Topas 8007 mPOF [50]	58	0.24	11	10
Topas 5013 [52]		0.40	20	12
Topas-Zeonex step index POF [65]	4	0.29	30	2
Zeonex 480R mPOF [54]	<5	0.52	30	2
Polycarbonate mPOF [46]	6	0.46	25	2

For the Topas 5013 mPOF the inscription time was not reported, whereas, the inscription

time reported in [52] for the Topas 8007 mPOF ranges from 58 to 338 minutes and the result with the shorter inscription time (58 minutes) is presented in Table 2.2.3. The results obtained with the 248 nm laser are presented in Table 2.2.4. Besides the inscription time, FWHM and grating reflectivity, the optimal energy per pulse in mJ is also given. Several FBGs were inscribed in each POF. If the energy per pulse is too high for the POF material, an overheating will occur, which causes an ablative process on the fiber [19]. Since the grating inscriptions were made in different POFs, a detailed study was performed to achieve the optimal energy per pulse to avoid overheating by the cumulative heating on each fiber material. In terms of minimizing fabrication times, this laser type was recently employed to fabricate FBGs in BDK doped fiber with a single UV laser pulse with a pulse energy of 6.3 mJ, providing an energy density per inscription of 974 mJ/cm^2 [21]. The pulse duration is 15 ns and a repetition rate of 1 Hz was applied. Since the laser pulse duration is very short when compared with the repetition rate, it is considered that each pulse has a total time of 1 second.

Table 2.2.4 POFBGs inscription with the pulsed UV KrF laser at 248 nm

POFs	Inscription time (seconds)	FWHM (nm)	Reflection (dB)	Optimal energy (mJ)
PMMA mPOF	25	0.4	32	6.0
Topas 8007 mPOF	25	0.6	31	5.5
Topas 5013 mPOF	20	0.6	23	6.0
Topas 5013 step-index POF	11	0.8	28	5.0
Zeonex 480R mPOF	15	0.7	28	3.5
Polycarbonate	14	0.6	23	3.0

The results presented in Table 2.2.4 show a reduction of the inscription time of at least 16 times compared with the inscription times listed in Table 2.2.3. The highest reduction of the inscription time was obtained for the mPOF made of Topas 8007, for which it was 130 times shorter. Furthermore, the FWHM was equal to or higher than the FWHM obtained with the CW laser system. Regarding the grating strength, the reflectivity of the gratings inscribed were close to or higher than the ones obtained with the CW laser. The improvement of the inscription time and grating strength is manly related to the pulsed laser @248 nm employed. However, such improvement can also be related to the pre-annealing made on the samples, since the results presented in [19] shows a writing time of 30 seconds with the same pulsed laser system at 248 nm presented in this work. This result was obtained for the 6-rings microstructured PMMA mPOF with a large core diameter of 18 μm, where it was not reported an annealing on the fiber prior to the grating inscription. In addition, the grating reflectivity was 20 dB and its 3-dB bandwidth was 0.16 nm. However, it was inscribed in the 1550 nm spectral region. The reflection spectrum of each POFBG is presented in Figure 2.2.2, where Fig. 2.2.2(a) presents the reflection for the PMMA POFBG, Figure 2.2.2(b) shows the spectrum of the Topas 8007 POFBG, Fig. 2.2.2(c) presents the reflection spectrum obtained for the Topas 5013 POFBG. The response of Topas 5013 step index POF is presented in Fig. 2.2.2(d), whereas the reflection spectra of Zeonex 480R and PC POFBGs are presented in Figs. 2.2.2(e) and 2.2.2(f), respectively. The reflection spectra presented in Figure 2.2.2 show a peak wavelength well above the noise floor for each material tested. Furthermore, the central wavelength in each case is in the 850 nm region, with the longest central wavelength of the PC and Topas 5013. However, the central wavelength of the PC POFBG was even higher and was reduced to about 866 nm after the blue-shift due to the post-annealing process. Similarly, the insets of Figure 2.2.2 present the transmission spectra of the POFBGs. To the authors' best knowledge, this is the first time that the transmission spectra of Zeonex, Topas and PC POFBGs are compared one-to-one. The differences of the initial power of each POF employed is due to the different losses of each fiber material, which was characterized in [27][46][52][53]. In addition, the POF connectorization to the silica pigtail can also induce different losses at POF transmission spectrum.

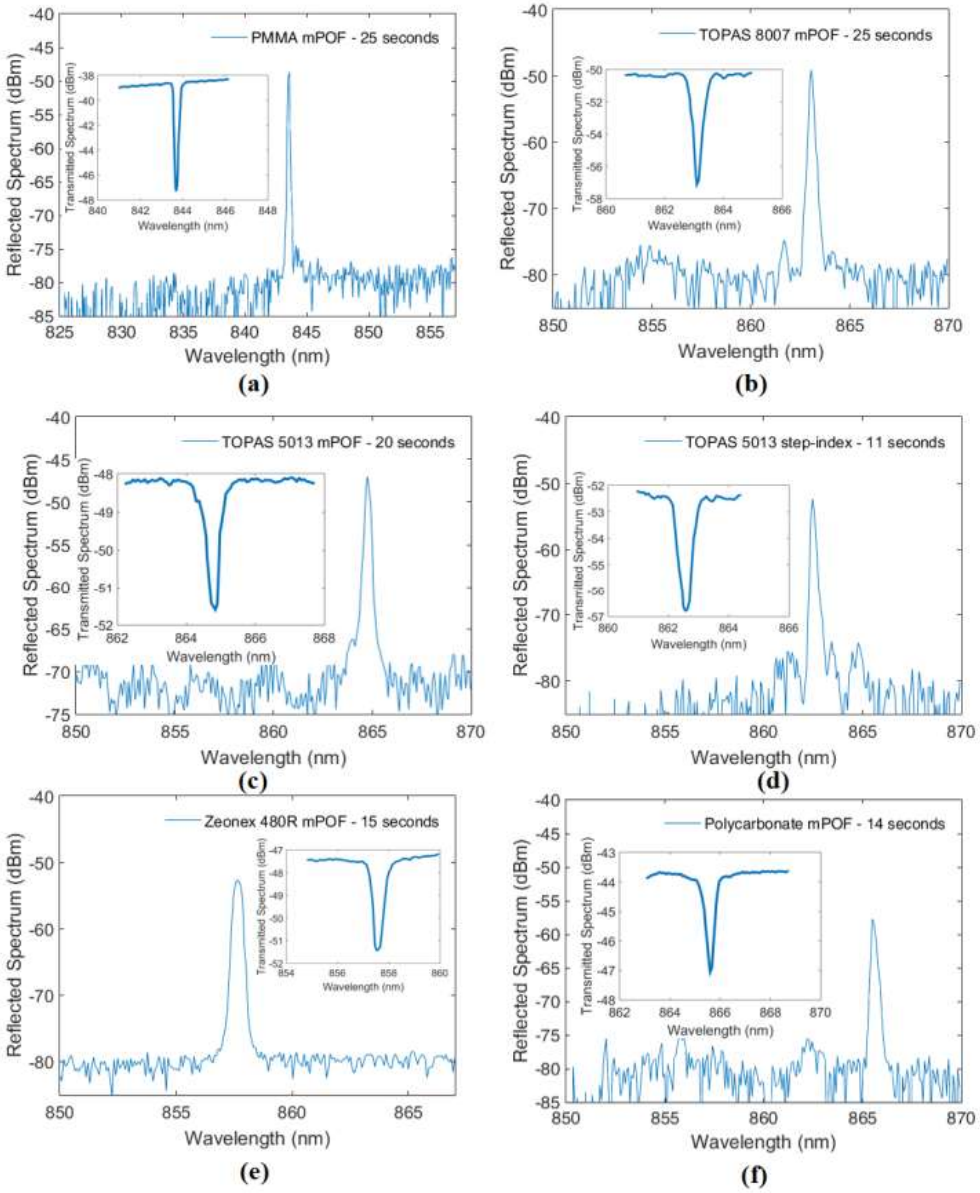

Figure 2.2.2 Reflection spectra of the POFGBs inscribed with the pulsed UV KrF @248 nm laser. The inscription times are also presented for (a) PMMA POFBG, (b) Topas 8007 POFBG, (c) Topas 5013 POFBG, (d) Topas 5013 step index POFBG, (e) Zeonex 480R POFBG and (f) Polycarbonate POFBG. The insets show the transmission spectrum of each grating.

Besides the necessity of keeping the laser and inscription setup stable for several minutes, the reduction of the gratings inscription time can also improve the FBG stability [27]. In addition, the heat treatment made on the fibers can influence the grating stability. For this reason, the POFBGs reflection spectra were monitored for several days to verify any instability on the grating strength, bandwidth and central wavelength. In particular, all samples were kept undisturbed for 40 days at room temperature (controlled environments conditions). Figure 2.2.3 presents the results obtained for each POFBG in terms of grating reflectivity, bandwidth and central wavelength, which were monitored over 40 days by measuring them every 5 days. Figures 2.2.3(a) and 2.2.3(b) show the gratings reflectivity and bandwidth, respectively, whereas Figure 3(c) presents the central wavelength of each POFBG. The results show a reduction in the reflectivity of all gratings by an amount lower than 3 dB that can be even smaller if the pre-annealing is made under high humidity conditions [66]. The only grating that presented a larger reduction in grating strength is the Topas 8007 POFBG. In addition, the bandwidth of each POFBG remains almost constant in all cases analyzed. The larger variation was obtained in the PC POFBGs for the

measurement made after 15 days, which might be due to some torsion in the fiber, since the value returned to the initial ones in the following measurements. However, all the POFBGs presented a stable central wavelength. Since the sensor applications for FBGs are related to the central wavelength monitoring, such stable wavelength enables the use of the presented setup for fast inscription of POFBGs in sensing applications of different parameters.

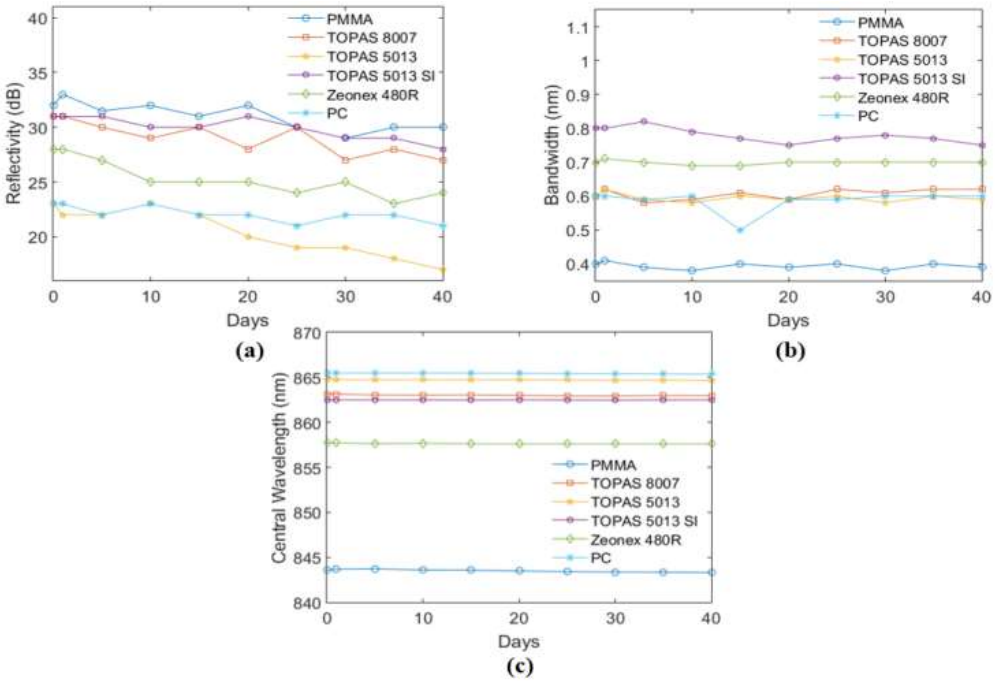

Figure 2.2.3 Stability of each POFBG after 40 days. (a) Gratings reflectivity, (b) bandwidth of the POFBGs and (c) central wavelength.

2.2.4 Conclusion

We presented the POFBG inscription with different POF materials with a pulsed UV KrF laser at 248 nm. The fibers employed in the grating inscription were PMMA, Topas 8007 and 5013, Zeonex and PC mPOFs and Topas 5013 step-index POFs. A pre-annealing was made of all fibers with a temperature below their glass transition temperatures and annealing times in the range of 24 hours. The comparison of the POFBGs inscribed with the technique presented in this work and with the conventional continuous 325 nm laser reported in the literature show a reduction in the inscription time of at least 16 times, where the maximum reduction was obtained for Topas 8007 mPOF (more than 130 times). Furthermore, a reflectivity of the spectra higher than the one obtained with the 325 nm laser was obtained in almost all cases. In addition, the created POFBGs with the pulsed laser at 248 nm show stability throughout 40 days, where slight modifications of their bandwidth, reflectivity and central wavelength were observed. The results presented in this work impact on the methods conventionally employed for the FBG inscription, where the use of a different laser setup, combined with a suitable heat treatment of the fiber, provides a substantial decrease of the inscription time without harming the grating strength, bandwidth and stability. In addition, the presented setup is similar to the one employed for FBG inscription in silica fibers, which means that, with slight modifications of the setup, it is possible to inscribed FBGs in different POF materials. The setup and the obtained results suggest that a much simpler fabrication of POFBGs is possible, which makes this technology more promising and easier to scale up, paving the way for its commercial applications. It is important to mention that with the pulsed 248 nm laser FBGs could be inscribed in 6-ring mPOFs, whereas this is not possible with the CW laser, for which typically only 3-ring mPOFs can be used. Since the loss of the mPOF decreases with the number of rings this makes the pulsed 248 nm laser FBG writing technology potentially even more advantageous.

2.3 Bragg gratings inscription in TS doped PMMA POF

[JP.3] R. Min, B. Ortega, X. Hu, C. Broadway, C. Caucheteur, C. Pun, H. Tam, P. Antunes, C. Marques, "Bragg gratings inscription in TS doped PMMA POF by using 248 nm KrF pulses" IEEE Photonics Technology Letters, 30(18), 1609-1612, 2018.

2.3.1 Introduction

During the last two decades polymer optical fiber Bragg gratings (POFBGs) have attracted huge attention driven by sensing and communication applications. Polymer optical fibers (POFs) show a smaller Young's modulus and larger thermo-optic coefficient compared with silica counterparts, which make them suitable for different sensing scenarios, such as strain [9], temperature [9], humidity [67], liquid level [11] and ultrasound [68]. The demonstrated biocompatibility also makes them a promising sensing technology for biomedical and bioengineering industry [69].

The first poly (methyl methacrylate) (PMMA) POFBG was reported in 1999 [17]. Since then, great progress has been made in the POFBG fabrication. Different materials such as Topas [52], Zeonex [54], CYTOP [64] or even polycarbonate [46] were introduced for different sensing modalities with unique advantages. Both microstructured and step-index POFs have been investigated. Until now, PMMA remains the preferred material for POFs composition. Due to the low photosensitivity of pure PMMA, a photosensitizer such as benzyl dimethyl ketal (BDK) [41], trans-4-stilbenemthanol (TS) [70] or diphenyl disulphide [69] can be added in the fiber core or cladding to enhance its photosensitivity. Among the various compositions and geometries of POFs, step-index POFs are the easiest ones to connectorize by using silica fibers pigtails [70]. In 2004, 90% reflectivity FBGs were obtained in step-index PMMA POFs with TS doped in the core by using 325 nm UV pulses after ~ 90 min exposure by using the phase mask technique [70]. Moreover, the etching technology allowed to obtain 40 min benefit in a 97% reflectivity grating by using a continuous 325 nm He-Cd laser system [61]. The same group also obtained low reflectivity gratings in 1 second, which have to be stabilized using a post-inscription thermal annealing [71]. Due to the PMMA POF periodic ablation in 248 nm wavelength mentioned by *Xiong et al.* in 1999 [17], this wavelength was not considered suitable for POFBG irradiation until *Oliveira et al*. [19] demonstrated the first POFBG in a pure PMMA microstructured fiber by using a 248 nm krypton fluoride (KrF) excimer laser system in few seconds of exposure, which greatly shortened the inscription time for POFBGs. Since then, one high pulse energy (6.3 mJ) was employed to fabricate FBGs in a BDK-doped microstructured PMMA fiber core [21]. Due to the benefits of KrF excimer laser such as high output pulse energy and repetition rate control, several works investigated the fabrication of several types of gratings in different POFs [23][28][29]. However, until now, no TS-doped PMMA POFBGs fabricated with 248 nm UV wavelength. Gratings at 850 nm spectral region are very suitable for various sensing applications since POF lengths of tens of centimeters are required and losses are much lower compared to the C+L bands. Consequently, our motivation is to study the fabrication of TS-doped POFBGs with the 248 nm laser system and develop fast and stable Bragg gratings inscription to achieve stable and useful optical components with lower transmission loss for sensing applications. We report the first TS-doped POFBG inscription under 248 nm UV irradiation with ~17 dB reflection above noise level in less than 1 second of exposure time. Moreover, temperature, humidity and strain characterizations are also measured for assessing potential sensing applications.

2.3.2 Bragg grating fabrication

In this work, a step-index PMMA POF is employed with a core diameter of 8.2 μm and a

cladding diameter of 150 μm. The cladding is pure PMMA, while the core is PMMA doped with diphenyl sulfide (DPS) (5% mole) and TS (1% w.t.). Both dopants are used to increase the refractive index and enhance the photosensitivity. A trans-cis structure change in the TS material under UV irradiation, estimated from 240 nm to 340 nm, leads to a refractive index decrease [70] where DPS facilitates the trans-cis inter-conversion under UV irradiation. A cross-section image of the fiber is shown in the inset of Figure 2.3.1. The fiber was annealed for 24 hours at 70 degrees in order to release the stress that was induced during the drawing process prior to the gratings fabrication. A Coherent Bragg Star Industrial-LN KrF excimer laser system operating at 248 nm wavelength was employed for the Bragg grating inscription. The experimental setup for POFBG inscription is shown in Figure 2.3.1. The laser beam was focused onto the fiber core utilizing a plano-convex cylindrical lens (Newport CSX200AR.10) with focal length of 20 cm. The effective spot size of the beam on the surface of the POF is 32.4 mm (height) and 20.0 mm (width). The UV laser beam illuminated a 567.5 nm pitch phase mask with a total length of 10 mm just before irradiating the fiber and, therefore, the FBG length was 10 mm.

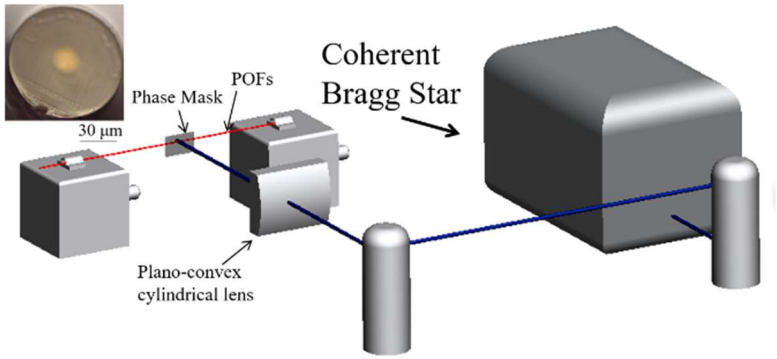

Figure 2.3.1 Experimental setup for POFBG inscription, inset: end face of the POF.

The reflected power spectrum was monitored after irradiation by using a super luminescent diode (Superlum SLD-371-HP1) and an optical spectrum analyzer (OSA) (Yokogawa AQ6373B) with 0.05 nm resolution bandwidth through butt coupling with a single-mode silica pigtail. A small amount of index gel was inserted to reduce Fresnel reflections. Several previous unfruitful attempts were done by using 1 pulse at 1 Hz repetition rate and 2.5 mJ pulse energy but further optimizations produced a grating with only 0.4 seconds inscription time at 100 Hz pulse rate. As explained below, the pulse repetition rate has strong influence on the POFBG reflected spectral power.

Figure 2.3.2 shows the POFBG reflected spectral power obtained with a 10 Hz repetition rate and a 0.50 ± 0.02 mJ pulse energy over 4 seconds (i.e., 40 pulses). We observe a full-width half-maximum (FWHM) bandwidth of 0.38 nm and a 17 dB peak-to-noise difference. The increase of pulse repetition rate is a promising method for grating inscription with shorter inscription time.

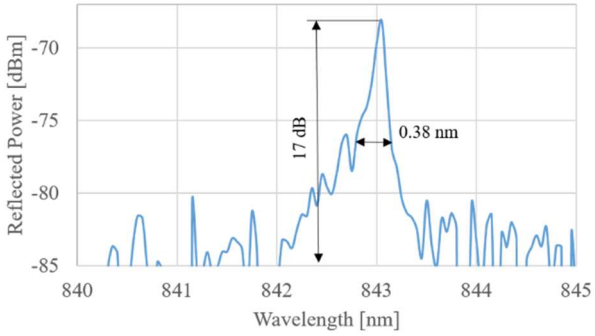

Figure 2.3.2 Reflected spectral power by a POFBG inscribed using 10 Hz repetition rate and pulse energy of 0.50 ± 0.02 mJ in 4 seconds (40 pulses).

Furthermore, in order to obtain shorter inscription times, the repetition rate was set to 50

Hz using the same pulse energy. Figure 2.3.3 shows the reflected power with an FWHM bandwidth of 0.46 nm, and 17 dB of reflectivity obtained in a 0.8 second exposure (40 pulses). The inscription time was reduced by 5 times when compared with the results shown in Figure 2.3.2.

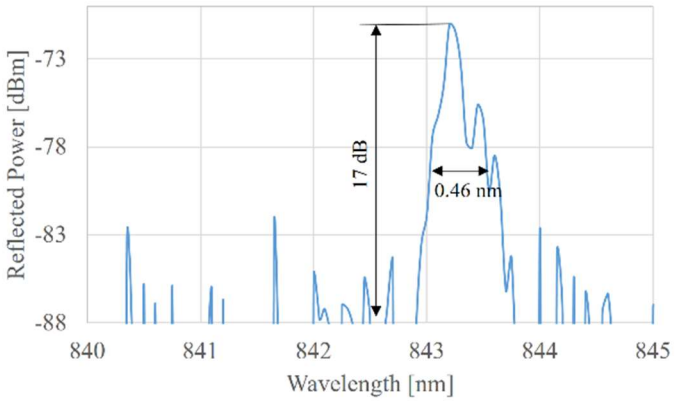

Figure 2.3.3 Reflected spectral power by a POFBG inscribed using 50 Hz repetition rate and pulse energy of 0.50±0.02 mJ in 0.8 seconds (40 pulses).

The repetition rate of the laser was further increased to 100 Hz and Figure 2.3.4 shows the reflected spectral power by the grating after 40 pulses by using the same pulse energy (0.50 ± 0.02 mJ). The POFBG still shows similar reflectivity response as the previous ones but the inscription time has been reduced down to 0.4 s.

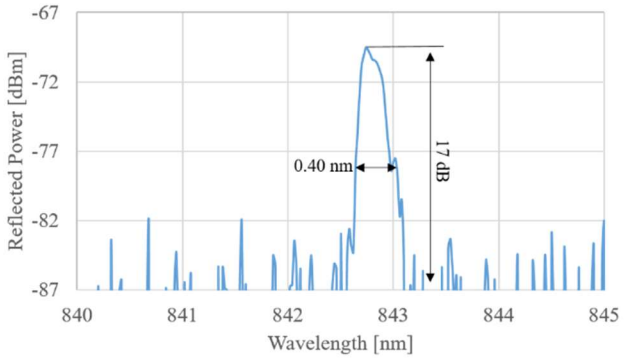

Figure 2.3.4 Reflected spectral power by a POFBG inscribed using 100 Hz repetition rate and pulse energy of 0.50 ± 0.02 mJ in 0.4 seconds (40 pulses).

Oliveira et al. [19] mentioned that it is possible to damage POF by using 50 Hz frequency and 3 mJ pulse energy after a few seconds. There are several methods to reduce or avoid damages, such as decreasing the pulse frequency, energy or pulse number. By using 1 Hz of frequency, a good performance is demonstrated in different undoped POFs [23]. Also, a single 6 mJ pulse leads to obtain gratings using BDK doped mPOF [21]. However, in our case, no POFBGs were obtained with a single pulse. Higher pulse repetition rates lead to achieve POFBGs in less than 1 second. As shown in [71], higher pulse repetition rates generate higher cumulative heating, and then higher temperatures are induced in the fiber. So, the aforementioned observation can be attributed to temperature variation. When a single pulse inscription is employed, the temperature is not high enough, the movement of polymer chains is confined and no sufficient free volume for the movement of TS molecules is generated. Conversely, when higher repetition rates are employed, higher temperature is achieved and sufficient free volume is enabled for the movement of TS molecules, which could switch from trans to cis forms with the associated negative refractive index change [61]. Figure 2.3.5 indicates that there is neither damage in the fiber core nor in the surface after

inscription by using the phase mask technology under 100 Hz repetition rate and pulse energy of 0.50 ± 0.02 mJ in 0.4 second (40 pulses). This demonstrates that the TS-doped POF can be useful in a POFBG fabrication setup, controlling the UV laser repetition rate to reduce the irradiation time without damaging the POF.

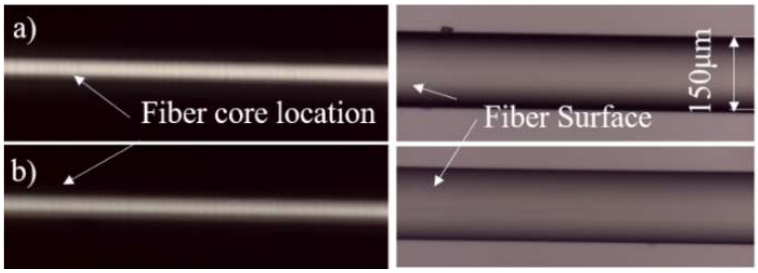

Figure 2.3.5 Microscope images of the TS doped POF surface: a) before irradiation; b) after 0.4 s irradiation by using phase mask technique under 100 Hz frequency and pulse energy 0.50 ± 0.02 mJ (40 pulses).

2.3.3 Bragg grating performance

For sensing applications, stability of the grating over time is a critical issue. Figure 2.3.6 shows the reflected spectral power by the grating two weeks after the initial inscription (see Figure 2.3.4) at room temperature. We can observe a blue shift of 0.7 nm and a power reduction of 1 dB. The grating profile is also modified, with the appearance of a sub-peak. This sub-peak could be related to coupling issues because the POF used is few-mode. A profitable comparison can be made to gratings inscribed using conventional CW 325 nm HeCd lasers, with exposures of 1 second, which need longer inscription time and present lower stability [71].

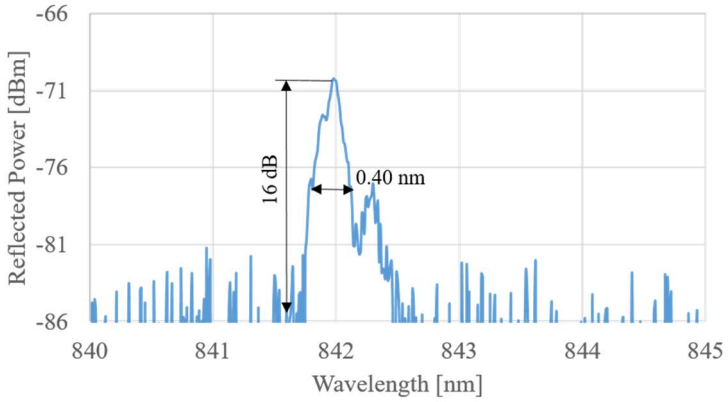

Figure 2.3.6 Grating with 100 Hz frequency and pulse energy 0.50 ± 0.02 mJ condition in 0.4 second (40 pulses) after two weeks.

Several gratings were inscribed with 40 pulses but using different repetition rates (10 Hz, 50 Hz and 100 Hz). In Figure 2.3.7, we can notice that the reflected power keeps stable for a long time showing no considerable impact of the repetition rate on the stability and therefore, it shows that this is an efficient method to obtain reasonable stable gratings with reduced fabrication times.

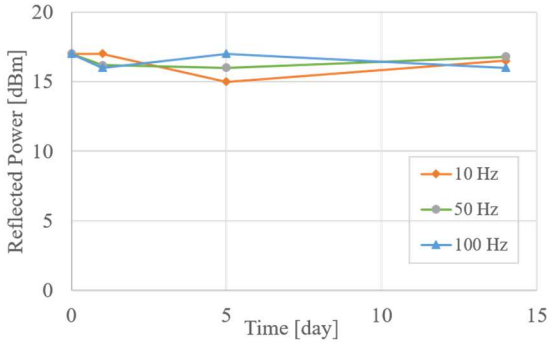

Figure 2.3.7 Reflected power of gratings fabricated with different laser pulse frequencies (10 Hz, 50 Hz and 100 Hz) at 40 pulses during two weeks.

In the following, the POFBG was connected to a single mode silica fiber with UV glue (Norland 78) and placed into a climate chamber (Angelantoni Industrie CH340) at a constant temperature of 22 ºC and 30 % of relative humidity (RH) during 80 min for stabilization. Then the RH was increased up to a value of 90 % in 20 % step, waiting 80 min between each one. The reflected spectrum was monitored using an 850 nm circulator, a super luminescent diode (Superlum SLD-371-HP1) and an optical spectrum analyzer (Yokogawa AQ6373B). Fig. 2.3.8 (a) shows that the central wavelength needs around 80 min to be stable under the 20 % humidity change. The total wavelength shift was 1.71 nm and the sensitivity was computed as 0.027 ± 0.005 nm/% RH as shown in Figure 2.3.8 (b).

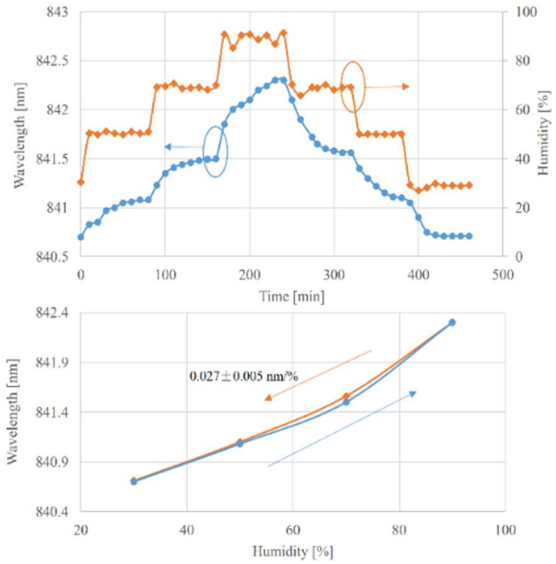

Figure 2.3.8 a) Measured wavelength shift under humidity change. b) Wavelength shift at different humidity levels.

Temperature sensitivity of the same grating was measured by using a Peltier plate, which contains a small v-groove where the temperature is set with a thermo-electric controller. Silicone grease was placed on the grating position to increase temperature conduction. The central wavelength of the grating was measured from 27 ºC to 52 ºC, in 10 ºC steps, every 10 min. The total central wavelength shift was about 1.22 nm, allowing to estimate a sensitivity of -0.42 ± 0.05 nm/ºC, as shown in Figure 2.3.9, a similar value obtained with Bragg gratings inscribed in the same fiber type but using the 325 nm HeCd laser system [61].

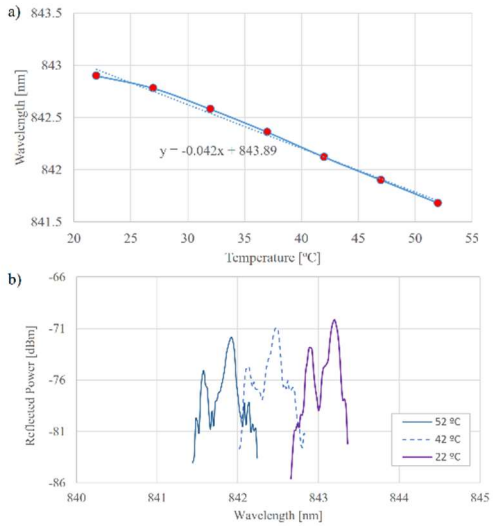

Figure 2.3.9 a) Wavelength shift under different temperatures. b) Reflected spectrum under different temperatures.

In order to characterize the strain sensitivity of the fabricated gratings, a 7.9 cm long fiber containing the grating was placed between two X-Y-Z stages where it was glued. The fiber was strained step-by-step while awaiting 5 min between each step at room temperature. The evolution of the central wavelength was monitored when the strain was changed from 0 to 1.26 % as depicted in Figure 2.3.10. A wavelength shift of 9 nm was observed under strain, which indicates a linear strain sensitivity of 7.18 ± 0.02 pm/με, which is similar with PMMA mPOFBG fabricated at 850 nm spectral region [8].

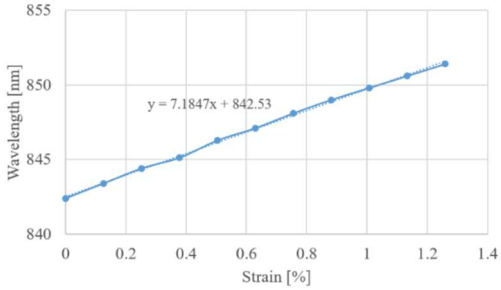

Figure 2.3.10 Wavelength shift under different strain.

As recently confirmed by the literature [23], different undoped POF materials need a maximum of 25 s of inscription time, but BDK-doped mPOF just requires one high pulse with 6.2 mJ of energy due to the high BDK absorption coefficient [21]. Based on these investigations, the performance described here is relevant due to the presence of the TS dopant. Due to the different refractive index change mechanism of BDK and TS dopants at 248 nm wavelength, we were not able to obtain a grating with a single pulse. However, the choice of adequate parameters of the pulsed UV laser allows to obtain FBG with less than 1 second exposure time.

2.3.4 Conclusion

In conclusion, we inscribed FBGs in Trans-4-stilbenemethanol-doped photosensitive step index PMMA POF at 850 nm wavelength by using phase mask methodology with a 248 nm KrF laser, with inscription times lower than 1 second. Humidity, temperature and strain sensitivities under stable conditions have been measured to assess the fabricated components for potential sensing applications.

2.4 Bragg grating inscription with low pulse energy in doped mPOF

[JP.4] R. Min, B. Ortega, K. Nielsen, O. Bang, C. Marques, "Bragg grating inscription with low pulse energy in doped microstructured polymer optical fibers" IEEE Sensors Letters, 2(2), 5000604, 2018.

2.4.1 Introduction

During the last two decades polymer optical fibers (POFs) have attracted the attention of many researchers due to the continuous reduction of the transmission attenuation among other reasons [72]. Due to the advantage of polymers over silica such as low Young's modulus and biological compatibility, polymer optical fiber Bragg gratings (POFBGs) have been considered as a promising technology for sensing [6] and short-range optical communications [5]. The first POFBG based on PMMA was reported in 1999 [17]. Since then, different kind of polymer materials such as PMMA, CYTOP, Topas, Zeonex or even polycarbonate have been used to fabricate Bragg gratings [25][46][54][64]. However, PMMA is known as the most used among all of the materials and high quality FBGs have been fabricated in pure PMMA microstructured polymer optical fiber (mPOF) using a 325 nm He-Cd CW laser, initially using 2 hours [25] and recently using less than 7 minutes [27]. Due to the low photosensitivity of pure PMMA, a photosensitizer such as trans-4-stilbenemthanol or benzyl dimethyl ketal (BDK) can be added in the fiber core or cladding to improve it [61][73][74]. Compared with pure PMMA, BDK-doped PMMA presents two absorption bands (one very pronounced at 250 nm region and other at 320-350 nm region) with evident photosensitivity enhancement at 248 nm region [73]. The addition of a dopant to the non-fully polymerized PMMA allows the selection of the wavelength needed to induce photopolymerization, where the wavelength of ~ 248 nm can be used for the BDK as a photoinitiator as discussed in [73]. In this way, *Luo et al.* reported the first Bragg grating in a BDK-doped core PMMA POF using a 355 nm laser [73]. Then a ~99 % reflective POFBG was obtained in a BDK-doped core PMMA mPOF after 13 min of irradiation with a 325 nm laser. In 2017, a 400 nm femtosecond pulsed laser was used for fast irradiation to produce FBGs in BDK-doped mPOF with just 40 seconds [34], where different UV powers were employed to obtain different grating responses.

Initially, 325 nm was demonstrated as the optimal wavelength to inscribe POFBGs, and 248 nm wavelength was not considered suitable for POFBG fabrication due to periodic ablation mentioned by *Peng et al.* in 1999 [16]. In 2000, the refractive index modification achieved with a 248 nm laser was investigated on PMMA chips for integrated-optical waveguides at low fluence (I = 17 mJ/cm^2) and low frequency (5 Hz). A 248 nm laser was employed to successfully inscribe the first POFBG using 3 mJ pulses in few seconds [19].

With the aim of reducing fabrication times, such a 248 nm laser was later employed to fabricate FBGs in BDK doped fiber with a single UV laser pulse with a high pulse energy of 6.3 mJ (974 mJ/cm^2) [21]. After irradiation, the strength of the grating continues growing for several minutes; similar to previously reported behavior in dye-doped PMMA optical fiber using 325 nm laser based grating inscription setup [75]. However, according to previous results [21], the irradiation of two or three ultraviolet pulses leads to some decrease in the induced index change so different UV pulse energy level has to be explored in order to optimize the fabrication process.

We demonstrate the use of low pulse energy (60 μJ/pulse) to get a grating with 40 % reflectivity in 90 pulses, of 15 ns duration each one. This work shows the impact of the pulse energy and the total UV energy on the grating growth. The fabricated grating shows a positive refractive index change and stability after fabrication which is very important and different from FBGs written with higher energy pulses recently reported in [21]. We also demonstrated energy efficient grating fabrication using 4 pulses of 200 μJ per pulse, achieving a suitable

grating transmission of about 7.5 dB.

2.4.2 Bragg grating inscription

A PMMA mPOF with 3 rings of holes and a BDK-doped core was used to inscribe Bragg gratings in this work. The three ring cladding microstructure has a hole-to-pitch ration of 0.47 with an average hole diameter of 1.74 μm and an average pitch of 3.70 μm , which makes it close to endlessly single-mode [76]. A cross-section image of the fiber is shown in the inset of Figure 2.4.1. A Coherent Bragg Star Industrial-LN krypton fluoride (KrF) excimer laser system operating at 248 nm wavelength with a 1 Hz repetition rate was employed for the Bragg grating inscription. The laser beam profile was measured as a rectangular Tophat function of 6.0 ×1.5 mm^2 size and 2×1 $mrad^2$ divergence. It was focused onto the fiber core utilizing a plano-convex cylindrical lens (Newport CSX200AR.10) with focal length of 20 cm. The effective spot size of the beam on the fiber surface is 20.0 mm in width and 32.4 μm in height. A slit was employed to control the width of the beam as shown in Figure 2.4.1. The UV light was passed through a 567.8 nm pitch phase mask over a 5 mm fiber length.

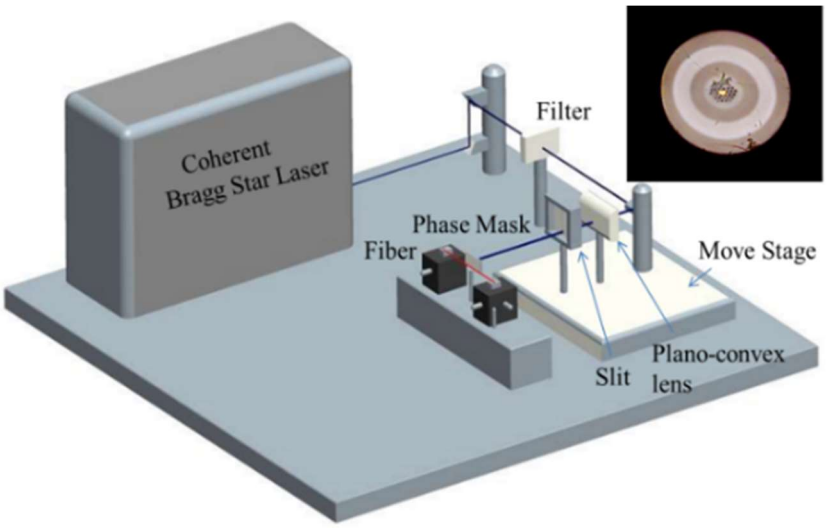

Figure 2.4.1 Experimental setup for POFBG inscription. Inset: mPOF cross-section image.

The reflected power spectrum was monitored during irradiation by using a super luminescent diode (Superlum SLD-371-HP1) and an optical spectrum analyzer (Yokogawa AQ6373B) with 0.02 nm resolution bandwidth. A linear step ND filter (Thorlabs NDL-10S-4) and a glass slide (can decrease 90 % of 248 nm UV power beam) were used to control the pulse energy. An energy power meter (packaged with Coherent Bragg Star Industrial-LN KrF excimer laser system) was used to measure pulse energy with ±1.0 % accuracy from nJ to J and the pulse energy fluctuates with ±5 % per pulse.

Figure 2.4.2 shows the post-inscription POFBG growth when it has been fabricated using 5 pulses of 200 μJ energy per pulse at 1 Hz repetition rate (6 times less than the energy used in previous work using a single UV pulse [21]). A red shift behavior was observed, and its reflected power keeps increasing for more than 100 seconds. No grating was achieved with only 1 pulse of this level of pulse energy.

It's worth noting that a grating with a strength of about 5 dBm in reflection has appeared after five 200 μJ pulses, which is comparable to the strength obtained with only one pulse of high energy reported in [21]. The difference is that at high pulse energy levels, the grating strength will decrease during the second pulses, as observed and discussed in [21], where the authors did not find an explanation for this behavior. However, it can be justified by excessive reaction (due to the core damage for long time UV exposure [73]) with high total UV energy received, which is a similar behavior as was previously reported in [73][75]. However, in our case Figure 2.4.2 shows that the grating growth continued after five low energy pulses with 1 Hz. A potential reason is that this low power pulse of 200 μJ has a gradual refractive index change on the polymer when compared to the abrupt change

observed for high energy pulses and after 5 pulses, we can reach to an adequate index change in the fiber core.

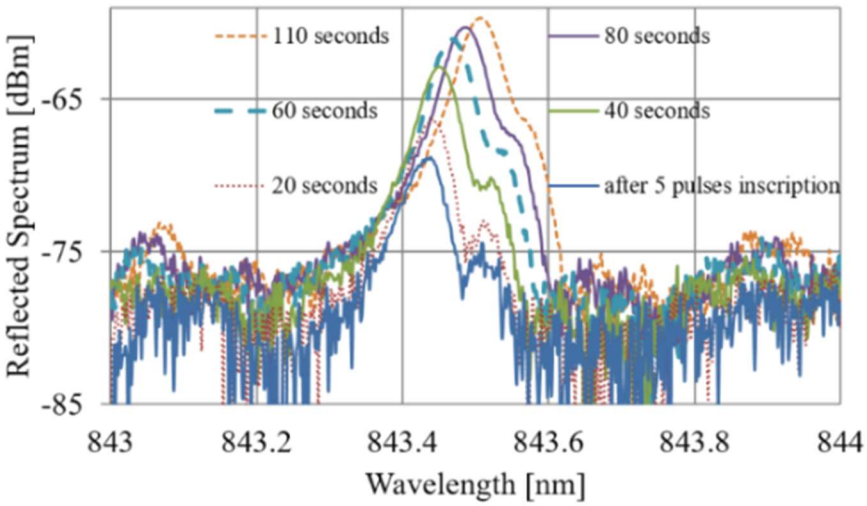

Figure 2.4.2 Post-inscription grating growth of a POFBG fabricated using 5 pulses of 200μJ energy per pulse at 1 Hz repetition rate.

In order to evaluate the lowest pulse energy suitable to fabricate Bragg gratings, a series of different tests were performed. Figure 2.4.3 shows the grating growth during irradiation of 60 μJ energy pulses at 1 Hz repetition rate as the number of irradiated pulses is increased up to 90 pulses. The grating appears after 20 pulses and its strength keeps increasing as the number of pulses increases. After 90 pulses the laser system was turned off and the reflected power of the grating kept relatively stable – a different behavior when compared with the result presented before in Figure 2.4.2. Figure 2.4.4 shows the transmission response of such gratings irradiated with a different number of 60 μJ pulses. A transmission rejection band of 2.2 dB, or 40 % equivalent reflectivity, was obtained with 90 pulses. Additional tests were carried out in order to check the stability of very weak gratings fabricated with 20 pulses and the reflected power measurement of the grating was very stable. Also, tests were performed with 32 μJ energy pulses however, it did not allow getting any grating, even trying with a large number of pulses, i.e. 600 pulses.

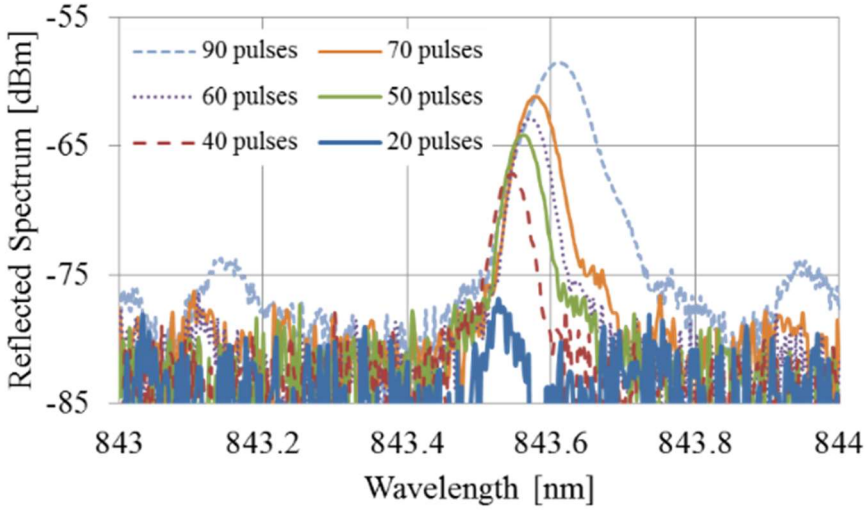

Figure 2.4.3 Reflection spectrum obtained with different number of pulses (1 Hz repetition rate) using a pulse energy of 60 μJ.

Our results indicate that a minimum pulse energy is need for a successful grating inscription, which after several tests is estimated as 60 μJ of energy per pulse. Importantly,

for the pulse energy levels of 60 µJ, 124 µJ, and 200 µJ, the gratings grew until a high level of reflection with no similar phenomenon happening as described in [21], where the second and third pulses was observed to reduce the reflected power of the grating [21][73][75]. A decrease in reflected power with increasing UV irradiation time was observed both with a PMMA fiber under 325 nm UV pulse irradiation (5 ns, 10 Hz) and a BDK-doped PMMA fiber under 355 nm pulsed laser irradiation [73]. The photosensitivity mechanisms of PMMA are still under research and the refractive index changes can be introduced by photo-crosslinking, photo degradation, or by photo polymerization [21]. During the FBG inscription, BDK acts as a photo-initiator and is activated by a transition within the molecular orbital of the >C = O group followed by α-splitting to produce free radicals. When illuminated by UV light, a series of reactions could happen as described in [73], where PMMA doped with BDK shows more than 15 times higher UV absorption compared with pure PMMA at 250 nm wavelength.

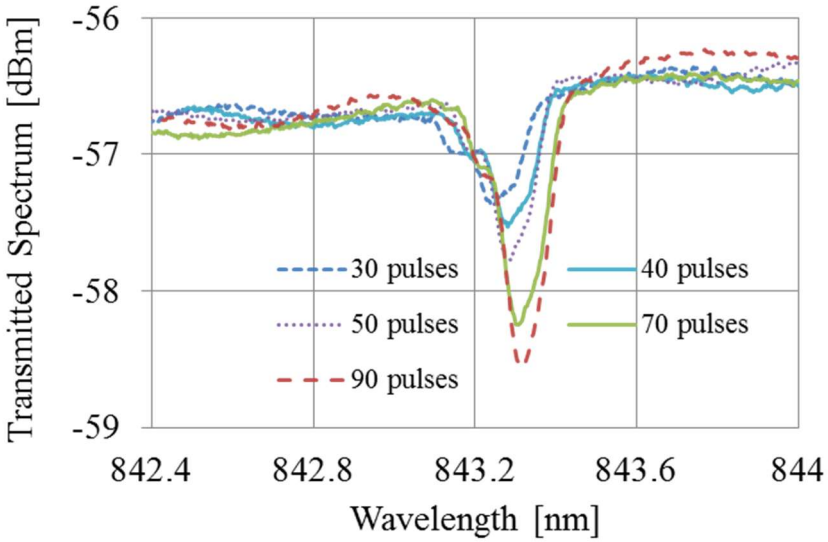

Figure 2.4.4 Transmission spectrum for 30, 40, 50. 70, and 90 pulses (1 Hz repetition rate) using a pulse energy of 60 µJ.

As shown in Table 2.4.1, the number of pulses required to achieve Bragg gratings with different pulse energies (60 µJ, 124 µJ, 200 µJ, 500 µJ and 2000 µJ) varies significantly. It is obvious that high pulse energy contributes to a shorter irradiation time since pulse energies of 200 µJ, 500 µJ and 2000 µJ require 4, 2 and 1 pulses, respectively. Figure 2.4.5 shows the stability of the gratings specified in Table 2.4.1 during an hour after irradiation in terms of wavelength shift and reflection band of the grating. All wavelengths indicate a red shift, as is expected due to the photo-polymerization mechanism [74] .

Table 2.4.1 Performance of the POFBG for different pulse energies and number of pulses.

Pulse energy (µJ)	Energy density per pulse (mJ/cm^2)	Total pulses	Reflection band (dB)	Energy density per inscription (mJ/cm^2)
60	37.0	90	22	3333.3
124	76.5	50	18	3825
200	123.4	4	24	493.6
200	123.4	5	23	617
500	308.6	2	20	617.2
2000	1234.6	1	20	1234.6

Analyzing Table 2.4.1, we can notice a tradeoff between pulse energy and energy density per inscription since the lowest energy density per inscription was not obtained when the lowest pulse energy is applied. The reflected power changes are more diverse, where Fig. 2.4.5 (b) indicates that grating with 60 µJ pulse energy shows a slight decreasing less

than 1 dB in 60 min and gratings with 200 µJ and 500 µJ show the trend of growth less than 3 dB.

In general, these results show a suitable stability of both the center wavelength and the reflectivity of the POFBGs. The reflection band changes do not show an obvious relationship with the pulse energy. However, it is to be expected that the reflected power changes have a relationship with the total UV energy received and the BDK dopant concentration in the fiber.

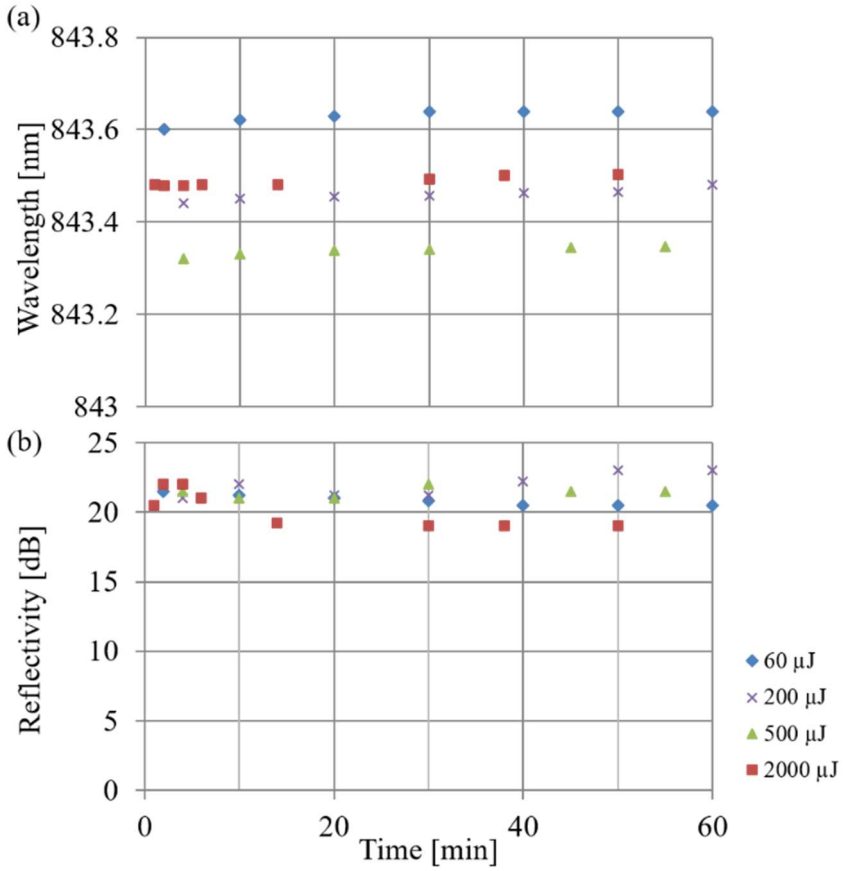

Figure 2.4.5 One-hour monitor after irradiation: a) wavelength response, b) reflectivity.

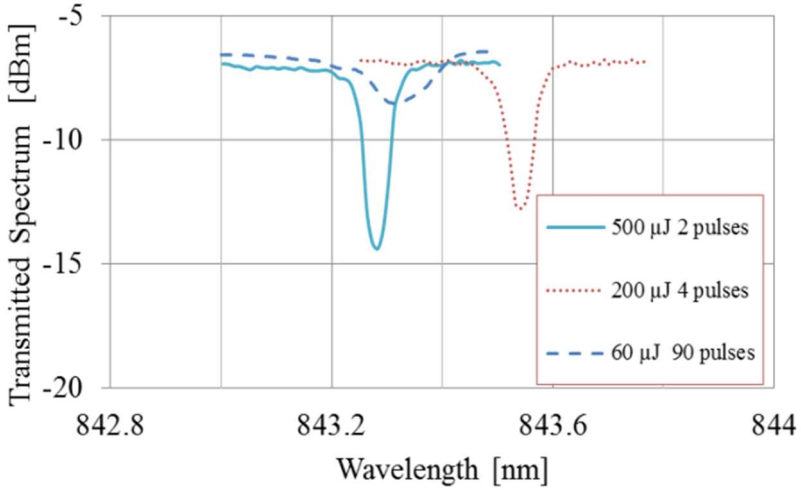

Figure 2.4.6 Transmission spectrum of gratings obtained with different pulse energy and number of pulses.

In order to provide a better insight into POFBGs fabricated by irradiation with low UV pulse energy, we obtained some results based on the transmitted power spectra as shown in Figure 2.4.6. Three of the POFBGs given in Table 2.4.1 (90 pulses with 60 µJ energy, 4

pulses with 200 μJ energy, and 2 pulses with 500 μJ energy) were analyzed and their transmission spectrum collected. The transmission dip of these POFBGs are 2.2 dB, 5.7 dB, and 7.5 dB, respectively. This result indicates a better performance when compared with BDK doped fiber irradiation with 400 nm femtosecond laser [34]. In [34] with 1 mW during 100 seconds a grating with a 0.2 dB transmission dip. In our experiment we can achieve gratings from 2 dB to 8 dB in transmission. From these results, the lowest energy density needed to inscribe a grating is 493.6 mJ/cm^2, 2 times less than reported in [21], where a single UV pulse was applied providing an energy density of 974 mJ/cm^2. The absorption performance at 250 nm and 400 nm UV wavelength may be able to explain this better performance [73].

As well known, strain characterization is also required for potential sensing applications as presented in many works in literature. For this purpose, the grating with 60 μJ and 90 pulses was placed on an XYZ translation stage. The central wavelength shift was monitored when the strain was changed from 0 to 1.1% at room temperature, as shown in Figure 2.4.7. The wavelength shift of 8.28 nm was observed with respect to the unstrained fiber, indicate a linear strain sensitivity of 0.753 ± 0.002 pm/με, similar with the previous FBGs in annealed POFs [8].

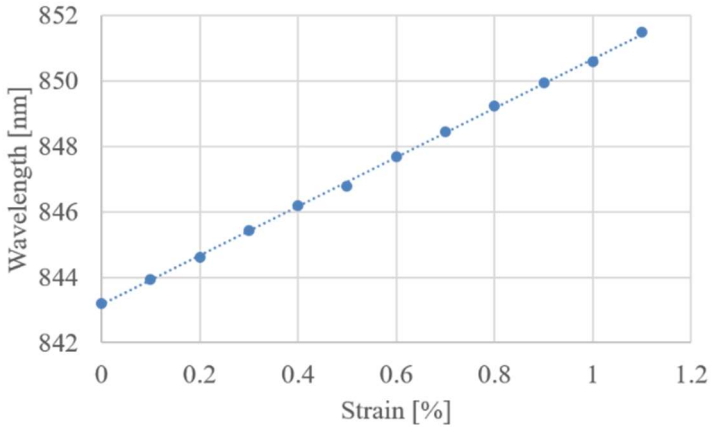

Figure 2.4.7 Central wavelength shifts vs. strain.

2.4.3 Conclusion

We demonstrated that with low UV power (60 μJ/pulse) we can achieve a suitable grating with a 2.2 dB dip in transmission and a reflectivity of 22 dB, which makes them suitable for many sensing applications. Analyzing the effect of different pulse energies and total UV energy on the quality of the grating, we found that with 200 μJ pulse energy we can achieve a suitable grating transmission dip of about 7.5 dB and a grating reflectivity of 24 dB with just 4 pulses, the most energy-saving way to achieve a reasonable grating with an energy density of 493.6 mJ/cm^2 for each inscription. The demonstrated gratings could be obtained without high pulse energy, which avoids high maintenance costs. This research can be useful for future investigations of different kind of Bragg grating devices fabrication for sensing fields in order to reduce the energy waste and pay attention to the minimum UV energy and total energy received. In addition, we will optimize the number of pulses for energies from 60 to 200 μJ in order to get a detailed optimization between the pulse energy and number of pulses with the aim to achieve the lowest energy density per inscription.

2.5 Bragg grating inscription in CYTOP POF

[JP.5] R. Min, B. Ortega, A. L. Junior, C. Marques, "Bragg grating inscription at 600 nm wavelength region in CYTOP POF with 248 nm KrF pulses" IEEE Sensors Letters, 2(3), 5000804, 2018.

2.5.1 Introduction

With the continued development of fabrication technologies and materials over the last two decades, polymer optical fiber (POF) has attracted huge attention for sensing and communication applications, due the advantage such as low Young's modulus and biocompatibility which make POF suitable for large strain measurements and medical sensing applications. POFs with large cores have been also shown as a cost attractive solution for short-range optical communication due to less operational complexity and simpler installation when compared with standard silica fiber [77]. Fiber Bragg gratings (FBGs) in POF exploit the advantages given by the low Young's modulus and biocompatible nature of the POF material and lead to develop a new generation of sensors. So far, most of the research is based on poly (methyl methacrylate) (PMMA) microstructured POFs (mPOFs) [41] and step index POF [61], where the mPOFs could show an endless single mode performance provided certain conditions are satisfied [34]. Such performance is difficult to achieve in PMMA step index POFs due to the higher refractive index difference between core and cladding. However, the connection between mPOF and silica fiber is a serious challenge due to holes from microstructure. Furthermore, some index matching gel can be employed to improve this coupling, but the gel gets inside the holes, and leads to a harmful effect on the light transmission. In this way, step index PMMA is a suitable POF to solve this issue and, recently, a single mode PMMA POF with doped core for photosensitivity increase was investigated and FBGs were inscribed to be used as optical sensors for medical applications [69]. Similarly, to other POFs, high fiber loss has proven a major issue in the widespread of sensing applications. The high transmission loss in PMMA POF are due to higher overtone vibrations of C-H groups which lead to broad-spectrum absorption with peaks in the infrared region [64].

Recent investigations on perfluorinated optical materials such as cyclic transparent fluoropolymers (CYTOP) show good transmission and overcomes this limitation. The wavelength of the maximum absorption is determined by the individual molecular structure. CYTOP only contains C-C, C-O and C-F bonds and shows higher transparency and low absorption losses due to the highly amorphous nature [64].

However, the benefit of low loss performance given by CYTOP also limits the photosensitivity of the fiber. In 2014, *Koerdt et al.* [78] reported the first FBG in CYTOP fiber at 1450 nm spectral region, where a 248 nm pulsed krypton fluoride (KrF) laser was used with an irradiation fluence of 5 kJ/cm^2 during less than 1 hour. The authors demonstrated that the core material of the Giga POF 50SR is photosensitive at 248 nm wavelength, but, unfortunately, the spectral response was not good for sensing and the sensitivity could not be measured also due to coupling issues. The reflected signal spectra of this multimode fiber showed a bandwidth of around 10 nm composed of several peaks corresponding to principal modes [79]. Each principal mode consists of several excited guided modes in the POF whose propagation constants are almost the same. The position of the single mode launching fiber determines the excited modes in the multimode POF.

Then, most of the attention about FBG in CYTOP POF is driven to femtosecond (fs) laser irradiation, as reported in 2015 [64]. This laser system allows the FBG inscription in any type of bulk material and optical fiber without photosensitivity [80] due to the extremely large light intensity through a small spatial region and ultra-short irradiation time. Also, the refractive index changes introduced by the fs pulses are highly localized. From the first FBG inscription in CYTOP POF with fs laser reported [64], the same group has published a considerable number of works with focus in sensing applications at 1550 nm spectral region

[81][82][83][84]. Due to point-by-point or plane-by-plane method limitation, the fs pulses irradiation is limited to typical periods of FBGs, due to the spatial resolution is limited by the diffraction limit [85]. Compared with silica fiber where the standard spectral region is at 1550 nm wavelength, POF shows huge advantages in 650 nm and 850 nm wavelength (including the compatibility to low cost LEDs close to the visible region as white and RGB LEDs). Thus, the fabrication of FBGs in low loss CYTOP fiber at these wavelengths is important for sensing and communication applications.

We demonstrate the first FBG irradiation with 248 nm UV pulses at 600 nm spectral region, and temperature and strain characterization tests to have been carried out to propose them as novel optical devices for visible communications and sensing applications.

2.5.2 Bragg grating fabrication

This work employed the commercial graded index multimode perfluorinated POF (GigaPOF-50SR, Chromis Fiberoptics), with core diameter of 50 μm, a 40 μm cladding layer and an additional polyester and polycarbonate over-cladding structure to protect the fiber, resulting in a total diameter of 490 μm [86] The fiber was etched with chloroform ($CHCl_3$) [64] during several minutes in the fume hood due to the use of such dangerous chemical product. The fiber was etched piece-by-piece to avoid any fiber twisting during etching process and reduce the POF fragility induced by the etching treatment. Then, the fiber was washed in flowing water for the removal of any residual chloroform. The final diameter of the fiber was about 90 μm without the over-cladding as shown in Figure 2.5.1.

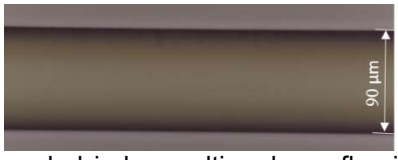

Figure 2.5.1. The commercial graded index multimode perfluorinated fiber after etching under microscope.

One razor blade was used to cleave the fiber end and it was butt-coupled to an 8° angle SM pigtail by using some index matching gel. As shown in Figure 2.5.2, a coherent KrF excimer pulsed laser emitting at 248 nm wavelength was used. The UV beam was focused onto the fiber core utilizing a plano-convex cylindrical lens (Newport CSX200AR.10) with focal length of 200 mm. The FBG was fabricated using the phase mask technique. The refractive index of CYTOP is about 1.34, so a 449.05 nm pitch phase mask is required to fabricate FBGs in CYTOP POF at 600 nm wavelength region.

A 20 cm long CYTOP fiber was placed on the XYZ translation stage and the 248 nm laser pulse energy was set at 0.6 mJ with a repetition rate of 40 Hz. The fiber was irradiated through the phase mask during 60 minutes. A supercontinuum laser (Fianium WL-SC-400-40) was used as optical source to characterize the reflectivity response of the grating and it should be noted that, due to the high power and broad wavelength (400 nm~2400 nm) of the source, one filter (Semrock 595 nm~700 nm) in order to protect the source in case of high power reflections.

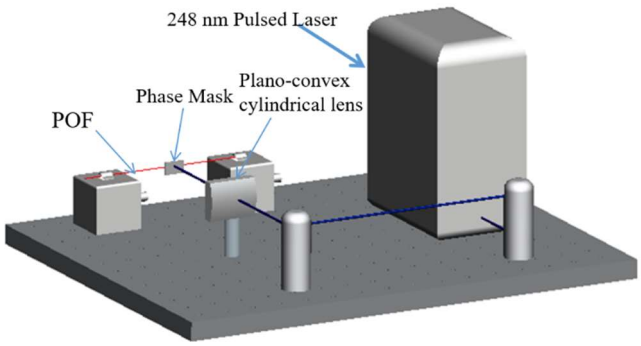

Figure 2.5.2 Experimental setup for POFBG inscription.

An optical spectrum analyzer (Yokogawa AQ6373B) with 0.2 nm resolution bandwidth was connected to a SM silica pigtail and an optical circulator was employed to measure the reflected power. The length of the inscribed FBG was 10 mm. Figure 2.5.3(a) shows the reflected spectrum obtained with butt-coupling method. Figure 2.5.3(b) shows an additional optical spectrum from the same FBG but a small change in the butt-coupling to illustrate how critical is the butt-coupling process for a good characterization of the FBG.

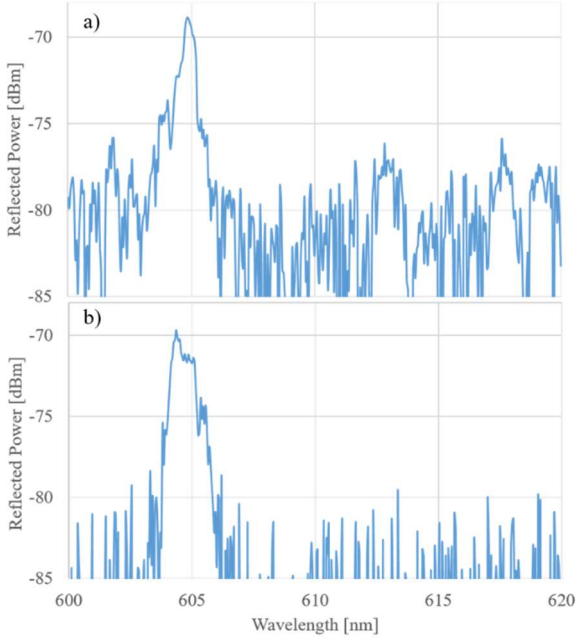

Figure 2.5.3 Reflected power spectrum by the FBG under different butt coupling. (a) Butt-coupling method. (b) Intentional misalignment in the butt coupling.

2.5.3 Temperature and strain characterization

Temperature, humidity and strain experiment results are presented to assess the potential sensing and optical communication applications. One end of the POF (grating inside) was cut as a flat face with a razor blade, then it was butt coupled with an APC SM pigtail by using an UV curable adhesive (Norland 68).

The grating was placed on a Peltier plate with temperature set by an electronic temperature controller. Some silicone grease was applied on the grating section to increase the heat conduction. It was measured from 32 ºC to 72 ºC with 20 ºC step and a temperature sensitivity of 11.2 ± 0.5 pm/ºC was obtained, providing a red shift performance, as shown in Figure 2.5.4. The results show a different behavior when compared with PMMA POF, which temperature sensitivity has been measured around −0.069 ± 0.001 nm/ºC [83] at 850 nm wavelength region. The CYTOP FBG fabrication with fs laser also showed a positive wavelength shift with increasing temperature, which can be explained in terms of the positive thermo-optic coefficient, which is close to 7.4×10^{-5}/K due to the linear expansion in bulk volume for CYTOPs [69]. Nevertheless, until now, no temperature sensitivity was reported at such wavelength.

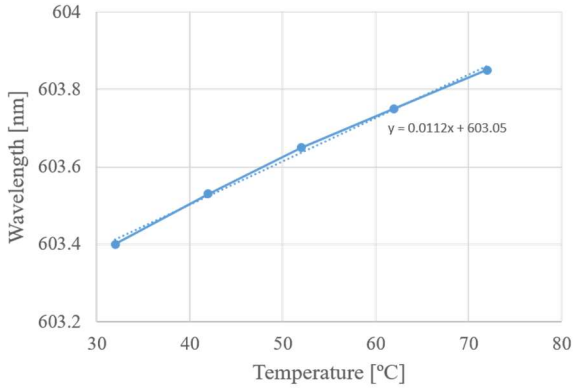

Figure 2.5.4 Wavelength shift under different temperature.

Humidity response of the FBG was also measured and the connectorised CYTOP POF was placed in the climatic chamber (Angelantoni Industrie CH340) with constant temperature at 30 ºC (a temperature chosen randomly and close to room temperature). The humidity level was from 50 % to 90%, and we can observe no wavelength shift for 40 % humidity change as shown in Figure 2.5.5. It indicates CYTOP POF is a good candidate for sensing applications under humidity change environment or in water.

The strain characterization was also investigated and the CYTOP POF was placed into a strain setup (see Figure 2.5.6 (a)) for this purpose. A 13.2 cm long CYTOP POF including a 1 cm long FBG was fixed with fiber clamps (Thorlabs HF001) and a translation stage was used with 0.1 mm step (0.075%) while the data was collected. The wavelength shift under different strain of the reflection spectrum is shown in Figure 2.5.6 (b). A wavelength shift of 2.0 nm was obtained with respect to the unstrained grating, which indicated a linear strain sensitivity of 0.533 pm/με at 600 nm spectral region. The maximum hysteresis occurs at about 1500 με, in which the deviation between the loading and unloading cycles is lower than 0.1 nm.

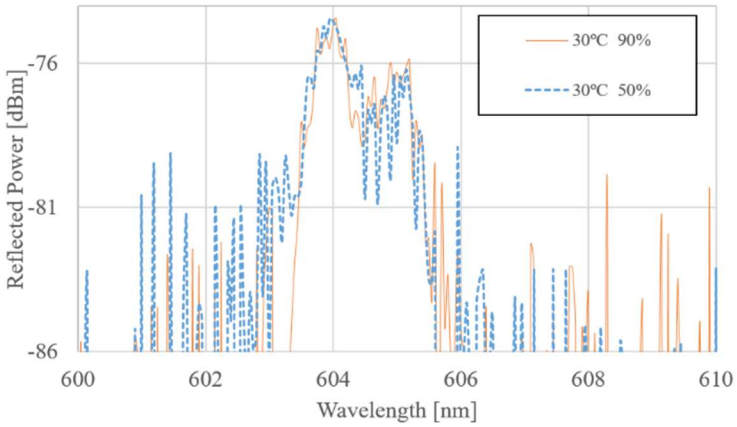

Figure 2.5.5 FBG spectrum under different humidity level at constant temperature.

To the best of our knowledge, no reports are published in the literature on the strain sensitivity of FBGs in POF at 600 nm region. The strain sensitivity of PMMA mPOF Bragg grating at 850 nm wavelength is about 0.711 pm/με [8] and at 1560 nm wavelength is around 1.58 pm/με [87]. Nevertheless, this lower sensitivity obtained in 600 nm region is consistent with the FBG wavelength shift with strain that presents an upward trend with respect to the Bragg wavelength increase, since the wavelength shift (Δλ) is defined as Eq. (2.1) for strain and temperature variations. Then, the term $(1-P_e)\,\lambda_B$ is the strain sensitivity, whereas $(\alpha+\xi)\,\lambda_B$ is the temperature sensitivity. For this reason, if the Bragg wavelength (λ_B) is in shorter wavelengths, the strain and temperature sensitivities will be lower when comparing with the one of λB in longer wavelength region, such as 850 nm or 1550 nm [83].

$$\Delta\lambda_B = [(1\text{-}P_e)\varepsilon + (\alpha + \xi)\Delta T]\lambda_B \quad (2.1)$$

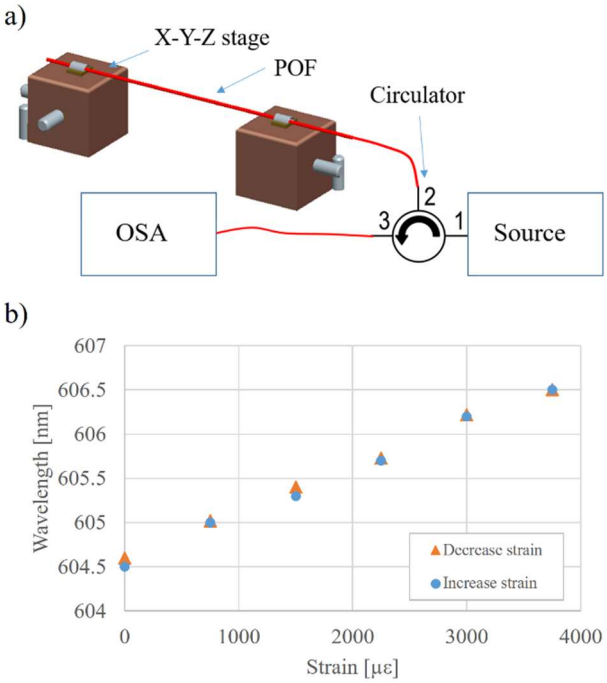

Figure 2.5.6 (a) Strain setup used. (b) Wavelength shift under different strain.

2.5.4 Discussion and Conclusion

The development of new sensors will benefit from the advantages of FBG in CYTOP fiber reported here. The refractive index of the CYTOP POF at 600 nm region is similar to the refractive index of water at 25 ºC [88] and such feature can be employed to detect oil and water layers in crude oil tanks [89]. Furthermore, this polymer is more chemically stable against chemical solutions and has a lower absorption of water than PMMA and other amorphous transparent thermoplastics [90]. These advantages make CYTOP POF sensor as a promising sensing technology in medical industry and also, as biosensors for compounds detection in aqueous solutions. Although CYTOP fibers present low optical losses at 1550 nm region, it generally needs a connectorization with silica fibers, which leads to further optical losses (see Figure 2.5.4). Moreover, the butt-coupling process is very sensitive to misalignments that results in large spectral changes in the reflection spectrum as shown in Figure 3. However, this is not a real limitation in applications using the visible wavelength range where low-cost components such as light sources, couplers and spectrometers are employed, and there is no need of butt-coupling between silica and POFs.

Visible light communications (VLC) also offer promising applications for FBGs in CYTOP POF, where they can be employed for signal routing and broadband optical source slicing [91]. Moreover, a FBG array in the visible wavelength range can also be used to generate different wavelengths from a single white light source [92] and color-shift keying (CSK) modulation can be implemented in VLCs [93].

In conclusion, we demonstrate the first FBG fabricated at 600 nm region in a commercial CYTOP POF using phase mask technology. This wavelength region is critical to be achieved by using fs laser systems due to the FBG period required. However, further efforts will be made in order to demonstrate stronger gratings. The temperature, humidity and strain characterization positively assess the use of these gratings for novel potential sensing and optical communication applications, which are also discussed. As future work we also plan to investigate the higher order modes' response to temperature and strain changes

2.6 References

1. K. O. Hill, Y. Fujii, D. C. Johnson, and B. S. Kawasaki, "Photosensitivity in optical fiber waveguides: Application to reflection filter fabrication," Appl. Phys. Lett. 32, 647 (1978).
2. G. Meltz, W. W. Morey, and W. H. Glenn, "Formation of Bragg gratings in optical fibers by a transverse holographic method.," Opt. Lett. **14**(15), 823–825 (1989).
3. K. O. Hill, B. Malo, F. Bilodeau, D. C. Johnson, and J. Albert, "Bragg gratings fabricated in monomode photosensitive optical fiber by UV exposure through a phase mask," Appl. Phys. Lett. **62**(10), 1035–1037 (1993).
4. Y. Qiu, Y. Sheng, and C. Beaulieu, "Optimal phase mask for fiber Bragg grating fabrication," J. Light. Technol. **17**(11), 2366–2370 (1999).
5. O. Ziemann, J. Krauser, P. Zamzow, and W. Daum, *POF Handbook*, 2nd ed. (Springer, 2008).
6. K. Peters, "Polymer optical fiber sensors - A review," Smart Mater. Struct. **20**(1), (2011).
7. A. Abang and D. J. Webb, "Influence of mounting on the hysteresis of polymer fiber Bragg grating strain sensors," Opt. Lett. **38**(9), 1376–1378 (2013).
8. A. Pospori, C. A. F. Marques, D. Sáez-Rodríguez, K. Nielsen, O. Bang, and D. J. Webb, "Thermal and chemical treatment of polymer optical fiber Bragg grating sensors for enhanced mechanical sensitivity," Opt. Fiber Technol. **36**, 68–74 (2017).
9. X. Chen, C. Zhang, D. J. Webb, G. D. Peng, and K. Kalli, "Bragg grating in a polymer optical fibre for strain, bend and temperature sensing," Meas. Sci. Technol. **21**(9), (2010).
10. A. R. Prado, A. G. Leal-Junior, C. Marques, S. Leite, G. L. de Sena, L. C. Machado, A. Frizera, M. R. N. Ribeiro, and M. J. Pontes, "Polymethyl methacrylate (PMMA) recycling for the production of optical fiber sensor systems," Opt. Express **25**(24), 30051–30060 (2017).
11. C. A. F. Marques, G.-D. Peng, and D. J. Webb, "Highly sensitive liquid level monitoring system utilizing polymer fiber Bragg gratings," Opt. Express **23**(5), 6058–6072 (2015).
12. M.C.J.Large, L. Poladian, G.W.Barton, and M. A. van Eijkelenborg, *Microstructured Polymer Optical Fibres* (Springer, 2008).
13. D. J. Webb, "Fibre Bragg grating sensors in polymer optical fibres," Meas. Sci. Technol. **26**(9), (2015).
14. G. Emiliyanov, P. E. Høiby, L. H. Pedersen, and O. Bang, "Selective serial multi-antibody biosensing with TOPAS microstructured polymer optical fibers," Sensors (Switzerland) **13**(3), 3242–3251 (2013).
15. H. U. Hassan, J. Janting, S. Aasmul, and O. Bang, "Polymer Optical Fiber Compound Parabolic Concentrator Fiber Tip-Based Glucose Sensor: In Vitro Testing," IEEE Sens. J. **16**(23), 8483–8488 (2016).
16. G. D. Peng, Z. Xiong, and P. L. Chu, "Photosensitivity and gratings in dye-doped polymer optical fibers," Opt. Fiber Technol. **5**(2), 242–251 (1999).
17. Z. Xiong, G. D. Peng, B. Wu, and P. L. Chu, "Highly Tunable Bragg Gratings in Single-Mode Polymer Optical Fibers," IEEE Photonics Technol. Lett. **11**(3), 352–354 (1999).
18. G. D. Peng and P. L. Chu, "Polymer optical fiber photosensitivities and highly tunable fiber gratings," Fiber Integr. Opt. **19**(4), 277–293 (2000).
19. R. Oliveira, L. Bilro, and R. Nogueira, "Bragg gratings in a few mode microstructured polymer optical fiber in less than 30 seconds," Opt. Express **23**(8), 10181–10187 (2015).
20. C. A. F. Marques, P. Antunes, P. Mergo, D. J. Webb, and P. Andre, "Chirped Bragg Gratings in PMMA Step-Index Polymer Optical Fiber," IEEE Photonics Technol. Lett. **29**(6), 500–503 (2017).
21. A. Pospori, C. A. F. Marques, O. Bang, D. J. Webb, and P. André, "Polymer optical fiber Bragg grating inscription with a single UV laser pulse," Opt. Express **25**(8), 9028–9038 (2017).
22. R. M. Ahmed, "Optical Study on Poly(methyl methacrylate)/Poly(vinyl acetate) Blends," Int. J. Photoenergy **2009**, 1–7 (2009).
23. C. A. F. Marques, R. Min, A. L. Junior, P. Antunes, A. Fasano, G. Woyessa, K. Nielsen, H. K. Rasmussen, B. Ortega, and O. Bang, "Fast and stable gratings inscription in POFs made of different materials with pulsed 248 nm KrF laser," Opt. Express **26**(2), 272–281

(2018).
24. C. Wochnowski, S. Metev, and G. Sepold, "UV-laser-assisted modification of the optical properties of polymethylmethacrylate," Appl. Surf. Sci. **154**, 706–711 (2000).
25. D. Saez-Rodriguez, K. Nielsen, O. Bang, and D. J. Webb, "Photosensitivity mechanism of undoped poly(methyl methacrylate) under UV radiation at 325 nm and its spatial resolution limit," Opt. Lett. **39**(12), 3421–3424 (2014).
26. C. A. F. Marques, L. B. Bilro, N. J. Alberto, D. J. Webb, and R. N. Nogueira, "Narrow bandwidth Bragg gratings imprinted in polymer optical fibers for different spectral windows," Opt. Commun. **307**, 57–61 (2013).
27. I.-L. Bundalo, K. Nielsen, C. Markos, and O. Bang, "Bragg grating writing in PMMA microstructured polymer optical fibers in less than 7 minutes," Opt. Express **22**(5), 5270–5276 (2014).
28. L. M. Pereira, A. Pospori, P. Antunes, M. F. Domingues, S. Marques, O. Bang, D. J. Webb, and C. A. F. Marques, "Phase-Shifted Bragg Grating Inscription in PMMA Microstructured POF Using 248-nm UV Radiation," J. Light. Technol. **35**(23), 5176–5184 (2017).
29. R. Min, B. Ortega, and C. Marques, "Fabrication of tunable chirped mPOF Bragg gratings using a uniform phase mask," Opt. Express **26**(4), 4411–4420 (2018).
30. Y. Luo, Q. Zhang, H. Liu, and G.-D. Peng, "Gratings fabrication in benzildimethylketal doped photosensitive polymer optical fibers using 355 nm nanosecond pulsed laser," Opt. Lett. **35**(5), 751–753 (2010).
31. C. J. S. Matos, P. I. Torres, L. C. G. Valente, I. C. S. Carvalho, and W. Margulis, "Bragg grating fabrication by the external method with 266-nm light," in *Proceedings of the SPIE, Volume 3572,* (SPIE, 1999), pp. 400–404.
32. A. Kameyama, M. Katt, and A. Yokotani, "A simplified fabrication technique for tilted fiber bragg grating for the simultaneous measurement of refractive index and temperature of liquids," J. Laser Micro Nanoeng. **9**(3), 230–233 (2014).
33. H. Deyerl, H. R. Serensen, J. B. Jensen, N. Plougmann, and M. Kristensen, "Fabrication and stability of fiber Bragg gratings for WDM applications using a 266nm CW-laser," in *Conference on Lasers and Electro-Optics* (IEEE, 2003), pp. 6–8.
34. X. Hu, G. Woyessa, D. Kinet, J. Janting, K. Nielsen, O. Bang, and C. Caucheteur, "BDK-doped core microstructured PMMA optical fiber for effective Bragg grating photo-inscription," Opt. Lett. **42**(11), 2209–2212 (2017).
35. T. A. Birks, J. C. Knight, and P. S. J. Russell, "Endlessly single-mode photonic crystal fiber," Opitcs Lett. **22**(13), 961–963 (1997).
36. A. Stefani, K. Nielsen, H. K. Rasmussen, and O. Bang, "Cleaving of TOPAS and PMMA microstructured polymer optical fibers: Core-shift and statistical quality optimization," Opt. Commun. **285**(7), 1825–1833 (2012).
37. W. Yuan, A. Stefani, M. Bache, T. Jacobsen, B. Rose, N. Herholdt-Rasmussen, F. K. Nielsen, S. Andresen, O. B. Sørensen, K. S. Hansen, and O. Bang, "Improved thermal and strain performance of annealed polymer optical fiber Bragg gratings," Opt. Commun. **284**(1), 176–182 (2011).
38. G. Woyessa, K. Nielsen, A. Stefani, C. Markos, and O. Bang, "Temperature insensitive hysteresis free highly sensitive polymer optical fiber Bragg grating humidity sensor," Opt. Express **24**(2), 1206–1213 (2016).
39. C. A. F. Marques, A. Pospori, G. Demirci, O. Çetinkaya, B. Gawdzik, P. Antunes, O. Bang, P. Mergo, P. André, and D. J. Webb, "Fast bragg grating inscription in PMMA polymer optical fibres: Impact of thermal pre-treatment of preforms," Sensors (Switzerland) **17**(4), 1–8 (2017).
40. W. Yuan, A. Stefani, and O. Bang, "Tunable polymer fiber Bragg grating (FBG) inscription: Fabrication of dual-FBG temperature compensated polymer optical fiber strain sensors," IEEE Photonics Technol. Lett. **24**(5), 401–403 (2012).
41. D. Sáez-Rodríguez, K. Nielsen, H. K. Rasmussen, O. Bang, and D. J. Webb, "Highly photosensitive polymethyl methacrylate microstructured polymer optical fiber with doped core," Opt. Lett. **38**(19), 3769–3772 (2013).
42. X. Hu, D. Saez-Rodriguez, C. Marques, O. Bang, D. J. Webb, P. Mégret, and C. Caucheteur, "Polarization effects in polymer FBGs: study and use for transverse force sensing," Opt. Express **23**(4), 4581–4590 (2015).
43. C. A. F. Marques, D. J. Webb, and P. Andre, "Polymer optical fiber sensors in human life safety," Opt. Fiber Technol. **36**, 144–154 (2017).

44. A. Fasano, G. Woyessa, J. Janting, H. K. Rasmussen, and O. Bang, "Solution-Mediated Annealing of Polymer Optical Fiber Bragg Gratings at Room Temperature," IEEE Photonics Technol. Lett. **29**(8), 687–690 (2017).
45. G. Woyessa, J. K. M. Pedersen, A. Fasano, K. Nielsen, C. Markos, H. K. Rasmussen, and O. Bang, "Zeonex-PMMA microstructured polymer optical FBGs for simultaneous humidity and temperature sensing," Opt. Lett. **42**(6), 1161–1164 (2017).
46. A. Fasano, G. Woyessa, P. Stajanca, C. Markos, A. Stefani, K. Nielsen, H. K. Rasmussen, K. Krebber, and O. Bang, "Fabrication and characterization of polycarbonate microstructured polymer optical fibers for high-temperature-resistant fiber Bragg grating strain sensors," Opt. Mater. Express **6**(2), 649–659 (2016).
47. A. G. Leal-Junior, A. Frizera, and M. José Pontes, "Sensitive zone parameters and curvature radius evaluation for polymer optical fiber curvature sensors," Opt. Laser Technol. **100**, 272–281 (2018).
48. A. Stefani, S. Andresen, W. Yuan, N. Herholdt-Rasmussen, and O. Bang, "High sensitivity polymer optical fiber-bragg-grating-based accelerometer," IEEE Photonics Technol. Lett. **24**(9), 763–765 (2012).
49. J. B. Jensen, P. E. Hoiby, G. Emiliyanov, O. Bang, L. H. Pedersen, and A. Bjarklev, "Selective detection of antibodies in microstructured polymer optical fibers," Opt. Express **13**(15), 5883–5889 (2005).
50. W. Yuan, L. Khan, D. J. Webb, K. Kalli, H. K. Rasmussen, A. Stefani, and O. Bang, "Humidity insensitive TOPAS polymer fiber Bragg grating sensor," Opt. Express **19**(20), 19731–19739 (2011).
51. I. P. Johnson, W. Yuan, A. Stefani, K. Nielsen, H. K. Rasmussen, L. Khan, D. J. Webb, K. Kalli, and O. Bang, "Optical fibre Bragg grating recorded in TOPAS cyclic olefin copolymer," Electron. Lett. **47**(4), 271–272 (2011).
52. C. Markos, A. Stefani, K. Nielsen, H. K. Rasmussen, W. Yuan, and O. Bang, "High-Tg TOPAS microstructured polymer optical fiber for fiber Bragg grating strain sensing at 110 degrees.," Opt. Express **21**(4), 4758–4765 (2013).
53. G. Woyessa, A. Fasano, A. Stefani, C. Markos, K. Nielsen, H. K. Rasmussen, and O. Bang, "Single mode step-index polymer optical fiber for humidity insensitive high temperature fiber Bragg grating sensors," Opt. Express **24**(2), 1253–1260 (2016).
54. G. Woyessa, A. Fasano, C. Markos, A. Stefani, H. K. Rasmussen, and O. Bang, "Zeonex microstructured polymer optical fiber: fabrication friendly fibers for high temperature and humidity insensitive Bragg grating sensing," Opt. Mater. Express **7**(1), 286–295 (2017).
55. K. Nielsen, H. K. Rasmussen, A. J. Adam, P. C. Planken, O. Bang, and P. U. Jepsen, "Bendable, low-loss Topas fibers for the terahertz frequency range," Opt. Express **17**(10), 8592–8601 (2009).
56. K. Nielsen, H. K. Rasmussen, P. U. Jepsen, and O. Bang, "Broadband terahertz fiber directional coupler," Opt. Lett. **35**(17), 2879–2881 (2010).
57. J. Anthony, R. Leonhardt, A. Argyros, and M. C. J. Large, "Characterization of a microstructured Zeonex terahertz fiber," J. Opt. Soc. Am. B **28**(5), 1013–1018 (2011).
58. G. Woyessa, A. Fasano, C. Markos, H. K. Rasmussen, and O. Bang, "Low Loss Polycarbonate Polymer Optical Fiber for High Temperature FBG Humidity Sensing," IEEE Photonics Technol. Lett. **29**(7), 575–578 (2017).
59. I. P. Johnson, K. Kalli, and D. J. Webb, "827 nm Bragg grating sensor in multimode microstructured polymer optical fibre," Electron. Lett. **46**(17), 3–4 (2010).
60. A. Stefani, W. Yuan, C. Markos, and O. Bang, "Narrow bandwidth 850 nm fiber Bragg grating in few-mode polymer optical fibers," IEEE Photonics Technol. Lett. **23**(10), 660–662 (2011).
61. X. Hu, C.-F. J. Pun, H.-Y. Tam, P. Mégret, and C. Caucheteur, "Highly reflective Bragg gratings in slightly etched step-index polymer optical fiber," Opt. Express **22**(15), 18807–18817 (2014).
62. X. Hu, C.-F. J. Pun, H.-Y. Tam, P. Mégret, and C. Caucheteur, "Tilted Bragg gratings in step-index polymer optical fiber," Opt. Lett. **39**(24), 6835–6838 (2014).
63. G. Statkiewicz-Barabach, D. Kowal, P. Mergo, and W. Urbanczyk, "Comparison of growth dynamics and temporal stability of Bragg gratings written in polymer fibers of different types," J. Opt. (United Kingdom) **17**(8), (2015).
64. A. Lacraz, M. Polis, A. Theodosiou, C. Koutsides, and K. Kalli, "Femtosecond Laser Inscribed Bragg Gratings in Low Loss CYTOP Polymer Optical Fiber," IEEE Photonics

Technol. Lett. **27**(7), 693–696 (2015).
65. G. Woyessa, A. Fasano, A. Stefani, C. Markos, K. Nielsen, H. K. Rasmussen, and O. Bang, "Single mode step-index polymer optical fiber for humidity insensitive high temperature fiber Bragg grating sensors," Opt. Express **24**(2), 1253–1260 (2016).
66. I.-L. Bundalo, K. Nielsen, G. Woyessa, and O. Bang, "Long-term strain response of polymer optical fiber FBG sensors," Opt. Mater. Express **7**(3), 967–976 (2017).
67. W. Zhang, D. J. Webb, and G. D. Peng, "Investigation into time response of polymer fiber bragg grating based humidity sensors," J. Light. Technol. **30**(8), 1090–1096 (2012).
68. C. Broadway, D. Gallego, A. Pospori, M. Zubel, D. J. Webb, K. Sugden, G. Carpintero, and H. Lamela, "Microstructured polymer optical fibre sensors for opto-acoustic endoscopy," in *SPIE Photonics Europe* (SPIE, 2016), p. 98860S.
69. J. Bonefacino, H.-Y. Tam, T. S. Glen, X. Cheng, C.-F. J. Pun, J. Wang, P.-H. Lee, M.-L. V. Tse, and S. T. Boles, "Ultra-fast polymer optical fibre Bragg grating inscription for medical devices," Light Sci. Appl. **7**(3), 17161 (2018).
70. J. Yu, X. Tao, and H. Tam, "Trans-4-stilbenemethanol-doped photosensitive polymer fibers and gratings," Opt. Lett. **29**(2), 156–158 (2004).
71. X. Hu, D. Kinet, P. Mégret, and C. Caucheteur, "Control over photo-inscription and thermal annealing to obtain high-quality Bragg gratings in doped PMMA optical fibers," Opitcs Lett. **41**(13), 2930–2933 (2016).
72. Y. Koike and M. Asai, "The future of plastic optical fiber," NPG Asia Mater. **1**(1), 22–28 (2009).
73. Y. Luo, Q. Zhang, H. Liu, and G.-D. Peng, "Gratings fabrication in benzildimethylketal doped photosensitive polymer optical fibers using 355 nm nanosecond pulsed laser," Opt. Lett. **35**(5), 751–753 (2010).
74. D. Kowal and G. Statkiewicz-Barabach, "Microstructured polymer optical fiber for long period gratings fabrication using an ultraviolet laser beam," Opt. Lett. **39**(8), 2242–2245 (2014).
75. H. B. Liu, H. Y. Liu, G. D. Peng, and P. L. Chu, "Novel Growth Behaviors of Fiber Bragg Gratings in Polymer Optical Fiber under UV Irradiation with Low Power," IEEE Photonics Technol. Lett. **16**(1), 159–161 (2004).
76. B. T. Kuhlmey, R. C. McPhedran, and C. M. de Sterke, "Modal cutoff in microstructured optical fibers," Opt. Lett. **27**(19), 1684–1686 (2007).
77. Y. Shi, E. Tangdiongga, A. M. J. Koonen, A. Bluschke, P. Rietzsch, J. Montalvo, M. M. De Laat, G. N. Van Den Hoven, and B. Huiszoon, "Plastic-optical-fiber-based in-home optical networks," IEEE Commun. Mag. **52**(6), 186–193 (2014).
78. M. Koerdt, S. Kibben, J. Hesselbach, C. Brauner, A. S. Herrmann, F. Vollertsen, and L. Kroll, "Fabrication and Characterization of Bragg Gratings in a Graded-index Perfluorinated Polymer Optical Fiber," Procedia Technol. **15**, 138–146 (2014).
79. R. Olshansky, "Propagation in glass optical waveguides," Rev. Mod. Phys. **51**(2), 341–367 (1979).
80. C. Florea and K. A. Winick, "Fabrication and characterization of photonic devices directly written in glass using femtosecond laser pulses," J. Light. Technol. **21**(1), 246–253 (2003).
81. R. Ishikawa, H. Lee, A. Lacraz, A. Theodosiou, K. Kalli, and Y. Mizuno, "Pressure Dependence of Fiber Bragg Grating Inscribed in Perfluorinated Polymer Fiber," IEEE Photonics Technol. Lett. **29**(24), 2167–2170 (2017).
82. A. Theodosiou, A. Lacraz, M. Polis, K. Kalli, M. Tsangari, A. Stassis, and M. Komodromos, "Modified fs-Laser Inscribed FBG Array for Rapid Mode Shape Capture of Free-Free Vibrating Beams," IEEE Photonics Technol. Lett. **28**(14), 1509–1512 (2016).
83. D. Vilarinho, A. Theodosiou, C. Leitão, A. G. Leal-Junior, M. de Fátima Domingues, K. Kalli, P. André, P. Antunes, and C. Marques, "POFBG-embedded cork insole for plantar pressure monitoring," MDPI Sensors **17**(12), (2017).
84. A. Theodosiou, M. Komodromos, and K. Kalli, "Carbon Cantilever Beam Health Inspection Using a Polymer Fiber Bragg Grating Array," J. Light. Technol. **36**(4), 986–992 (2018).
85. K. Toma, Y. Masaki, M. Kusaba, K. Hirosawa, and F. Kannari, "Control of grating-coupled ultrafast surface plasmon pulse and its nonlinear emission by shaping femtosecond laser pulse," J. Appl. Phys. **118**(10), (2015).
86. Thorlabs, "Graded-index polymer optical fiber (GI-POF)," https:

//www.thorlabs.com/catalogPages/1100.pdf.

87. B. Ortega, R. Min, D. Sáez-Rodríguez, Y. Mi, K. Nielsen, and O. Bang, "Bandpass transmission filters based on phase shifted fiber Bragg gratings in microstructured polymer optical fibers," in *Proceedings of SPIE - The International Society for Optical Engineering* (2017), **10232**.
88. R. Gravina, G. Testa, and R. Bernini, "Perfluorinated plastic optical fiber tapers for evanescent wave sensing," Sensors **9**(12), 10423–10433 (2009).
89. A. G. Leal-Junior, C. Marques, A. Frizera, and M. J. Pontes, "Multi-interface level in oil tanks and applications of optical fiber sensors," Opt. Fiber Technol. **40**, 82–92 (2018).
90. M.-H. Hung, P. R. Resnick, B. E. Smart, and W. H. Buck, "Fluorinated plastics, amorphous," in *Concise Polymeric Materials Encyclopedia*, J. C. Salamon, ed. (CRC, 1999), pp. 499–501.
91. V. Performance, M. Length, T. Curtis, E. Spicer, P. W. Shumate, C. W. Lundgren, G. Optron-, V. P. S. N. J. Orost, P. Press, and N. York, "Led Spectral Slicing for Sing Le-Mode Local Loop Applications," Electron. Lett. **24**(7), 389–390 (1988).
92. L. U. Khan, "Visible light communication: Applications, architecture, standardization and research challenges," Digit. Commun. Networks **3**(2), 78–88 (2017).
93. E. Monteiro and S. Hranilovic, "Design and Implementation of Color-Shift Keying for Visible Light Communications," J. Light. Technol. **32**(10), 2053–2060 (2014).

Chapter 3

Fabrication of different types of gratings

3.1 Moiré phase-shifted fiber Bragg gratings

[JP.6] R. Min, C. Marques, O. Bang, B. Ortega, "Moiré phase-shifted fiber Bragg gratings in polymer optical fibers" Optical Fiber Technology, 41, 78-81, 2018.

3.1.1 Introduction

Phase-Shifted fiber Bragg gratings (PS-FBG) in silica fibers have been demonstrated during the last decade as attractive very narrow filters for a variety of applications such as real-time monitoring, switching and demodulating [1][2]. Very recently published papers report PS-FBG applications also in the microwave photonics field, such as tunable bandstop-to-bandpass microwave photonic filters, which opens new perspectives for these devices [3].

It is well-known that a narrowband transmission filter can be obtained from an FBG when a single-phase shift is introduced inside the grating whose location and magnitude can be adjusted according to the desired transmission band. Moreover, multiple phase shifts can be used to tailor the transmission spectrum for wavelength demultiplexing in DWDM applications [4].

Polymer optical fibers (POFs) have several advantages over silica fibers, such as a larger elongation before breakage, a higher thermo-optic coefficient, and a lower Young's modulus. These advantages will provide a broad tuning range either straining or heating the fiber, and easy handling due to its low stiffness and therefore, lower installations cost. Although the product of bandwidth and channel length is somewhat reduced due to the higher loss [5], POFs are already extensively used in buildings, cars, trains, airplanes and other important short-range applications. Recently, the introduction of the new polymer called CYTOP [6] with reduced losses at telecom wavelengths has led to new promising applications for POFs.

FBGs in silica fibers is a very mature filtering technology both for telecommunication and sensors [7] since a large variety of high performance FBGs can be fabricated by creating a UV light induced periodic variation in the refractive index of the fiber core. Since the first polymer FBG was reported in 1999 [8], several promising devices have been demonstrated, such as embedded POF FBG sensors [9], microstructured POF (mPOF) sensors at 827nm [10], Fabry–Pérot cavity based on polymer FBG as refractive index sensor [11], FBGs in low-loss multi-mode CYTOP POFs [12], and mPOF FBG sensors in the polymer Topas [13], which is humidity insensitive. Despite of this, POF and mPOF gratings are still under research. Fast high quality FBG fabrication requires highly photosensitive fibers; so far great advances have been done in doping POFs [14]. Furthermore, previous work [15] demonstrates that grating time stability can be correctly addressed by proper fiber annealing.

High resolution applications require the fabrication of polymer FBGs with sharp characteristics which, in combination with the large sensitivity of polymers, will lead to a new generation of accurately tunable devices. Therefore, the fabrication of phase-shifted gratings in polymer optical fiber is identified as one of the challenges for the development of novel sensors or communication subsystems. However, the literature only provides a single report on a phase-shifted FBG (PS-FBG) in POFs, which was for use at THz

frequencies [16] by using a point-by-point FBG fabrication method. In terms of minimizing fabrication times of gratings, a 248 nm UV laser was employed to fabricate FBGs in benzyl dimethyl ketal (BDK) doped fiber with a single UV laser pulse [17].

We report an easy way to produce PS-FBGs in POF with the phase-mask technique to achieve quality gratings for photonics applications. Here we use two gratings with slight different periods, which have been superimposed in the fiber in order to form a Moiré structure with a π phase shift in the center of the device [18]. A very narrowband transmission filter is achieved using two UV pulses of 15 ns duration [19] each one, and strain and temperature sensitivities are provided.

3.1.2 Phase-shifted Moiré FBG fabrication

A PS-FBG consists of a grating where a discrete phase shift is inserted at a certain point inside the grating. Punctual modification of the refractive index of the fiber core or relative spatial shift of the fiber with respect to the phase mask, when using phase-mask based grating fabrication, are alternatives to fabricating a PS-FBG, although both require very high spatial resolution equipment.

However, the phase-shifted structure can be reproduced as a Moiré grating, where two gratings of equal amplitude but different periods, $\boldsymbol{\Lambda_1}$ and $\boldsymbol{\Lambda_2}$ superimposed [18]. This structure has one rapidly and one slowly varying envelope, which periods are $\boldsymbol{\Lambda_s}$ and $\boldsymbol{\Lambda_c}$, respectively, as shown in Figure 3.1.1(a) and there is an intrinsic π phase-shift at the crossover point. According to the theory, other phase shift values can be achieved by super-imposing gratings with different amplitudes and multiple phase-shifts can be obtained either by using longer gratings or by changing $\boldsymbol{\Lambda_1}$ or $\boldsymbol{\Lambda_2}$ while the grating length is maintained.

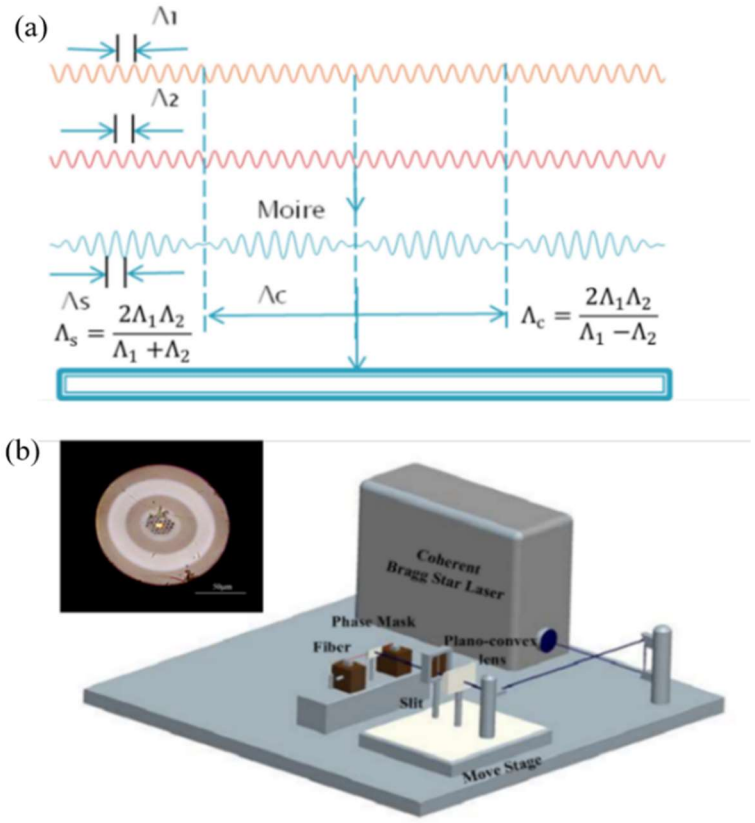

Figure 3.1.1 a) Moiré grating structure. b) Experimental setup for FBG fabrication, inset: Transverse structure of the mPOF.

In our setup, a 248 nm Coherent Bragg Star Industrial-LN krypton fluoride (KrF) emitting an output pulse power of 2.5 mJ energy and 15 ns duration was employed for grating inscription. A slit was employed to control the width of the beam. The fiber was mounted horizontally in between two v-grooves with 0.1% strain and the beam was focused onto the fiber using a plano-convex cylindrical lens (Newport CSX200 AR.10) (see Figure 3.1.1(b)). A mPOF made of PMMA with a three-ring hexagonal cladding microstructure (see Fig. 3.1.1(b) has a hole-to-pitch ratio of 0.47 with an average hole diameter of 1.74 μm and an average pitch of 3.70 μm [19], which makes it close to endlessly single-mode. The fiber core is doped with BDK to increase the photosensitivity to UV [19]. Before use the fiber, it was annealed for 24 hours at 70 ºC. The UV light was passed through a 567.80 nm pitch phase mask over a 2.5 mm fiber length. Initially, a first uniform grating with a period of 289.4 nm was fabricated with one pulse shown in Figure 3.1.2. The fiber was manually connectorised with around 4 dB insertion losses per connector. An Optical Spectrum Analyzer (YOKAGAWA AQ6373B) was employed to measure the grating spectral response with 0.01 nm resolution bandwidth. According to Figure 3.1.1 (a) and provided the grating length L_0=2.5 mm is equal to Λ_c and the fiber length between two flexure stage accessories L is 202 mm, the required pitch of the second grating can be calculated:

$$\Lambda_2 = \frac{L_0 \Lambda_1}{L_0 - 2\Lambda_1} = 289.47 \text{ nm} \tag{3.1}$$

During the second grating fabrication, the fiber length is $L + \Delta L$, which can be calculated as follows:

$$\Delta L = \frac{\Lambda_2 - \Lambda_1}{\Lambda_1} * L = 0.046 \text{ mm} \tag{3.2}$$

Therefore, since both gratings are spatially superimposed, a Moiré grating is obtained and a phase shift is formed inside [18].

Figure 3.1.2 shows the reflected signal of the first uniform grating and also when the second grating is overlapped with two pulses irradiation, where a phase shift has appeared. The new opened reflection 3 dB band is 0.035 nm. Repetitive experimental results confirm that a PS-FBG can be easily achieved by this method.

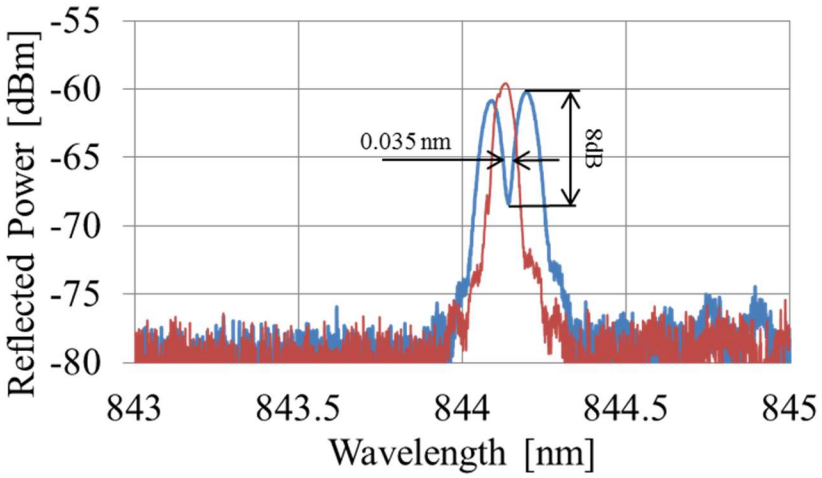

Figure 3.1.2 Reflected power of uniform grating and phase shifted grating.

The simulation of the response of a single phase shifted grating can be easily done by inserting a phase shift matrix with Matrix method [20]. Figure 3.1.3 shows the theoretical and experimental PS-FBG transmission and reflectivity response of one grating. The full

width at half-maximum of the FBG stopband is about 0.1 nm and, as a result of the phase-shift, a sub-picometer transmission band appears with 3 dB insertion losses. The PS-FBG reflectivity of both peaks (#1 and #2), separated by the notch are more than 80%. The experimental results fit well with the simulation results where the slight difference could be due to any non-homogeneity from UV laser beam, imperfections in the POF manufacturing, or even the real grating length inscribed to be less than the phase mask length.

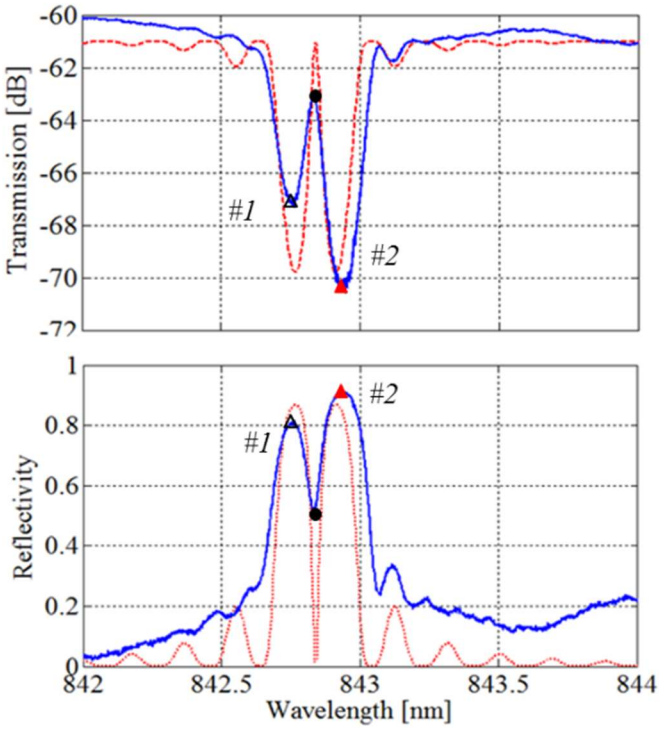

Figure 3.1.3 Experimental (dashed blue line) and simulations (solid red line) of the spectral response of the PS-FBG: (a) transmission, (b) reflectivity.

As explained above, this method can be easily employed to obtain multiple phase shifted gratings by changing Λ_2 (see eqs. (1) and (2)). Figure 3.1.4 depicts the reflectivity response of a PS-FBG based on Moiré structure resulting from the second grating fabricated with ΔL = 0.0705 mm, which corresponds to Λ_2= 289.501 nm (Λ_c= 1.875 mm), according to eq. (2) and therefore two phase shifts are encountered as expected along the 2.5 mm long grating, as expected from Figure 3.1.1. Furthermore, the experiment also confirmed three phase shifts when the second overlapped grating is written using ΔL = 0.0936 mm, which results to Λ_2= 289.534 nm (Λ_c= 1.25 mm).

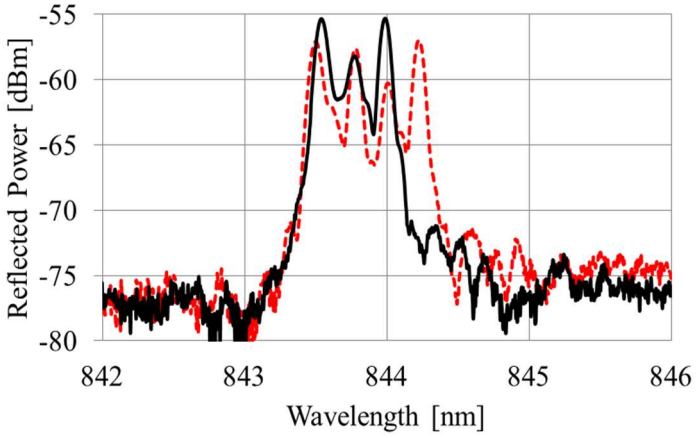

Figure 3.1.4 Reflection power of multiple phase shifted FBGs (solid line, two PS-FBGs, dashed line, three PS-FBGs).

3.1.3 Strain and temperature characterization

In this section, the fabricated PS-FBGs were tested under different strain and temperature. The PS-FBG was placed into a translation stage to strain the fiber stepwise in time. The evolution of wavelength and reflectivity for both peaks and notch of the PS-FBG reflectivity spectrum was monitored when the strain was changed from 0 to 1.1% every 5 min at room temperature, as depicted in Figure 3.1.5 (a). A wavelength shift of 7.32 nm was observed with respect to the unstrained grating, which indicates a linear strain sensitivity of 0.708±0.005 pm/με for both peaks and notch (see Figure 3.1.5 (a), which is similar with the previous uniform FBGs in annealed POFs [15]. Figure 3.1.5 (b) indicates the reflected power increases slightly with strain as expected for uniform polymer FBGs for this range of strain [21].

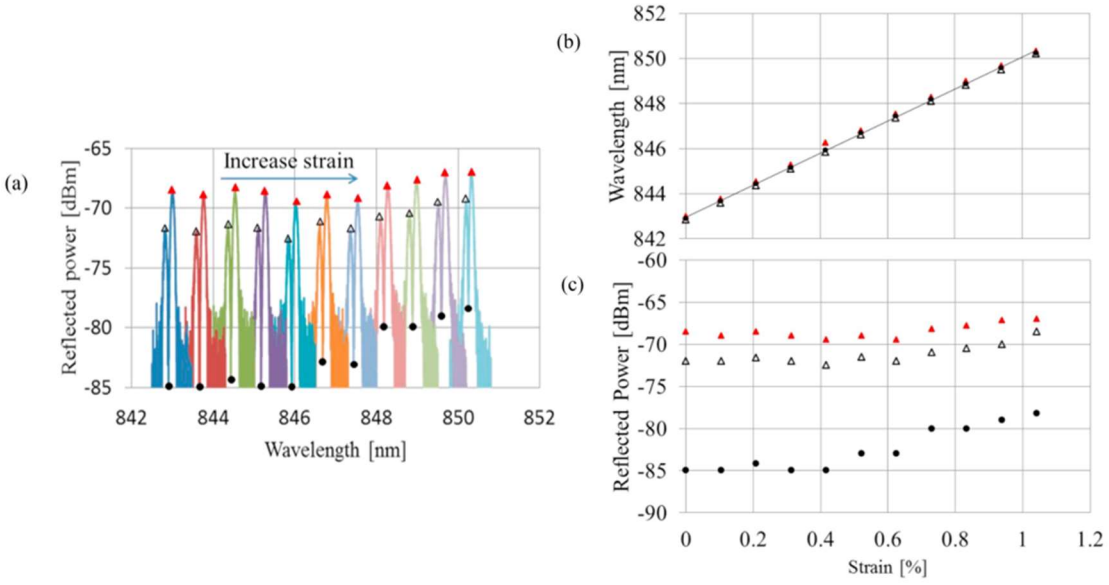

Figure 3.1.5 (a) Spectra behavior with the increase of strain, (b) Central wavelength changes and (c) maximum reflected power for both peaks (#1 and #2) and notch of the PS-FBG under different strain. (Black triangles: peak #1 of the PS-POFBG; black circles: notch of the PS-POFBG; red triangles: peak #2 of the PS-POFBG).

Temperature sensitivity is measured with other fabricated PS-FBG to avoid the effect of strain measurement. The grating was put on a Peltier plate which contains a small v-groove and the temperature was controlled by a temperature electronic controller. Some silicone grease was placed on the fiber to increase the temperature conduction. We measure wavelength and reflected power response of the grating from 25 °C to 55 °C every 5 min. The total wavelength shifts about 2.00 nm with temperature increase from 25 °C to 55 °C. The achieved temperature sensitivity was about -0.069 ± 0.005 nm/°C, after fitting to a linear model. It can be seen that a 2 nm change can be achieved with a temperature variation of only 30 °C, which is bigger than the attained in silica PS-FBG by some hundreds-degree temperature variation (~10.3 pm/°C) [22]. Also, this achieved temperature sensitivity is similar to the values already reported for uniform FBGs in the same polymer fiber [23].

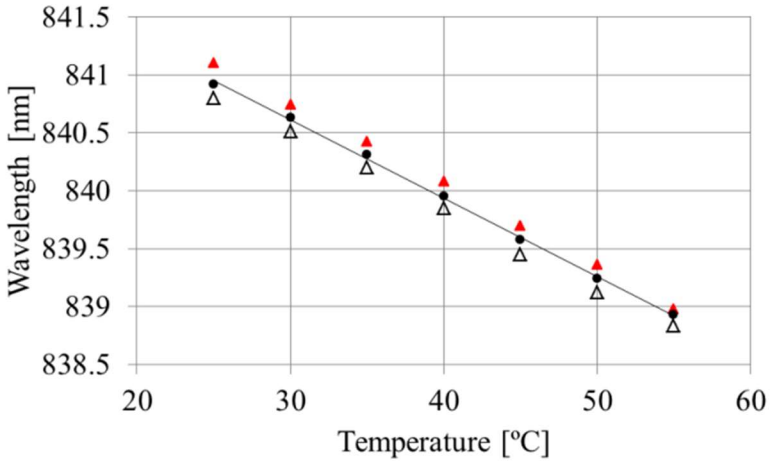

Figure 3.1.6 Wavelength responses of one PS-FBG under different temperature.

3.1.4 Conclusions

In conclusion, we demonstrate a simple method to fabricate of PS-FBGs in POFs using the phase mask technique. We obtained the phase shift by superimposing two quasi similar uniform fiber Bragg gratings to form a Moiré structure by using two UV pulses irradiation for each grating. Furthermore, the flexibility of such technique has been shown by fabricating gratings with multiple phase shifts. POFs are very attractive for the deployment of current and future high bandwidth access networks and the phase shifted devices open new opportunities for applications in WDM networks and also for microwave photonic applications. Strain and temperature sensitivity have been measured as suitable for future highly tunable devices, which will be developed based on easy handling and low cost materials provided stress relaxation issues and related stability are correctly addressed.

3.2 Tunable chirped mPOF Bragg gratings

[JP.7] R. Min, B. Ortega, C. Marques, "Fabrication of tunable chirped mPOF Bragg gratings using a uniform phase mask" Optics Express, 26(4), 4411-4420, 2018.

3.2.1 Introduction

Chirped Bragg gratings are promising devices in optical fiber technology due to their well-known applications such as dispersion compensation [24], beam forming [25], microwave photonics filtering [26] and a variety of sensing applications [27][28]. Several different chirping methodologies have been demonstrated in silica fiber. Previous works demonstrate chirped gratings fabrication by using refractive index gradient [24], temperature gradient [29], strain gradient [30] and also, varying the period of the grating [31]. Actually, the use of chirped phase mask is the most convenient way to fabricate chirped Bragg gratings by a single exposure process. This method offers high repeatability and easy implementation. However, fabricated gratings are limited by the phase mask chirp and a number of phase masks are required to fabricate gratings with different chirp parameters, which leads to an expensive technique. Oppositely, chirped Bragg gratings irradiated under strain gradient offer flexibility since the fiber is subjected under strain which is modified during the UV beam scanning and therefore, the chirp parameter can be accurately controlled [30]. Furthermore, non-uniform fiber diameter is obtained by tapering the fiber and applied strain results in a strain gradient. Consequently, different chirp parameters can be obtained by accurately control of the etching process [32].

Polymer optical fibers (POFs) have some advantages compared to silica fibers, such as a lower Young's modulus, a higher thermo-optic coefficient and a larger elongation before breakage which are exploited in a large variety of applications in sensing and telecommunications field [5][33][34][35]. Fabrication of polymer optical fiber Bragg gratings (POFBGs) is under research during the last two decades where recent achievements include uniform fiber Bragg gratings (FBGs) [5], birefringent Bragg gratings [36], tilted fiber Bragg gratings [37] and phase-shifted grating [17]. Unlike chirped Bragg gratings fabrication in silica fiber is a mature technology, chirped gratings in POFs are still a challenge. In 2005, a simple method based on axial tension and uniform heating was theoretically proposed to obtain linearly chirped Bragg gratings in POF tapers [38]. However, the first chirped POFBG was successfully fabricated by using a chirped phase mask in 2017 [39]. Nevertheless, this latter result was obtained by using special phase masks, leading to expensive and fixed fabrication parameters. Flexible fabrication techniques based on uniform phase masks are then required to be adopted as mass production of these optical components for different applications.

Regarding the UV-induced refractive index change in POF, high photosensitivity benzyl dimethyl ketal (BDK) doped microstructured POFs (mPOFs) have been recently reported [40][41]. The use of 248 nm UV pulsed laser system has been proposed to obtain the shortest time Bragg gratings fabrication with a single pulse Bragg gratings fabrication in doped fibers [19] and with few pulses using undoped fibers [42].

To the best of our knowledge, we present the first chirped Bragg grating in POF fabricated by using a uniform phase mask. Tapered optical fibers in the grating segment are employed in combination with strain in order to obtain tunable chirped Bragg gratings in microstructured BDK core doped POF.

3.2.2 Basics of chirped Bragg grating using tapered fibers

Considering a grating written in a tapered fiber with radius profile r (z) under external tension F along the fiber axis. The Bragg wavelength, λ_B, shifts $\Delta\lambda_B$ (z) at z position, which can be calculated as [32]:

$$\frac{\Delta\lambda_B(z)}{\lambda_B} = (1 - p_e)\frac{F}{\pi E r(z)^2} \tag{3.3}$$

where E is Young's modulus and $p_e = 0.04$ is the photoelastic constant for polymer material. As a result, the inscription of a Bragg grating using a phase mask with uniform period leads to a chirped grating with a chirp profile given by the radius profile of the taper and the tension applied to the fiber during fabrication. The Bragg wavelength along the grating is given by:

$$\lambda_B(z) = \lambda_B(0) + \Delta\lambda_B \cdot f \tag{3.4}$$

where $\lambda_B(0)$ is the Bragg wavelength at z=0 and $\Delta\lambda_B$ is the total chirp of the grating. The chirp function of the chirped gratings f (z) and the fiber radius r (z) are related by the following expression [32]:

$$r(z) = \frac{r(0)r(L)}{\sqrt{[r(0)^2 - r(L)^2]f(z/L) + r(L)^2}} \tag{3.5}$$

where L is the grating length. Therefore, by accurate control of r (z), it is easy to obtain various chirped grating profiles when the external tension is applied.

3.2.3 Experimental chirped fiber Bragg grating with etched technology

All fibers used in this work were pre-annealed at 70 ºC for 12 hours, to remove any residual stresses created during the drawing process and also to remove possible twists present on it. Each fiber sample (long POF pieces up to 20 cm) were cleaved using a portable cleaver [43] and attached to demountable FC/PC connectors in order to simplify the interrogation of the POFBG. The use of tapered POFs to fabricate Bragg gratings with high performance utilizing the material changes exhibited in the POF due to etching process was well demonstrated in [44]. Pure acetone can be efficiently used to remove the cladding of PMMA POF. Two different POFs were used: a) PMMA mPOF with a three-ring cladding microstructure and BDK doped core close to endlessly single-mode (Fiber 1) [40] and b) Endlessly single-mode PMMA mPOF with BDK produced using the selected center hole doping technique (Fiber 2) [41]. Fiber 1 shows an average hole diameter and pitch of 1.74 μm and 3.7 μm respectively, with the external and core diameter of 130 μm and 8 μm, respectively. The ratio of the hole diameter to the pitch was calculated to be 0.47, therefore, the fiber could have either a single or a few modes, depending on the wavelength. Fiber 2 has the average hole diameter and pitch of 1.5 μm and 3.79 μm, respectively. Thus, the ratio of the hole diameter to the pitch was calculated to be 0.4, confirming that the mPOF is endlessly single-mode [41]. The diameters of the core and the cladding are 6 μm and 150 μm, respectively. Each piece of fiber used in this work was tilted and immersed in a container full of acetone in order to get different radius along the fiber based on the volatile property of acetone (see Figure 3.2.1(a)). The etching time depends on the required cladding thickness [45]. Figure 3.2.1(b) shows an example of linearly tapered fiber with L = 1 cm, r (0) = 64 μm and r (L) = 55 μm. Due to the limited of microscope sight, here we just show a part of L, instead of the total length.

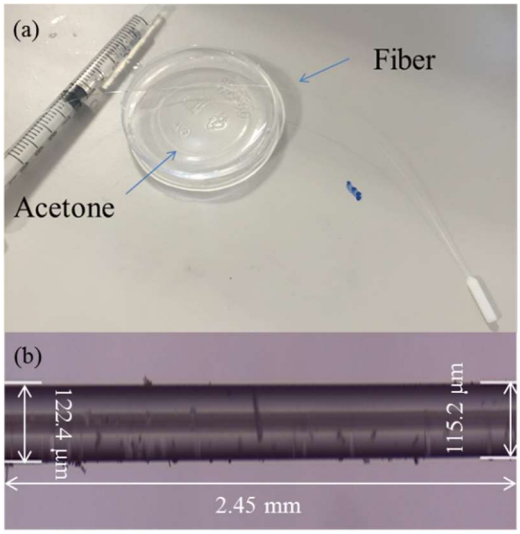

Figure 3.2.1 (a) Photograph of acetone container, (b) Linearly tapered fiber profile showing a part of L.

A Coherent Bragg Star Industrial-LN krypton fluoride (KrF) excimer laser system operating at 248 nm wavelength was employed for the chirped Bragg grating inscription with a 2.5 mJ energy per pulse. The laser beam profile was measured as a rectangular Tophat function of 6.0×1.5 mm^2 size and divergence 2×1 $mrad^2$. The laser beam is focused in the fiber core utilizing a plano-convex cylindrical lens (Newport CSX200AR.10) with effective focal length of 200.0 mm. The effective spot size of the beam on the fiber surface is 16.0 mm in width and 32.4 µm in height. For the grating inscription, we used the typical phase mask technique as depicted in Figure 3.2.2. A 10 mm long uniform phase mask, which defines the physical length of the grating structure, of 567.8 nm period was employed in the setup and the grating is subjected to 1% strain during fabrication. The reflected optical power by the FBG was monitored during irradiation by employing a super luminescent diode (Superlum SLD-371-HP1) and an optical spectrum analyzer (Yokogawa AQ6373B) with 0.02 nm resolution bandwidth. A cross-section image of the Fiber 1 is shown in inset of Figure 3.2.2.

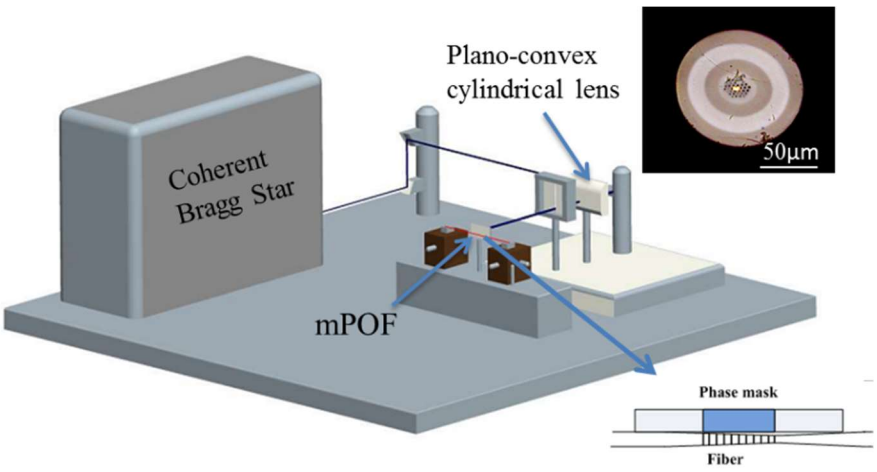

Figure 3.2.2 (a) Experimental setup for chirped Bragg grating inscription based on uniform phase mask. Inset: mPOF cross-section (Fiber 1).

Figure 3.2.3 shows the 1 cm long grating response of Fiber 1 just after fabrication where a 0.26 nm chirp was created due to 1% strain applied to the 1 cm long linear taper where initial and final diameter are 128 μm and 110 μm, respectively, being (r (0) = 64 μm and r (L) = 55 μm), which leads to a taper of 9 μm/cm. Figure 3.2.3 also shows a uniform Bragg grating with the sake of comparing it with the chirped grating obtained under 1.0 % strain. We can observe that the uniform Bragg grating, fabricated on a not tapered optical fiber piece under 1% strain, reflects a narrower and stronger bandpass compared with the chirped one [5]. The higher bandwidth of the chirped grating is directly related with the linear variation of the period since the resonance condition occurs for various wavelengths, resulting in a grating with a bandwidth much higher than conventional FBGs.

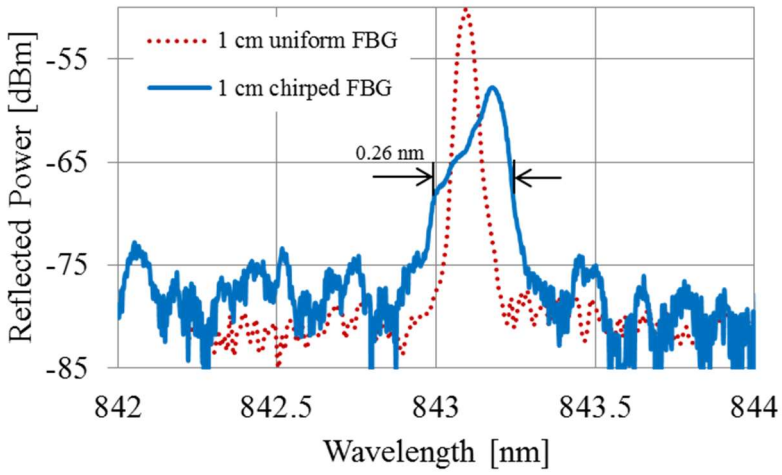

Figure 3.2.3 Reflected optical power by the FBG fabricated on a 1% strained tapered fiber section obtaining a chirped FBG. Also, reflected spectrum of a uniform FBG for comparison with chirped grating after irradiation.

It shall be noted that the method used in this work is applying tension to the fiber during the inscription process. The grating is chirped during inscription due to the stress-optic effect caused by the strain gradient along the fiber. When the tension is removed, the chirp due to the stress-optic effect disappears, but another chirp is developed as different parts of the taper relax differently from the initial strain gradient. The same phenomenon occurs using tapered silica fibers [46]. Using this method presented here, the chirped grating can be packaged as strain-free. It can create a larger chirp (than the method with no strain applied) for the same applied strain level, because the stress-optic effect has an opposite sign to the lengthening effect, and a chirp cancellation occurs.

Then, after two minutes of the fabrication we increase the strain to demonstrate the stability of the chirped grating. Figure 3.2.4 shows the spectrum of the reflected power when 1.3% strain was applied; the initial bandwidth was 0.7 nm (see red line in Figure 3.2.4 (a)) but it increased up to 1.25 nm in 160 s (see blue line in Figure 3.2.4 (a)) due to the photosensitivity increase of BDK doped fiber, similar to post growth performance described in [19]. Figure 3.2.4 (b) shows the chirped POFBG reflected bandwidth response evolution in time. From Figure 3.2.4 we can notice a slight instability of the response over the time and it shall be noted that this results were collected after two minutes of the fabrication where the grating is in growing and spectral stabilization process [19]. The time to reach stability was around 280 s and the temporal stability in this case affects the bandwidth, but surprisingly not the reflected power [19]. So far it is still not clear about the mechanism. But we do believe that the thermal stress induced by UV irradiation in POF plays an important role. The thermal stress might induce the refractive index change with an opposite sign of that induced by UV photoreactions to the polymer fiber. The polymer FBG becomes stable when the thermal stress is completely relaxed. After this, the grating

presents high level of stability for a long time (controlling the environmental room conditions).

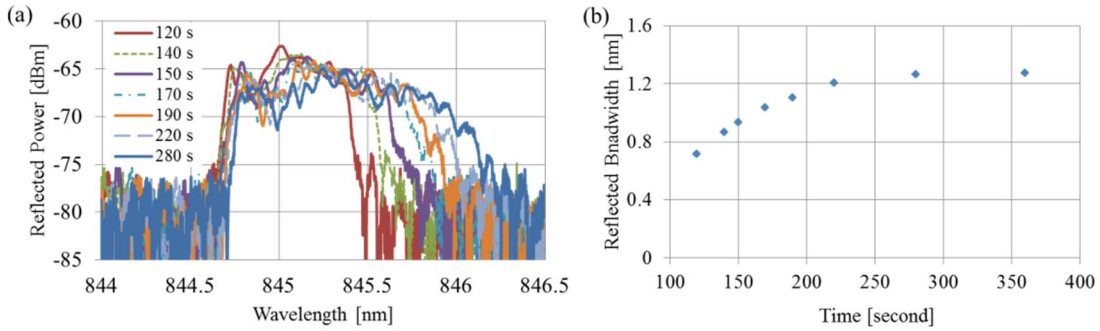

Figure 3.2.4 (a) Reflected power by chirped POFBG (Fiber 1) under 1.3 % strain two minutes after irradiation. (b) Chirped POFBG optical bandwidth response vs time during 360 seconds.

3.2.4 Strain and temperature response of chirped fiber Bragg grating

After the previous experiment, we released the strain and the resonance shifted to 835 nm with 1.6 nm bandwidth as displayed in Figure 3.2.5 (a). Similar performance happens in tapers fabrication using silica fibers where the strain gradient is formed along the grating when the fiber is held under tension producing a varying shift in the periodic refractive index and consequently, results in a tunable chirped grating [47]. As long as the strain is increased, the POFBG reflected spectral bandpass narrows up to 1% strain condition (irradiation was carried out under 1 % strain) whereas additional strain causes a central wavelength shift to longer wavelengths as well as broader bandwidths, as shown in Figure 3.2.5 (a). Figures 3.2.5 (b) and 3.2.5 (c) show the spectral response of two gratings fabricated in two different tapered sections of Fiber 1 with r (0) = 63 μm and r (L) = 59 μm (taper of 4 μm/cm) and r (0) = 64 μm and r (L) = 50 μm (taper of 14 μm/cm), respectively, under different strain conditions. The grating in Figure 5(b) shows a narrower bandwidth than the one depicted in Figure 3.2.3. Only 0.5 nm bandwidth is observed after the strain release whereas 1 nm bandwidth is measured under 1.65 % strain. However, the grating in Figure 3.2.5 (c) shows a 2.6 nm bandwidth under 1.50 % strain which is broader than others due to the strong tapered profile also showing a high strain sensitivity [48]. It shall be noted that the deep peak in reflected bandwidth of chirped fiber Bragg grating under 1.50 % strain (see Figure 3.2.6 (c)) is due to some mismatch in the position of the grating respect to the tapered section, which will become clearer with strain increase. An accurate and smooth control of such strong tapered profiles is required by using expensive and high-resolution setup.

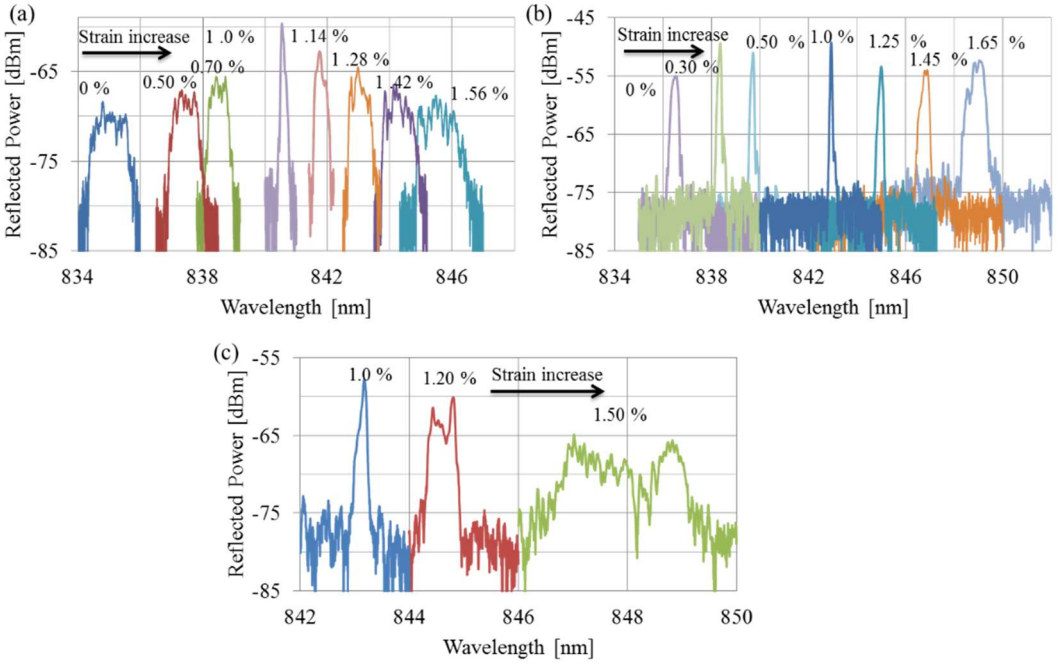

Figure 3.2.5 Chirped FBG tunability by using strain on different tapers: (a) 9 μm/cm, (b) 4 μm/cm, (c) 14 μm/cm.

The recoverability of the grating with r (0) = 63 μm and r (L) = 59 μm has been examined through the strain increasing and decreasing processes. In the experiment, the strain was gradually applied to the grating up to 1.65 % and then slowly decreased to zero strain. Judging from the variation of the resonance wavelengths and the peak intensities of the grating during the increasing-decreasing experiment, hysteresis is observed in the resonance wavelength and intensity as displayed in Figure 3.2.6. Figure 3.2.6 (a) shows a maximum variation of 4.7 dB of the peak intensities during the increasing-decreasing experiments, observed at a strain of 0.75%. Figure 3.2.7 (b) shows the maximum resonance wavelength change, around 0.5 nm, which is achieved at a strain of 0.3%. Also, Figure 3.2.6 (b) shows the chirped POFBG response as a function of the strain and an average sensitivity of 0.71 ± 0.02 pm/με is achieved. The reflected bandwidth vs strain is shown in Figure 3.2.6 (c) and indicates a great potential to explore when large strain is applied to the chirped POFBG.

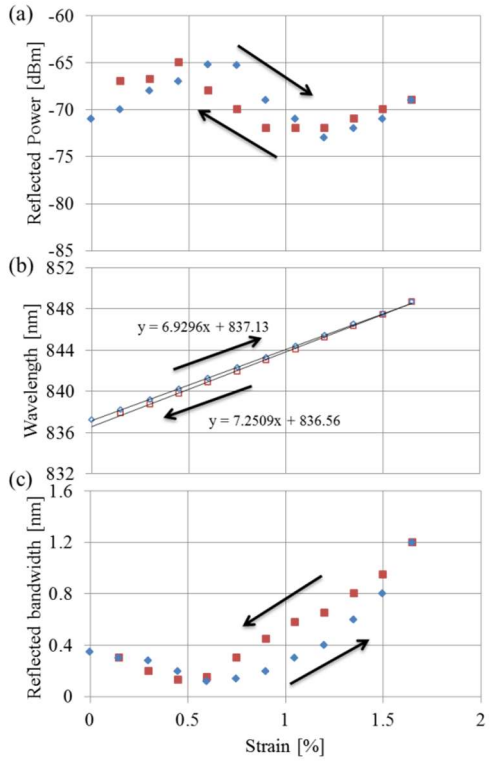

Figure 3.2.6 Strain increasing-decreasing cycle of chirped POFBG (Fiber 1): (a) reflected peak power, (b) resonance wavelength and (c) reflected bandwidth.

A tapered section of Fiber 2 [41] with r (0) = 66.5 μm and r (L) = 61 μm was irradiated to produce chirped POFBGs with the same conditions presented in previous cases. The results under different strains are shown in Figure 3.2.7(a) and indicate that etching technology for chirped POFBGs fabrication can be explored using POFs with different characteristics such as fiber diameter. From Figure 3.2.7(a) we can also achieve a high sensitivity level. The bandwidths of three different tapered samples (with both fiber types) are shown in Figure 3.2.7(b), indicating that stronger tapers lead to broader bandwidths.

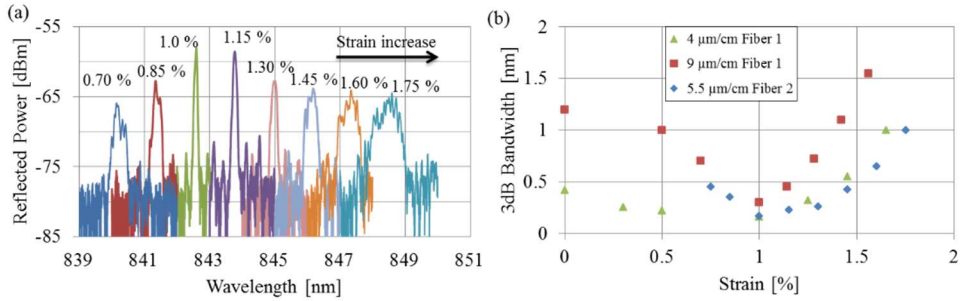

Figure 3.2.7 (a) Reflected power spectrum of a 5.5 μm/cm tapered chirped Bragg grating under different strain using Fiber 2, (b) 3dB bandwidth of POFBG using three different tapered samples vs strain.

A chirped POFBG based on Fiber 1 was placed in the climatic chamber (Angelantoni Industrie CH340) with 50% humidity under varying temperature values. The temperature was increased from 22 ºC to 52 ºC with steps of 5 ºC and each temperature value was held during 10 minutes. Figure 3.2.8 (a) shows the chirped POFBG response as a function of the temperature and a sensitivity of -56.7 pm/ºC is achieved (see Figure 3.2.8 (b)).

Regarding to reflected bandwidth response, it keeps close to stable as shown in Figure 3.2.8 (c).

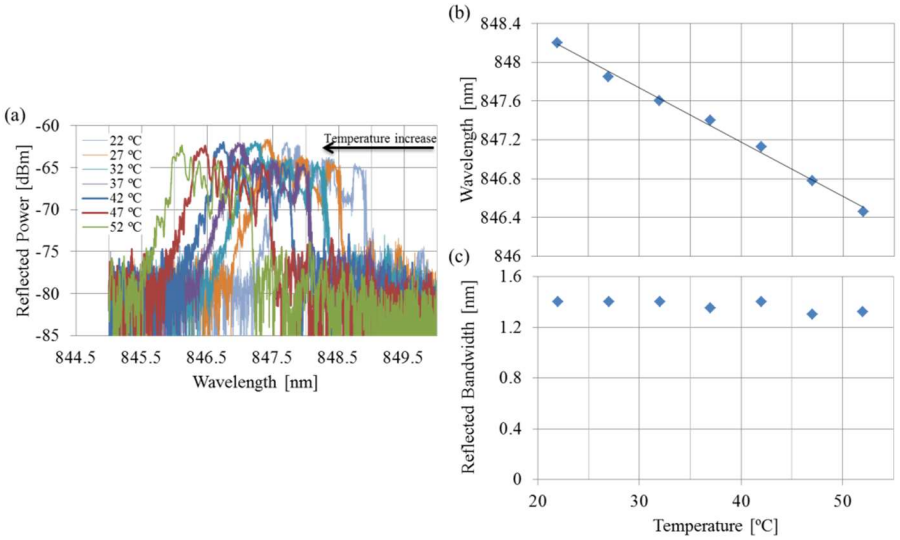

Figure 3.2.8 (a) Dependence of the reflected power spectrum of chirped FBG under 1.6 % strain on the temperature, (b) Central wavelength vs temperature under 1.6 % strain, (c) Reflected 3 dB bandwidth vs temperature under 1.6 % strain.

Figure 3.2.9 (a) shows the grating stability under two-hours monitoring in the second day after fabrication. The grating shows a stable response with less than 1.5 dB decrease in reflected power. Also Figure 3.2.9 (b) shows the same grating one week later and the measurement confirms the stability of the spectral profile and strength although higher level of noise was measured due to significant connectorization losses. A shift of 0.5 nm is observed which can be attributed to random changes in environmental conditions, such as temperature and air humidity variations, being responsible for the observed drift of the Bragg peaks positions within ± 0.5 nm margin.

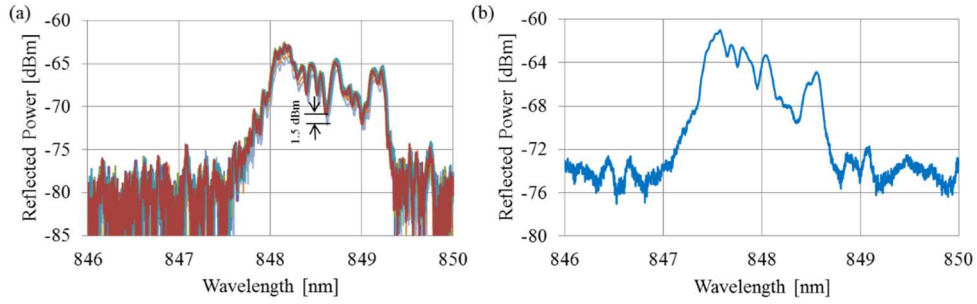

Figure 3.2.9 (a) Grating stability in two hours monitoring under 1.6% strain, (b) response after one week under 1.6 % strain.

3.2.5 Conclusion

We demonstrated the fabrication of tunable chirped Bragg gratings in polymer optical fiber using a uniform phase mask for the first time to our knowledge. Chirped POFBGs fabricated with different tapered profiles indicate the potentiality of this method. The strain and temperature sensitivity measurements demonstrate their tunability properties. By proper etching of the section we obtained 2.6 nm reflected bandwidth under 1.50 % strain, and stronger tapered profiles would lead to chirped POFBGs with broader bandwidths. This work paves the way for different photonics applications of chirped fiber Bragg grating in POF.

3.3 Hot water-assisted fabrication of Chirped mPOF Bragg grating

[JP.8] R. Min, B. Ortega, C. Broadway, C. Caucheteur, G. Woyessa, O. Bang, P. Antunes, C. Marques, "Hot water-assisted fabrication of chirped polymer optical fiber Bragg gratings" Optics Express, 26(26), 34655-34664, 2018.

3.3.1 Introduction

Polymer optical fibers (POFs) bring new opportunities for fiber Bragg grating (FBG) devices due to a lower Young's modulus and a larger range of applying strain [5]. Furthermore, POFs are ideal candidates for bio-sensing applications [49][50][51][52] due to their flexibility in bending, biocompatibility and non-brittle nature. Since the first polymer optical fiber Bragg grating (POFBG) was reported in 1999 [8], different polymer materials are used for FBG fabrication with specific purposes, such as low attenuation CYTOP [12], high temperature resistance and humidity insensitive Zeonex [53], polycarbonate [54], Topas [55], and mixtures thereof [56]. However, poly (methyl methacrylate) (PMMA) is the most common material for Bragg grating devices [5][8].

POFBGs are usually obtained using the phase mask technology, which is a simple and reliable method. However, the phase mask can only inscribe gratings with a given period, i.e., with a specific Bragg wavelength, whereas a Bragg grating centered at a different wavelength requires a new phase mask with another pitch value or using additional techniques, such as post-annealing [57], shown to provide a 230 nm tuning range [58], or straining the POF during FBG writing, shown to provide a 12 nm tuning range [59]. At the same time, non-uniform devices, such as chirped FBGs (CFBG) are attractive for other applications, such as dispersion compensation [60] and biomedical sensing [61], where POF materials show huge advantages compared with silica fibers, such as a lower Young's modulus, higher sensitivities, and biocompatibility and biodegradability [62]. In 2005, CFBGs in POF were proposed for the first time by *Liu et al.* [38] based on taper technology. Recently, the first CFBG in POF was fabricated by using chirped phase mask technology [39], whereas tunable POF CFBGs have been obtained using taper technology [63] for a variety of applications, such as bio-medical thermal detection [64] or variable delay lines [65]. The use of a chirped phase mask is expensive and not flexible, whereas taper technology needs accurate tapering process and chirp characteristic changes with strain.

Recently, *Woyessa et al.* [58] reported the effect of the relativity humidity (RH) during annealing on the properties of PMMA based POFBGs. Such effect is due to the fact that water acts as plasticizer for PMMA and lowers its glass transition temperature (*Tg*). *Fasano et al.* [66] investigated the effect of PMMA based POFBGs immersion in methanol/water solutions at room temperature, and a clear permanent wavelength blue shift was obtained after several hours although sealed conditions are required due to fast evaporation of methanol. *Pospori et al.* [67] reported a novel thermal annealing methodology for tuning POFBGs to longer wavelengths based on stretching the optical fiber with 1% or 2 % strain during the annealing process. This annealing employs hot water without a high accurate temperature control, and the same research group also demonstrated [15] that annealing under 55 °C and 60 °C temperature water can also enhance the stress and force sensitivities of Bragg gratings in POF with different response time. This effect can be explained as molecular relaxation of the polymer when the fiber material temperature is raised above the β-transition temperature [68]. All these works [15][58][66][67] focus on permanent wavelength shift of uniform POFBG.

We propose to produce permanent CFBGs by applying gradient thermal annealing to uniform POFBG which reduces the overall cost for fabricating POF CFBGs and leads to obtain flexible gratings response compared with strain tapered POF CFBG [63] or chirped phase mask fabrication techniques.

3.3.2 Polymer optical fiber Bragg grating fabrication

POFBGs were inscribed using a 248 nm KrF (Coherent Bragg Star Industrial-LN) laser system emitting 15 ns duration pulses. The fiber was an endlessly single-mode BDK-doped PMMA mPOF [41] which was fabricated in *DTU Fotonik* with the center hole doping technique. Before using the fiber, it was annealed with 55 °C hot water [15] for 10 mins. Details about the fabrication setup, POF cleaving and connection between POF and silica fiber for testing can be found in [19][43]. A uniform phase mask with 567.8 nm period was used to fabricate a 10 mm long FBG at 850 nm wavelength region. Figure 3.3.1 shows a uniform FBG reflected power spectrum after irradiation with a single pulse (15 ns of duration).

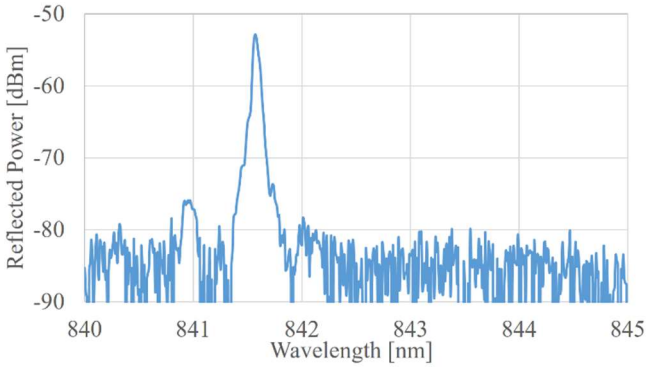

Figure 3.3.1 Reflected spectral power of a 10 mm long uniform FBG inscribed by a single 15 ns pulse.

3.3.3 Gradient thermal annealing

The setup employed for thermal annealing is shown in Figure 3.3.2 (a) where a uniform POF grating is immersed in a container (height: 2 cm, radius 6.5 cm) filled with water (~1.4 cm height). A hot plate was used to control the temperature of the water, which was monitored by a multi-function standard CEM DT-8820 environment meter. The sensor probe was immersed in the hot water and attached to the move stage, which controls the distance from the hot plate of each measurement. The reflected spectral power of the grating was monitored by a super luminescent diode (Superlum SLD-371) and an optical spectrum analyzer (AQ6373B) connected by using a silica optical fiber circulator (Thorlabs TW850R5A1). Figure 3.3.2(b) shows the temperature of the water measured at different depths of the container by moving the stage attached to the temperature sensor. As expected, the water heating by a hot plate was linear with the water depth (the temperature in the container showed a decrease of 0.23 ± 0.02 ºC/mm from the bottom hot plate). In order to get uniform thermal annealing of the POFBG with a uniform temperature, the grating must be kept parallel to the hot plate, as shown in Figure 3.3.2 (a).

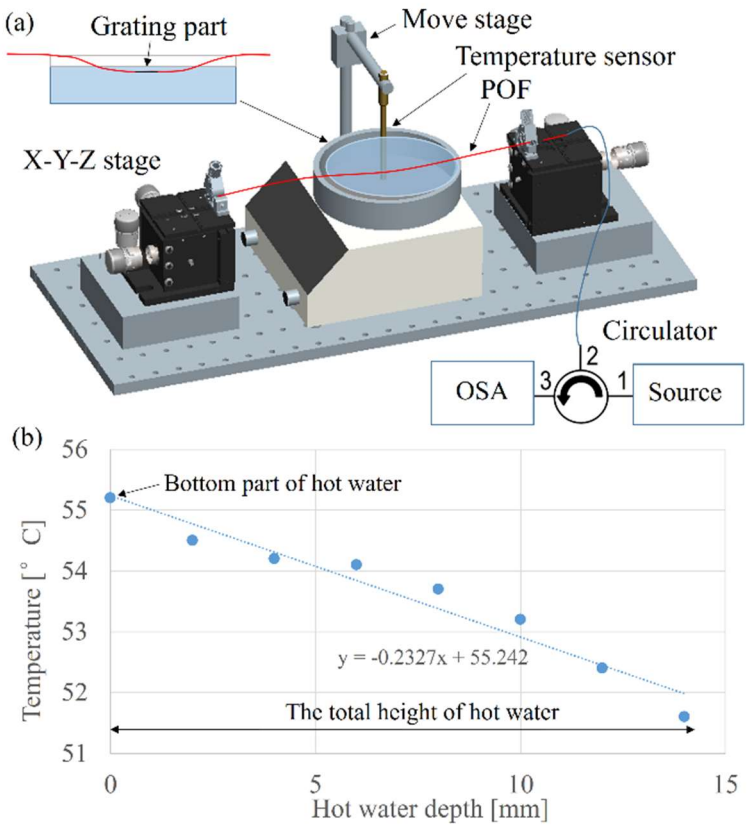

Figure 3.3.2 (a) Experimental setup for annealing POFBG, (b) Temperature vs hot water depth in the container.

Figure 3.3.3 (a) shows the Bragg wavelength shift during the annealing process with 52.5 ± 1.0 °C (grating part in ~12 mm depth of hot water). From Figure 3.3.3 (a), we can notice that the central wavelength of the grating shifts about 14 nm when the grating is brought out from the hot water after 90 mins immersion, compared to the response before immersing showing similar behavior than reported by *Pospori et al.* [15] where a uniform FBG was annealed in hot water at 55 ºC and 60 ºC. After that, we observed that the wavelength shift was stable after 10 mins, according to stability of gratings response under humidity conditions [69]. The bandwidth of the grating evolution is also plotted in Figure 3.3.3 (a). Just after immersing in hot water, the reflected power and the bandwidth increased during the first ~ 4 mins, then kept considerably stable, and the reflected spectrum bandwidth remained stable during annealing (Figure 3.3.3 (b)), similar performance reported in [70]. After this process, both the wavelength and the reflected spectrum was stable after thermal annealing, as was checked after 5 days. The wavelength shift is due to the complex heterogeneous nature of fiber shrinkage and molecular relaxation [15]. *Stajanca et al.* [68] also reported it under higher temperature, where the Bragg wavelength shift followed a more stretched exponential decay.

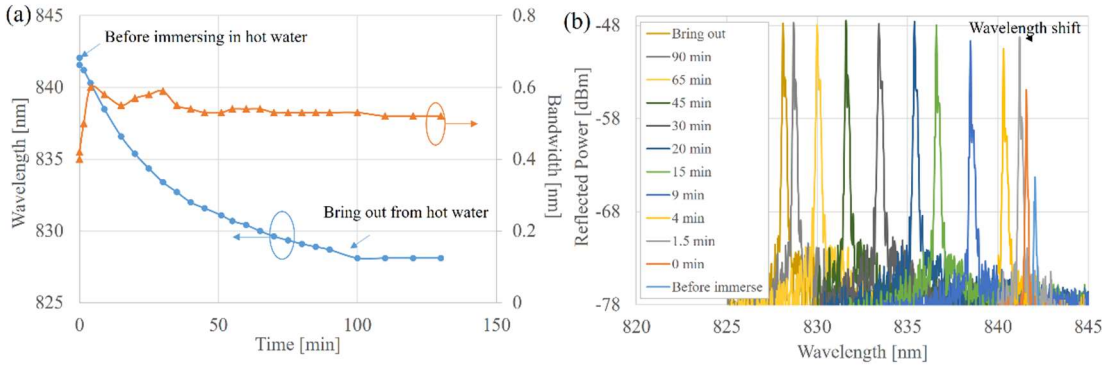

Figure 3.3.3 Measurements during uniform annealing: (a) POFBG central wavelength and bandwidth, (b) Reflected spectral power.

Next experiment aims to use the benefits of gradient temperature in a hot water container with a hot plate at the bottom. Figure 3.3.4 shows the experimental setup for gradient thermal annealing where one magnet was used to fix the POF to the bottom of the container so the grating was immersed in the hot water at an angle of 45º, chosen to avoid damage of the fiber due to strong curvatures at steeper angles. As shown in Figure 3.3.2 (b), the linear temperature change with height in the container is 0.23± 0.02 ºC/mm, so the temperature varies along the grating with 0.17 ± 0.02 ºC/mm when the fiber was oriented at 45º angle direction.

The temperature at the bottom of the container was 55.2 ± 1 ºC whereas 51.5 ± 1 ºC was measured at the top (see Figure 3.3.2(b)). Figure 3.3.5 plots the central wavelength shift with time of another FBG, similarly to Figure 3.3.3, but showing larger wavelength shift due to higher temperature at the bottom of the container, as shown in Figure 3.3.2(b). It is important to note that since the chirped gratings presented here and, in the following, have an asymmetric reflection spectrum, we define the Bragg wavelength as the center between the recorded outer edges, defined as the first minima (see marker points in Figure 3.3.3 (b)). The measurements confirm that chirped performance is obtained as Figure 3.3.5(b) shows that the bandwidth increases from 0.3 nm to ~1.1 nm, which is more than twice the bandwidth obtained with uniform annealing in Figure 3.3.3(a).But after ~20 minutes, although the central wavelength continued to decrease, the bandwidth stopped increasing with time.

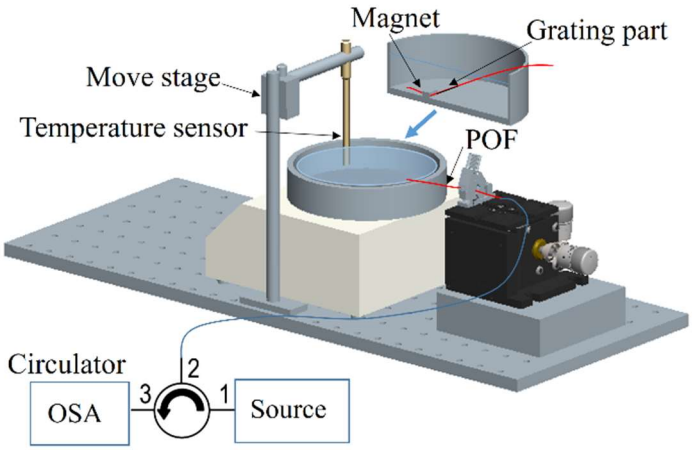

Figure 3.3.4 Experimental setup for gradient thermal annealing.

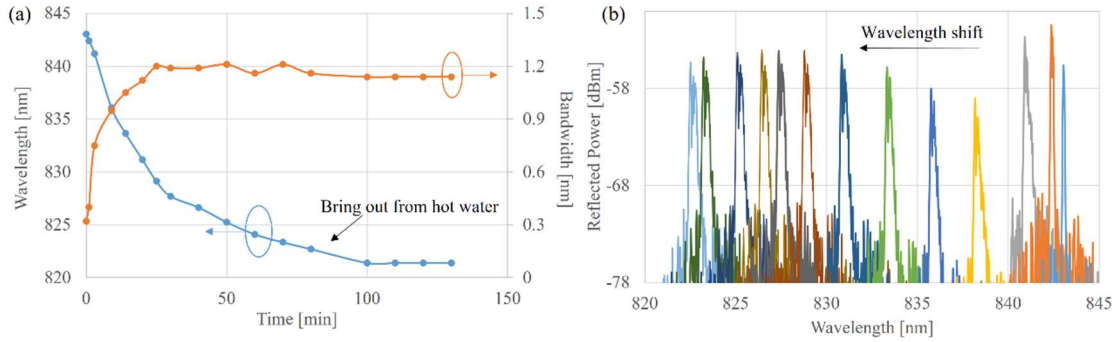

Figure 3.3.5 Measurements during gradient annealing: (a) POFBG central wavelength shift and bandwidth, (b) Reflected spectral power.

However, the obtained chirp was somewhat limited due to the limitation in the gradient thermal annealing setup, which offered ~3 ºC difference along the water container. In the following, we proposed a new method for enhanced gradient thermal annealing also based on hot water, as depicted in Figure 3.3.6. In this case, only a 4 mm section of the POFBG was immersed in the water, whereas the rest of the grating (the total POFBG length was 10 mm) was kept outside the water. Despite the room temperature was 22 ºC, the area close to the hot water container would be larger but much lower than 55 ± 1 ºC, and therefore, a higher gradient thermal annealing was obtained when compared to the fully immersed grating in hot water. Figure 3.3.7 shows the obtained results with different gratings (#1, #2 and #3) under different annealing periods. Figure 3.3.7(a) and 3.3.7(c) show the spectra obtained after up to 40 s and 155 s annealing time, respectively, showing the bandwidth increases with time, with larger values than obtained in Figure 3.3.5 (a). In Figure 3.3.7(b) and Figure 3.3.7(d) we can observe bandwidths around 1.75 nm in ~40 s and 5.5 nm in ~150 s, which lead to group delay dispersion (GDD) values of 56.5 and 18 ps/nm, respectively, in a 1cm long grating. Once the desired chirp is achieved, the grating is brought out from hot water, although the bandwidth of the grating continued to slightly increase up to 5 % as shown in Figure 3.3.7(a). It can be considered as still having a small thermal annealing effect just after bringing it out from hot water, and then was stable afterwards. Also, the wavelength shifts 1.5 ± 0.3 nm towards the blue wavelength, as shown in Figure 3.3.3 (a), according to uniform polymer FBG response after annealing with hot water [15] whereas the bandwidth keeps roughly similar. Figure 3.3.7(e) and 3.3.7(f) show the results of another experiment (Grating 3) with longer annealing time of 510 s where the grating chirp reached 11 nm bandwidth once the grating was brought out from the water with stable behavior. Of course, the specific structure of the chirped grating, i.e. reflected spectrum, depends on the actual thermal gradient over the fiber, and therefore, fine control of the grating position relative to the water surface is required. Further work is currently being done on the time delay characterization of the chirped gratings to learn about the actual structure in order to optimize the method for obtaining chirped gratings with flat spectral response.

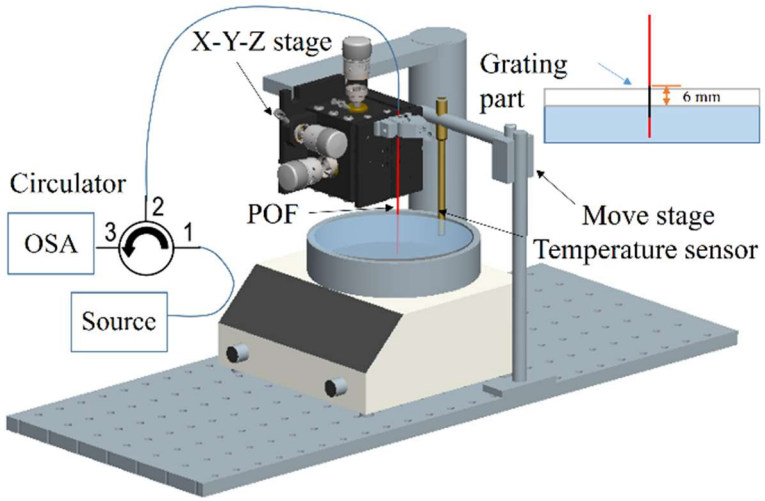

Figure 3.3.6 Improved experimental setup for gradient thermal annealing.

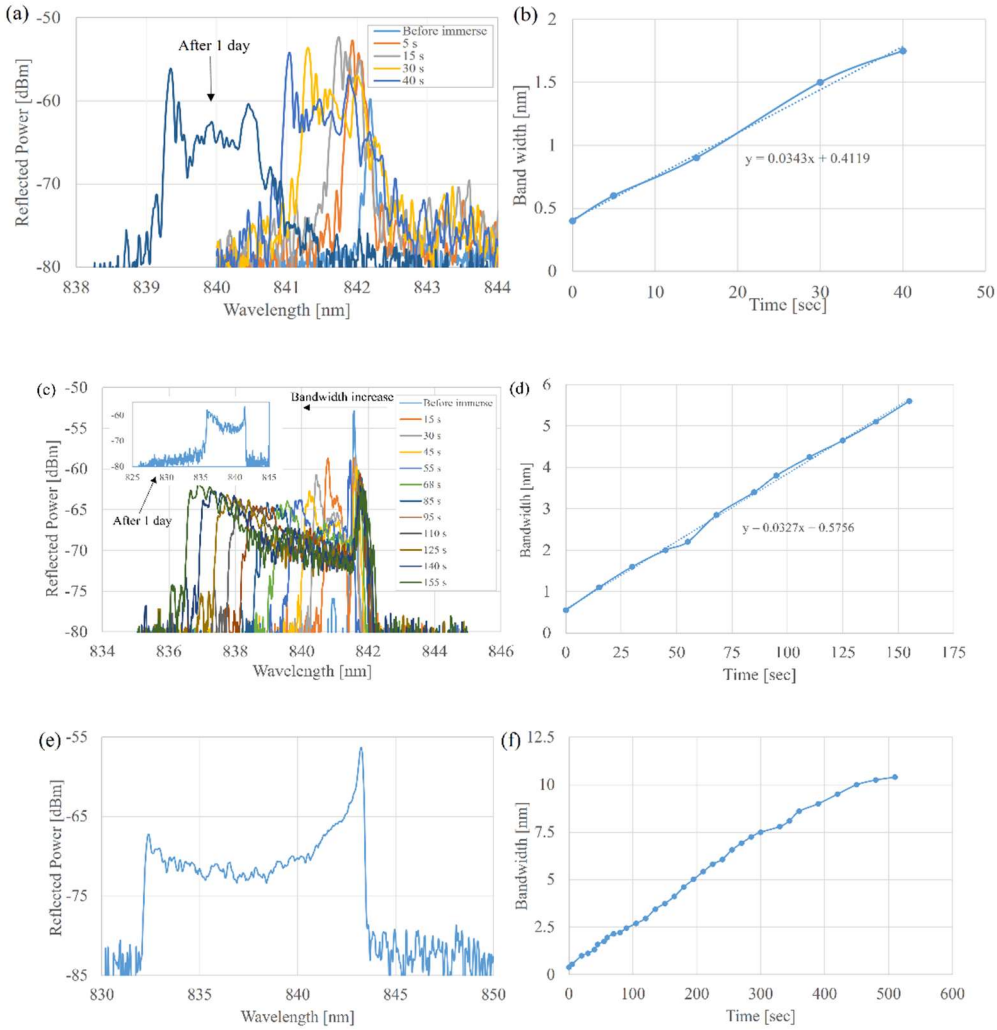

Figure 3.3.7 POFBG under strong gradient annealing: Grating #1: (a) Reflected spectral power (total annealing time of 40 s), (b) Bandwidth vs time; Grating #2: (c) Reflected spectral power (total annealing time of 155 s), (d) Bandwidth vs time; Grating #3: (e) Reflected spectral power once the grating is brought out after 510 s annealing time, (f) Bandwidth vs time (total annealing time of 510 s).

3.3.4 Characterization of POF chirped FBG

We report the full characterization of the chirped POFBG obtained in Figure 3.3.7(a) in terms of temperature, strain and humidity. The temperature sensitivity was measured by placing the grating on a Peltier plate, which contains a small v-groove and allows the temperature control by an electronic temperature controller. Some silicone grease was used to increase the temperature conduction. The central wavelength of the grating reflection bandpass was measured every 10 mins during 60 mins when temperature was changed from 27 ºC to 52 ºC in steps of 5 ºC. The central wavelength shifts towards the blue wavelengths about 3.2 nm (see Figure 3.3.8(a)), which corresponds to a sensitivity around -0.106 ± 0.005 nm/ºC, a bit higher than reported for uniform POFBGs about (-0.077 ± 0.007 nm/ºC) [59] due to the different pre-annealing conditions. The reflected power of grating increased with temperature, whereas the bandwidth and the spectrum were similar as shown in Figure 3.3.8(b), similar to the behavior shown by tapered CFBG under various temperature [63]. Although the reflected spectral power showed a non-flat profile, differently than reported in [63], note that the presence of peaks at both wavelength edges and, also, sharp slopes allow to provide precise measurements of the grating bandwidth and central wavelength as required for applications.

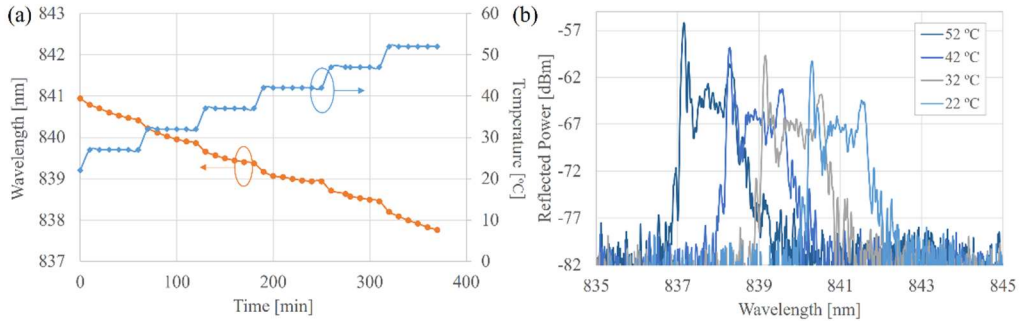

Figure 3.3.8 (a) Central wavelength shift (the center of the wavelength spacing between the first minima (nulls)) vs time when temperature is changed. (b) Reflected spectra vs temperature.

In order to characterize the strain sensitivity of the chirped POFBG, a 15 cm long fiber containing the grating was placed on the X-Y-Z translation stage and fixed with glue between two X-Y-Z stages spaced by a distance of 11.3 cm. The fiber was strained 0.18 % step-by-step awaiting 5 min between each step at room temperature. The evolution of the central wavelength was monitored when the strain was changed from 0 to 1.44 % and also, decreasing it, as depicted in Figure 3.3.9. A small hysteresis is observed in the resonance wavelength as shown in Figure 3.3.9(a). The bandwidth keeps stable during strain, which is a different performance compared with tapered CFBG [63]. A wavelength shift of 11.6 nm was observed for the applied 1.44% strain, which indicates a linear strain sensitivity of 8.05 ± 0.05 nm/%, similarly to the results obtained with annealed PMMA mPOFBG at 850 nm spectral region [15].

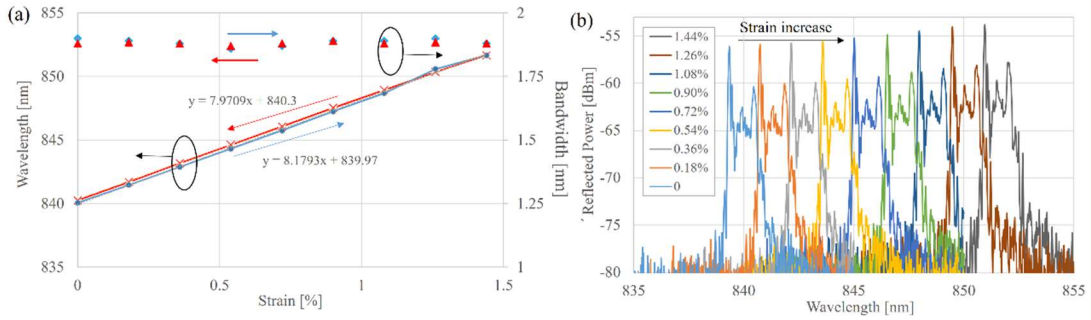

Figure 3.3.9 (a) Central wavelength during strain increasing (blue) and decreasing (red) cycle of chirped POFBG. (b) Reflected Spectra vs strain.

Finally, the chirped POFBG was placed in the temperature chamber (Angelantoni Industrie CH340) at a constant temperature of 22 ºC and 30% of relative humidity (RH) to perform the humidity characterization measurements. The RH was increased up to 90% in a step of 20% RH with a stabilization period of 70 mins. The cycle can be observed in the Figure 3.3.10(a) and the optical spectra evolution is shown in Figure 3.3.10 (b). The total wavelength shift was 1.5 nm and the sensitivity was calculated to be 0.025 ± 0.005 nm/%RH, according to the measurements shown in Figure 3.3.10, the obtained result is similar to one obtained with annealed phase-shifted PMMA mPOFBG at 850 nm spectral region [17].

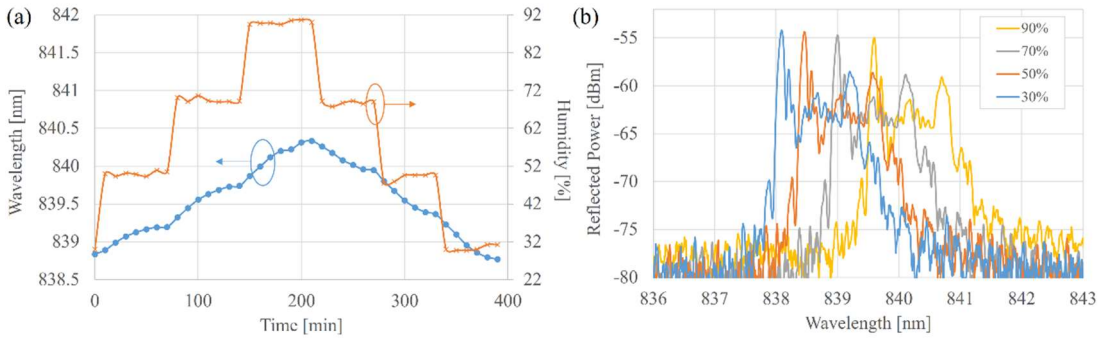

Figure 3.3.10 (a). Central wavelength of the chirped grating vs time when humidity is changed. (b) Reflected spectrum vs humidity.

3.3.5 Conclusion

We have demonstrated a new low-cost fabrication technique of chirped POFBGs based on hot water assisted gradient thermal annealing of uniform POFBGs. The proposed method is simple since no special phase mask or additional etching process is needed, and it enables an easy and flexible tuning of the wavelength and chirp performance with a permanent and stable chirp characteristic. A chirp larger than 11 nm has been obtained for the first time in less than 10 min. The central wavelength linearly changes with temperature, strain and humidity whereas the bandwidth keeps stable, similar to CFBG response when a chirped phase mask is employed for fabrication. Sensitivity measurements to external parameters have been provided for future potential applications such as high-resolution large bandwidth thermal detection in bio-sensing and delay lines in microwave photonics subsystems. Moreover, the use of liquids with different specific heat coefficients will also lead to variations on the temperature gradient. In this way, investigations of different liquids and temperature gradients will be considered as future work.

3.4 Long period gratings

[JP.9] R. Min, C. Marques, K. Nielsen, O. Bang, B. Ortega, "Fast inscription of long period gratings in microstructured polymer optical fibers" IEEE Sensors Journal, 5(1), 1919-1923, 2018.

3.4.1 Introduction

During the last two decades, long period fiber gratings (LPGs) have attracted significant attention due to their successful applications for both optical communications [71] and sensing [72]. The advantage of LPGs includes low insertion loss, ease of fabrication and low back reflection. Various LPGs based on silica fiber have been explored as WDM channel isolation filter [73], erbium-doped multi-wavelength fiber laser [74], highly sensitive refractometer [75] and sensor for different parameters such as strain [76], temperature [77], refractive index [77] and biochemical sensing [78][79]. Furthermore, properties of polymer optical fibers (POF) such as the large range of strain and small Young's modulus make LPGs even more attractive in these fibers. As a recent application, an all-plastic fiber-based pressure sensor based on LPG in microstructured POF (mPOF) has been explored [80]. However, the fabrication technology of LPGs in POF is still under research. Only a few papers mentioned the fabrication process of LPGs in mPOF [80][81][82][83]. The first LPG was fabricated in mPOF by mechanical deformation and heating [81]. UV photo inscription of LPG in mPOF was reported in 2010 with point-by-point technique [82]. Also, trans-4-stilbenmethanol was employed as external cladding dopant and demonstrated a reduced fabrication time down to six times compared to pure PMMA fibers with the same technique, which lead to reduce the coupling points as well as to shorten the irradiation time for each point (42 s against 2 min) [84]. In terms of minimizing fabrication times, which is a critical issue for commercial application, a 248 nm UV laser was used to inscribe a high quality fiber Bragg grating (FBG) in an undoped PMMA mPOF within less than 30 s [85].Then, this laser type was employed to fabricate FBGs in benzyl dimethyl ketal (BDK) doped fiber with a single UV laser pulse [19] and it holds the minimum inscription time obtained until now. As demonstrated in previous work [19], BDK dopant acts as a photo initiator which triggers a photo-polymerization process when irradiated with UV light and therefore, the photosensitivity of this fiber is increased.

We present the shortest inscription time for the LPG in an mPOF, and we also investigate the temperature and strain sensitivities.

3.4.2 Long period grating fabrication

A PMMA mPOF with 3 rings of holes and a BDK doped core was used to inscribe LPGs. The three ring cladding microstructure has a hole-to-pitch ratio of 0.47 with an average hole diameter of 1.74 um and an average pitch of 3.70 um [40], which makes it close to endlessly single-mode [86]. A cross-section image of the fiber is shown in Figure 3.4.1. The fiber was annealed for 24 hours at 70 degrees before use in order to improve stability and quality of the inscribed gratings [21]. After cleaving it with a special room temperature cleaver [43] and polishing with sand paper, the fiber was connectorized and held onto the fabrication setup under 0.1% strain, as depicted in Figure 3.4.2. A Coherent Bragg Star Industrial-LN krypton fluoride (KrF) excimer laser system operating at 248 nm wavelength was employed for the LPG inscription. The laser pulse duration was 15 ns and the pulse energy was set at 2.95 mJ. The laser beam profile was measured as a rectangular Tophat function of 6.0×1.5 mm^2 size and 2×1 $mrad^2$ divergence. It was focused onto the fiber core utilizing a plano-convex cylindrical lens (Newport CSX200AR.10) with focal length of 20 cm. The translation stage was employed to shift the laser beam with a

precision of 10 μm and a slit was employed to control the width of the beam where the point-by-point technique was employed to inscribe LPGs.

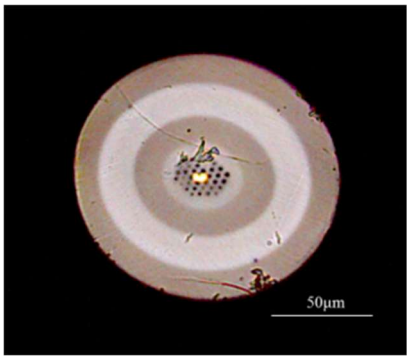

Figure 3.4.1 Cross-section of the mPOF.

The grating transmission spectrum was monitored during fabrication by using a super luminescent diode (Superlum SLD-371-HP1) and an optical spectrum analyzer (Yokogawa AQ6373B) with 0.02 nm resolution bandwidth. According to the slit width, each point was 0.2 mm long, the beam was shifted 1 mm for inscribing every point and a total of 25 steps were completed, obtaining an LPG total length of 25 mm. Each inscription point was irradiated by two pulses from the UV laser, which gives a writing time per inscription point of two 15 ns pulse with 1 Hz frequency. This is a significant reduction from the 42s per point writing time reported in a previous work [83].

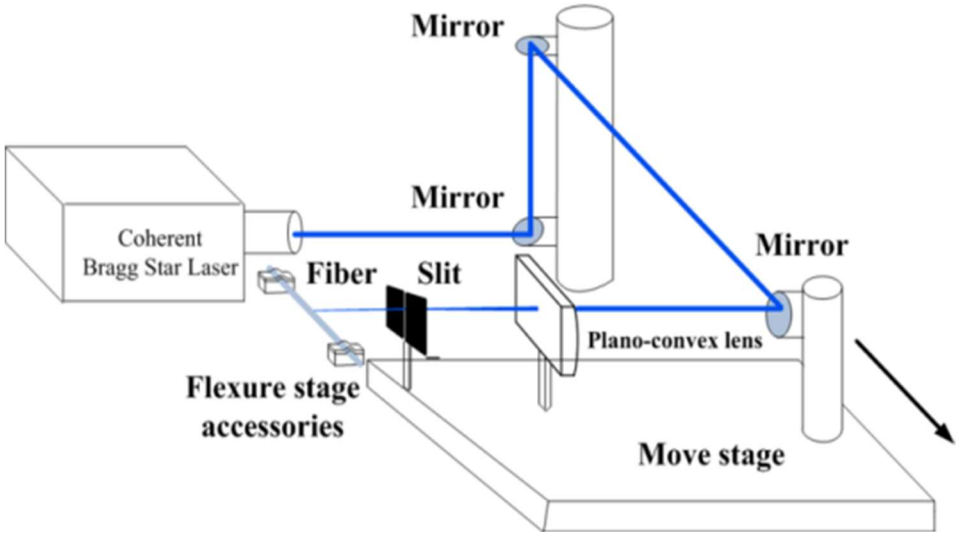

Figure 3.4.2 Experimental setup for LPG inscription.

Figure 3.4.3 shows the transmission of the LPG spectrum with only one irradiated pulse in each coupling point. The transmission of the grating was about -3.0 dB at 870.05 nm just after fabrication. The results are presented as normalized transmission response respect to the output spectrum of the optical source. According with [19], just one KrF laser pulse with a duration of 15 ns introduces a refractive index change in the fiber core with enhanced photosensitivity by the BDK dopant. Also, it shall be noted that some experiments about single and multiple pulses were already explored for FBG inscription in [19]. In this way, both one and two pulses for each coupling point would lead to LPG fabrication, where the LPG inscription of 25 mm is achieved due to the uniformity of BDK doping in the fiber.

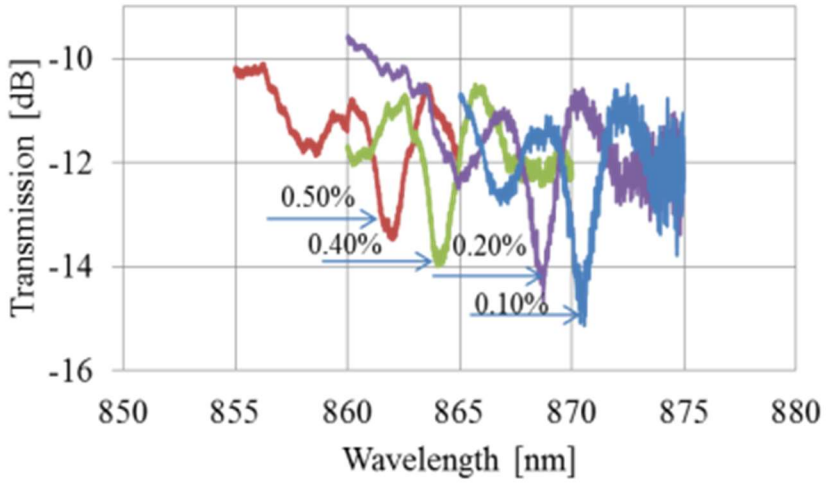

Figure 3.4.3 Transmission of the LPG with one irradiated pulse per coupling point under different strain.

Another LPG was inscribed using two pulses for each coupling point in order to obtain a stronger grating. Figure 3.4.4 shows the LPG transmission spectra just after fabrication when different levels of strain are applied. When the laser is stopped and the fiber is under 0.05 % strain, the grating peak is centered at 869. 5 nm and the transmission only drops 4.5 dB, whereas the grating peak becomes more clear when it is further strained (0.88 % and 1.0 %), and intensity reaches around 9.0 dB.

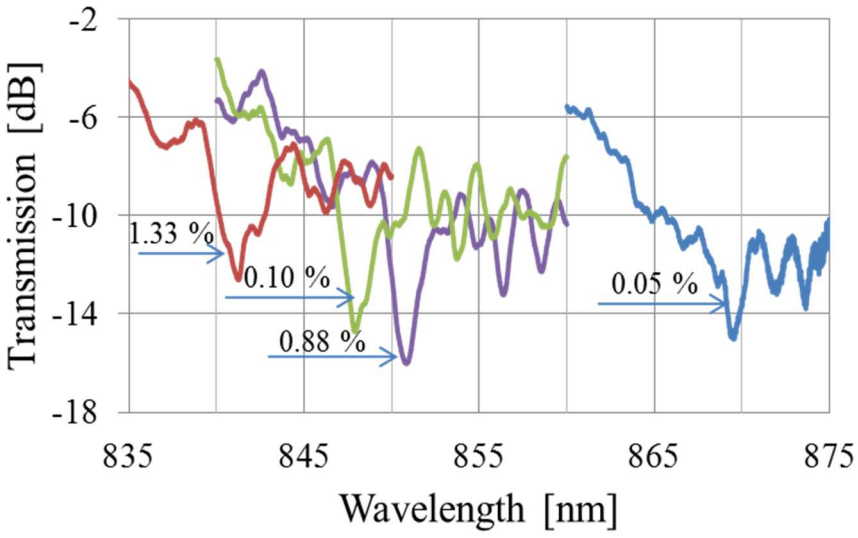

Figure 3.4.4 Transmission of the LPG under different strain after inscription with two pulses for each coupling point.

However, after two weeks, the grating response shows a -20 dB peak centered at 866.9 nm wavelength when a 0.1% strain is applied, as shown in Figure 3.4.5. Such intensity growth after fabrication has been previously reported in FBG irradiated in annealed BDK doped PMMA fibers [19] and dye-doped PMMA polymer fibers [87].

Transmission spectra were also collected after two weeks with different levels of strain measurement as shown in Figure 3.4.6, and all cases show larger resonant dip than measured spectra just after fabrication, according to Figure 3.4.4. The transmission values at the resonance of the LPG for different values of strain in figures 3.4.4 and 3.4.6 have

been plotted in Figure 3.4.7 for the sake of comparison.

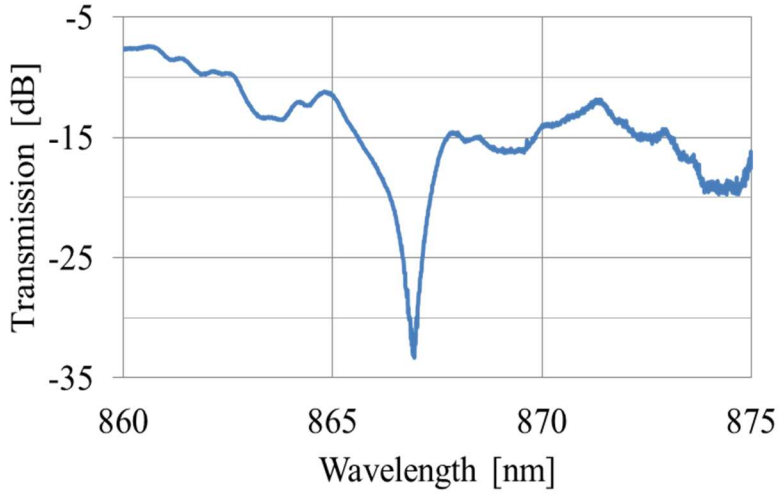

Figure 3.4.5 Transmission of LPG with 0.1% strain two weeks after fabrication.

3.4.3 Strain and temperature characterization

In the following, we measured the strain and temperature sensitivities of the fabricated LPGs in order to complete their characterization. To measure the former one, a 22 cm long connectorized fiber including an inscribed LPG was fixed with epoxy glue on the flexure stage accessories (Thorlabs THH001), and then fixed on the translation stage. The flexure stage fixing avoids sliding and also strain can be easily controlled by the translation stage. The total fiber length between the glued points was about 18.1 cm and the length was changed by 20 µm (0.1105% strain) in every measurement step. After 12 steps, a total 1.326 % strain was applied and then, decreasing strain was applied by using the same steps, after strain experiment we move epoxy glue carefully with a sharp blade.

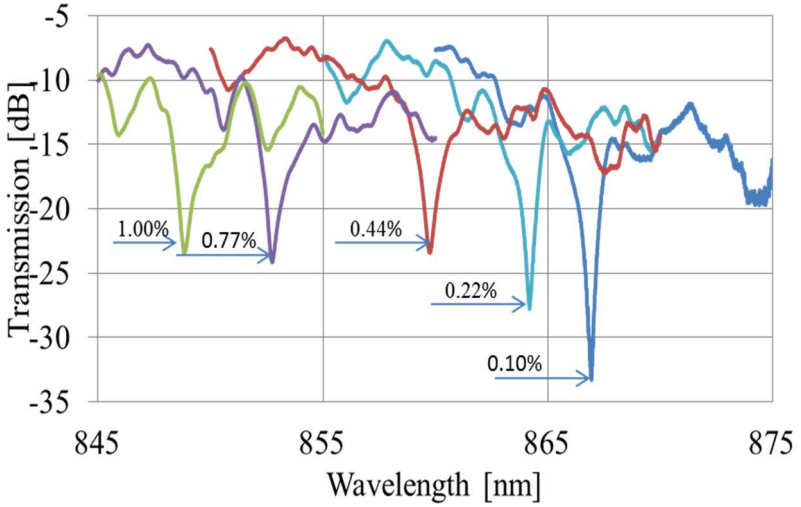

Figure 3.4.6 LPG transmission responses under different strain after two weeks.

Figure 3.4.8 shows the peak wavelength variation against different levels of strain and sensitivity about -2.3 ± 0.05 nm/mstrain was measured for increasing strain whereas, -2.25

± 0.05 nm/mstrain for decreasing strain due to polymer hysteresis. The measured sensitivity is slightly larger than presented in the literature, which ranges from -1.40 to -1.44 nm/mstrain for increasing strain and between -1.30 and -1.40 nm/mstrain for decreasing strain [88]. This phenomenon is probably due to fiber annealing for 24 hours at 70 ºC as reported in [89] since the annealed fibers can produce an increase in the strain sensitivity.

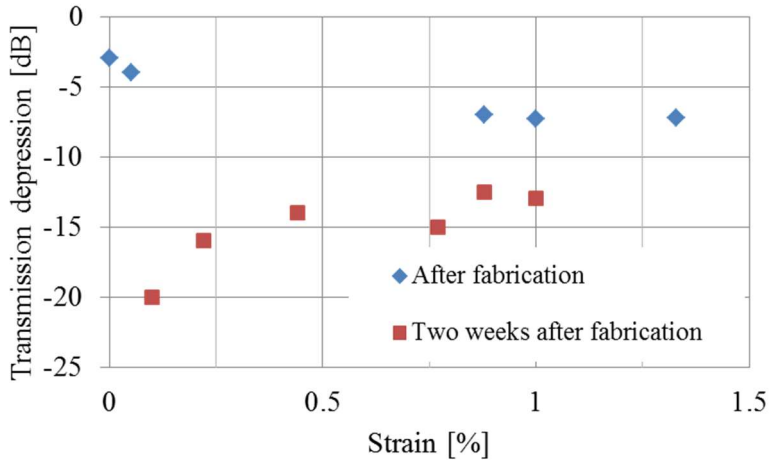

Figure 3.4.7 Transmission depression of the grating with strain.

We also studied the temperature response of the LPG inscribed which was fixed on the flexure stage and placed in the climatic chamber (Angelantoni Industrie CH340) with 50% humidity under varying temperature values. The temperature was increased from 22 ºC to 52 ºC with steps of 5 ºC. Each temperature value was held during one hour to ensure stabilization.

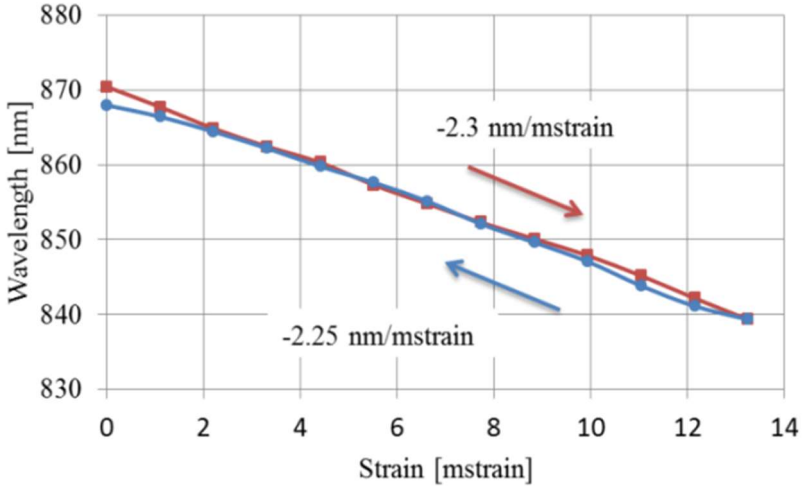

Figure 3.4.8 Wavelength change induced by increasing and decreasing strain.

At the same time, we explored the stable behavior of the grating response during the characterization experiment. As depicted in Figure 3.4.9, when the temperature is changed from 27 ºC to 32 ºC, the grating needs about 1 hour to become stable and before stability is reached, the grating shifts towards blue and then towards red wavelengths. However,

when the temperature is increased from 47 ºC to 52 ºC, the grating needs less than 10 minutes to become stable and central wavelength only shifts by a small amount.

The large range shift, observed for temperature change between 27 ºC and 42 ºC is probably due to the combined effect of humidity and temperature [69] since the water diffusion is a slow process. Oppositely, the grating becomes stable after a short time when the temperature is increased, as reported in [90], when the temperature is increased under 55% RH conditions.

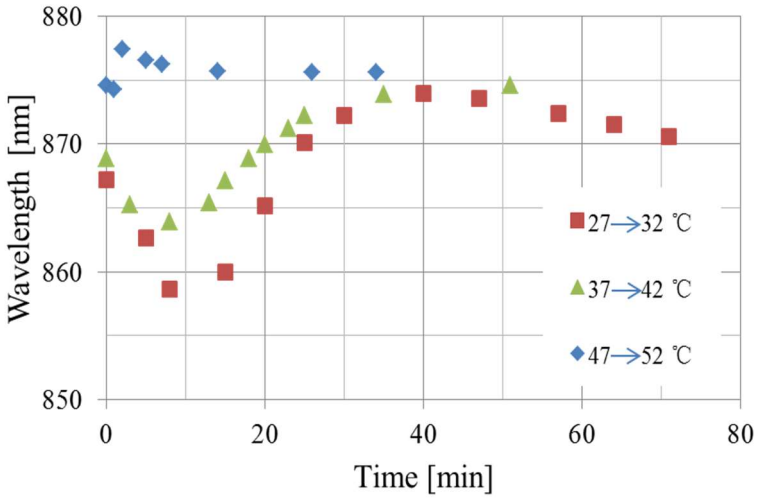

Figure 3.4.9 Time evolution of the LPG central wavelength for different temperature variations.

Provided temperature is stabilized for each measurement, the obtained temperature sensitivity was 0.276 ± 0.02 nm/ºC, as shown in Figure 3.4.10. The resonance wavelength of the grating shows a linear behavior with temperature. This behavior is different from previous results [91] where high nonlinearity and hysteresis was obtained when measurements were collected after 5 min. The linear behavior is probably due to the larger measuring times employed in our experiment since we also found high nonlinearity in the grating behavior during the first 5 min due to the combination of temperature and humidity. Longer times (~ 1 hour) between each measurement allow to get a stable response and, consequently the wavelength shows a linear behavior with the temperature variation. Such behavior with temperature variation of LPG was also reported in mPOF with trans-4-stilbenmethanol as external cladding dopant [83]. However, the measured sensitivity is slightly larger than presented in the literature. From [83], in the linear part of the temperature characteristics the thermal sensitivity was roughly 0.035 nm/ºC, which is almost one order less when compared with our result. It can be due to fiber drawing conditions; chemical composition of polymer and it is dependent of thermal history processing of each fiber.

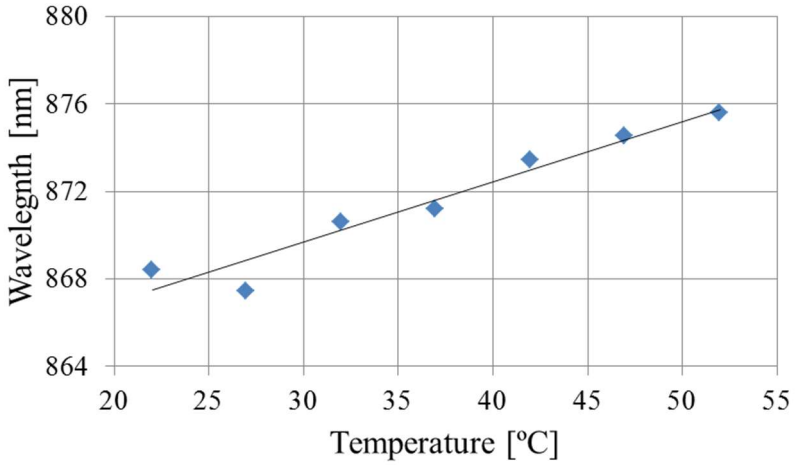

Figure 3.4.10 Central wavelength dependence on the temperature.

Figure 3.4.11 shows the transmission of the LPG after 50 days after fabrication, showing a good stability of the grating. The achieved strain sensitivity is -1.97 ± 0.05 nm/mstrain, slightly lower than before, which indicates the sensitivity decreases slowly with time.

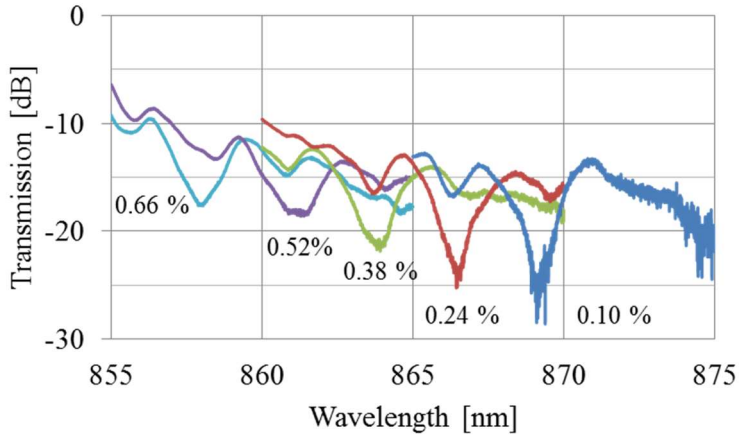

Figure 3.4.11 LPG transmission behavior with strain (50 days after fabrication).

3.4.4 Conclusion

To summarize, we demonstrated fast inscription of LPGs in polymer optical fibers using two 248 nm UV laser pulses per point by using point–by- point technique. The device has been fabricated in a single mode mPOF which core has been doped with BDK for photosensitivity enhancement to UV radiation. The inscription time for each coupling point has been shortened by 21 times compared with the best one reported in the literature. The grating response shows a notch depth of 20 dB centered at 866.9 nm wavelength under 0.1% strain. The strain and thermal characterization of the LPG showed the strain and temperature sensitivity of -2.3 ± 0.05 nm/mstrain and 0.276 ± 0.02 nm/ºC, respectively. Furthermore, we explored the stability of the grating response under different conditions to demonstrate its large potential for telecommunications and sensing applications.

3.5 References

1. N. F. Naim, M. S. Ab-Rahman, H. A. Bakarman, and A. A. A. Bakar, "Real-Time Monitoring in Passive Optical Networks Using a Superluminescent LED With Uniform and Phase-Shifted Fiber Bragg Gratings," J. Opt. Commun. Netw. **5**(12), 1425 (2013).
2. T.-Y. Kim, M. Hanawa, S.-J. Kim, S. Hann, Y. H. Kim, W.-T. Han, and C.-S. Park, "Optical delay interferometer based on phase shifted fiber Bragg grating with optically controllable phase shifter," IEEE Photonics Technol. Lett. **14**(10), 1834–1836 (2006).
3. X. Han and J. Yao, "Bandstop-to-bandpass microwave photonic filter using a phase-shifted fiber bragg grating," J. Light. Technol. **33**(24), 5133–5139 (2015).
4. G. P. A. and S. Radic, "Phase Shifted Fiber Bragg Gratings and Their Application for Wavelength Demultiplexing," IEEE Photonics Technol. Lett. 995–997 (1994).
5. D. J. Webb, "Fibre Bragg grating sensors in polymer optical fibres," Meas. Sci. Technol. **26**(9), (2015).
6. Y. Koike and T. Lshigure, "Progress of low-loss GI polymer optical fiber from visible to 1.5-um wavelength," in *ECOC97* (1997), pp. 22–25.
7. K. M. Chung, L. Dong, C. Lu, and H. Y. Tam, "Novel fiber Bragg grating fabrication system for long gratings with independent apodization and with local phase and wavelength control," Opt. Express **19**(13), 12664–12672 (2011).
8. Z. Xiong, G. D. Peng, B. Wu, and P. L. Chu, "Highly Tunable Bragg Gratings in Single-Mode Polymer Optical Fibers," IEEE Photonics Technol. Lett. **11**(3), 352–354 (1999).
9. G. Rajan, M. Ramakrishnan, Y. Semenova, E. Ambikairajah, G. Farrell, and G. D. Peng, "Experimental study and analysis of a polymer fiber bragg grating embedded in a composite material," J. Light. Technol. **32**(9), 1726–1733 (2014).
10. I. P. Johnson, K. Kalli, and D. J. Webb, "827 nm Bragg grating sensor in multimode microstructured polymer optical fibre," Electron. Lett. **46**(17), 3–4 (2010).
11. M. F. S. Ferreira, G. Statkiewicz-Barabach, D. Kowal, P. Mergo, W. Urbanczyk, and O. Frazão, "Fabry-Perot cavity based on polymer FBG as refractive index sensor," Opt. Commun. **394**, 37–40 (2017).
12. A. Lacraz, M. Polis, A. Theodosiou, C. Koutsides, and K. Kalli, "Femtosecond Laser Inscribed Bragg Gratings in Low Loss CYTOP Polymer Optical Fiber," IEEE Photonics Technol. Lett. **27**(7), 693–696 (2015).
13. W. Yuan, L. Khan, D. J. Webb, K. Kalli, H. K. Rasmussen, A. Stefani, and O. Bang, "Humidity insensitive TOPAS polymer fiber Bragg grating sensor," Opt. Express **19**(20), 19731–19739 (2011).
14. Y. Luo, Q. Zhang, H. Liu, and G.-D. Peng, "Gratings fabrication in benzildimethylketal doped photosensitive polymer optical fibers using 355 nm nanosecond pulsed laser," Opt. Lett. **35**(5), 751–753 (2010).
15. A. Pospori, C. A. F. Marques, D. Sáez-Rodríguez, K. Nielsen, O. Bang, and D. J. Webb, "Thermal and chemical treatment of polymer optical fiber Bragg grating sensors for enhanced mechanical sensitivity," Opt. Fiber Technol. **36**, 68–74 (2017).
16. S. F. Zhou, L. Reekie, Y. T. Chow, H. P. Chan, and K. M. Luk, "Phase-shifted fiber bragg gratings for terahertz range," IEEE Photonics Technol. Lett. **24**(20), 1875–1877 (2012).
17. L. M. Pereira, A. Pospori, P. Antunes, M. F. Domingues, S. Marques, O. Bang, D. J. Webb, and C. A. F. Marques, "Phase-Shifted Bragg Grating Inscription in PMMA Microstructured POF Using 248-nm UV Radiation," J. Light. Technol. **35**(23), 5176–5184 (2017).
18. D. C. J. Reid, C. M. Ragdale, I. Bennion, J. Buus, and W. J. Stewart, "Phase-shifted Moire grating fibre resonators," Electron. Lett. **26**(1), 10–12 (1990).
19. A. Pospori, C. A. F. Marques, O. Bang, D. J. Webb, and P. André, "Polymer optical fiber Bragg grating inscription with a single UV laser pulse," Opt. Express **25**(8), 9028–9038 (2017).
20. T. Erdogan, "Fiber Bragg Spectra," J. Light. Technol. **15**(8), 1277–1294 (1997).
21. W. Yuan, A. Stefani, M. Bache, T. Jacobsen, B. Rose, N. Herholdt-Rasmussen, F. K. Nielsen, S. Andresen, O. B. Sørensen, K. S. Hansen, and O. Bang, "Improved thermal and strain performance of annealed polymer optical fiber Bragg gratings," Opt. Commun. **284**(1), 176–182 (2011).
22. S. F. O. Silva, L. A. Ferreira, F. M. Araújo, J. L. Santos, and O. Frazão, "Fiber bragg grating

structures with fused tapers," Fiber Integr. Opt. **30**(1), 9–28 (2011).
23. C. Marques, A. Pospori, D. Sáez-Rodríguez, K. Nielsen, O. Bang, and D. J. Webb, "Fiber optic liquid level monitoring system using microstructured polymer fiber Bragg grating array sensors: performance analysis," in *Proc. SPIE 9634* (2015), pp. 96345V–96345V–4.
24. K. O. Hill, K. Takiguchi, F. Bilodeau, B. Malo, T. Kitagawa, S. Thériault, D. C. Johnson, and J. Albert, "Chirped in-fiber Bragg gratings for compensation of optical-fiber dispersion," Opt. Lett. **19**(17), 1314–1316 (2008).
25. B. Ortega, J. Capmany, J. L. Cruz, D. Pastor, and M. V. Andres, "Variable delay line for phased-array antenna based on a chirped fiber grating," IEEE Trans. Microw. Theory Tech. **48**(8), 1352–1360 (2002).
26. C. Wang and J. Yao, "A nonuniformly spaced microwave photonic filter using a spatially discrete chirped FBG," IEEE Photonics Technol. Lett. **25**(19), 1889–1892 (2013).
27. O. Frazão, M. Melol, P. V. S. Marques, and J. L. Santos, "Measurement Science and Technology Chirped Bragg grating fabricated in fused fibre taper for strain–temperature discrimination," Meas. Sci. Technol. **16**, 984–988 (2005).
28. H. Y. Chang, Y. C. Chang, H. J. Sheng, M. Y. Fu, W. F. Liu, and R. Kashyap, "An ultra-sensitive liquid-level indicator based on an etched chirped-fiber bragg grating," IEEE Photonics Technol. Lett. **28**(3), 268–271 (2016).
29. J. Lauzon, S. Thibault, J. Martin, and F. Ouellette, "Implementation and characterization of fiber Bragg gratings linearly chirped by a temperature gradient," Opt. Lett. **19**(23), 2027–2029 (2008).
30. P. C. Hill and B. J. Eggleton, "Strain gradient chirp of fibre Bragg gratings," Electron. Lett. **30**(14), 1172–1174 (2002).
31. R. Kashyap, P. F. McKee, R. J. Campbell, and D. L. Williams, "Novel method of producing all fibre photoinduced chirped gratings," Electron. Lett. **30**(12), 996–998 (1994).
32. J. L. Cruz, L. Dong, S. Barcelos, and L. Reekie, "Fiber Bragg gratings with various chirp profiles made in etched tapers," Appl. Opt. **35**(34), 6781–6787 (2008).
33. C. A. F. Marques, D. J. Webb, and P. Andre, "Polymer optical fiber sensors in human life safety," Opt. Fiber Technol. **36**, 144–154 (2017).
34. I. T. Monroy, H. P. A. Vd Boom, A. M. J. Koonen, G. D. Khoe, Y. Watanabe, Y. Koike, and T. Ishigure, "Data transmission over polymer optical fibers," Opt. Fiber Technol. **9**(3), 159–171 (2003).
35. A. Nespola, S. Abrate, R. Gaudino, C. Zerna, B. Offenbeck, and N. Weber, "High-speed communications over polymer optical fibers for in-building cabling and home networking," IEEE Photonics J. **2**(3), 347–358 (2010).
36. X. Hu, D. Saez-Rodriguez, C. Marques, O. Bang, D. J. Webb, P. Mégret, and C. Caucheteur, "Polarization effects in polymer FBGs: study and use for transverse force sensing," Opt. Express **23**(4), 4581–4590 (2015).
37. X. Hu, C.-F. J. Pun, H.-Y. Tam, P. Mégret, and C. Caucheteur, "Tilted Bragg gratings in step-index polymer optical fiber," Opt. Lett. **39**(24), 6835–6838 (2014).
38. H. Liu, H. Liu, G. Peng, and T. W. Whitbread, "Tunable dispersion using linearly chirped polymer optical fiber Bragg gratings with fixed center wavelength," IEEE Photonics Technol. Lett. **17**(2), 411–413 (2005).
39. C. A. F. Marques, P. Antunes, P. Mergo, D. J. Webb, and P. Andre, "Chirped Bragg Gratings in PMMA Step-Index Polymer Optical Fiber," IEEE Photonics Technol. Lett. **29**(6), 500–503 (2017).
40. D. Sáez-Rodríguez, K. Nielsen, H. K. Rasmussen, O. Bang, and D. J. Webb, "Highly photosensitive polymethyl methacrylate microstructured polymer optical fiber with doped core," Opt. Lett. **38**(19), 3769–3772 (2013).
41. X. Hu, G. Woyessa, D. Kinet, J. Janting, K. Nielsen, O. Bang, and C. Caucheteur, "BDK-doped core microstructured PMMA optical fiber for effective Bragg grating photo-inscription," Opt. Lett. **42**(11), 2209–2212 (2017).
42. C. A. F. Marques, A. Pospori, G. Demirci, O. Çetinkaya, B. Gawdzik, P. Antunes, O. Bang, P. Mergo, P. André, and D. J. Webb, "Fast bragg grating inscription in PMMA polymer optical fibres: Impact of thermal pre-treatment of preforms," Sensors (Switzerland) **17**(4), 1–8 (2017).
43. D. Saez-Rodriguez, R. Min, B. Ortega, K. Nielsen, and D. J. Webb, "Passive and Portable Polymer Optical Fiber Cleaver," IEEE Photonics Technol. Lett. **28**(24), 2834–2837 (2016).
44. K. Bhowmik, G. D. Peng, Y. Luo, E. Ambikairajah, V. Lovric, W. R. Walsh, and G. Rajan,

"Etching process related changes and effects on solid-core single-mode polymer optical fiber grating," IEEE Photonics J. **8**(1), (2016).
45. X. Hu, C.-F. J. Pun, H.-Y. Tam, P. Mégret, and C. Caucheteur, "Highly reflective Bragg gratings in slightly etched step-index polymer optical fiber," Opt. Express **22**(15), 18807–18817 (2014).
46. L. Dong, J. L. Cruz, L. Reekie, and J. A. Tucknott, "Fabrication of chirped fibre gratings using etched tapers," Electron. Lett. **31**(11), 908–909 (2002).
47. G. M. Williams, E. J. Friebele, and M. A. Putnam, "Fabrication of tapered, strain-gradent chirped fibre Bragg gratings," Electron. Lett. **31**(4), 309–310 (2002).
48. G. Rajan, Y. M. Noor, B. Liu, E. Ambikairaja, D. J. Webb, and G. D. Peng, "A fast response intrinsic humidity sensor based on an etched singlemode polymer fiber Bragg grating," Sensors Actuators, A Phys. **203**, 107–111 (2013).
49. J. Bonefacino, H.-Y. Tam, T. S. Glen, X. Cheng, C.-F. J. Pun, J. Wang, P.-H. Lee, M.-L. V. Tse, and S. T. Boles, "Ultra-fast polymer optical fibre Bragg grating inscription for medical devices," Light Sci. Appl. **7**(3), 17161 (2018).
50. X. Cheng, J. Bonefacino, B. O. Guan, and H. Y. Tam, "All-polymer fiber-optic pH sensor," Opt. Express **26**(11), 14610–14616 (2018).
51. G. Emiliyanov, J. B. Jensen, O. Bang, P. E. Hoiby, L. H. Pedersen, E. M. Kjær, and L. Lindvold, "Localized biosensing with Topas microstructured polymer optical fiber," Opt. Lett. **32**(5), 1059–1059 (2007).
52. H. U. Hassan, J. Janting, S. Aasmul, and O. Bang, "Polymer Optical Fiber Compound Parabolic Concentrator Fiber Tip-Based Glucose Sensor: In Vitro Testing," IEEE Sens. J. **16**(23), 8483–8488 (2016).
53. G. Woyessa, A. Fasano, C. Markos, A. Stefani, H. K. Rasmussen, and O. Bang, "Zeonex microstructured polymer optical fiber: fabrication friendly fibers for high temperature and humidity insensitive Bragg grating sensing," Opt. Mater. Express **7**(1), 286–295 (2017).
54. A. Fasano, G. Woyessa, P. Stajanca, C. Markos, A. Stefani, K. Nielsen, H. K. Rasmussen, K. Krebber, and O. Bang, "Fabrication and characterization of polycarbonate microstructured polymer optical fibers for high-temperature-resistant fiber Bragg grating strain sensors," Opt. Mater. Express **6**(2), 649–659 (2016).
55. C. Markos, A. Stefani, K. Nielsen, H. K. Rasmussen, W. Yuan, and O. Bang, "High-Tg TOPAS microstructured polymer optical fiber for fiber Bragg grating strain sensing at 110 degrees.," Opt. Express **21**(4), 4758–4765 (2013).
56. G. Woyessa, A. Fasano, A. Stefani, C. Markos, K. Nielsen, H. K. Rasmussen, and O. Bang, "Single mode step-index polymer optical fiber for humidity insensitive high temperature fiber Bragg grating sensors," Opt. Express **24**(2), 1253–1260 (2016).
57. I. P. Johnson, D. J. Webb, K. Kalli, M. C. J. Large, and A. Argyros, "Multiplexed FBG sensor recorded in multimode microstructured polymer optical fibre," in *SPIE Photonics Europe* (2010), p. 77140D.
58. G. Woyessa, K. Nielsen, A. Stefani, C. Markos, and O. Bang, "Temperature insensitive hysteresis free highly sensitive polymer optical fiber Bragg grating humidity sensor," Opt. Express **24**(2), 1206–1213 (2016).
59. W. Yuan, A. Stefani, and O. Bang, "Tunable polymer fiber Bragg grating (FBG) inscription: Fabrication of dual-FBG temperature compensated polymer optical fiber strain sensors," IEEE Photonics Technol. Lett. **24**(5), 401–403 (2012).
60. P. I. Reyes, N. Litchinitser, M. Sumetsky, and P. S. Westbrook, "160-Gb/s tunable dispersion slope compensator using a chirped fiber bragg grating and a quadratic heater," IEEE Photonics Technol. Lett. **17**(4), 831–833 (2005).
61. D. Tosi, E. G. Macchi, M. Gallati, G. Braschi, A. Cigada, S. Rossi, G. Leen, and E. Lewis, "Fiber-optic chirped FBG for distributed thermal monitoring of ex-vivo radiofrequency ablation of liver," Biomed. Opt. Express **5**(6), 1799–1811 (2014).
62. D. Shan, C. Zhang, S. Kalaba, N. Mehta, G. B. Kim, Z. Liu, and J. Yang, "Flexible biodegradable citrate-based polymeric step-index optical fiber," Biomaterials **143**, 142–148 (2017).
63. R. Min, B. Ortega, and C. Marques, "Fabrication of tunable chirped mPOF Bragg gratings using a uniform phase mask," Opt. Express **26**(4), 4411–4420 (2018).
64. S. Korganbayev, R. Min, M. Jelbuldina, X. Hu, C. Caucheteur, O. Bang, B. Ortega, C. Marques, and D. Tosi, "Thermal Profile Detection Through High-Sensitivity Fiber Optic Chirped Bragg Grating on Microstructured PMMA Fiber," J. Light. Technol. **36**(20), 4723–4729 (2018).

65. R. Min, S. Korganbayev, C. Moladi, C. Broadway, X. Hu, C. Caucheteur, O. Bang, P. Antunes, D. Tosi, C. Marques, and B. Ortega, "Largely tunable dispersion chirped polymer FBG," Opt. Lett. **43**(20), 5106–5109 (2018).
66. A. Fasano, G. Woyessa, J. Janting, H. K. Rasmussen, and O. Bang, "Solution-Mediated Annealing of Polymer Optical Fiber Bragg Gratings at Room Temperature," IEEE Photonics Technol. Lett. **29**(8), 687–690 (2017).
67. A. Pospori, C. Marques, G. Sagias, H. Lamela-Rivera, and D. . Webb, "Novel thermal annealing methodology for permanent tuning polymer optical fiber Bragg gratings to longer wavelengths," Opitcs Express **14**(5), 1732–1739 (2016).
68. P. Stajanca, O. Cetinkaya, M. Schukar, P. Mergo, D. J. Webb, and K. Krebber, "Molecular alignment relaxation in polymer optical fibers for sensing applications," Opt. Fiber Technol. **28**, 11–17 (2016).
69. W. Zhang, D. J. Webb, and G. D. Peng, "Investigation into time response of polymer fiber bragg grating based humidity sensors," J. Light. Technol. **30**(8), 1090–1096 (2012).
70. A. G. Leal-Junior, A. Theodosiou, C. Marques, M. J. Pontes, K. Kalli, and A. Frizera, "Compensation Method for Temperature Cross-Sensitivity in Transverse Force Applications with FBG Sensors in POFs," J. Light. Technol. **36**(17), 3660–3665 (2018).
71. A. M. Vengsarkar, P. J. Lemaire, J. B. Judkins, V. Bhatia, T. Erdogan, and J. E. Sipe, "Long-period fiber gratings as band-rejection filters," J. Light. Technol. **14**(1), 58–64 (1996).
72. S. W. James and R. P. Tatam, "Optical fibre long-period grating sensors: Characteristics and application," Meas. Sci. Technol. **14**(5), (2003).
73. X. Liu, L. Zhan, S. Luo, Y. Wang, and Q. Shen, "Individually switchable and widely tunable multiwavelength erbium-doped fiber laser based on cascaded mismatching long-period fiber gratings," J. Light. Technol. **29**(21), 3319–3326 (2011).
74. U. Tiwari, S. M. Tripathi, K. Thyagarajan, M. R. Shenoy, V. Mishra, S. C. Jain, N. Singh, and P. Kapur, "Tunable wavelength division multiplexing channel isolation filter based on dual chirped long-period fiber gratings," Opt. Lett. **36**(19), 3747–3749 (2011).
75. L. Rindorf and O. Bang, "Highly sensitive refractometer with photonic crystal fiber long-period grating," Opitcs Lett. **33**(6), 563–565 (2007).
76. X. Zhong, Y. Wang, J. Qu, C. Liao, S. Liu, J. Tang, Q. Wang, J. Zhao, K. Yang, and Z. Li, "High-sensitivity strain sensor based on inflated long period fiber grating," Opt. Lett. **39**(18), 5463–5466 (2014).
77. J. Li, W. Zhang, S. Gao, P. Geng, X. Xue, Z. Bai, and H. Liang, "Long-period fiber grating cascaded to an S fiber taper for simultaneous measurement of temperature and refractive index," IEEE Photonics Technol. Lett. **25**(9), 888–891 (2013).
78. L. Rindorf, J. B. Jensen, M. Dufva, L. H. Pedersen, P. E. Høiby, and O. Bang, "Photonic crystal fiber long-period gratings for biochemical sensing.," Opt. Express **14**(18), 8224–31 (2006).
79. C. Chen, A. Laronche, G. Bouwmans, L. Bigot, Y. Quiquempois, and J. Albert, "Sensitivity of photonic crystal fiber modes to temperature, strain and external refractive index," Opt. Express **16**(13), 9645–9653 (2008).
80. I.-L. Bundalo, R. Lwin, S. Leon-Saval, and A. Argyros, "All-plastic fiber-based pressure sensor," Appl. Opt. **55**(4), 811–816 (2016).
81. M. P. Hiscocks, M. A. van Eijkelenborg, A. Argyros, and M. C. J. Large, "Stable imprinting of long-period gratings in microstructured polymer optical fibre," Opt. Express **14**(11), 4644–4649 (2006).
82. D. Sáez-Rodríguez, J. L. Cruz, I. Johnson, D. J. Webb, M. C. J. Large, and A. Argyros, "Water diffusion into UV inscripted long period grating in microstructured polymer fiber," IEEE Sens. J. **10**(7), 1169–1173 (2010).
83. D. Kowal and G. Statkiewicz-Barabach, "Microstructured polymer optical fiber for long period gratings fabrication using an ultraviolet laser beam," Opt. Lett. **39**(8), 2242–2245 (2014).
84. D. Saez-Rodriguez, K. Nielsen, O. Bang, and D. J. Webb, "Photosensitivity mechanism of undoped poly(methyl methacrylate) under UV radiation at 325 nm and its spatial resolution limit," Opt. Lett. **39**(12), 3421–3424 (2014).
85. R. Oliveira, L. Bilro, and R. Nogueira, "Bragg gratings in a few mode microstructured polymer optical fiber in less than 30 seconds," Opt. Express **23**(8), 10181–10187 (2015).
86. B. T. Kuhlmey, R. C. McPhedran, and C. M. de Sterke, "Modal cutoff in microstructured optical fibers," Opt. Lett. **27**(19), 1684–1686 (2007).
87. H. B. Liu, H. Y. Liu, G. D. Peng, and P. L. Chu, "Novel Growth Behaviors of Fiber Bragg

Gratings in Polymer Optical Fiber under UV Irradiation with Low Power," IEEE Photonics Technol. Lett. **16**(1), 159–161 (2004).

88. G. Statkiewicz-barabach, D. Kowal, M. K. Szczurowski, P. Mergo, and W. Urbanczyk, "Hydrostatic Pressure and Strain Sensitivity of Long Period Grating Fabricated in Polymer Microstructured Fiber," IEEE Photonics Technol. Lett. **25**(5), 496–499 (2013).
89. C. A. F. Marques, R. Min, A. L. Junior, P. Antunes, A. Fasano, G. Woyessa, K. Nielsen, H. K. Rasmussen, B. Ortega, and O. Bang, "Fast and stable gratings inscription in POFs made of different materials with pulsed 248 nm KrF laser," Opt. Express **26**(2), 272–281 (2018).
90. W. Zhang, D. J. Webb, and G.-D. Peng, "Enhancing the sensitivity of poly(methyl methacrylate) based optical fiber Bragg grating temperature sensors," Opt. Lett. **40**(17), 4046–4049 (2015).
91. C. A. F. Marques, G.-D. Peng, and D. J. Webb, "Highly sensitive liquid level monitoring system utilizing polymer fiber Bragg gratings," Opt. Express **23**(5), 6058–6072 (2015).

Chapter 4

Novel applications of polymer fiber gratings

4.1 Strain sensing

[JP.10] R. Min, B. Ortega, C. Broadway, X. Hu, C. Caucheteur, O. Bang, P. Antunes, C. Marques, "Microstructured PMMA POF chirped Bragg gratings for strain sensing" Optical Fiber Technology, 41, 78-81, 2018.

4.1.1 Introduction

Over the last three decades, fiber Bragg gratings (FBG) inscribed in silica fiber have become a mature and recognized technology for both sensing and telecommunications. Compared to conventional sensing techniques, fiber sensors present significant advantages such as immunity to electromagnetic interference, lightweight and compactness for numerous sensing applications. These include strain [1], temperature [1], refractive index [2] [3], deformation [4], ultrasound [5] and liquid level indications [6]. Polymer optical fibers (POFs) share several of the advantages of silica fibers. Recently, POF sensors are receiving increased attention for their fundamental mechanical advantages over silica fibers including a lower Young's modulus, a higher thermo-optic coefficient, a higher elastic limit and biocompatibility for sensing applications. Materials such as poly (methyl methacrylate) (PMMA) [7], cyclic transparent optical polymer (CYTOP) [8], Topas [9] and Zeonex [10] have been successfully used for POF fabrication to date. Non-uniform FBGs have been recently implemented in POF: tilted FBGs (TFBG) [11], phase-shifted FBGs (PS-FBG) [12] and chirped FBGs (CFBG) [13], where the applications of these devices are attractive due to the benefit of POF.

POFBGs have been reported for strain measurement [14] by monitoring the resonant wavelength shift. However, other parameters such as temperature and humidity also cause wavelength shifts. Such effect is typically overcome by incorporating some interrogation scheme in order to distinguish one parameter from another, either by using different polymers, reference sensors or other related techniques [15]. One option is Topas, a humidity insensitive optical fiber material with a humidity sensitivity of less than 0.59 ± 0.02 pm/% at 1568 nm, 50 times lower than PMMA fibers [16]. Nonetheless, Topas and PMMA have similar temperature sensitivity. Static strain sensing requires appropriate compensation under varying ambient temperature levels [16].

Zhang et al. [17] investigated the response of PMMA POF grating based humidity sensors with different diameters and demonstrated that shorter response times could be obtained with lower fiber diameters. A dual FBG structure has been proposed to avoid the effects of temperature and humidity fluctuation, where an effective reference FBG is isolated from the parameter for measurement [18]. It has been reported that the humidity furcation effect on the wavelength shift of a grating under strain is different when compared with a strain free FBG [18]. In silica fiber, CFBGs glued at a slant orientation can be used as displacement sensor and accelerometer through bandwidth measurement with temperature insensitive performance [19][20], and tapered CFBGs have been demonstrated for strain sensing [21], where a 3-dB bandwidth modulation is shown that remains insensitive to humidity and temperature changes. Also, CFBGs have found important applications in healthcare, mechanical engineering, and shock waves analysis, among others [22][23].

We present a tapered CFBG in PMMA mPOF, combining the benefits of tapered chirped

Bragg gratings and fundamental POF characteristics. A sensitivity of 0.90 pm/με is obtained, higher value when compared with uniform FBGs, and fast measurements can be obtained through bandwidth measurements. This bandwidth observation is shown to be stable against humidity and temperature, making this concept suitable for its usage in temperature and humidity variable environments.

4.1.2 Strain response

Endlessly single-mode BDK-doped PMMA mPOF [24] was produced by using the center hole doping technique. In order to remove any residual stress incurred during the drawing process, the fiber was pre-annealed at 70 ºC for 12 hours without humidity control in temperature chamber. A 20 cm long fiber sample was cleaved with a portable cleaver [25] and polished with sand paper to enhance the quality of the end face. Prior to inscription, the fiber section was tapered in acetone using a computer driven translation stage to obtain the desired profile, as shown in Figure 4.1.1 (a).

A CFBG was inscribed using the phase mask method (total length 10 mm) and a single 15 ns pulse from a 2.5 mJ pulsed Coherent Bragg Star Industrial-LN krypton fluoride (KrF) excimer laser at 248 nm. The reflected spectral power of the CFBG is shown in Figure 4.1.1 (b).

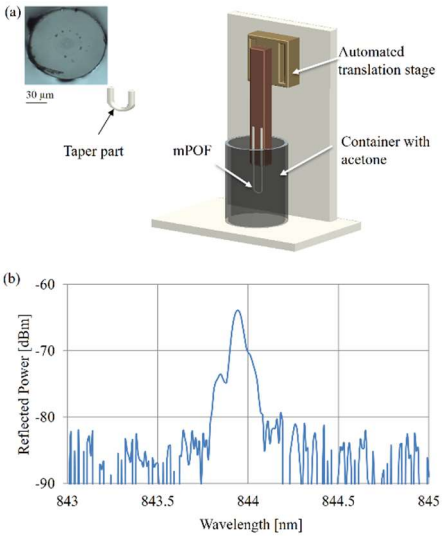

Figure 4.1.1 (a) Taper setup for POF, inset: end face of mPOF; (b) Reflected power by an FBG obtained with one pulse KrF laser irradiation.

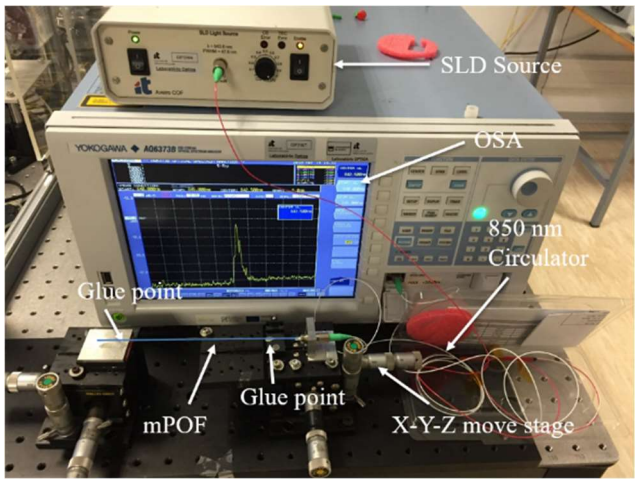

Figure 4.1.2 Strain measurement setup.

The strain sensitivity was tested using the setup depicted in Figure 4.1.2. The fiber was fixed with epoxy in order to avoid sliding. Axial strain was applied to the fiber through longitudinal displacement controlled by a 3D translation stage. The grating reflected spectrum was monitored using a super luminescent diode (Superlum SLD-371-HP1) and an optical spectrum analyzer (Yokogawa AQ6373B) with 20 pm spectral resolution.

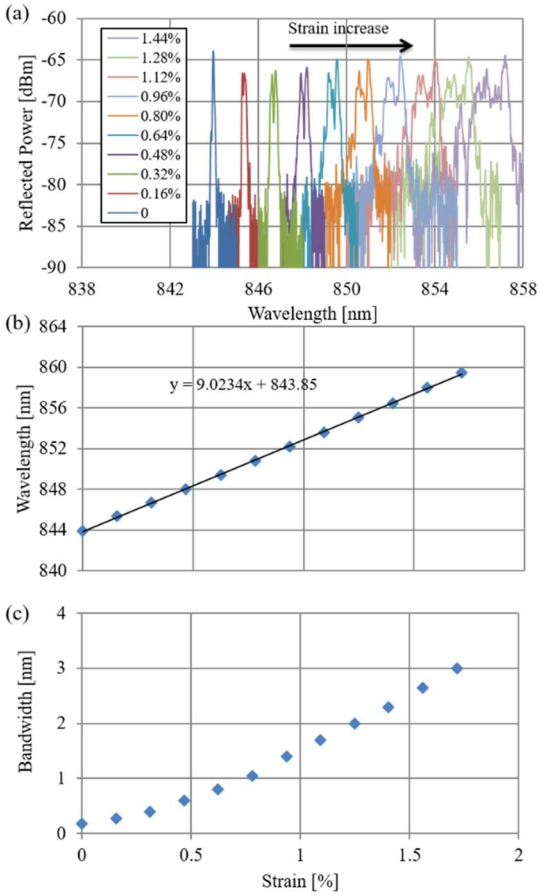

Figure 4.1.3 (a) Spectral reflected power vs strain; (b) Wavelength shift vs strain; (c) Bandwidth vs strain.

Figure 4.1.3 (a) shows how the reflected power spectrum of the grating changes with the application of strain. A 12.62 cm section of POF had strain applied on the grating in 200 μm steps, causing a positive wavelength shift as shown in Figure 4.1.3 (a). Figure 4.1.3 (b) indicates that the central wavelength of the grating increases with strain. The obtained strain sensitivity is 0.90 ± 0.02 pm/με, higher than that of a uniform POFBG in the same material and geometry (~0.71 pm/με) due to the tapered etching of the fiber [26]. Figure 4.1.3 (c) shows the bandwidth of the grating increase with strain, which can be used to measure this magnitude instead of measuring the central wavelength of the grating provided temperature and humidity sensitivities are compensated.

4.1.3 Temperature response

Figure 4.1.4(a) shows the reflected optical spectrum of the grating when temperature is set between 22 to 52 ºC under 60 % humidity without strain. In this condition, the temperature response achieves a stable value in less than 5 minutes, and the temperature sensitivity is measured as -57.9 ± 2.0 pm/ºC. This value is similar to the one reported for PS-FBGs [12] with the same polymer fiber material and geometry. Figure 4.1.4(c) shows the 3-dB bandwidth of the grating which is around 0.18 ± 0.02 nm under temperature increase from 22 to 52 ºC. This data confirms the temperature independent behavior previously observed

in silica fiber [23].

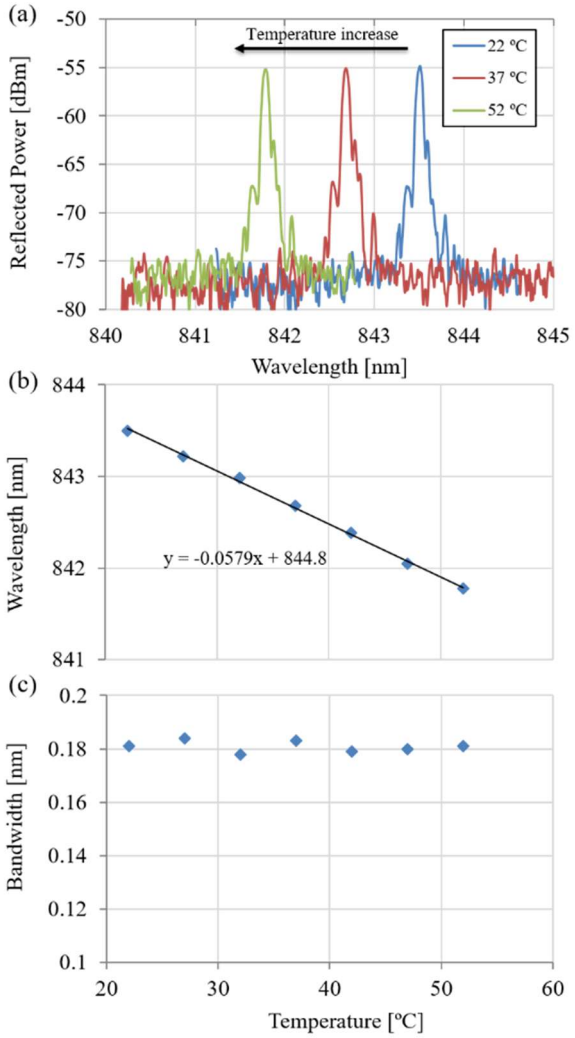

Figure 4.1.4 (a) Grating spectral response under temperature variations; (b) Central wavelength shift vs temperature; (c) 3-dB bandwidth vs temperature.

Figure 4.1.5(a) shows the reflected spectrum of the grating between 22 ºC and 52 ºC with 60 % humidity and 1.25 % strain. Figure 4.1.5(b) indicates the 3-dB bandwidth fluctuation under temperature increases from 22 to 52 ºC, with data collected every 5 min intervals in order to get temperature stabilization after each 5 ºC step. The 3-dB bandwidth remains constant at 2.00 ± 0.05 nm over the temperature increase from 22 to 52 ºC. The temperature sensitivity was found to be -58.8 ± 2.0 pm/ ºC (see Figure 4.1.5(b)), similar to the one obtained without applied strain.

4.1.4 Humidity response

Humidity is usually a challenge for practical applications of POFBGs [17]. During the experiment described as follows, the grating was left at a constant temperature of 22 ºC and no strain was applied. Figure 4.1.6(a) shows the central wavelength stabilization curve when humidity was decreased from 60% to 30%, with stability was observed after 50 minutes. Figure 4.1.6(b) indicates the resulting curve when the ambient humidity is changed from 30 % to 90 %, 100 minutes are required until stability is observed. The obtained humidity sensitivity of the grating is 26.0 ± 0.5 pm/% with no applied strain, higher than the values (19.9 ± 2.5 pm/%) obtained by *Pereira et al.* [12] with PS-FBGs in the same wavelength region (due to the high etch) [26]. Figure 4.1.6(c) depicts the reflected power spectrum of the grating under

30 % humidity, during humidity change and at 90 % humidity. We observe that the profile is acceptably homogeneous under these changes. We can observe that the 3-dB bandwidth is 0.18 ± 0.02 nm, as shown in Figure 4.1.6(d).

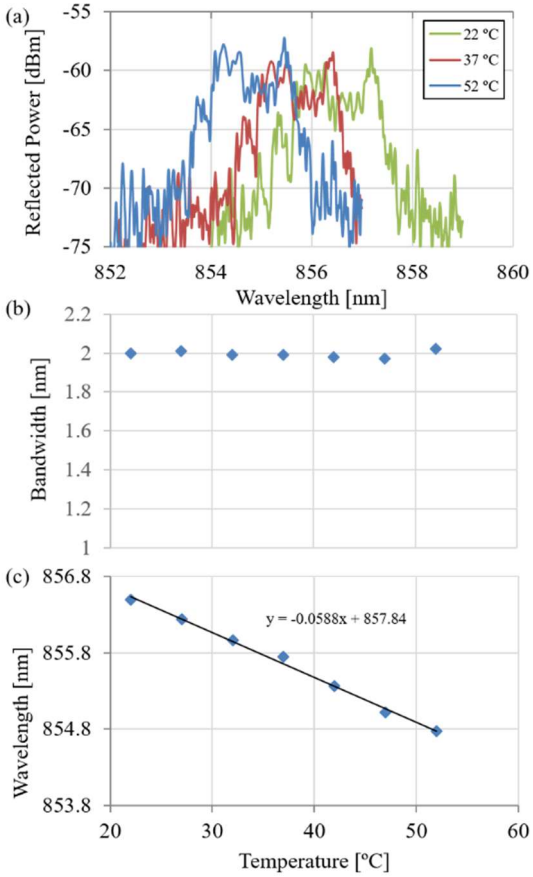

Figure 4.1.5 (a) Grating spectral response with temperature change under 1.25 % strain; (b) 3-dB bandwidth under 1.25 % strain vs temperature; (c) Central wavelength shift under 1.25 % strain vs temperature.

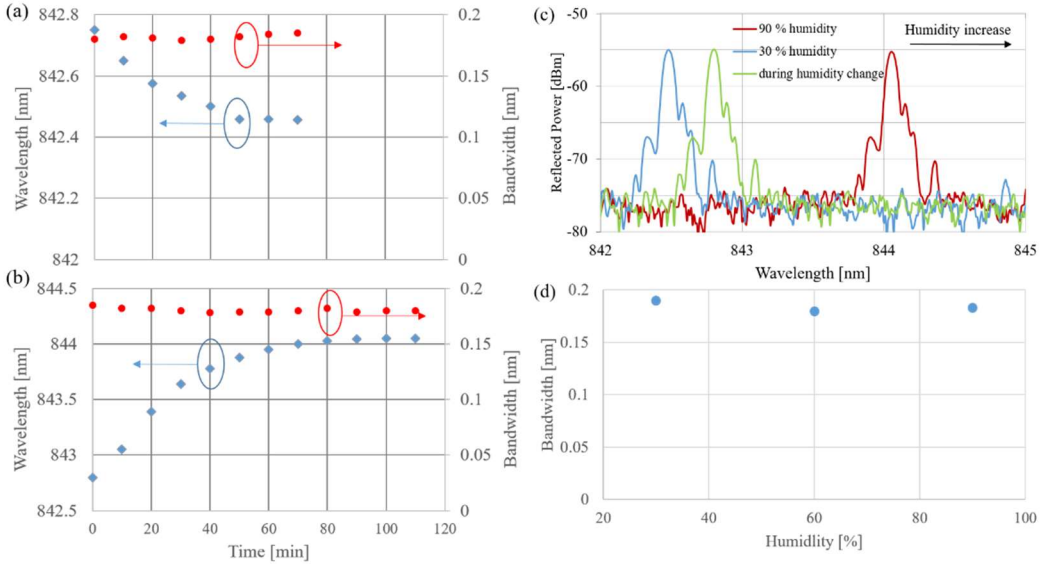

Figure 4.1.6 (a) FBG central wavelength and 3-dB bandwidth vs time under humidity change from 60% to 30%; (b) FBG central wavelength and 3-dB bandwidth vs time under humidity change from 30% to 90%; (c) Reflected spectral power vs wavelength under different humidity changes; (d) 3-dB bandwidth vs humidity change from 30% to 90%.

Figure 4.1.7(a) displays the reflected spectrum of the grating under 30 % humidity, during humidity change and 90 % humidity for a grating subjected to an axial strain of 1.25 %. The humidity sensitivity of the grating is 11.7 ± 0.4 pm/%, slightly lower than the value obtained without strain. A similar performance is explained in [18] as a reduced swelling coefficient in the fiber under strain when compared with the fiber under no strain condition.

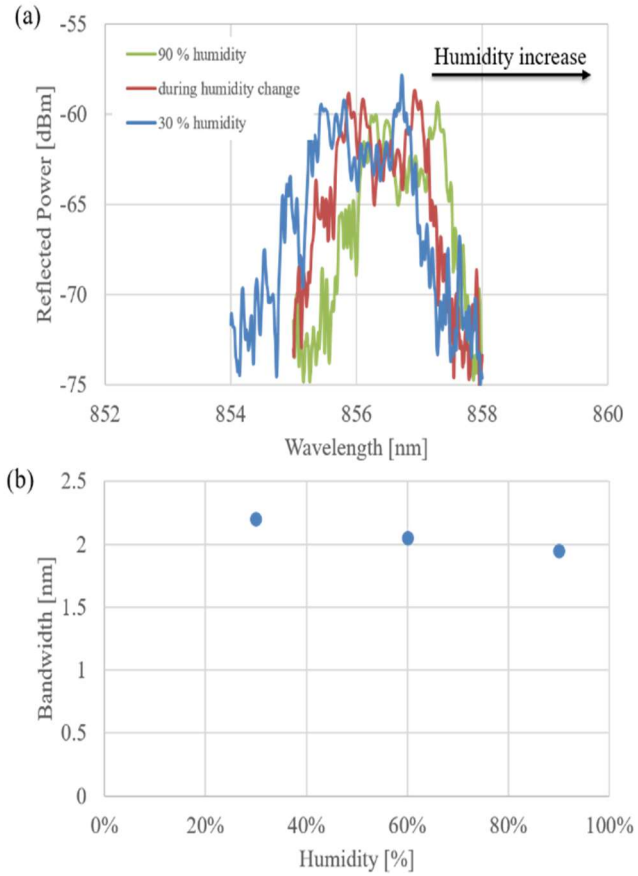

Figure 4.1.7 (a) Reflected spectral power vs wavelength under humidity change, (b) 3-dB bandwidth vs humidity change from 30% to 90%.

We found the 3-dB bandwidth decreases with humidity increases and a sensitivity about -4.2 ± 0.4 pm/% is obtained under high strain condition and 60 % humidity fluctuation. Actually, from Figure 4.1.7(b), this sensitivity is lower than the one shown by the central wavelength. Therefore, our CFBG in POF performs comparably to ones in silica, showing the bandwidth decreases as long as humidity increases under high strain conditions.

4.1.5 Conclusion

We presented a tapered CFBG in PMMA mPOF for strain sensing, with a measured sensitivity of 0.90 ± 0.02 pm/με. We have shown wavelength and bandwidth measurements, where the latter are less sensitive to humidity changes when the fiber is under no strain. A low humidity sensitivity performance around -4.2 ± 0.4 pm/% was achieved under high strain conditions. The grating response time is significantly improved by measuring the 3-dB bandwidth, which is a great benefit towards commercial strain sensing applications using POFBGs, especially under variable temperature and humidity conditions.

4.2 Thermal profile detection

[JP.11] S. Korganbayev, R. Min, M. Jelbuldina, X. Hu, C. Caucheteur, O. Bang, B. Ortega, C. Marques, D. Tosi, "Thermal profile detection through high-sensitivity fiber optic chirped Bragg grating on microstructured PMMA fiber Chirped FBG" IEEE/OSA Journal of Lightwave Technology, 36(20), 4723–4729, 2018.

4.2.1 Introduction

Established over two decades, optical fiber sensors for measurement of temperature have been demonstrated and implemented in several applications in harsh environments, oil and gas, and industrial monitoring [27]. Fiber Bragg Grating (FBG) sensors [28][29][30] are the most popular technology for multi-point measurement, and present systems enable sensing networks with up to hundreds of sensing points with spatial resolution at the centimeter scale [31]. On the other side, distributed tempe rature sensors based on Raman scattering enable long-haul distributed sensing, for distances up to tens of kilometers and spatial resolution 10~100 cm [32]. One of the most recent challenges for fiber optic temperature sensing technologies is the application in healthcare [33]. In this framework, FBG sensors represent an effective technology, thanks to their miniature size and compact form factor, electro-magnetic compatibility, biocompatibility in compliance to ISO10993 standard, and possibility to be embedded in commercial catheters. However, an essential feature of fiber optic sensors for medical applications is the possibility to detect temperature spatial distributions, often labeled thermal maps [34] (temperature as a function of space and time), with a narrow spatial resolution and on the same fiber. The spatial resolution is defined as the distance between each sensing point. FBG sensors have small length (15 mm typically) and can operate in wavelength-division multiplexing [35]; with present draw-tower inscription setups they can achieve a centimeter-level spatial resolution for medical applications [36], while maintaining the fiber protective jacket. An alternative to FBG sensors is represented by optical frequency-domain backscatter reflectometry (OFDR) [37][38], which is based on a white-light interferometer that detects the small Rayleigh backscatter signature of the fiber. OFDR system can further reduce the spatial resolution below the millimeter while maintaining a measurement time close to 1 Hz. However, distributed sensing system based on OFDR [39][40] are built on interferometers with a reference trigger, that constitute a bulky optical hardware, that requires a swept laser interferometer [39] or a microwave photonic circuit [40]. In addition, distributed systems do not have a specific active (or sensing) region in which the change of reflectivity is detected and encoded into a change of spectrum, but rather the entire fiber acts as a sensor along its entire length.

The possibility of measuring temperature pattern within a 1550 mm with a sub-centimeter spatial resolution, region through a compact biocompatible sensor has a significant impact in medical devices. A major field of application is in the monitoring of minimally invasive thermo therapies for cancer care [23], whereas a miniature applicator for microwave [41], radiofrequency (RF) [42], or laser [43] delivers a highly spatially confined heat field. In this application, thermal gradients have slopes reaching 35 ºC/mm and 1 ºC/s [23][34]. The measurement of blood temperature during laser-based treatment of tissues [44] and intravascular interventional surgery [45] also records steep spatial temperature gradients. Chirped FBG (CFBG), particularly having a linear chirp profile, have been used to extend the functionality of uniform FBG in this application [46]. While prior to the early 2010s, CFBGs have been mainly used as mechanical strain sensors [47][48], recent works have shown the possibility of using CFBGs for biomedical applications in thermal ablation [49].The principle of operation is encoded in the CFBG spectrum: a different CFBG reflection spectrum is observed as a function of each temperature spatial distribution. In particular, *Korganbayev et al.*[23] in 2018 proposed a method for demodulating the CFBG by means of an iterative optimization technique, that estimates the temperature profile by applying the same thermal profile to a CFBG theoretical model [47] and observing when the estimated and measured spectra show the best agreement. A drawback of this arrangement is that the temperature sensitivity of a standard CFBG on a glass fiber is typically 10 pm/ºC, which results in small spectral variations in the inner CFBG bandwidth. In order to increase the sensitivity, recent

works showed promising results on the fabrication of CFBGs on polymethyl methacrylate (PMMA) polymer optical fiber (POF) [13][50][51]. *Marques et al.* [13] reported the inscription of a CFBG on an undoped step-index POF with sensitivity of −131 pm/ºC. *Min et al.* [51] reported a tunable CFBG on a microstructed POF (mPOF) tapered fiber with benzyl dimethyl ketal (BDK) doping achieving −56.7 pm/ºC sensitivity. Thus, by utilizing a CFBG on a single mode POF instead of a standard glass fiber results in a thermal sensitivity increase of about one order of magnitude, which allows spectral detection technique to be more effective, and allow the measurement of temperature patterns with a better accuracy. In this work we describe the fabrication and application of an mPOF CFBG for the detection of temperature patterns in thermal ablation. A mPOF CFBG with sensitivity −191.4 pm/ºC and 1 cm length has been fabricated and used f or *in situ* detection of temperature pattern in a radiofrequency ablation setup [52]. In a first experiment, the mPOF CFBG has been located on a heating plate, detecting a linear temperature profile. Then, the mPOF CFBG has been used for detecting the temperature in proximity of the ablation thermal peak, with a profile close to Gaussian. A demodulation technique for the mPOF CFBG is introduced, which allows converting the CFBG spectrum into the temperature measured in each section of the grating, with 1 mm spatial resolution. The proposed result represents an important benchmark for application of PMMA CFBG in healthcare for detection of thermal maps with narrow spatial resolution, with immediate application in thermo therapies.

4.2.2 mPOF CFBG inscription and interrogation

The mPOF used in this work was a three-ring microstructure PMMA POF with BDK doped in the core [24]. Due to the average hole diameter and pitch in the fiber, we believe the mPOF shows an endlessly single mode behavior [24]. Before the use, about 20 cm length piece was pre-annealed at 70 ºC for 24 hours in order to remove residual stress during the drawing process. Then, the fiber sample was connected to the ferrule on one end, in order to connect it to a standard single mode fiber (SMF) through a mating sleeve: due to the different diameter between the mPOF and the SMF, it was necessary to partially etch the end-side of the mPOF fiber to match the size of the SMF. For the non-uniform etching process, the polymer fiber was tilted and immersed in a container full of 2:1 mixed acetone and liquid alcohol; one linear translation stage was programmed to move the fiber with constant speed performing a non-uniform etching, with a process similar to [25]. Afterwards, glue was used to fix the mPOF-SMF connector, drying the glue at room temperature for several hours to stabilize the structure [25]. Finally, the end face of the mPOF fiber was polished with sand paper to enhance the end face quality. A 248 nm wavelength pulsed Coherent Krypton Fluoride (KrF) excimer laser system was employed for the chirped Bragg grating inscription with a 2.5 mJ pulse [51] (see Figure 4.2.1). The laser beam profile was measured as a rectangular Tophat function of 6.0×1.5 mm^2 size and divergence 2×1 $mrad^2$, the UV beam focused on the fiber utilizing a plano-convex cylindrical lens with an effective focal length of 200.0 mm. The grating inscription was performed using 1067.03 nm phase mask, under 1% strain, in order to obtain a chirp profile [53]. The result is a 10 mm grating corresponding to the physical length of the phase mask, whereas the chirp profile is obtained through the strain pattern. Figure 4.2.2 shows the obtained CFBG and non-uniform tapering on mPOF, as measured on the experimental setup. The grating length of 10 mm results in a maximum reflectivity of −34.27 dB measured by spectral analysis and having about 25 dB amplitude over the noise floor. The full-width half-maximum (FWHM) bandwidth is 0.94 nm, which corresponds to a chirp rate approximately 0.09 nm/mm.

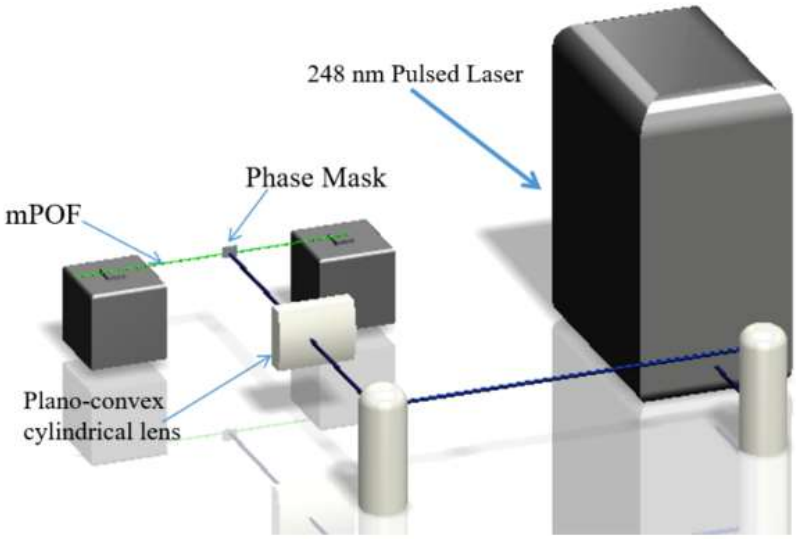

Figure 4.2.1 Schematic of CFBG inscription on mPOF.

The experimental setup used for the CFBG analysis has been arranged in order to expose the grating to spatially uniform and non-uniform thermal gradients, in order to observe the variations of the spectrum under different conditions. This task has been implemented using a water bath in order to obtain a uniform temperature, and a hot plate in order to induce a thermal gradient. Finally, the CFBG has been exposed to a thermal ablation using a radio frequency generator-based setup. For the experimental analysis, we used a Luna OBR4600optical backscatter reflectometer (OBR, Luna Inc., Roanoke, VA, US) as an interrogation setup to detect the mPOF CFBG spectrum with 1525–1610 nm wavelength range and 33 pm wavelength resolution. The use of an OBR instead of a standard interrogator of FBG analyzer allows the detection of a smaller amount of power, since the PMMA fiber and its connector are lossy devices. In addition, the OBR can measure the group delay. The experimental setup for calibration and linear temperature profile consists of a water bath, hot plate (IKA magnetic stirrer/C-Mag HS4) and reference thermometer (IKA electronic contact thermometer/ETS D-5, accuracy ±0.2 ºC). For temperature measurement with mPOF CFBG during radiofrequency ablation experiment, a Leanfa Hybrid generator (450 kHz) was used to ablate porcine liver phantom [49].

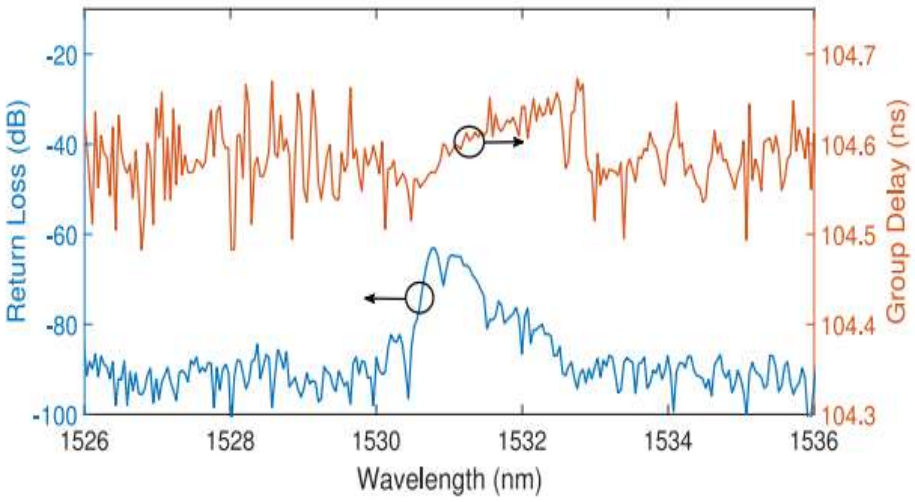

Figure 4.2.2 Reflection spectrum (left) and group delay (right) of mPOF CFBG inreference condition, before exposure to thermal ablation.

In order to detect the temperature profiles in each experimental validation, the method of spectral reconstruction developed in [23] and also reported in [34] has been adjusted to the specific type of grating, and implemented. A schematic of the algorithm is shown in Figure 4.2.3. In this method, we assume that the temperature profile over the grating length has a known shape, dependent on a small set of parameters. Thus, a model of the grating built by coupled mode theory (CMT) [47] has been implemented, estimating the grating parameters [23]. Subsequently, at each measurement, a temperature profile is applied to the CMT model until the root mean square error between the simulated grating and the measured spectrum is minimized.

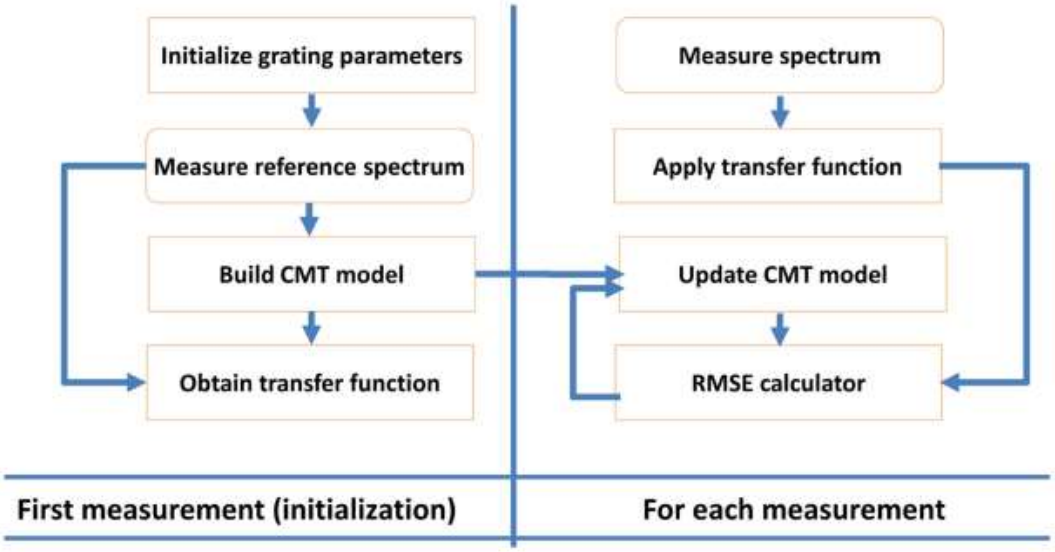

Figure 4.2.3 Reconstruction algorithm. Before the first measurement we input model grating parameters. After, transfer function, ratio of measured reference spectrum and CMT model spectrum without applied temperature, is calculated. Then, algorithm calculates root-mean-square error (RMSE) between filtered measured spectrum and updated CMT model to minimize cost function. As a result, the final temperature profile is obtained.

This method has been consolidated in [23], and allows the detection of either a linear thermal pattern, such as the gradient observed by exposing the CFBG to a hot plate setup, or a Gaussian shaped pattern as typically observed during radiofrequency [49] or laser [23] ablation, which is the main application area for the mPOF CFBG. Calling ΔT(z) the temperature profile, where z is the axis of the fiber, a linear profile is expressed as a 2 parameters estimation:

$$\Delta T(z) = A_0 + A_1 \cdot z \tag{4.1}$$

Where A_1 is the thermal gradient, and A_0 is the temperature offset. For a thermal ablation pattern [23], we assume a Gaussian pattern:

$$\Delta T(z) = A \cdot \exp[-\frac{(z-z_0)^2}{2\sigma^2}] \tag{4.2}$$

Where A, z_0, and σ are the amplitude, center value, and standard deviation respectively.

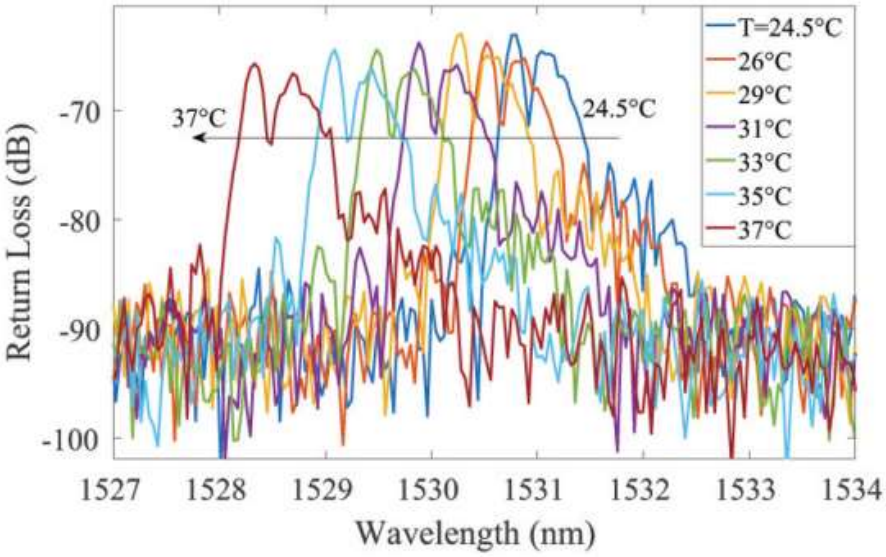

Figure 4.2.4 Reflection spectra of the mPOF CFBG, positioned in water bath during temperature increase, for different temperatures.

It should be highlighted that high temperature sensitivity of mPOF compared with silica CFBG (about 15 times larger in magnitude) can provide unprecedented temperature profile measurement sensitivity [13]: since a local temperature variation causes a much larger shift of the respective portion of the grating, compared to [23] we observe a much larger spectral variation that is helpful to the spectral reconstruction method.

The hereby proposed temperature reconstruction technique maintains the same procedural steps reported in [23]. While in [23] the grating under analysis was a silica CFBG having a much larger chirp coefficient, in the present work it is necessary to adjust the model to match the geometrical and optical parameters of the mPOF grating taking into account, in particular, the significant changes in terms of chirp rate coefficient (~1 order of magnitude narrower than a silica fiber) and thermal sensitivity(~1 order of magnitude larger and with opposite sign than a silica fiber). The solution that we propose is to maintain a relatively high number of simulated gratings (M=100), which provides an adequate discretization profile of each element constituting the chirped grating, and to estimate the other parameters from the optical spectrum: 1529.5~1530.7 wavelength bandwidth grating strength kL_g = 0.34, refractive index change δ_{neff} = 10^{-5}, refractive index of mPOF n_{eff} = 1.4895, and thermal sensitivity -191.4 pm/ºC. The main variation that we need to implement is in the grating length, as we artificially set the length of the overall CFBG to 10 cm, rather than 1 cm as its geometrical size. The reason for this change is that the temperature reconstruction method is effective in converting the spectral changes when each discrete grating element is spaced from the adjacent elements; this condition occurs for gratings having chirp rate of 1 nm/mm to 2 nm/mm as it was applied in [23] but does not apply to the present mPOF CFBG that has a chirp rate of 0.09 nm/mm, much lower than previous gratings. Thus, in order to maintain the structure of the algorithm without changing the optimization routine, we artificially expand the grating length by a factor 10 in order to have an artificial chirp rate of 0.94 nm/mm, similar to the previous values reported in [23], and compensating in part the limitations of the inscription setup to fabricate wideband CFBGs on a fiber with polymer compound. After inputting all the parameters of the grating including the artificial length, the algorithm computes the optimization routine and extract the temperature profile over the grating artificial length, that is then rescaled down by a factor 10 to the 0~1 cm axis.

4.2.3 Experiment

Before calibration the mPOF CFBG has been placed inside the water bath for 12 hours in order to absorb all possible water and, subsequently, prevent humidity effect on spectral shift during the experiment. Calibration of the CFBG has been done through the measurements of a spatially uniform temperature: the CFBG is positioned inside the water bath and the reference temperature is measured with the thermometer. The temperature has been increased from 24.5 ºC to 37.0 ºC, measuring the CFBG spectrum during the heating cycle; this range allows the full CFBG spectrum to be within the wavelength range of the interrogator, and is compatible with biomedical applications [34][45]. For each measurement the Bragg wavelength has been estimated by calculating the center of the FWHM of the grating. In Figure 4.2.4, the spectra of the FBG during thermal calibration are observed: it is possible to notice, as expected by [13], that the spectrum shifts towards the shortest wavelengths during the heating cycle. As shown in Figure 4.2.5, by evaluating the Bragg wavelength shift as a function of temperature, the thermal sensitivity of the CFBG sensor has been estimated as −191.4 pm/ºC, after fitting to a linear model. This value is similar to sensitivity achieved in [54] equal to −180.0 pm/ºC. This obtained sensitivity value has been used in the following experiments, in the CMT model for spectral reconstruction. The small errors in calibration can be explained by not uniform heat distribution in the water bath, heat absorption effect, accuracy of the thermometer, and to a non-linear thermal coefficient of the PMMA fiber [55]. The sensitivity observed for this grating is similar to previously reported POF gratings operating in near infrared [13][51] and much larger than cyclo-olefin copolymer [56] that has lesser sensitivity to humidity.

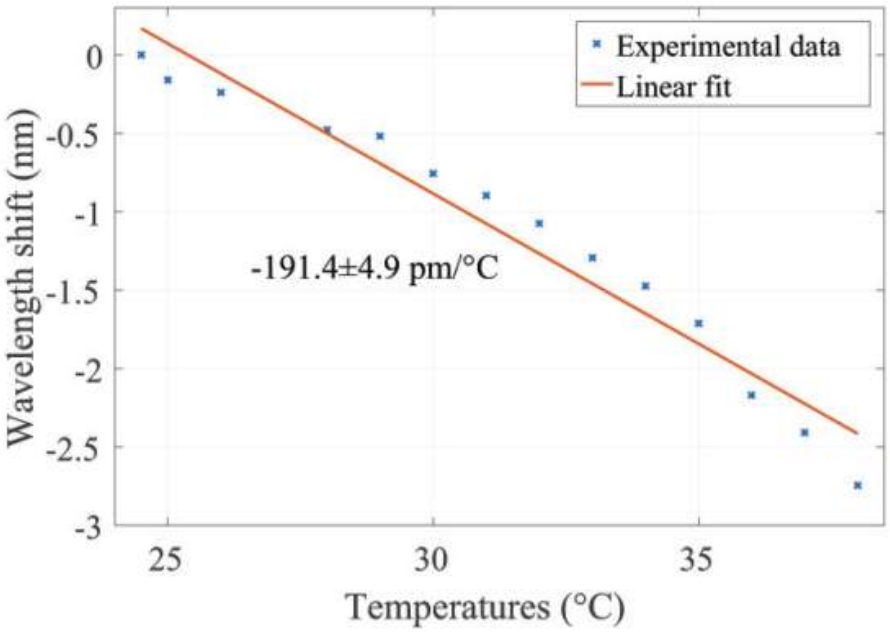

Figure 4.2.5 mPOF CFBG central wavelength shift as a function of temperature; the chart shows the experimental data and a linear fit.

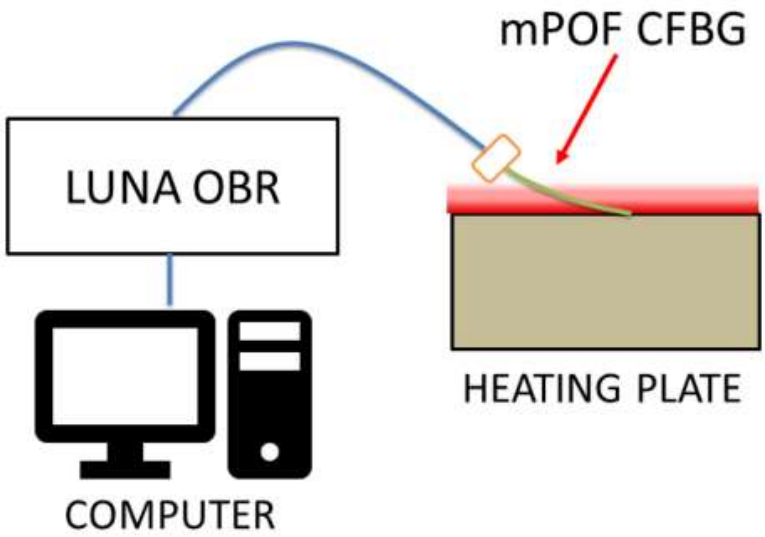

Figure 4.2.6 Schematic of linear gradient experiment: tail of the CFBG is placed at distance from heating plate and tip is fixed on the plate. LUNA OBR measures mPOF CFBG spectra during the heating experiment.

Following the method in [23] and used also in [57] to calibrate a CFBG by means of a controlled heating source, an experiment has been designed having a linear thermal gradient in order to evaluate the capability of the CFBG to respond to a non-uniform spatial gradient [58]. The setup of this measurement is shown in Figure 4.2.6. For linear temperature gradient, the tip of the CFBG sensor corresponding to the right portion (longest wavelengths) of the spectrum has been placed at the center of the hot plate, while the tail (shortest wavelengths) has been positioned at 2 cm from the plate. Due to the fact that temperature acting on the tip is higher than a tail temperature, we can observe an approximately linear thermal gradient along the CFBG length.

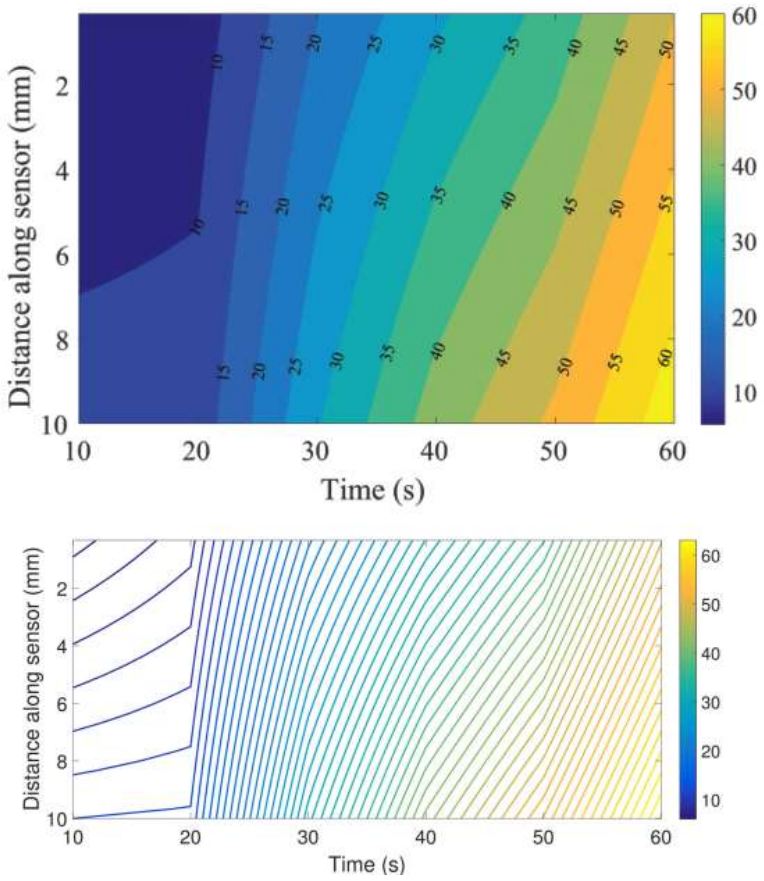

Figure 4.2.7 Measurement of linear temperature gradient with a mPOF CFBG as a function of distance along grating and time. The color bar shows temperature in ºC degrees. Upper chart: thermal map; Lower chart: isothermal curves.

The gradient is induced between the tip and the tail of the grating by the different amount of heating acting on each side of the CFBG: considering the short length of the CFBG, we assume that the temperature profile follows the linear pattern as in Eq. (4.1).The Figure 4.2.7 shows that in this setup, as expected, the thermal reconstruction returns a linear gradient along the grating. The thermal map reports that as the plate heats, and temperature increases from the tip to the tail of the grating, the gradient progressively enlarges until the hot plate reaches 60 ºC; at this time, the tail of the grating is exposed to 49 ºC, accounting for a gradient of 11 ºC/cm. This experiment shows that the CFBG responds in a different way to a non-uniform pattern, and the spectral reconstruction method can estimate the thermal map.

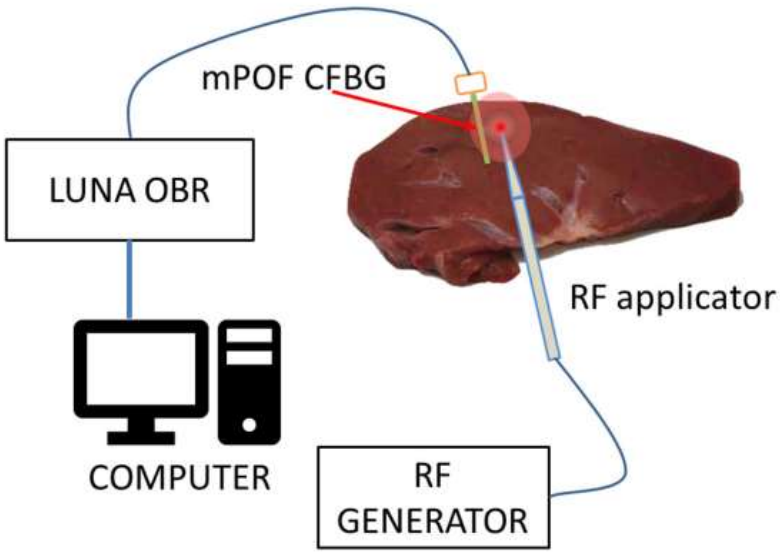

Figure 4.2.8 Schematic of thermal ablation experiment: the LUNA OBR measures spectra from mPOF CFBG, which is placed in proximity of RF applicator during the ablation.

This experiment focused on temperature measurement with mPOF CFBG during radiofrequency ablation (RFA) on porcine liver. RFA is a medical treatment aimed at the minimally invasive ablation of tumors after their localization and has been practiced as a clinical procedure [52][59]. The use of fiber optic sensors in measurement of the thermal patterns during RFA was introduced in [49]: in this work, the use of the mPOF CFBG provides a much larger sensitivity to temperature variation (18.7 times larger than [49]).

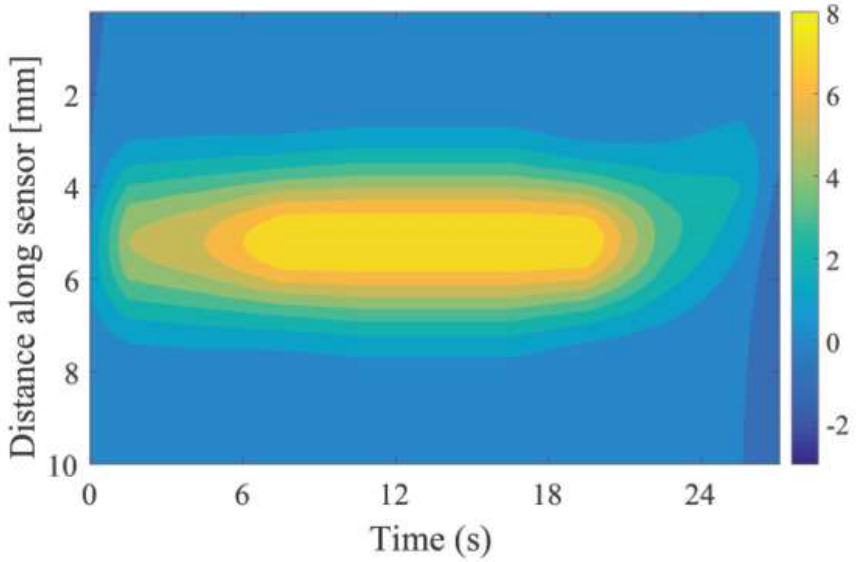

Figure 4.2.9 Measurement of Gaussian temperature gradient with a mPOF CFBG: thermal profile reconstructed with the CFBG as a function of distance along grating and time during ablation. The color bar shows temperature in ºC degrees.

The mPOF CFBG has been placed in proximity of a radiofrequency applicator (Figure 4.2.8) to measure temperature at the edge of ablated volume. The applicator is a research-grade single tip electrode having 5 mm thickness and percutaneously shaped tip, inserted in situ at the center of the target zone. The applicator is connected to the RF generator, that supplied a 450 kHz continuous power (50 W) to the electrode. The power has been

maintained constant through the experiment for 27 seconds, to mimic a rapid thermal ablation of a small target zone. The applicator has been placed at a distance of approximately 10 mm from the CFBG sensor, in order to avoid exposing the grating to excessive temperature.

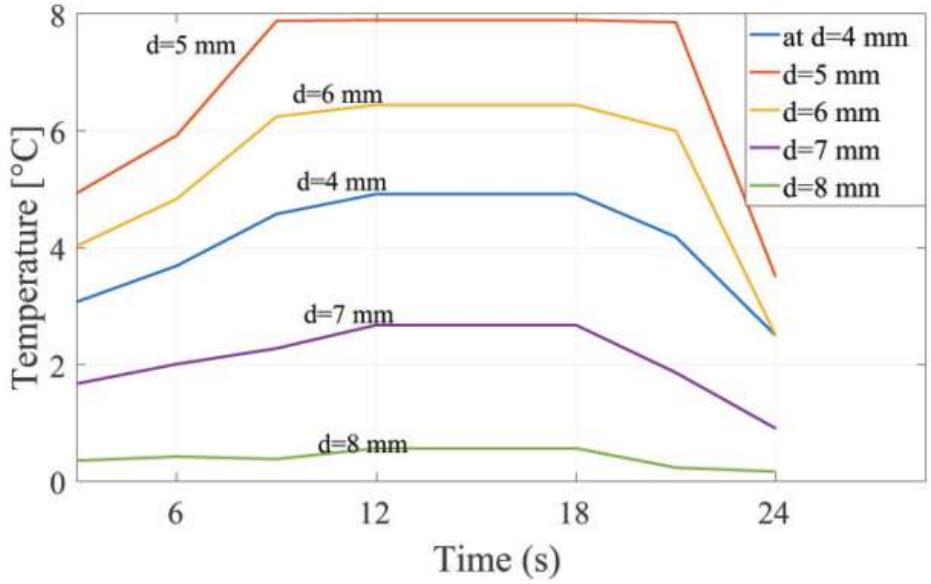

Figure 4.2.10 Temperature graphs for Gaussian-shaped RFA temperature profile; the chart reports the temperature as a function of time, for different values of position along the grating length.

The reflection spectrum of the mPOF FBG has been progressively detected by LUNA OBR4600 and further analyzed using the spectral reconstruction technique; for the temperature gradient estimation, we use the Gaussian model in Eq. (4.2). The results of thermal reconstruction are shown in Figure 4.2.9 and 4.2.10. Figure 4.2.9 shows the whole thermal map; it is clearly seen in Figure 4.2.10 that temperature reaches maximum 8 ºC at 9 s and starts decreasing after 18 s, that correlates with the ablation cycle during experiment. Results are in line with [49] considering the temperature regions outside of the central peak value. The RF power has been automatically disconnected by the RF generator after 18 s, in correspondence to the impedance of the tissue rising over threshold value [49]: this causes the tissue to cooldown until reaching room temperature.

4.2.4 Conclusion

In this work, we reported the measurement of thermal profiles using a mPOF CFBG fiber optic sensor, with a detection method based on spectral reconstruction. The higher sensitivity to temperature variations (−191.4 pm/ºC) with respect to glass fiber, and the low chirp rate of the mPOF grating require modification of the reconstruction algorithm. We have conducted two sets of experiments: linear temperature profile along 10 mm mPOF CFBG, and a radiofrequency ablation that induces Gaussian shaped temperature gradient. Experiments validate that proposed use of mPOF CFBG can provide significant advantages for thermal sensing in biomedical applications. Future work will be addressed to evaluate the response of the mPOF CFBG in closer proximity to the applicator, using a longer grating length and possibly a larger chirp rate, and to improve the spectral reconstruction method to work with specific mPOF CFBG coefficients

4.3 Dispersion compensation

[JP.12] R. Min, S. Korganbayev, C. Monardi, C. Broadway, X. Hu, C. Caucheteur, O. Bang, P. Antunes, D. Tosi, C. Marques, B. Ortega, "Largely tunable dispersion chirped polymer FBG" Optics Letters, 43(20), 5106-5109, 2018.

4.3.1 Introduction

Chirped fiber Bragg gratings (CFBGs) in silica fibers are attractive components which have been implemented for a variety of applications, such as long distance dispersion compensation [60], optoelectronic oscillator [61], mode locked fiber laser [62], accelerometer [20] or biomedical sensing [49]. Furthermore, microwave photonics is also a promising application area where dispersive elements are required, which includes beamforming for phased array antenna [63], signal generation [64] or reconfigurable transversal filters [65] amongst others. Indeed, CFBGs based on silica fiber is a very mature technology and several techniques have been demonstrated for fabricate and tuning, such as temperature gradient [66], strain gradient [67], varying the period the grating [68] and tuning with ferrofluidic defects in microstructured optical fiber [68]. However, polymer optical fibers (POFs) show higher thermo-optic coefficient, larger elongation before breakage and lower Young's modulus compared with silica fiber. Accordingly, a broader tuning range under temperature and strain, easy handling due to its low stiffness and lower installation costs are some of their main advantages [69], besides its biocompatibility. During the last decade, the use of polymer optical fiber (POF) has been increasing for short reach applications such as home networks [70][71] and low cost interconnects in datacenters [72] or sensors [73], which leads to current growing interest in novel fiber wavelength sensitive components.

Since the first fiber Bragg grating (FBG) in POF was reported in 1999 [74], FBGs in POF have become attractive devices for optical communication and sensing. Examples of them are phase-shifted FBG [12], tilted FBG [75] or FBGs in low loss cyclic transparent amorphous fluoropolymers (CYTOP) POFs [76], as reported in recent literature. CFBGs in POF were theoretically proposed for tunable dispersion in 2005 [54] by applying both strain and temperature, showing a potential large dispersion tuning range from 110 to 2400 ps/nm. However, experimentally, the first CFBG in POF was successfully fabricated by using a chirped phase mask in 2017 [13] as well as CFBGs have been recently fabricated in POF at 850 nm by using a uniform phase mask and non-uniform tapered fibers [51].

We present the first dispersion experimental demonstration of largely tunable dispersive FBGs in POF, where a dispersion range from positive 11.15 to 513.6 ps/nm and negative 490.60 to 15.90 ps/nm has been achieved, therefore, CFBGs in POF are confirmed as very promising dispersive devices for a variety of applications.

4.3.2 Grating device fabrication

The use of tapered silica fibers in 1996 [77] allowed to demonstrate variable group delay slope of the CFBG by applying different strain values. Liu et al. [54] provided simulation results for a similar approach in polymer fibers. We present a tunable dispersion CFBG inscribed in an endlessly single-mode benzyl dimethyl ketal (BDK)-doped poly (methyl methacrylate) (PMMA) microstructured POF (mPOF) [24], which was fabricated in DTU Fotonik by using the center hole doping technique. In order to remove any residual stress of the fiber from the drawing process, the fiber was pre-annealed at 80ºC for 24 hours. A 20 cm long fiber sample was connected to a ferrule, cleaved with a portable cleaver [25] and polished with sand paper to enhance the end face quality. As explained in [78], acetone can be employed to obtain POF etching. In our experiment, prior to the inscription process, the fiber section was immersed in acetone while a constant speed automatic translation stage was used to shift the fiber during the etching process, resulting in a non-uniform etching time for different fiber sections. Consequently, a linear tapered section, as shown in Figure 4.3.1 (a), is obtained with high reliability and repeatability, the tapered fiber diameter has been

measured along the taper of two points separated by 10 mm as 65 μm and 55 μm, lead to a linear taper profile of 1 μm/mm. The tapered fiber was subjected to 1% strain during exposure by a single pulse (with duration of 15 ns) with 2.5 mJ energy from a 248 nm KrF laser at 248 nm where a 10 mm long uniform phase mask of 1064 nm period was used, delivering a 10 mm long CFBG. The laser beam profile was measured as a rectangular Tophat function of 6.0×1.5 mm2 size and 2×1 mrad2 and a slit of 10 mm width sets the length of the grating. It was focused onto the fiber core utilizing a plano-convex cylindrical lens (Newport CSX200AR.10) with focal length of 20 cm. Additional details can be found in [24].

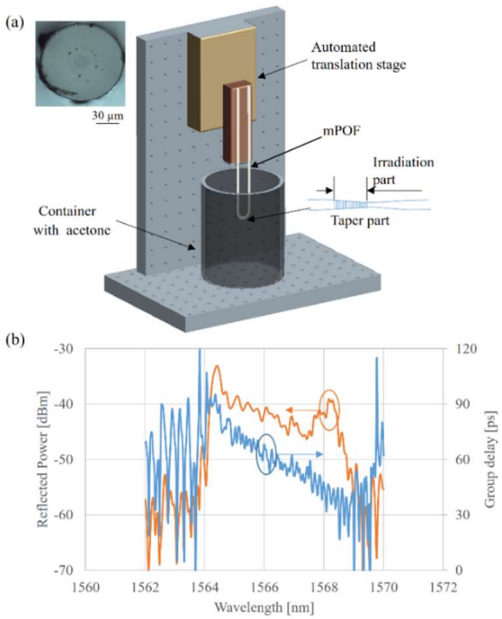

Figure 4.3.1 (a) Taper setup for mPOF; inset: end face of mPOF. (b) Reflected spectral power and group delay after fabrication and strain released.

Given that microstructuring is typically known to scatter circa 20% of the incident light during a successful inscription, some inhomogeneities may exist in the fibers refractive index profile. In symmetric microstructured fibers, inscription is successful provided no capillaries are in the light path of the inscription laser beam. Oppositely, in the worst case, the FBG profile is affected and the fiber is directionally sensitive. However, work by Broadway et al. has shown that for He-Cd inscription of PMMA mPOF, lateral directivity appears mechanically homogeneous over a 20-degree arc, even at pressures as low as 1kPa [79]. An optical backscatter reflectometer (LUNA 4600) with wavelength resolution of 33 pm was used to measure the reflected power and group delay. Figure 4.3.1(b) shows the reflected spectral power and the group delay of the fabricated CFBG after strain release, performing similarly to taper CFBG in silica fibers [53]. The maximum bandwidth was 4.86 nm, corresponding to a chirp of 0.486 nm/mm and a dispersion value around 11.15 ps/nm.

4.3.3 Dispersion measurement

A 5 cm long POF including a 1 cm long CFBG was subjected between two fiber clamps (Thorlabs HF001) fixed on the translation stage, as shown in Figure 4.3.2, which shifts every 10 μm step (0.005%). Figures 4.3.3(a) and (b) show the strain dependence of the reflected spectral power and group delay of the grating. It is clearly shown that chirped grating response strongly varies with the applied strain. The slope of the group delay vs wavelength (i.e. grating dispersion) varies according to the bandwidth change since the maximum grating delay is given by the grating length. The group delay shows a positive slope for strain levels higher than 1% and a negative when strain decreases from the value employed during the grating inscription. The reason for that is due to stress optic effect, which is opposite to the lengthening effect [30] and a chirp cancellation occurs. As expected, the central wavelength of the grating shifts to longer wavelengths when strain increases. Figure 4.3.3(c) shows a

strain sensitivity of 1.26± 0.02 pm/με, similar to uniform POFBG in the same material at 1530 nm (~1.3 pm/με) [80].

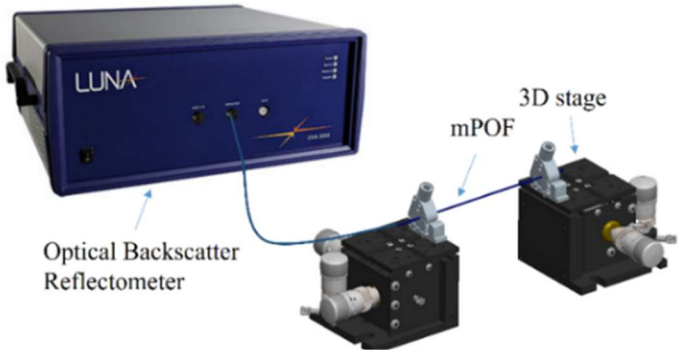

Figure 4.3.2. Experimental setup for strain measurements.

Figure 4.4.4 shows the bandwidth dependence and the dispersion with the applied strain. In Figure 4.4.4 (a), the negative slope region shows a bandwidth decrease with strain of 5.01 nm/%, whereas higher values of strain than 1% lead to an increase of 8.71 nm/%. Figure 4.4.4 (b) shows the dependence of the grating dispersion with the strain, where a dispersion increase from 11.15 to 513.60 ps/nm is achieved by increasing the strain up to 1.04 %. Negative dispersion of 490.60 ps/nm is measured for strain values of 0.94 % and it decreases to 15.90 ps/nm when 1.5% strain is applied. During 0.94% to 1.04 % strain, two opposite sign dispersion appeared due to the process of the conversion of the group delay slope. Since the grating is inscribed under 1% strain, the chirp is caused because of the stress- optic effect (i.e. strain gradient along the fiber). However, in this case, the grating pitch is not varying over the taper. After release, the chirp due to the stress-optic effect disappears, but another chirp appears due to different parts of the taper relax differently from the initial strain gradient (reversely to the lengthening effect [53]. Therefore, larger chirps can be created and the chirped grating can be packaged strain-free [51]. Detailed theory is provided following the analysis of r (radius) and L (fiber length) in chirped gratings using the transfer matrix method [47].

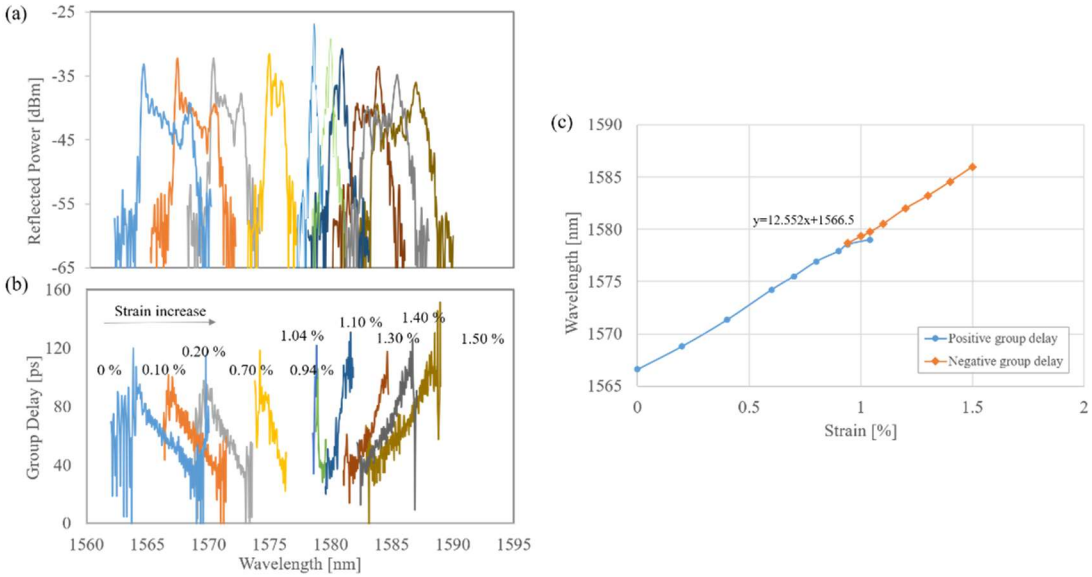

Figure 4.3.3 (a) Reflected spectrum vs strain. (b) Group delay vs strain. (c) Central wavelength shift vs strain.

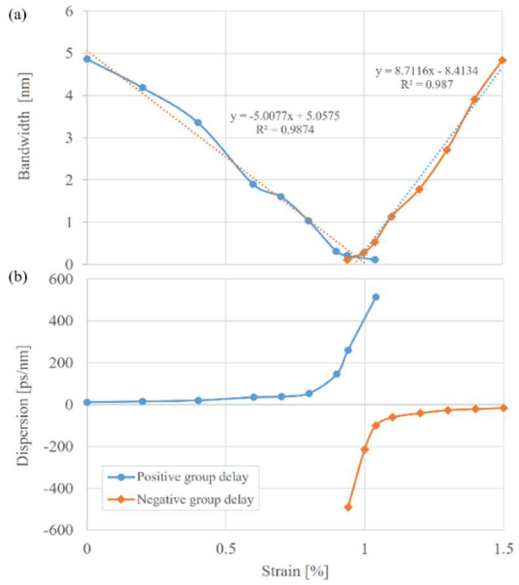

Figure 4.3.4 Characterization of the CFBG response: (a) bandwidth vs strain. (b) Dispersion vs strain.

Figure 4.3.3 (c) shows the central wavelength shift with the applied strain, which we propose to be compensated with the effect of temperature. Consequently, we characterized the CFBG response between 30 ºC and 52 ºC. The grating was placed on a Peltier plate with the temperature maintained by an electronic temperature controller. Figures 4.3.5 (a) and (b) show the obtained reflected spectral power and the group delay measurements. Figure 4.3. 6 shows a linear dependence of the central wavelength with the temperature, yielding a sensitivity of 0.0719 nm/ºC. We can, therefore, conclude that we can achieve a 1.6 nm tuning range over 22 ºC temperature tuning. Note that this value is larger than the 1.3 nm achieved in silica FBG when 100ºC temperature change is applied [81].

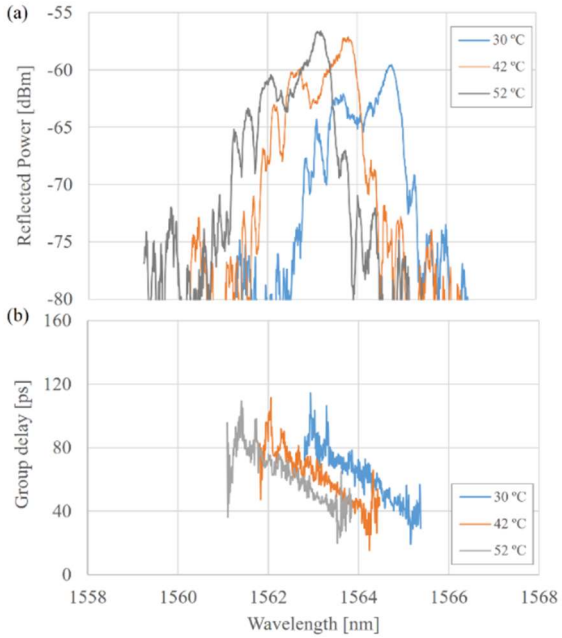

Figure 4.3.5 CFBG response characterization at different temperatures: (a) Reflected spectral power vs wavelength, (b) Group delay vs wavelength.

Figure 4.3.7 shows that the bandwidth and dispersion of the CFBG are stable when the temperature varies in the range 30-52 ºC. The dispersion is estimated as 26.2 ± 0.4 ps/nm and keeps constant within the margin of error. The measured blue shift of the central

wavelength with temperature can be employed to compensate the wavelength shift obtained when external strain is applied for the sake of dispersion tunability, which makes this dispersion device even more flexible. Figure 4.3.4 shows a large range of dispersion, from 145.8 ps/nm at 0.9% strain to 513.6 ps/ nm at 1.04% strain under a central wavelength shift of 1.76 nm.

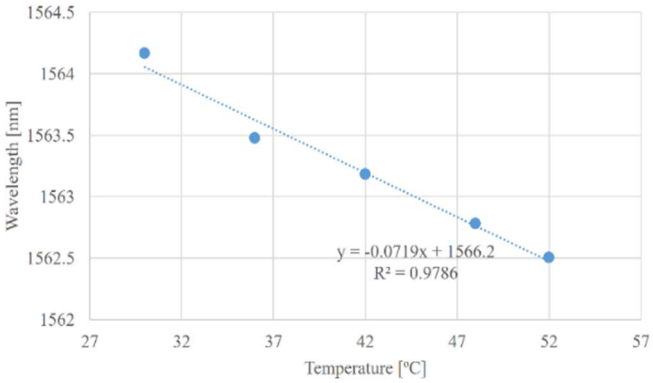

Figure 4.3.6 Linear dependence of the central wavelength under different temperatures.

For example, to offset the center wavelength increase induced by 0.14 % applied strain, the required temperature rise is 24 ºC, which is suitable for the temperature range for POFBG technology. In silica FBG, the temperature and strain sensitivities are 11.3 pm/ºC and 1.06 pm/με, so 132 ºC temperature change would be required to compensate the wavelength shift due to 0.14 % applied strain, which is not practical for real application [81].

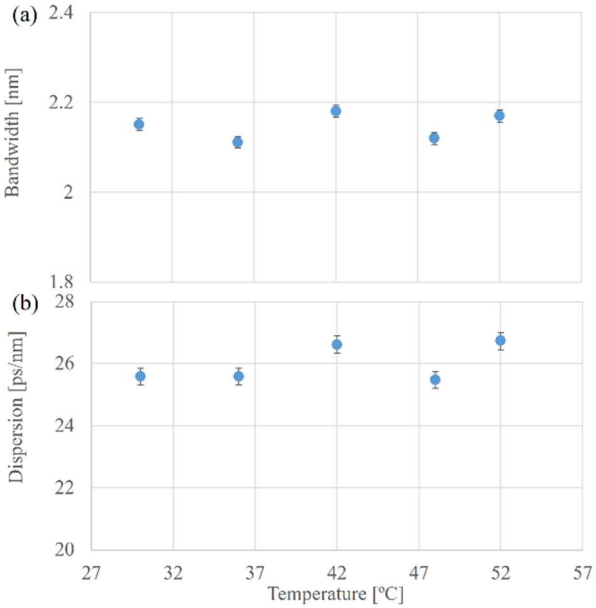

Figure 4.3.7 (a) Bandwidth vs Temperature. (b) Dispersion vs Temperature.

4.3.4 Conclusion

In conclusion, for the first time to our knowledge, the tunable dispersion of a chirped fiber Bragg grating inscribed in POF by using non-uniform tapered fibers technique has been demonstrated. We also propose to employ temperature in order to compensate the central wavelength shift due to the applied strain, and therefore, promising tunable CFBG devices are presented for future optical systems.

4.4 References

1. Y. J. Rao, "In-fibre Bragg grating sensors," Meas. Sci. Technol. **8**(4), 355–375 (1997).
2. A. Iadicicco, A. Cusano, S. Campopiano, A. Cutolo, and M. Giordano, "Thinned fiber Bragg gratings as refractive index sensors," IEEE Sens. J. **5**(6), 1288–1294 (2005).
3. C. Caucheteur, V. Voisin, and J. Albert, "Near-infrared grating-assisted SPR optical fiber sensors: design rules for ultimate refractometric sensitivity," Opt. Express **23**(3), 2918–2932 (2015).
4. T. H. T. Chan, L. Yu, H. Y. Tam, Y. Q. Ni, S. Y. Liu, W. H. Chung, and L. K. Cheng, "Fiber Bragg grating sensors for structural health monitoring of Tsing Ma bridge: Background and experimental observation," Eng. Struct. **28**(5), 648–659 (2006).
5. J. Guo and C. Yang, "Highly Stabilized Phase-Shifted Fiber Bragg Grating Sensing System for Ultrasonic Detection," IEEE Photonics Technol. Lett. **27**(8), 848–851 (2015).
6. H. Y. Chang, Y. C. Chang, H. J. Sheng, M. Y. Fu, W. F. Liu, and R. Kashyap, "An ultra-sensitive liquid-level indicator based on an etched chirped-fiber bragg grating," IEEE Photonics Technol. Lett. **28**(3), 268–271 (2016).
7. D. Saez-Rodriguez, K. Nielsen, O. Bang, and D. J. Webb, "Photosensitivity mechanism of undoped poly(methyl methacrylate) under UV radiation at 325 nm and its spatial resolution limit," Opt. Lett. **39**(12), 3421–3424 (2014).
8. A. Lacraz, M. Polis, A. Theodosiou, C. Koutsides, and K. Kalli, "Femtosecond Laser Inscribed Bragg Gratings in Low Loss CYTOP Polymer Optical Fiber," IEEE Photonics Technol. Lett. **27**(7), 693–696 (2015).
9. W. Yuan, L. Khan, D. J. Webb, K. Kalli, H. K. Rasmussen, A. Stefani, and O. Bang, "Humidity insensitive TOPAS polymer fiber Bragg grating sensor," Opt. Express **19**(20), 19731–19739 (2011).
10. G. Woyessa, A. Fasano, C. Markos, A. Stefani, H. K. Rasmussen, and O. Bang, "Zeonex microstructured polymer optical fiber: fabrication friendly fibers for high temperature and humidity insensitive Bragg grating sensing," Opt. Mater. Express **7**(1), 286–295 (2017).
11. X. Hu, P. Mégret, and C. Caucheteur, "Surface plasmon excitation at near-infrared wavelengths in polymer optical fibers," Opt. Lett. **40**(17), 3998–4001 (2015).
12. L. M. Pereira, A. Pospori, P. Antunes, M. F. Domingues, S. Marques, O. Bang, D. J. Webb, and C. A. F. Marques, "Phase-Shifted Bragg Grating Inscription in PMMA Microstructured POF Using 248-nm UV Radiation," J. Light. Technol. **35**(23), 5176–5184 (2017).
13. C. A. F. Marques, P. Antunes, P. Mergo, D. J. Webb, and P. Andre, "Chirped Bragg Gratings in PMMA Step-Index Polymer Optical Fiber," IEEE Photonics Technol. Lett. **29**(6), 500–503 (2017).
14. X. Chen, C. Zhang, D. J. Webb, G. D. Peng, and K. Kalli, "Bragg grating in a polymer optical fibre for strain, bend and temperature sensing," Meas. Sci. Technol. **21**(9), (2010).
15. A. G. Leal-Junior, A. Theodosiou, C. Marques, M. J. Pontes, K. Kalli, and A. Frizera, "Compensation Method for Temperature Cross-Sensitivity in Transverse Force Applications with FBG Sensors in POFs," J. Light. Technol. **36**(17), 3660–3665 (2018).
16. W. Zhang and D. J. Webb, "Humidity responsivity of poly(methyl methacrylate)-based optical fiber Bragg grating sensors," Opt. Lett. **39**(10), 3026–3029 (2014).
17. W. Zhang, D. J. Webb, and G. D. Peng, "Investigation into time response of polymer fiber bragg grating based humidity sensors," J. Light. Technol. **30**(8), 1090–1096 (2012).
18. W. Yuan, A. Stefani, and O. Bang, "Tunable polymer fiber Bragg grating (FBG) inscription: Fabrication of dual-FBG temperature compensated polymer optical fiber strain sensors," IEEE Photonics Technol. Lett. **24**(5), 401–403 (2012).
19. C. Shen and C. Zhong, "Novel temperature-insensitive fiber Bragg grating sensor for displacement measurement," Sensors Actuators, A Phys. **170**(1–2), 51–54 (2011).
20. W. Zhou, X. Dong, K. Ni, C. C. Chan, and P. Shum, "Temperature-insensitive accelerometer based on a strain-chirped FBG," Sensors Actuators, A Phys. **157**(1), 15–18 (2010).
21. J. A. Tucknott, L. Reekie, L. Dong, M. G. Xu, and J. L. Cruz, "Temperature-independent strain sensor using a chirped Bragg grating in a tapered optical fibre," Electron. Lett.

31(10), 823–825 (2002).
22. D. Tosi, "Review of chirped fiber bragg grating (CFBG) fiber-optic sensors and their applications," Sensors (Switzerland) **18**(7), (2018).
23. S. Korganbayev, Y. Orazayev, S. Sovetov, A. Bazyl, E. Schena, C. Massaroni, R. Gassino, A. Vallan, G. Perrone, P. Saccomandi, M. Arturo Caponero, G. Palumbo, S. Campopiano, A. Iadicicco, and D. Tosi, "Detection of thermal gradients through fiber-optic Chirped Fiber Bragg Grating (CFBG): Medical thermal ablation scenario," Opt. Fiber Technol. **41**(11), 48–55 (2018).
24. X. Hu, G. Woyessa, D. Kinet, J. Janting, K. Nielsen, O. Bang, and C. Caucheteur, "BDK-doped core microstructured PMMA optical fiber for effective Bragg grating photo-inscription," Opt. Lett. **42**(11), 2209–2212 (2017).
25. D. Saez-Rodriguez, R. Min, B. Ortega, K. Nielsen, and D. J. Webb, "Passive and Portable Polymer Optical Fiber Cleaver," IEEE Photonics Technol. Lett. **28**(24), 2834–2837 (2016).
26. A. Pospori, C. A. F. Marques, D. Sáez-Rodríguez, K. Nielsen, O. Bang, and D. J. Webb, "Thermal and chemical treatment of polymer optical fiber Bragg grating sensors for enhanced mechanical sensitivity," Opt. Fiber Technol. **36**, 68–74 (2017).
27. S. J. Mihailov, "Fiber bragg grating sensors for harsh environments," Sensors **12**(2), 1898–1918 (2012).
28. A. D. Kersey, M. A. Davis, H. J. Patrick, M. LeBlanc, M. K. P. Koo, C. G. Askins, M. A. Putnam, and E. J. Friebele, "Fiber Grating Sensors," J. Light. Technol. **15**(8), 1442–1463 (1997).
29. C. Broadway, R. Min, A. G. Leal Junior, C. Marques, and C. Caucheteur, "Towards commercial polymer fiber Bragg grating sensors: review and applications," J. Light. Technol. **37**(11), 2605–2615 (2018).
30. J. Albert, L. Y. Shao, and C. Caucheteur, "Tilted fiber Bragg grating sensors," Laser Photonics Rev. **7**(1), 83–108 (2013).
31. Y. Wang, J. Gong, D. Y. Wang, B. Dong, W. Bi, and A. Wang, "A quasi-distributed sensing network with time-division-multiplexed fiber bragg gratings," IEEE Photonics Technol. Lett. **23**(2), 70–72 (2011).
32. S. W. Tyler, J. S. Selker, M. B. Hausner, C. E. Hatch, T. Torgersen, C. E. Thodal, and S. G. Schladow, "Environmental temperature sensing using Raman spectra DTS fiber-optic methods," Water Resour. Res. **46**(4), 1–11 (2010).
33. E. Schena, D. Tosi, P. Saccomandi, E. Lewis, and T. Kim, "Fiber optic sensors for temperature monitoring during thermal treatments: An overview," Sensors (Switzerland) **16**(7), 1–20 (2016).
34. D. Tosi, E. Schena, C. Molardi, and S. Korganbayev, "Fiber optic sensors for sub-centimeter spatially resolved measurements: Review and biomedical applications," Opt. Fiber Technol. **43**(3), 6–19 (2018).
35. D. J. Webb, M. W. Hathaway, D. A. Jackson, S. Jones, L. Zhang, and I. Bennion, "First in-vivo trials of a fiber Bragg grating based temperature profiling system," J. Biomed. Opt. **5**(1), 45–50 (2002).
36. M. Rothhardt, M. Becker, C. Chojetzki, E. Lindner, and H. Bartelt, "Fabrication and applications of Draw Tower Gratings," in *Bragg Gratings, Photosensitivity, Poling Glass Waveguides* (2016), p. BTh1B.1.
37. B. J. Soller, D. K. Gifford, M. S. Wolfe, and M. E. Froggatt, "High resolution optical frequency domain reflectometry for characterization of components and assemblies," Opt. Express **13**(2), 666–674 (2005).
38. M. Froggatt and J. Moore, "High-spatial-resolution distributed strain measurement in optical fiber with rayleigh scatter," Appl. Opt. **37**(10), 1735–1740 (1998).
39. Z. Ding, C. Wang, K. Liu, J. Jiang, D. Yang, G. Pan, Z. Pu, and T. Liu, "Distributed Optical Fiber Sensors Based on Optical Frequency Domain Reflectometry: A review," Sensors (Basel) **18**(4), 1072 (2018).
40. A. L. Ricchiuti, J. Hervás, D. Barrera, S. Sales, and J. Capmany, "Microwave Photonics Filtering Technique for Interrogating a Very-Weak Fiber Bragg Grating Cascade Sensor," IEEE Photonics J. **6**(6), 5501410 (2014).
41. R. C. G. Martin, C. R. Scoggins, and K. M. McMasters, "Safety and efficacy of microwave ablation of hepatic tumors: A prospective review of a 5-year experience," Ann. Surg. Oncol. **17**(1), 171–178 (2010).
42. P. L. Pereira, "Actual role of radiofrequency ablation of liver metastases," Eur. Radiol.

17(8), 2062–2070 (2007).
43. P. Saccomandi, E. Schena, M. A. Caponero, F. M. Di Matteo, M. Martino, M. Pandolfi, and S. Silvestri, "Theoretical analysis and experimental evaluation of laser-induced interstitial thermotherapy in ex vivo porcine pancreas," IEEE Trans. Biomed. Eng. **59**(10), 2958–2964 (2012).
44. W. Liu, Y. Kong, X. Shi, X. Dong, H. Wang, J. Zhao, and Y. Li, "Determination of temperature and residual laser energy on film fiber-optic thermal converter for diode laser surgery," Comput. Assist. Surg. **22**(1), 251–257 (2017).
45. X. Zou, N. Wu, Y. Tian, J. Ouyang, K. Barringhaus, and X. Wang, "Miniature Fabry–Perot Fiber Optic Sensor for Intravascular Blood Temperature Measurements," IEEE Sens. J. **13**(6), 2155–2160 (2013).
46. P. C. Won, J. Leng, Y. Lai, and J. A. R. Williams, "Distributed temperature sensing using a chirped fibre Bragg grating," Meas. Sci. Technol. **15**(8), 1501–1505 (2004).
47. M. Pisco, A. Iadicicco, S. Campopiano, A. Cutolo, and A. Cusano, "Structured chirped fiber Bragg gratings," J. Light. Technol. **26**(12), 1613–1625 (2008).
48. S. Yashiro, T. Okabe, N. Toyama, and N. Takeda, "Monitoring damage in holed CFRP laminates using embedded chirped FBG sensors," Int. J. Solids Struct. **44**(2), 603–613 (2007).
49. D. Tosi, E. G. Macchi, M. Gallati, G. Braschi, A. Cigada, S. Rossi, G. Leen, and E. Lewis, "Fiber-optic chirped FBG for distributed thermal monitoring of ex-vivo radiofrequency ablation of liver," Biomed. Opt. Express **5**(6), 1799–1811 (2014).
50. D. J. Webb, "Fibre Bragg grating sensors in polymer optical fibres," Meas. Sci. Technol. **26**(9), (2015).
51. R. Min, B. Ortega, and C. Marques, "Fabrication of tunable chirped mPOF Bragg gratings using a uniform phase mask," Opt. Express **26**(4), 4411–4420 (2018).
52. S. Rossi, M. Di Stasi, E. Buscarini, P. Quaretti, F. Garbagnati, L. Squassante, C. T. Paties, D. E. Silverman, and L. Buscarini, "Percutaneous RF interstitial thermal ablation in the treatment of hepatic cancer.," Am. J. Roentgenol. **167**(3), 759–768 (1996).
53. L. Dong, J. L. Cruz, L. Reekie, and J. A. Tucknott, "Fabrication of chirped fibre gratings using etched tapers," Electron. Lett. **31**(11), 908–909 (2002).
54. H. Liu, H. Liu, G. Peng, and T. W. Whitbread, "Tunable dispersion using linearly chirped polymer optical fiber Bragg gratings with fixed center wavelength," IEEE Photonics Technol. Lett. **17**(2), 411–413 (2005).
55. A. Sophie, M. Patrick, O. Heidi, G. Thomas, T. Hugo, C. A. F. Marques, D. J. Webb, G.-D. Peng, P. Mergo, and B. Francis, "Thermal effects on the photoelastic coefficient of polymer optical fibers," Opt. Lett. **41**(11), 2517–2520 (2016).
56. M. Rosenberger, G. L. Roth, B. Adelmann, B. Schmauss, and R. Hellmann, "Temperature Referenced Planar Bragg Grating Strain Sensor in fs-Laser Cut COC Specimen," IEEE Photonics Technol. Lett. **29**(11), 885–888 (2017).
57. P. Saccomandi, A. Varalda, R. Gassino, D. Tosi, C. Massaroni, M. A. Caponero, R. Pop, S. Korganbayev, G. Perrone, M. Diana, A. Vallan, G. Costamagna, J. Marescaux, and E. Schena, "Linearly chirped fiber Bragg grating response to thermal gradient: from bench tests to the real-time assessment during in vivo laser ablations of biological tissue," J. Biomed. Opt. **22**(09), 097002 (2017).
58. P. Bettini, E. Guerreschi, and G. Sala, "Development and experimental validation of a numerical tool for structural health and usage monitoring systems based on chirped grating sensors," Sensors (Switzerland) **15**(1), 1321–1341 (2015).
59. T. Livraghi, L. Solbiati, M. F. Meloni, G. S. Gazelle, E. F. Halpern, and S. N. Goldberg, "Treatment of Focal Liver Tumors with Percutaneous Radio-frequency Ablation: Complications Encountered in a Multicenter Study," Radiology **226**(2), (2003).
60. P. I. Reyes, N. Litchinitser, M. Sumetsky, and P. S. Westbrook, "160-Gb/s tunable dispersion slope compensator using a chirped fiber bragg grating and a quadratic heater," IEEE Photonics Technol. Lett. **17**(4), 831–833 (2005).
61. Z. Tang, S. Pan, D. Zhu, R. Guo, Y. Zhao, M. Pan, D. Ben, and J. Yao, "Tunable optoelectronic oscillator based on a polarization modulator and a chirped FBG," IEEE Photonics Technol. Lett. **24**(17), 1487–1489 (2012).
62. X. He, Z. Liu, and D. N. Wang, "Wavelength-tunable, passively mode-locked fiber laser based on graphene and chirped fiber Bragg grating," Opt. Lett. **37**(12), 2394–2396 (2012).
63. B. Ortega, J. Capmany, J. L. Cruz, D. Pastor, and M. V. Andres, "Variable delay line for

phased-array antenna based on a chirped fiber grating," IEEE Trans. Microw. Theory Tech. **48**(8), 1352–1360 (2002).
64. C. Wang and J. Yao, "Photonic generation of chirped millimeter-wave pulses based on nonlinear frequency-to-time mapping in a nonlinearly chirped fiber bragg grating," IEEE Trans. Microw. Theory Tech. **56**(2), 542–553 (2008).
65. J. Capmany, B. Ortega, and D. Pastor, "A tutorial on microwave photonic filters," J. Light. Technol. **24**(1), 201–229 (2006).
66. J. Lauzon, S. Thibault, J. Martin, and F. Ouellette, "Implementation and characterization of fiber Bragg gratings linearly chirped by a temperature gradient," Opt. Lett. **19**(23), 2027–2029 (2008).
67. P. C. Hill and B. J. Eggleton, "Strain gradient chirp of fibre Bragg gratings," Electron. Lett. **30**(14), 1172–1174 (2002).
68. R. Kashyap, P. F. McKee, R. J. Campbell, and D. L. Williams, "Novel method of producing all fibre photoinduced chirped gratings," Electron. Lett. **30**(12), 996-998(2) (1994).
69. A. Candiani, W. Margulis, C. Sterner, M. Konstantaki, and S. Pissadakis, "Phase-shifted Bragg microstructured optical fiber gratings utilizing infiltrated ferrofluids," Opt. Lett. **36**(13), 2548–2550 (2011).
70. H. Yang, S. Member, S. C. J. Lee, E. Tangdiongga, C. Okonkwo, H. P. A. Van Den Boom, F. Breyer, S. Randel, and A. M. J. Koonen, "47.4 Gb/s Transmission Over 100 m Graded-Index Plastic Optical Fiber Based on Rate-Adaptive Discrete Multitone Modulation," J. Light. Technol. **28**(4), 352–359 (2010).
71. F. Forni, Y. Shi, N. C. Tran, H. P. A. Van Den Boom, E. Tangdiongga, and A. M. J. Koonen, "Multiformat wired and wireless signals over large-core plastic fibers for in-home network," J. Light. Technol. **36**(16), 3444–3452 (2018).
72. Y. Shao, R. Cao, Y. K Huang, Philip N. Ji, S. Zhang "112-Gb/s transmission over 100m of graded-index plastic optical fiber for optical data center applications," in *Optical Fiber Communication Conference* (2012).
73. C. A. F. Marques, D. J. Webb, and P. Andre, "Polymer optical fiber sensors in human life safety," Opt. Fiber Technol. **36**, 144–154 (2017).
74. Z. Xiong, G. D. Peng, B. Wu, and P. L. Chu, "Highly Tunable Bragg Gratings in Single-Mode Polymer Optical Fibers," IEEE Photonics Technol. Lett. **11**(3), 352–354 (1999).
75. X. Hu, C.-F. J. Pun, H.-Y. Tam, P. Mégret, and C. Caucheteur, "Tilted Bragg gratings in step-index polymer optical fiber," Opt. Lett. **39**(24), 6835–6838 (2014).
76. R. Min, B. Ortega, A. Leal-Junior, and C. Marques, "Fabrication and Characterization of Bragg Grating in CYTOP POF at 600-nm Wavelength," IEEE Sensors Lett. **2**(3), 1–4 (2018).
77. J. L. Cruz, L. Dong, S. Barcelos, and L. Reekie, "Fiber Bragg gratings with various chirp profiles made in etched tapers," Appl. Opt. **35**(34), 6781–6787 (2008).
78. X. Hu, C.-F. J. Pun, H.-Y. Tam, P. Mégret, and C. Caucheteur, "Highly reflective Bragg gratings in slightly etched step-index polymer optical fiber," Opt. Express **22**(15), 18807–18817 (2014).
79. C. Broadway, D. Gallego, A. Pospori, M. Zubel, D. J. Webb, K. Sugden, G. Carpintero, and H. Lamela, "Microstructured polymer optical fibre sensors for opto-acoustic endoscopy," in *SPIE Photonics Europe* (SPIE, 2016), p. 98860S.
80. W. Yuan, A. Stefani, M. Bache, T. Jacobsen, B. Rose, N. Herholdt-Rasmussen, F. K. Nielsen, S. Andresen, O. B. Sørensen, K. S. Hansen, and O. Bang, "Improved thermal and strain performance of annealed polymer optical fiber Bragg gratings," Opt. Commun. **284**(1), 176–182 (2011).
81. Bai-Ou Guan, Hwa-Yaw Tam, Xiao-Ming Tao, and Xiao-Yi Dong, "Simultaneous strain and temperature measurement using a superstructure fiber Bragg grating," IEEE Photonics Technol. Lett. **12**(6), 675–677 (2002).

Chapter 5
General discussion of the results

This chapter aims to discuss the results obtained throughout the thesis by means of proper comparison to other results in the previous literature.

5.1 Gratings fabrication

Although 325 nm was the first irradiation wavelength reported by *Peng'* group [1] and initially 248 nm wavelength was not considered suitable for polymer fiber Bragg grating writing due to high absorption, the first Bragg grating successful inscription in 30 seconds using low flow and repetition rate at 248 nm UV light opened a new field of interest for grating irradiation [2]. Since then, the research work on gratings inscription using 248 nm wavelength has been continuously growing. A typical POF FBG irradiation system is described in [2], where the pulse power and repetition rate can be optimized [3][4] in order to shorten the fabrication time.

Pospori et al. [5] and *us* [6] fabricated FBGs in BDK doped POF using 248 nm and 266 nm wavelength irradiation, respectively, and obtained strong POFBGs with a single short laser pulse (15 and 8 ns of duration, respectively), which is even compatible with fiber drawing process. Bragg gratings inscription in the 850 nm spectral region was also obtained by using step index PMMA POF irradiation using a 248 nm krypton fluoride (KrF) excimer laser system, which only took 0.4 seconds with 100 Hz pulse repetition. In this fiber, the cladding material is pure PMMA while the core is PMMA doped with TS (1% w.t.) and diphenyl sulfide (DPS) (5% mole) to enhance the photosensitivity and increase the refractive index [4]. We demonstrated the inscription of gratings in POFs made of different materials (Topas, Zeonex and Polycarbonate) under 248 nm wavelength and compared with the same fiber irradiation under 325 nm, resulting a reduction of the irradiation times at least 16 times and better stability when 248 nm wavelength is employed. We also obtained the first 600 nm wavelength grating with commercial CYTOP POF using a 248 nm KrF laser system with a repetition of 40 Hz and average pulse energy of ~0.60 mJ during ~60 min [7], leading to potential applications in the visible range.

5.2 Different types of gratings

Recently, a novel bandpass transmission filter based on PS-FBG at telecom wavelength [8] was obtained using Moiré method by 325 nm Kimmon laser system exposure about 20 mins, as shown in Figure 5.2.1. A Moiré structure is formed by superimposing two gratings of equal amplitude but slightly different periods. Figure 5.2.2 (a) shows the result of two superimposed pulses on a single mode BDK doped mPOF by using a 248 nm KrF laser emitting an output pulse power of 2.5 mJ energy and 15 ns duration [9]. The obtained grating showed 0.035 nm bandwidth and 8 dB in rejection band, with high level of flexibility and no need of strain accuracy. At 850 nm wavelength region, PS FBG was also obtained directly during the grating fabrication by placing a narrow blocking aperture in the center of the UV beam (see Figure 5.2.2 (b)) [10], which could also extend to multi-PS FBG. A high-quality Bragg grating structure was obtained with -16.3 dB and -13.2 dB dips in transmission. The only drawback is the accuracy required for the

narrow blocking line which must be put on the phase mask.

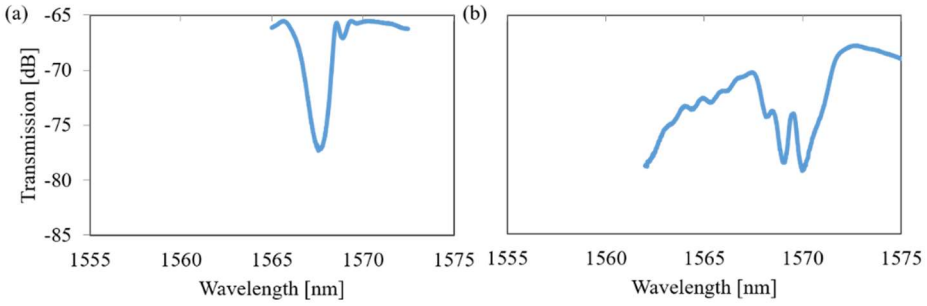

Figure 5.2.1 PS-FBG fabricated by 325 nm UV irradiation: a) Uniform FBG (first fabrication step), b) PS-FBG (Moiré structure based on two overlapped uniform gratings) -graphs adapted from [8]-.

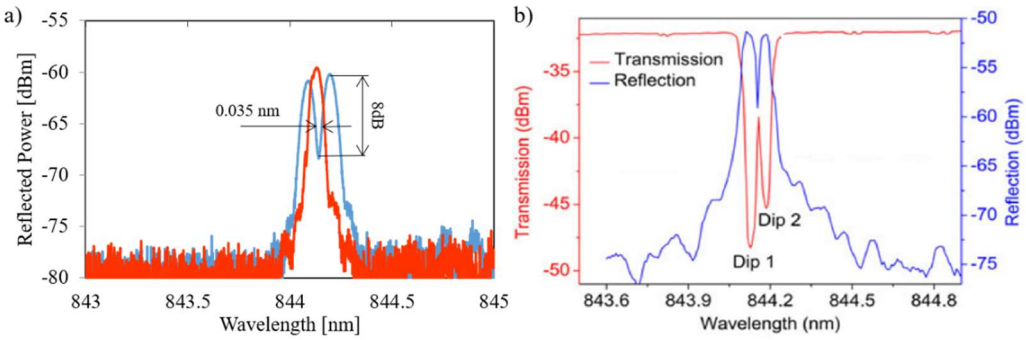

Figure 5.2.2 PS-FBG fabrication by 248 nm irradiation: a) Moiré overlapping method; image adapted from [9], b) a narrow blocking in the center -graphs adapted from [10]-.

Although chirped FBGs in POF were proposed for the dispersion tuning without wavelength shift in 2005 [11], the first chirped FBG in POF was inscribed using an KrF excimer laser operating at 248 nm and a 25-mm long chirped phase mask customized for 1550-nm grating inscription in 2017 [12]. The laser pulse rate was 1 Hz (5 mJ) and only few pulses were employed to obtain the grating response depicted in Figure 5.2.3 (a), showing a 3.9 nm bandwidth and 1.2 nm/cm chirp. The chirped phase mask method offers large stability with high cost and no flexibility as its main drawbacks. Since then, different techniques have been demonstrated to be valid for fabricating chirped gratings in POF. *Theodosiou et al.* used femtosecond direct writing method to obtain chirped FBG in commercial CYTOP POF [13], which consisted of 2000 periods with a total length of ~ 4.5 mm and 10 nm bandwidth (chirp of ~2.22 nm/mm), as shown in Figure 5.2.3 (b). Flexible chirped grating writing is demonstrated by this method but limitations are encountered for low wavelengths.

However, in this thesis we presented the first tunable chirped FBG, which was fabricated in a tapered BDK doped mPOF by using a uniform phase mask under 248 nm UV [14]. The spectral reflected power of a 10 mm grating with chirp of ~0.26 nm/mm under 1.6% strain is shown in Figure 5.2.3 (c) and the tunable properties were given by the strain and temperature sensitivity with 0.71 ± 0.02 pm/με and 56.7 pm/ºC [14][15]. Furthermore, also in this thesis, largely chirped POFBGs have been also fabricated by hot water assisted gradient thermal annealing, as shown in Figure 5.2.3 (d) [16], where one grating with ~1.1 nm/mm chirp was obtained. The simplicity of this method is one of its main advantages since no special phase mask or additional etching are needed and it enables easy control

tuning of the central wavelength and chirp characteristics.

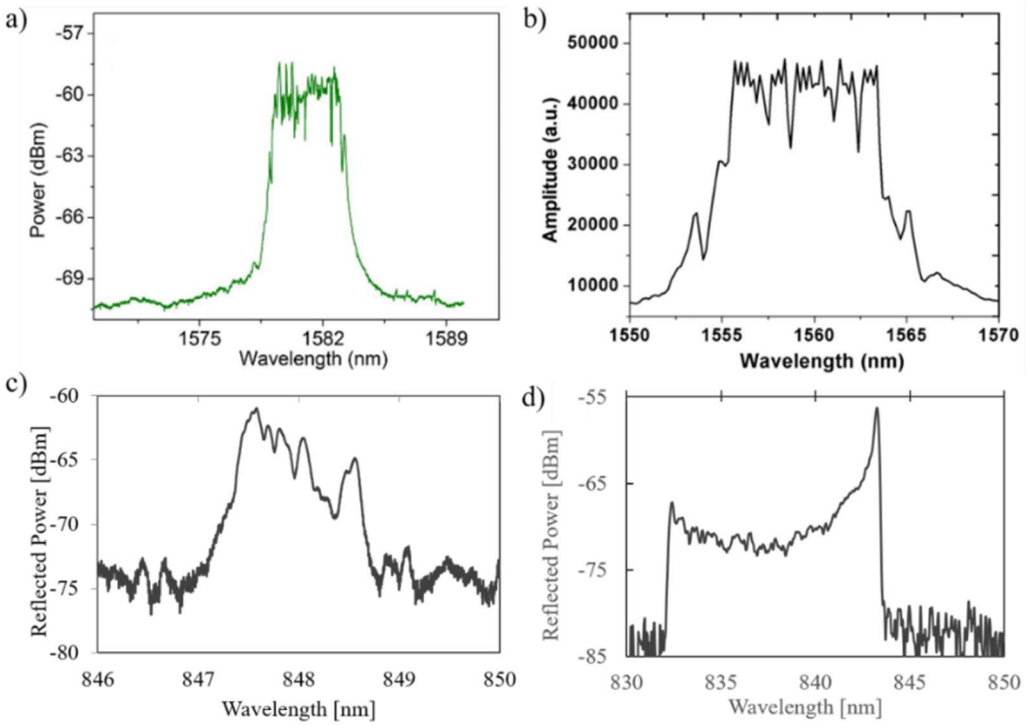

Figure 5.2.3 The reflected spectral power of chirped POFBG fabricated by different techniques: a) Chirped phase mask, b) Femtosecond directly writing on CYTOP POF, c) Under 1.6 % strain with tapering method, d) Thermal annealing.

Finally, regarding long period gratings in POF, the extense literature during the last years shows different mechanisms and methods to be used for fabricating them in POF [17][18][19][20][21][22]. The first LPG was fabricated in mPOF by mechanical deformation and heating [23]. UV photo inscription of LPG in mPOF was reported in 2010 with point-by-point technique [17]. In terms of minimizing fabrication times, which is a critical issue for commercial application, in this thesis, we demonstrated a -20 dB transmission LPG in mPOF using point by point method with an slit width of 0.2 mm [24]; the beam was shifted 1 mm for inscribing every point and 25 steps were completed to obtain an LPG total length of 25 mm. Each inscription point was irradiated by two 15 ns pulses emitted by the UV laser at 1 Hz frequency repetition rate and therefore, 2s irradiation time means a significant reduction from the 42s per point writing time reported in a previous work [21]. The strain sensitivity about -2.3 ± 0.05 nm/mstrain was measured for increasing strain whereas -2.25 ± 0.05 nm/mstrain for decreasing strain due to polymer hysteresis, which is slightly larger than presented in the previous literature, ranging from -1.40 to -1.44 nm/mstrain for increasing strain and between -1.30 and -1.40 nm/mstrain for decreasing strain [25].

5.3 Gratings applications

Dispersion compensation using chirped POFBG was first proposed in 2005 [11], but the experimental demonstration of a largely tunable dispersive device based on a chirped FBG in mPOF has been reported by *Min et al.* [26], as included in this thesis. The reflected spectral power shows a bandwidth from 0.11 to 4.86 nm and the group delay variation under strain corresponds to a tunable dispersion from 513.6 to 11.15 ps/nm, a bandwidth from 0.42 to 5.04 nm and dispersion from 2126 to 178 ps/nm reported with chirped FBG in silica fiber [27], chirped POFBG shows large varies performance with potential applications

in both optical communications and microwave photonics systems.

Among the POF applications, due to polymer characteristics mentioned in the Introduction section of this thesis, strain sensing is the most popular application. However, strain sensing under variable temperature and humidity conditions is always an issue for POF sensing. *Min et al.* [28] demonstrated the effective bandwidth of the tunable chirped POFBG is highly dependent on the strain and remains practically constant with temperature and humidity changes, which can be used in combination with wavelength measurement, to develop strain sensors under temperature and humidity variable environments. The strain sensitivity is 9.02 ± 0.02 pm/με (Figure. 4.1.3) which is higher than previous results [14] due to larger etching [29]. One of the recent challenges for fiber optic temperature sensing is found in biomedical applications. An essential feature of these systems is the possibility to detect temperature spatial distributions, also known as thermal maps [30]. A linearly chirped POFBG has been demonstrated as a semi-distributed temperature sensor capable to monitor the temperature profile along the grating length for minimally invasive scenarios [31]. High sensitivity of chirped POFBG supports the detection of spatially non-uniform temperature by means of spectral reconstruction, which indicates that chirped FBG in mPOF can provide significant advantages for thermal detecting in bio-medical applications. Furthermore, chirped POFBGs fabricated with chirped phase mask have been also demonstrated to provide accurate distributed pressure sensing [12]. The grating was subjected to pressure at various spatial position points of the grating and the reflected spectral power showed a wavelength dip related to the pressed region, which can be used for different sensing applications.

One interesting application is provided by health equipment for dynamic monitoring of gait. An array of five FBGs inscribed in CYTOP fiber [32] was embedded in a cork insole. The advantages of POF (e.g. higher flexibility and robustness) enabled monitoring patients with higher body mass compared with similar systems based on silica fiber, with a mean sensitivity of ~8.14 PM/kPa, which is almost four times higher compared with silica FBGs (~2.51 pm/kPa). Other relevant applications of FBG on POF previously reported include detect surface plasmon resonance (SPR) with tilted POF FBG [33] which is an accurate and reliable technique for determining the change of density at the interface between a dielectric medium and a metal which attracts huge attention for biochemical sensing in microfluidic systems. And piezoelectric transducers of ultrasounds are widely used in biomedical area, but the main drawback is their sensitivity to electromagnetic fields. Optical fibers are promising to replace piezo electric transducers, with the benefit of electromagnetic interference immunity and with good sensor sensitivity and proper size for ultrasonic detection. POF shows better robustness and sensitivity to pressure than silica fiber, as required by ultrasound detectors. *Broadway et al.* [34] presented the first ultrasonic detection at 5, 10 and 15 MHz by using a tilted FBG in commercial CYTOP fiber, which paves the way towards its eventual applications.

5.4 References

1. Z. Xiong, G. D. Peng, B. Wu, and P. L. Chu, "Highly Tunable Bragg Gratings in Single-Mode Polymer Optical Fibers," IEEE Photonics Technol. Lett. **11**(3), 352–354 (1999).
2. R. Oliveira, L. Bilro, and R. Nogueira, "Bragg gratings in a few mode microstructured polymer optical fiber in less than 30 seconds," Opt. Express **23**(8), 10181–10187 (2015).
3. R. Min, B. Ortega, K. Nielsen, O. Bang, and C. Marques, "Bragg Grating Inscription With Low Pulse Energy in Doped Microstructured Polymer Optical Fibers," IEEE Sensors Lett. **2**(2), 2–5 (2018).
4. R. Min, B. Ortega, X. Hu, C. Broadway, C. Caucheteur, C. F. J. Pun, H. Y. Tam, P. Antunes, and C. Marques, "Bragg gratings inscription in TS-doped PMMA POF by using 248-nm KrF pulses," IEEE Photonics Technol. Lett. **30**(18), 1609–1612 (2018).
5. A. Pospori, C. A. F. Marques, O. Bang, D. J. Webb, and P. André, "Polymer optical fiber Bragg grating inscription with a single UV laser pulse," Opt. Express **25**(8), 9028–9038 (2017).
6. L. Pereira, R. Min, X. Hu, C. Caucheteur, O. Bang, B. Ortega, C. Marques, P. Antunes, and J. L. Pinto, "Polymer optical fiber Bragg grating inscription with a single Nd:YAG laser pulse," Opt. Express **26**(14), 18096–18104 (2018).
7. R. Min, B. Ortega, A. Leal-Junior, and C. Marques, "Fabrication and Characterization of Bragg Grating in CYTOP POF at 600-nm Wavelength," IEEE Sensors Lett. **2**(3), 1–4 (2018).
8. B. Ortega, R. Min, D. Sáez-Rodríguez, Y. Mi, K. Nielsen, and O. Bang, "Bandpass transmission filters based on phase shifted fiber Bragg gratings in microstructured polymer optical fibers," in Proceedings of SPIE - The International Society for Optical Engineering (2017), 10232.
9. R. Min, C. Marques, O. Bang, and B. Ortega, "Moiré phase-shifted fiber Bragg gratings in polymer optical fibers," Opt. Fiber Technol. **41**, 78–81 (2018).
10. L. M. Pereira, A. Pospori, P. Antunes, M. F. Domingues, S. Marques, O. Bang, D. J. Webb, and C. A. F. Marques, "Phase-Shifted Bragg Grating Inscription in PMMA Microstructured POF Using 248-nm UV Radiation," J. Light. Technol. **35**(23), 5176–5184 (2017).
11. H. Liu, H. Liu, G. Peng, and T. W. Whitbread, "Tunable dispersion using linearly chirped polymer optical fiber Bragg gratings with fixed center wavelength," IEEE Photonics Technol. Lett. **17**(2), 411–413 (2005).
12. C. A. F. Marques, P. Antunes, P. Mergo, D. J. Webb, and P. Andre, "Chirped Bragg Gratings in PMMA Step-Index Polymer Optical Fiber," IEEE Photonics Technol. Lett. **29**(6), 500–503 (2017).
13. A. Theodosiou, X. Hu, C. Caucheteur, and K. Kalli, "Bragg Gratings and Fabry-Perot Cavities in Low-Loss Multimode CYTOP Polymer Fiber," IEEE Photonics Technol. Lett. **30**(9), 857–860 (2018).
14. R. Min, B. Ortega, and C. Marques, "Fabrication of tunable chirped mPOF Bragg gratings using a uniform phase mask," Opt. Express **26**(4), 4411–4420 (2018).
15. R. Min, B. Ortega, and C. Marques, "Tunable chirped fiber bragg gratings in mPOF," in Optics InfoBase Conference Papers (2018), p. Part F98-B.
16. R. Min, B. Ortega, C. Broadway, C. Caucheteur, G. Woyessa, O. Bang, P. Antunes, and C. Marques, "Hot water-assisted fabrication of chirped polymer optical fiber Bragg gratings," Opt. Express **26**(26), 34655–34664 (2018).
17. D. Sáez-Rodríguez, J. L. Cruz, I. Johnson, D. J. Webb, M. C. J. Large, and A. Argyros, "Water diffusion into UV inscripted long period grating in microstructured polymer fiber," IEEE Sens. J. **10**(7), 1169–1173 (2010).
18. Z. C. Li, H. Y. Tam, L. X. Xu, and Q. J. Zhang, "Fabrication of long-period gratings in poly(methyl methacrylate-co-methyl vinyl ketone-cobenzyl methacrylate)-core polymer optical fiber by use of a mercury lamp," Opt. Lett. **30**(10), 1117–1119 (2005).
19. D. Kowal, G. Statkiewicz-Barabach, P. Mergo, and W. Urbanczyk, "Inscription of long period gratings using an ultraviolet laser beam in the diffusion-doped microstructured polymer optical fiber," Appl. Opt. **54**(20), 6327–6333 (2015).
20. Y. Luo, Z. Li, R. Zheng, R. Chen, Q. Yan, Q. Zhang, G. Peng, G. Zou, H. Ming, and B. Zhu, "Birefringent azopolymer long period fiber gratings induced by 532 nm polarized laser," Opt. Commun. **282**(12), 2348–2353 (2009).
21. D. Kowal and G. Statkiewicz-Barabach, "Microstructured polymer optical fiber for long

period gratings fabrication using an ultraviolet laser beam," Opt. Lett. **39**(8), 2242–2245 (2014).
22. R. Lwin, A. Argyros, S. G. Leon-Saval, and M. C. J. Large, "Strain sensing using long period gratings in microstructured polymer optical fibres," in 21st International Conference on Optical Fibre Sensors (2011), 7753, p. 775396.
23. M. P. Hiscocks, M. A. van Eijkelenborg, A. Argyros, and M. C. J. Large, "Stable imprinting of long-period gratings in microstructured polymer optical fibre.," Opt. Express **14**(11), 4644–4649 (2006).
24. R. Min, C. Marques, K. Nielsen, O. Bang, and B. Ortega, "Fast Inscription of Long Period Gratings in Microstructured Polymer Optical Fibers," IEEE Sens. J. **18**(5), 1919–1923 (2018).
25. G. Statkiewicz-barabach, D. Kowal, M. K. Szczurowski, P. Mergo, and W. Urbanczyk, "Hydrostatic Pressure and Strain Sensitivity of Long Period Grating Fabricated in Polymer Microstructured Fiber," IEEE Photonics Technol. Lett. **25**(5), 496–499 (2013).
26. R. Min, S. Korganbayev, C. Moladi, C. Broadway, X. Hu, C. Caucheteur, O. Bang, P. Antunes, D. Tosi, C. Marques, and B. Ortega, "Largely tunable dispersion chirped polymer FBG," Opt. Lett. **43**(20), 5106–5109 (2018).
27. X. Dong, P. Shum, N. Ngo, C. Chan, J. Ng, and C. Zhao, "A largely tunable CFBG-based dispersion compensator with fixed center wavelength," Opt. Express **11**(22), 2970–2974 (2003).
28. R. Min, B. Ortega, C. Broadway, X. Hu, C. Caucheteur, O. Bang, P. Antunes, and C. Marques, "Microstructured PMMA POF chirped Bragg gratings for strain sensing," Opt. Fiber Technol. **45**, 330–335 (2018).
29. G. Rajan, M. Yusof, M. Noor, N. H. Lovell, E. Ambikaizrajah, G. Farrell, and G. Peng, "Polymer micro-fiber Bragg grating," Opitcs Lett. **38**(17), 38–41 (2013).
30. D. Tosi, E. Schena, C. Molardi, and S. Korganbayev, "Fiber optic sensors for sub-centimeter spatially resolved measurements: Review and biomedical applications," Opt. Fiber Technol. **43**(3), 6–19 (2018).
31. S. Korganbayev, R. Min, M. Jelbuldina, X. Hu, C. Caucheteur, O. Bang, B. Ortega, C. Marques, and D. Tosi, "Thermal Profile Detection Through High-Sensitivity Fiber Optic Chirped Bragg Grating on Microstructured PMMA Fiber," J. Light. Technol. **36**(20), 4723–4729 (2018).
32. D. Vilarinho, A. Theodosiou, C. Leitão, A. G. Leal-Junior, M. de Fátima Domingues, K. Kalli, P. André, P. Antunes, and C. Marques, "POFBG-embedded cork insole for plantar pressure monitoring," MDPI Sensors **17**(12), (2017).
33. X. Hu, P. Mégret, and C. Caucheteur, "Surface plasmon excitation at near-infrared wavelengths in polymer optical fibers," Opt. Lett. **40**(17), 3998–4001 (2015).
34. C. Broadway, K. Kalli, A. Theodosiou, M. Zubel, K. Sugden, P. Megret, and C. Caucheteur, "L-band CYTOP Bragg gratings for ultrasound sensing," in Micro-Structured and Specialty Optical Fibres V (2018), 10681(May), p. 1068109.

Chapter 6

Conclusions and future research lines

This last chapter summarizes the main conclusions obtained throughout this work and points out some future interesting research lines to carry out during the next years. Novel contributions of this thesis in the POF gratings fabrication process and also novel devices and applications are described as follows, although several aspects require further research to make these devices real “off the shelf” sensors and filters in the near future. The advantages and characteristics of polymers have been successfully proved as promising for strain, temperature and humidity sensors and also for filters or variable delay lines in communications networks.

6.1 Conclusions

6.1.1 Gratings fabrication

POFBGs were inscribed in different POF materials by using a pulsed UV KrF laser at 248 nm. The fibers employed in the grating inscription were PMMA, Topas 8007 and 5013, Zeonex and PC mPOFs and Topas 5013 step-index POFs. The comparison of the POFBGs inscribed with the technique presented in this work and with the conventional continuous 325 nm laser reported in the literature show a reduction in the inscription time of at least 16 times, where the maximum reduction was obtained for Topas 8007 mPOF (more than 130 times). The results presented in this work have an impact on the methods conventionally employed for the FBG inscription, since the use of a different laser setup, combined with a suitable annealing of the fiber, provides a substantial decrease of the inscription time without harming the grating strength, bandwidth and stability. In addition, the presented setup is similar to the one employed for FBG inscription in silica fibers. The transmission loss and the connection between silica fiber and mPOF are still issues for commercial application, which needs further research to be improved.

FBG inscription in BDK doped PMMA mPOF using a single low energy pulse (8 ns) from a Q-switched Nd: YAG laser system operating at 266 nm was demonstrated. The grating exhibits more than 84% reflectivity, and a refractive index change of 0.5×10^{-4} in the core of the fiber. The results show the potential to reduce POFBG production costs, by employing cheaper laser systems (the laser system employed in this work is about 5 times cheaper when compared to the KrF 248 nm excimer laser system and the femtosecond laser system) and also, reducing the inscription time to a pulse width (in this case to 8 ns). Besides our work brings new chances for POFBG fabrication at 266 nm wavelength, similarly as FBG in other POF material, the transmission loss and the connection between silica fiber and mPOF need to be improved.

FBG in Trans-4-stilbenemethanol-doped photosensitive step-index PMMA POF at 850 nm wavelength was investigated by using phase mask methodology with a 248 nm KrF laser, with inscription times lower than 1 second. Humidity, temperature and strain sensitivities under stable conditions were also measured to assess the fabricated components for potential sensing applications. However, the transmission losses are still an issue for commercial applications, which needs some time to come through.

We demonstrated that low UV power (60 μJ/pulse) leads to achieve a grating with a 2.2 dB dip in transmission and a reflectivity of 22 dB, which makes them suitable for many

sensing applications. The demonstrated gratings can be obtained without high pulse energy, which avoids high maintenance costs. This research can be useful for future investigations of different kind of Bragg grating devices fabrication for sensing fields in order to reduce the energy waste and pay attention to the minimum UV energy and total spent energy.

FBGs were fabricated at 600 nm region in a commercial CYTOP POF using phase mask technology. FBGs operating at this wavelength region is critical to be achieved by using fs laser systems due to the FBG period required. However, further efforts are required in order to demonstrate stronger gratings. The temperature, humidity and strain characterization positively assess the use of these gratings for novel potential sensing and optical communication applications, which are also discussed throughout the thesis. As future work we also plan to investigate the response of higher order modes coupling to temperature and strain changes.

6.1.2 Devices and applications

We demonstrate the fabrication of a PS-FBG in polymer optical fibers using the phase mask technique. The phase shift is obtained by superimposing two quasi similar uniform fiber Bragg gratings to form a Moiré structure by using two UV pulses irradiation for each grating. Furthermore, the flexibility of such technique has been shown by fabricating gratings with multiple phase shifts. POFs are very attractive for the deployment of current and future high bandwidth access networks and the phase shifted devices open new opportunities for applications in WDM networks and also for microwave photonic applications. Strain and temperature sensitivity have been measured to propose them as highly tunable devices, which will be developed based on easy handling and low-cost materials provided stress relaxation issues and related stability are correctly addressed.

We have presented the fabrication of tunable chirped Bragg gratings in polymer optical fiber using a uniform phase mask for the first time to our knowledge. Chirped POFBGs have been fabricated with different tapered profiles for the sake of illustrating the potentiality of this method. The strain and temperature sensitivity measurements as 0.71 ± 0.02 pm/με and -56.7 pm/ºC, demonstrate their tunability properties. By proper etching of the section we obtained 2.6 nm reflected bandwidth under 1.50 % strain, and stronger tapered profiles would lead to chirped POFBGs with broader bandwidths. This work paves the way for different photonics applications of chirped fiber Bragg grating in POF. Good accuracy and control of the etching profile of the fiber is required so further investigations are required for better results.

A new low cost fabrication technique of chirped POFBGs based on hot water assisted gradient thermal annealing of uniform POFBGs has been presented in this thesis. The proposed method is simple since no special phase mask or additional etching process is needed, and it enables an easy and flexible tuning of the wavelength and chirp performance with a permanent and stable chirp characteristic. A chirp larger than 11 nm has been obtained for the first time in less than 10 min. The central wavelength linearly changes with temperature, strain and humidity whereas the bandwidth keeps stable, similar to CFBG response when a chirped phase mask is employed for fabrication. Sensitivity measurements to external parameters have been provided for future potential applications such as high-resolution large bandwidth thermal detection in bio-sensing and delay lines in microwave photonics subsystems. Moreover, the use of liquids with different specific heat coefficients will also lead to variations on the temperature gradient. In this way, investigations of different liquids and temperature gradients will be considered as future work. Not fully annealed POF were used in this experiment with the corresponding limited long-time stability performance.

LPGs have been inscribed in polymer optical fibers by using point–by- point technique with two 248 nm UV laser pulses per point. The device has been fabricated in a single mode mPOF which core has been doped with BDK for photosensitivity enhancement to UV radiation. The inscription time for each coupling point has been shortened by 21 times compared with the best one reported in the literature. Furthermore, we explored the stability of the grating response under different conditions to demonstrate its large potential for telecommunications and sensing applications. High resolution control system is required for this method and research to look for potential applications is to be done.

Tapered chirped POF FBGs were investigated for sensing with measured sensitivity of 0.90 ± 0.02 pm/με. We have shown wavelength and bandwidth measurements, where the latter are less sensitive to humidity changes when the fiber is under no strain. A low humidity sensitivity performance around -4.2 ± 0.4 pm/% was achieved under high strain conditions. The grating response time is significantly improved by measuring the 3-dB bandwidth, which is a great benefit towards commercial strain sensing applications using POFBGs.

Thermal profiles were measured by using a mPOF CFBG fiber optic sensor, with a detection method based on spectral reconstruction. The higher sensitivity to temperature variations (−191.4 pm/◦C) with respect to glass fiber, and the low chirp rate of the mPOF grating require modification of the reconstruction algorithm. We have conducted two sets of experiments: linear temperature profile along 10 mm mPOF CFBG, and a radiofrequency ablation that induces Gaussian shaped temperature gradient. Experiments validate that the proposed mPOF CFBG can provide significant advantages for thermal sensing in biomedical applications.

The tunable dispersion devices were implemented by using tapered chirped POF FBGs. We also proposed to employ temperature in order to compensate the central wavelength shift due to the applied strain, and therefore, promising tunable CFBG devices are presented for future optical systems. Step-index BDK POF could be also interesting for this application due to high photosensitivity and larger strength of the fabricated gratings. In the overall, this work paves the way for chirped POF FBG in both sensing and optical communication applications.

6.2 Future research lines

Although the POFBG technology has been dramatically improved recently, there is still room for a further improvement and optimization. For PMMA based POF, the benzyl dimethyl ketal (BDK) dopant in POF seems promising, but the concentration in the fiber core still needs to be optimized for enhanced photosensitivity. At the same time, dopants can increase the transmission loss of POF, and strong and stable gratings in undoped POF are still worth to be investigated.

As explained throughout this thesis, the work has been mainly focused on the experimental results on POF gratings fabrication and applications. However, further work on modelling and simulation of the gratings response would be also worth to optimize the components design and the fiber choice, also predicting the thermal, strain and humidity sensitivities for sensing applications. More specifically, with regard to fibers, exploring the gratings fabrication in few modes or multimode POF can be attractive, i.e., for low cost communications systems. As shown in the different experimental setups employed in this work, the connection of silica fiber with mPOF, single mode POF and multimode POF is always critical and imposes limitations on the proper measurement of devices. To overcome this problem, we employed one simple cleaver to cut the polymer fibers and we used commercial ferrules for connecting them with normal silica fiber, but our solution may be further improved for commercial applications.The strength of the fabricated devices and other general aspects such as gratings stability and repeatability including annealing processes for different polymer fibers can be also further improved to obtain reliable off-the-shelf components.

Special grating devices in POF show attractive performance, similarly to silica fiber ones. The fabrication technology for chirped POFBG is one of the main achievements during our study, but there is still room for improving towards commercial products. We will follow this research line to explore novel fabrication technology for chirped POFBG.

About the application based on chirped POFBG, future work could be addressed to evaluate the response of the mPOF CFBG in closer proximity to the applicator, using a longer grating length and possibly a larger chirp rate, and to improve the spectral reconstruction method valid for specific mPOF CFBG coefficients. For biomedical applications, further research must be conducted towards the development of future devices with new materials such as hydrogel and polydimethylsiloxane.

Besides chirped POFBG applications, phase shifted POFBG can be used for high-

sensitivity ultrasonic sensing system, which is also an interesting topic to be explored, and also the use of large angle tilted POFBG for surface plasmon resonance measurement as promising for biomedical applications.

To conclude, the novel applications show the potential of POFBG for biomedical and dispersion compensation. However, the POFBG applications are not limited to these fields and additional applications can be developed in the near future for various industrial sectors including the aerospace, civil, energy, and environmental sectors.

ANNEX: List of publications

A. Journal publications included in the compendium

[JP.1] L.P. Pereira, **R. Min**, X. Hu, B. Ortega, C. Marques, C. Caucheteur, P. Antunes, J. Pinto, "Polymer optical fiber Bragg grating inscription with a single Nd:YAG laser pulse. "**Optics Express**, 26(10), 18096-18104, 2018. **(Impact factor: 3.356, Optics-Q1)**

[JP.2] C. Marques, **R. Min**, A. L. Junior, P. Antunes, A. Fasano, G. Woyessa, K. Nielsen, H. K. Rasmussen, B. Ortega, and O. Bang, "Fast and stable gratings inscription in POFs made of different materials with pulsed 248 nm KrF laser" **Optics Express**, 26(2), 2013-2022, 2018. **(Impact factor: 3.356, Optics-Q1)**

[JP.3] R. Min, B. Ortega, X. Hu, C. Broadway, C. Caucheteur, C. Pun, H. Tam, P. Antunes, C. Marques, "Bragg gratings inscription in TS doped PMMA POF by using 248 nm KrF pulses" **IEEE Photonics Technology Letters**, 30(18), 1609 - 1612, 2018. **(Impact factor: 2.446, Optics-Q2)**

[JP.4] R. Min, B. Ortega, K. Nielsen, O. Bang, C. Marques, "Bragg grating inscription with low pulse energy in doped microstructured polymer optical fibers" **IEEE Sensors Letters**, 2(2), 5000604, 2018.

[JP.5] R. Min, B. Ortega, A. L. Junior, C. Marques, "Bragg grating inscription at 600 nm wavelength region in CYTOP POF with 248 nm KrF pulses" **IEEE Sensors Letters**, 2(3), 5000804, 2018.

[JP.6] R. Min, C. Marques, O. Bang, B. Ortega, "Moiré phase-shifted fiber Bragg gratings in polymer optical fibers" **Optical Fiber Technology**, 41 ,78-81,2018. **(Impact factor: 1.35, Optics-Q3)**

[JP.7] R. Min, B. Ortega, C. Marques, "Fabrication of tunable chirped mPOF Bragg gratings using a uniform phase mask." **Optics Express**, 26(4), 4411-4420, 2018. **(Impact factor: 3.356, Optics-Q1)**

[JP.8] R. Min, B. Ortega, C. Broadway, C. Caucheteur, G. Woyessa, O. Bang, P. Antunes, C. Marques, Hot water-assisted fabrication of chirped polymer optical fiber Bragg gratings" **Optics Express**, 26(26), 34655-34664, 2018. **(Impact factor: 3.356, Optics-Q1)**

[JP.9] R. Min, C. Marques, K. Nielsen, O. Bang, B. Ortega, "Fast inscription of long period gratings in microstructured polymer optical fibers" **IEEE Sensors Journal**, 5(1), 1919 - 1923 , 2018. **(Impact factor: 2.617, Instruments-Q1)**

[JP.10] R. Min, B. Ortega, C. Broadway, X. Hu, C. Caucheteur, O. Bang, P. Antunes, C. Marques "Microstructured PMMA POF chirped Bragg gratings for strain sensing" **Optical Fiber Technology**, 41, 78-81, 2018. **(Impact factor: 1.35, Optics-Q3)**

[JP.11] S.Korganbayev, **R.Min**, M. Jelbuldina, X. Hu, C. Caucheteur, O.Bang, B.Ortega, C. Marques, D. Tosi, "Thermal profile detection through high-sensitivity fiber optic chirped Bragg grating on microstructured PMMA fiber Chirped FBG" **IEEE/OSA Journal of Lightwave Technology** , 36(20), 4723 –4729, 2018. **(Impact factor: 3.652, Optics-Q1)**

[JP.12] R. Min, S. Korganbayev, C. Monardi, C. Broadway, X. Hu, C. Caucheteur, O. Bang, P. Antunes, D. Tosi, C. Marques, B. Ortega, "Largely tunable dispersion chirped polymer FBG" **Optics Letters**, 43(20), 5106-5109, 2018. **(Impact factor: 3.589, Optics-Q1)**

B. Journal and conference papers strongly related but not included in the compendium:

Journals:

[JP.13] D. Saez-Rodríguez, **R. Min**, B. Ortega, K. Nielsen, D. J. Webb, "Passive and Portable Polymer Optical Fiber Cleaver" **IEEE Photonics Technology Letters** 28(24), 2834-2837, 2016. **(Impact factor: 2.446, Optics-Q2)**

[JP.14] C. Marques, A. L-Junior, **R. Min**, M. F. Domingues, C. Leitão Leitão, P. Antunes, B. Ortega, P.S André, "Advances on Polymer Optical Fiber Gratings Using a KrF Pulsed Laser System Operating at 248 nm " **MDPI Fibers**, 6(3), 2018.

[JP.15] R.Min, B. Ortega, C. Marques, "Latest Achievements in Polymer Optical Fiber Gratings: Fabrication and Applications" **MDPI Photonics**, 6(2), 2019.

Conferences:

[CP.1] R. Min, C. Broadway, X. Hu, O. Bang, C. Caucheteur, B. Ortega, C. Marques. "Chirped mPOF Bragg grating for strain sensing " OSA OFS-26, Lausanne, Switzerland, September, 2018.

[CP.2] R. Min,B. Ortega ,C. Marques, "Tunable Chirped fiber Bragg gratings in mPOF " OSA Advanced Photonics Congress ETH Zurich, Zürich, Switzerland, July, 2018.

[CP.3] R. Min, C. Marques, B. Ortega, O. Bang, "LPG inscription in mPOF for optical sensing " SPIE Photonics Europe, France, Vol. Proc. 10681, pp. 10681 - 10681-7, April, 2018.

[CP.4] R. Min, B. Ortega, K. Nielsen, O. Bang, "Stable Fibre Bragg Gratings inscribed in doped microstructured polymer optical fibre based on PMMA " The 26th International Conference on Plastic Optical Fibres, Averio, Portugal, 2017.

[CP.5] B.Ortega, **R. Min**, D. S. Rodríguez, Y. Mi, K. Nielsen, O. Bang, "Bandpass transmission filters based on phase shifted fiber Bragg gratings in microstructured polymer optical fibers" SPIE Europe V, vol. 10232, p. 1023209. Prague, 2017.

[CP.6] D. Saez-Rodríguez, **R. Min**, B. Ortega, K. Nielsen, D. J. Webb, "Passive Polymer Optical Fiber Cleaver" The 25th International Conference on Plastic Optical Fibres Aston, UK 2016.